

**Die Expedition ARCTIC '93  
Der Fahrtabschnitt ARK-IX/4  
mit FS „Polarstern“ 1993**

**The Expedition ARCTIC '93  
Leg ARK-IX/4  
of RV „Polarstern“ 1993**

---

**edited by Dieter K. Fütterer  
with contributions of the participants**



Cruise Report ARK-IX/4  
Tromsø - Murmansk - Bremerhaven  
Contents

1	INTRODUCTION AND CRUISE SUMMARY .....	5
2	CRUISE ITINERARY .....	7
3	WEATHER CONDITIONS .....	13
4	REMOTE SENSING OF SEA ICE	
4.1	Airborne radar surveys .....	16
4.2	AVHRR imaging.....	20
4.3	Line-scan camera observations.....	21
4.4	Microwave emissivity .....	22
5	OCEANOGRAPHIC STUDIES	
5.1	Physical and chemical parameters of the water column .....	26
5.1.1	First results of the CTD-measurements .....	27
5.1.2	Tracer measurements.....	31
5.1.2.1	Sampling for Tritium, Helium, <sup>14</sup> C, <sup>18</sup> O and <sup>85</sup> Kr analyses .....	31
5.1.2.2	Chlorofluorocarbons and carbon tetrachloride .....	33
5.1.2.3	Other tracerwork.....	35
5.1.3	Chemical oceanography .....	37
5.1.3.1	Nutrients and oxygen.....	37
5.1.3.2	Total carbonate .....	38
5.2	Acoustic Doppler Current Profiler (ADCP) observations .....	40
5.3	Moorings .....	41
5.4	Meteorological buoys.....	41
6	SEA-ICE STUDIES AND SAMPLING	
6.1	Sea-ice conditions along the cruise track .....	42
6.1.1	Ice conditions in the Svalbard and Franz Josef Land area .....	42
6.1.2	Ice conditions in the Laptev Sea.....	43
6.2	Albedo of the ice cover during late summer time and energy exchange processes.....	47
6.3	Thickness, structure and properties of sea ice .....	51
6.4	Sea-ice biology .....	55
6.4.1	Abundance of the sea ice organisms.....	55
6.4.2	Structure and dynamics of sea ice food web .....	62
6.4.3	Study of the under-ice fauna .....	63
6.4.4	Observations of sea-ice organisms in the field using an endoscope ...	64
6.4.5	Stain dilution experiments.....	65
6.4.6	Continuous chlorophyll measurements.....	68
6.5	Sediments in sea ice .....	69
6.6	Distribution, structure and hydrography of surface melt puddles.....	73
6.7	Iceberg observations .....	76
7	BIOLOGICAL INVESTIGATIONS	
7.1	Phytoplankton and particle flux.....	79
7.1.1	Mooring of sediment trap .....	84

7.2.	Distribution of zooplankton and community structures .....	84
7.3	Egg production in dominant copepod species .....	90
7.4	Zoobenthos .....	94
7.4.1	Meiofauna .....	94
7.4.2	Macrofauna .....	97
7.5	Benthic microbial ecology .....	106
8	<b>GEOLOGICAL INVESTIGATIONS</b>	
8.1	Sediment echography and high resolution sub-bottom profiling .....	111
8.2	Sediment sampling and description .....	122
8.3	Physical properties .....	128
8.4	Sediment characteristics and lithostratigraphy .....	129
8.4.1	Sediments from the Barents Sea continental slope between Svalbard and Franz Josef Land .....	129
8.4.2	Sediments from the Laptev Sea shelf and continental margin .....	136
8.4.3	Sediments from the Vilkitski Strait .....	148
8.5	Geochemical changes in the sediments .....	150
8.5.1	Pore water geochemistry .....	150
8.5.2	Calcium carbonate hexahydrate precipitations .....	153
9	<b>REFERENCES</b> .....	155
10	<b>ANNEX</b>	
10.1	Station list ARK-IX/4 .....	157
10.2	Benthos sampling list .....	171
10.3	List of smearslices prepared and examined during the cruise .....	175
10.4	Graphical core descriptions .....	177
10.5	General guidelines for data and sample distribution .....	227
10.5.1	Physical and chemical oceanography .....	227
10.5.1.1	Statement for the distribution of oceanographic and hydrochemical data .....	227
10.5.1.2	Working titles of oceanographic and hydrochemical themes .....	228
10.5.2	Remote sensing .....	229
10.5.2.1	Guidelines for the exchange of remote sending data .....	229
10.5.2.2	Working titles of remote sensing themes .....	230
10.5.3	Physical sea-ice studies .....	230
10.5.3.1	Data exchange and joint data evaluation for sea-ice studies .....	230
10.5.4	Sea-ice biology .....	232
10.5.4.1	Distribution procedure for ice biological samples and data .....	232
10.5.4.2	Scientific working titles and collaborations for sea-ice biological studies .....	233
10.5.5	Marine biological investigation .....	234
10.5.5.1	Sample and data distribution procedure for benthic and planktic biological material .....	234
10.5.5.2	Intended scientific work on biological material and data .....	235
10.5.6	Marine Geology .....	237
10.5.6.1	Sediment sample distribution guidelines for ARK-IX/4 materials .....	237
10.5.6.2	Working titles on sampled geological material and data .....	238
10.6	List of participating institutions .....	241
10.7	List of participants and ship's crew .....	243

## 1 INTRODUCTION AND CRUISE SUMMARY

As an obvious indication of the promising evolution of the bilateral scientific cooperation between Russia and Germany the fourth Leg of the ninth expedition of RV *Polarstern* into the Arctic Ocean (ARK-IX/4) was carried out as a joint Russian-German multidisciplinary oceanographic expedition (ARCTIC'93) to the Eurasian continental margin of the Barents and Laptev Seas. The scientific program aboard RV *Polarstern* covered a broad field of scientific objectives spanning paleoceanography, marine biology, physical and chemical oceanography as well as sea-ice research and remote sensing in a region which has been inaccessible to western scientists until this expedition. General planning of this expedition started as early as 1988; the scientific program resulted from many discussions between scientists of several disciplines primarily from the Alfred Wegener Institute (AWI) in Bremerhaven, the Research Center for Marine Geosciences GEOMAR in Kiel and the Arctic and Antarctic Research Institute (AARI) in St. Petersburg and several institutes within the Russian Academy of Sciences (RAS) which are involved in ecological and geo-scientific research. Planning was finalized during a bilateral workshop on "Russian-German Cooperation in and around the Laptev Sea" in St. Petersburg, 10-13 May 1993.

RV *Polarstern* of AWI operated in the ice-covered areas of the outer shelf and continental slope of the Laptev Sea (ARK-IX/4) while the Russian hydrographic vessel RV *Ivan Kireyev* carried out a complementary program in the ice-free shallow waters of the southern Laptev Sea (TRANSDRIFT-I). Participation of RV *Ivan Kireyev* was organized and coordinated by AARI, St. Petersburg and GEOMAR, Kiel.

RV *Polarstern* took on a complement of Russian scientists in Murmansk in early August and departed for the region of Svalbard and Franz Joseph Land where two transects extending from the continental shelf into the deep Nansen Basin were sampled for sea ice, oceanographic, biological and geological research. Sailing east RV *Polarstern* met with RV *Ivan Kireyev* in the eastern Laptev Sea for intercalibration of oceanographic equipment. RV *Polarstern* performed an extensive sampling program in the Laptev Sea on four transects from the shelf into the deep ocean basins, most of this in heavy pack ice. A final meeting and exchange of data and samples between the two vessels occurred in late September.

The multidisciplinary scientific program aboard *Polarstern* included four major objectives:

- (1) The marine geology program focused on sampling sediments of the Eurasian continental margin for high resolution paleoclimate and paleoceanographic studies.
- (2) The main topic of the marine biological investigations included the comparison of different ecological conditions of the permanently ice-covered regions of the northern Barents and Laptev seas.
- (3) The sea-ice program focused on: (i) ice physics such as growth processes of sea ice, its structure and properties; (ii) ice biology including abundance of organisms in sea ice, structure and dynamics of the food web as well as the coupling processes between sea ice and the pelagic environment and (iii) ice-transported sediment as a major process for ARCTIC Ocean sedimentation.
- (4) The oceanographic program focused on the specific role of the different Eurasian shelf seas in forming surface and subsurface water masses and on quantifying their relative contributions.

The great success of this concerted Russian-German ARCTIC'93 expedition represents a major breakthrough in Arctic Ocean research cooperation. More than 70 Russian, German and scientists from some other countries cooperated excellently in this integrated field study aboard RV *Polarstern* and RV *Ivan Kireyev*. After this most rewarding experience it is planned to continue this cooperation by jointly working on samples and data, by mutual data exchange and by joint publishing of the results where appropriate. Further joint expeditions are planned for the years to come.

The present report describes the scientific program and first results of RV *Polarstern*'s Leg ARK-IX/4 of ARCTIC'93; the initial report and preliminary results from TRANSDRIFT-I of RV *Ivan Kireyev* will be published elsewhere in this series.

#### Acknowledgements

The scientific participants in *Polarstern* cruise ARK-IX/4 take this opportunity to thank captain Jonas and his crew for the magnificent treatment on board and for their untiring and able assistance during work under sometimes harsh conditions. Their skill and permanent support provided the ideal climate for a successful cruise.

## 2 CRUISE ITINERARY

RV *Polarstern* left Tromsø early in the morning of August 6, 1993, with 40 scientists and 44 crew members heading for the Russian port of Murmansk where 11 Russian cruise participants, observer, ice pilot and additional nine scientists, were boarded. The short port call in Murmansk was taken as an opportunity for a flying visit of the city of Murmansk by a large number of scientists. Early in the morning of August 8, RV *Polarstern* left Murmansk and sailed in calm sea with northwesterly heading for Bjørnøya and Spitsbergen.

A first test station for a number of sampling gears was successfully run in the morning of August 9 in the Bear Island Trough supported by bright sunshine and calm sea. In the late evening of the same day *Polarstern* crossed the polar front; at the same time dense fog arose.

The scientific work program started in the early morning of August 10 off the southern tip of Spitsbergen. At the western end of Storfjordrenna and in the mouth of the Storfjord four oceanographic moorings were deployed. On rapid transit heading north on August 11 *Polarstern* cleared west of Kong Karls Land and Kvitøya. First drift ice which rapidly became denser was met abeam Hopen Bank at 77° 30' N / 24° 40' E.

The first working area of Transect A on the Nansen Basin continental slope north of Kvitøya was reached in the early morning of August 12. The same day the first flight mission of the sea-ice airborne radar survey was carried out in the area between Svalbard and Franz Josef Land. During the expedition the sea-ice distribution was monitored by the INTAARI airborne radar system in four flight missions on different occasions, two in the Barents Sea and two in the Laptev Sea.

During the period from August 12 to August 14 station work was carried out along Transect A with sampling and probing for biological, geological and oceanographic projects. Because of dense ice coverage (9-10/10) no towed gears could be used. For the same reason the attempt failed to recover two oceanographic moorings which had been deployed during *Polarstern* cruise EPOS-II (1991) in water depth of 500 and 2500 m respectively.

At noon of August 14 *Polarstern* started her transit from Transect A heading east over a distance of 140 nm for the next working area of Transect C north of Franz Josef Land. Heavy ice conditions of 9-10/10 coverage and bad visibility hindered a speedy headway; average speed decreased to merely 1-2 knots. On the following days of August 15 and 16 two stations on large ice flows for sea-ice sampling and research were carried out *en route*. Station time was used on board *Polarstern* for geological sampling.

On August 17 a position in the vicinity of the planned Transect C was reached. In consideration of the extremely heavy ice conditions further headway to the East would have required too much loss of time. Therefore, it was decided to remove Transect C to a more westerly position extending from the northwestern edge of Franz Josef Land. Sampling along planned Transects B and E was completely abandoned to save time for the main objectives of the expedition in the Laptev Sea. With minor revisions of planned sampling positions because of sometimes extremely

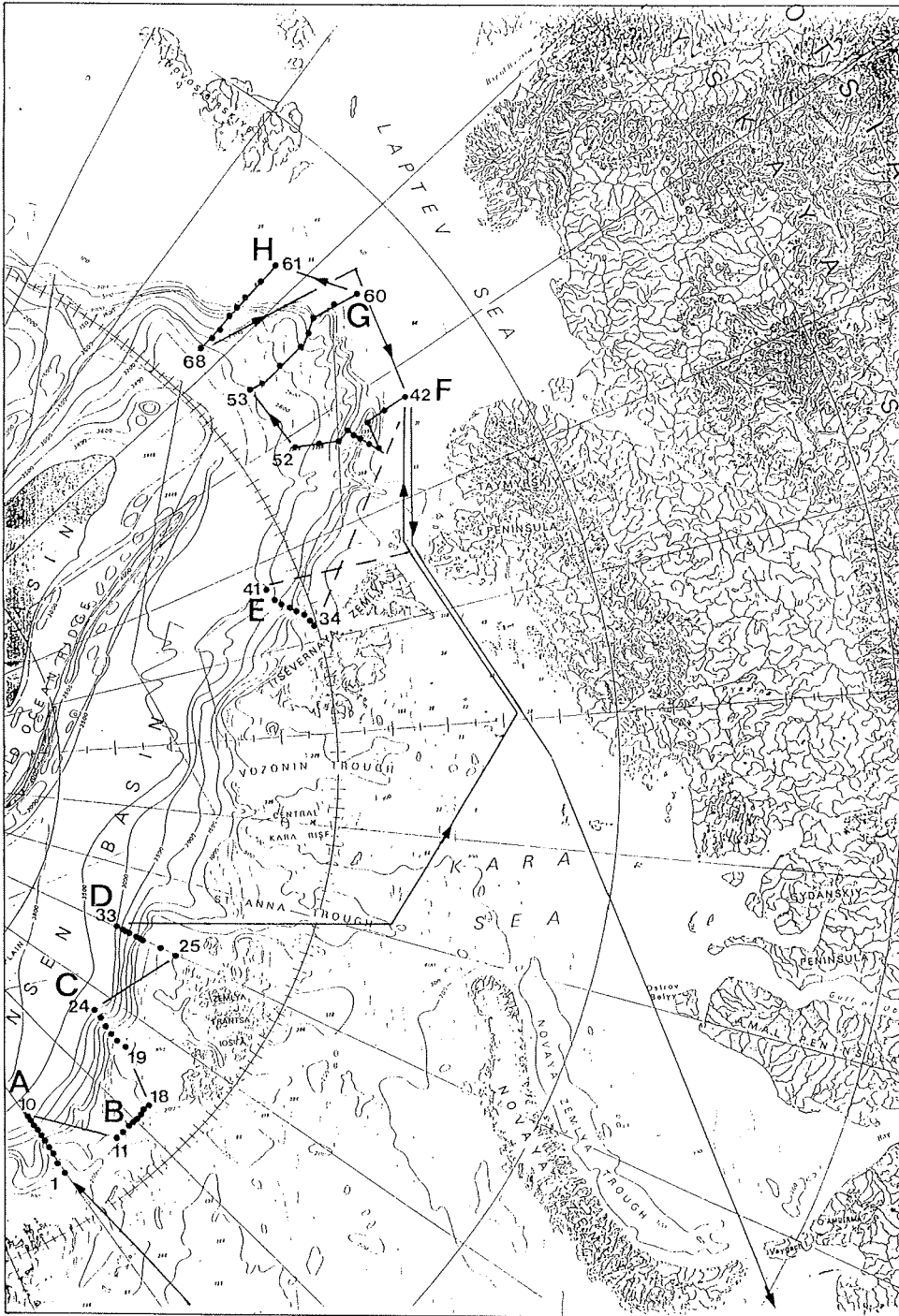


Fig. 2-1: Cruise track and sampling stations of RV *Polarstern* along the continental margin of the eastern Barents and Laptev Seas as originally planned.

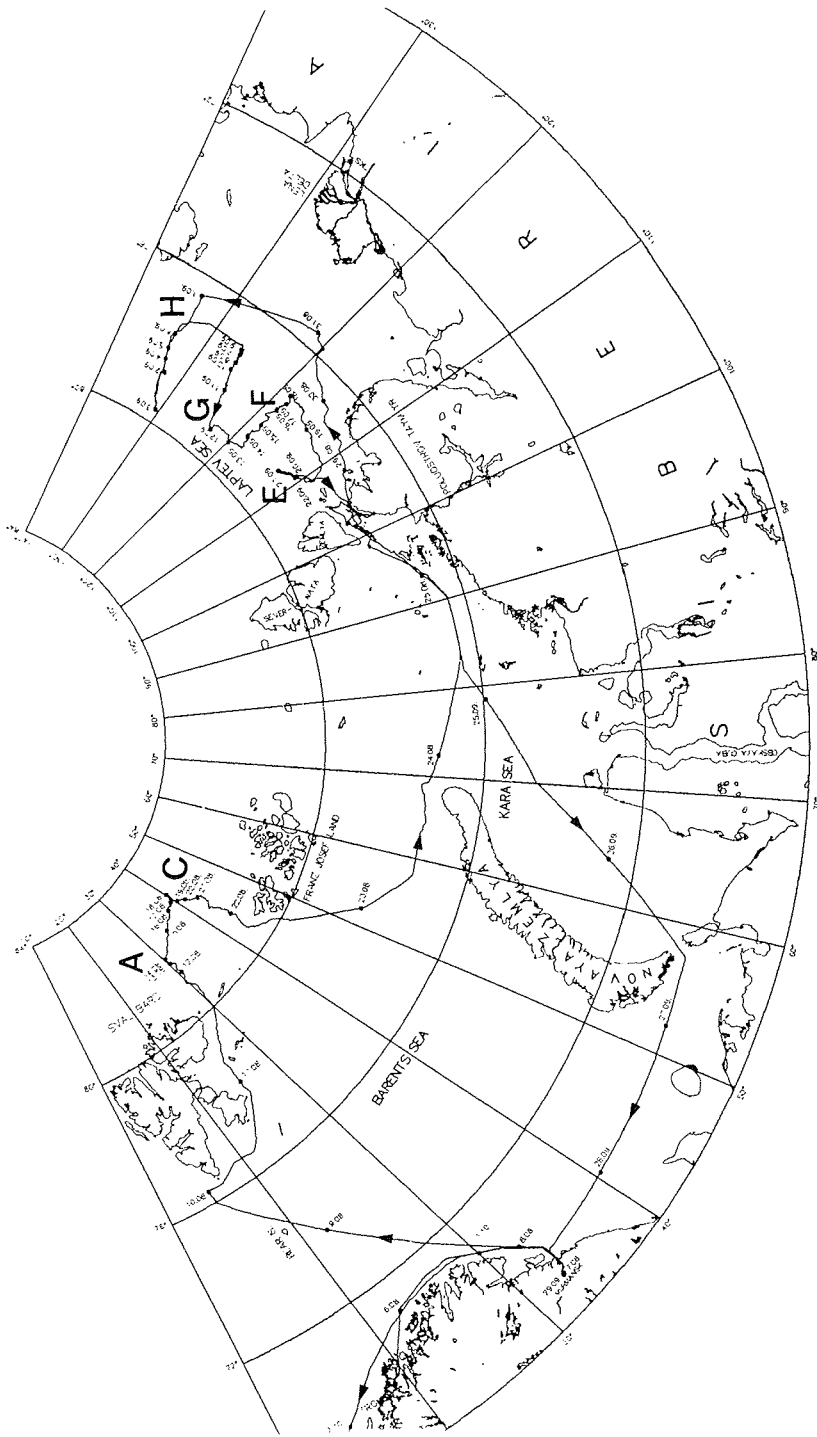


Fig. 2-2: Cruise track of RV *Polarstern* during ARK-IX/4 and location of sampling Transects A and C in the northern Barents Sea and E, F, G, and H in the Laptev Sea.

difficult ice condition a complete sampling program for all disciplines was accomplished on Transect C from the deep Nansen Basin to the northwestern shelf of Franz Josef Land. The most northern position of cruise ARK-IX/4 was reached on this transect on August 18 at 82° 46' N / 40° 13' E.

On August 19 the second airborne radar mission took place on a flight pattern north of Franz Josef Land. This flight yielded an excellent overlapping with the satellite-borne Synthetic Aperture Radar (SAR) scenes of the European Research Satellite (ERS-1). In addition these data, together with AVHRR images received on board *Polarstern*, offered an excellent support for navigating the ship out of the ice.

After finishing station work on Transect C in the evening of August 21, *Polarstern* left the area of Franz Josef Land heading for a long transit to the Laptev Sea. At the beginning, heavy multi-year ice of 8-9/10 coverage together with dense fog and bad visibility hindered a good headway. Not until late evening of August 22 Franz Josef Land was cleared abeam. Sudden clearance from fog enabled a marvelous view on the steep cliffs and extensive ice fields of Alexandra Land and Prince George Land. The drift ice border was passed during the following night of August 23 at 79° 55' N / 46° 36' E.

Meeting fine weather and calm sea *Polarstern* made good headway while passing eastern Barents Sea. In the morning of August 24, large fields of drift ice of 6-8/10 coverage were passed off the northern tip of Novaya Zemlya as forecasted from AVHRR images. Likewise favourable conditions were met while passing the northern Kara Sea heading for the Nordenskiöld Archipelago off the Taymyr Peninsula. The Strait of Vilkitski, the narrow between Severnaya Zemlya and Cape Chelyuskin, the most northern tip of continental Asia, was reached in the night of August 25.

Long-lasting strong easterly winds during the past days of August had concentrated thick multi-year ice in the western Laptev Sea forming a hardly passable ice barrier, called The Taymyr Ice Massive, at the eastern exit of Vilkitski Strait into the Laptev Sea. *Polarstern* decided to wait in Vilkitski Strait until one of the Russian nuclear icebreakers, operating in this part of the Northern Searoute, would be available for convoy. While waiting *Polarstern* used the time to carry out an intensive biological, geological and oceanographical sampling program successfully.

Not until the early morning of August 29 when the nuclear icebreaker *Soyuz* followed by an icegoing freighter showed up the convoy could be formed. In the following night the two nuclear icebreakers *Rossiya* and *Arctica* and a second freighter closed up. *Polarstern* followed the impressive convoy now formed by three nuclear icebreakers and two ice-strengthened freighters. The extremely heavy ice conditions of thick and heavily pressed and ridged multi-year ice off the Taymyr Peninsula represented a real challenge even for the powerful nuclear icebreakers. After a distance of approximately 140 nm and heaving passed the zone of heavy press-ice the convoy was disbanded in the early morning of August 31 near the ice edge in the western Laptev Sea at 75° 47' N / 119° 43' E.

In the course of August 31 *Polarstern* steamed out of the ice and headed in open waters for an agreed upon rendezvous with RV *Ivan Kireyev* in the eastern Laptev Sea at 76° 30' N / 133° 10' E, northwest of Kotelnyy Island. Because of high swell the meeting in the afternoon of September 1 became more difficult than expected.

Finally, it was restricted to the exchange of samples, equipment and spare parts. For the intercalibration of the hydrographic equipment on *Polarstern* and *Ivan Kireyev* this site was used for CTD measurements from both vessels. At the same time biological and geological sampling took place.

In the course of September 1 the first airborne radar flight mission in the Laptev Sea was accomplished which enabled an excellent and complete overview on the actual ice distribution in the Laptev Sea. Using these information *Polarstern* left the rendezvous with *Ivan Kireyev* in the evening of September 1 heading north in open water along the ice edge for the deep sea of the Amundsen Basin. During the following days up to September 6, intensive station work was carried out on 12 positions on Transect H between 79° 38' N, 130° 33' E in the deep Amundsen Basin and 76° 30' N / 133° 10' E on the shallow Laptev Sea shelf. Shallow water depths and short distances between stations resulted in a rapid sequence of stations and corresponding work load for all scientists involved. Because of generally favourable ice conditions in the eastern Laptev Sea the sea ice program had to be reduced to one station only at 79° 38' N / 130° 33' E where a thin flow of one-year ice was sampled.

During the night of September 7, *Polarstern* hauled to the ice edge in the West to start sampling Transect G in the extension of Lena river delta to the north from the shelf at 77° 02' N / 126° 25' E to the deep Amundsen Basin at 79° 15' N / 122° 53' E. During the next days up to September 12, altogether 10 positions were sampled on Transect G for oceanography (9 stations), biology (6 stations), geology (8 stations) and sea ice (4 stations).

Strong westerly winds during these days had broken up to some extent the still dense ice cover (approx. 9/10) enabling *Polarstern* to make good progress and save time between stations. Transiting west in the night of September 13 *Polarstern* started sampling on Transect F in the western Laptev Sea at 79° 10' N / 110° 50' E. Two meteorological drift buoys were deployed on ice flows *en route* which will transfer position of the ice flow and data of wind, humidity and air pressure via satellite. On Transect F stretching from the deep Nansen Basin at 79° 10' N / 119° 50' E to the western Laptev Sea shelf at 77° 11' N / 118° 44' E altogether 12 positions were sampled for oceanography (12 stations), biology (7 stations), geology (8 stations) and sea ice (5 stations).

During these days of mid September temperature decreased strongly to minus 15° C. This made work on deck more difficult, but what was more important, led rapidly to formation of new ice and to as rapidly decreasing ice conditions. Besides these adversities all station work on Transect F could successfully be finished on September 18. An important help for ship's navigation during these days were the SAR-scenes of the second airborne radar mission which was accomplished on September 14, covering the western Laptev Sea.

In agreement with the nuclear icebreakers operating in Vilkitski Strait and the western Laptev Sea *Polarstern* started her direct transit to Maly Taymyr Island at the eastern entrance of Vilkitski Strait in the evening of September 18 without icebreaker support. This transit proceeded unexpectedly smoothly, at first favoured by large leads over the shelf break, opening and closing regularly in the course of tides, later

by bright sunshine which provided excellent conditions for helicopter surveys. Additional information was available from NOAA-AVHRR satellite images.

Already on September 20, station work on an additional Transect E could start from near Maly Taymyr Island at 78° 16' N / 109° 14' E to the northeast into the southwestern Laptev Sea. This transect was terminated on September 21, at 78° 45' N / 112° 42' E and 1200 m water depth when by again decreasing temperature and increasing formation of new ice, conditions changed strongly to the worse. After to some extent vigorous struggle with more and more rigid pack ice *Polarstern* reached the open water of Vilkitski Strait in the morning of September 23.

Near the shore of Helland Hansen Island in the western Vilkitski Strait a second *ad hoc* rendezvous with *Ivan Kireyev* was accomplished. Both vessels laid alongside for a period of four hours enabling an intensive exchange of visitors. This opportunity was used to exchange all sample material and scientific equipment for transport back to Germany and Russia respectively.

In the afternoon of September 24 *Polarstern* left the area of Vilkitski Strait heading west for Murmansk. Favourable weather with easterly winds provided a comfortable cruise through the southern Kara Sea, Kara Strait between Nowaya Zemlya and Vaygach Peninsula and the southeastern Barents Sea. On September 29 *Polarstern* arrived in Murmansk where the Russian participants in the ARK-IX/4 cruise disembarked. The port call in Murmansk was used for scientists and crew for sight-seeing and a bus tour into the vicinity of Murmansk. In the evening captain and chief scientist gave a reception on board *Polarstern* for the information of directors and senior scientists as well as officials of various Murmansk based scientific institutions and establishments of navy and economy.

Early in the morning of October 1, *Polarstern* left Murmansk and sailed for Bremerhaven. After 61 days on sea, a distance of approximately 8000 nautical miles many of which in heavy pack ice, *Polarstern* in the morning of October 5, reached the port of Bremerhaven bringing to an end a scientifically unexpected successful cruise which, in the future, may be called a milestone in Russian-German cooperation in the Arctic Ocean.

### 3 WEATHER CONDITIONS

#### 3.1 Specific Meteorological Features in the Laptev Sea during ARC-IX/4 (Erhard Röd)

The following summarized synoptic review of baric patterns and circulation systems is to frame the phenomenology of fog given below.

During the first two weeks (8 August through 15 August) between low pressure over the Norwegian Sea and a well developed subpolar high over Severnaya Zemlya and Franz Josef Land the wind was mainly from S to SE with 2 to 5 Bft. This warm air advection held the temperature near to freezing point. The pressure at the ship ranged from 1020 to 1034 hPa. From this peak value constant pressure fall indicated the decay of the anticyclonic regime, caused by cyclonic eddies S and W of the ships route.

The lowest pressure of the whole cruise was achieved on 31 August with 992 hPa. The vortex over Taymyr Peninsula generated rather strong NE-wind with 4 to 8 Bft during the week of 23 August to 28 August. From 30 August to 10 September the flow switched repeatedly between SE and NW with 4 to 6 Bft, corresponding to the varying position of the low centres over the Taymyr Peninsula and the Kara Sea respectively. The latter continued moving east just north of the site of *Polarstern* bringing about a pressure drop to 1002 hPa on 10 September. This curl became stationary later on near the Wrangel Island. The northwesterly flow in its cold sector initiated the advection of colder and drier air. In the meantime a high had settled over Barents Sea and spread gradually its control towards Laptev Sea raising the pressure above the 1020 hPa level again.

Towards the end of operations in the Laptev Sea a long high pressure belt extending from the East Siberian Sea to Scandinavia with low pressure over the continent made the wind turn to SE, later in Vilkitski Strait to NE with 4 to 6 Bft. Due to channelling the turbulent flow gusted here up to 40 knots. September 10, brought the onset of an essential colder period with temperatures between  $-4^{\circ}$  C and the absolute minimum of the cruise of  $-15^{\circ}$  C.

To summarize the conditions described above the pressure was relatively high with an average of 1019 hPa corresponding to dominating anticyclonic regime in the Arctic with only two well developed cyclonic interruptions. Cyclogenetic processes as a counterpart originated mainly over European and Asian Russia due to summer conditions with low pressure over the warmer continent. On 22 days the outflow from this subpolar high brought northeasterly to northwesterly winds. On other 22 days winds from S to SE were responsible for most of the intense fog events. The mean temperature of the first half of the cruise was near freezing point and approximately  $-5^{\circ}$  C during the second half.

#### 3.1 Fog during the RV *Polarstern* cruise ARK-IX/4 of (Erhard Röd)

In the summer in the Arctic regions fog is of outstanding importance for all research activities, ship manoeuvres and especially for flight operations of planes or helicopters; all the other meteorological parameters being only of minor or indirect

influence. Wind for instance, an interesting factor over open sea, in the presence of ice loses completely its impact on ships movement and is significant only in an indirect way by the displacement of the pack-ice and by advection of different air masses.

On the other hand, fog is conditioned itself by the complex interrelation of all meteorological factors in a very tricky way sometimes hard to be understood and even harder to be predicted. It is notorious, that different processes can contribute to the formation of fog: radiative cooling of the air adjacent to the surface under clear sky conditions, advection of preexisting fog-areas, mixing of air masses with different properties, cooling of moist and relatively warm air by the colder sea or ice. The latter mechanism seems to be the most frequent over sea and ice in the Arctic (e.g. the fog over the Newfoundland Banks).

The forecast of fog therefore frequently can be reduced to a prognostic estimate of wind direction and speed. Southerly winds bringing (mostly) warm air over the colder surface are likely to produce fog. Cold air from northerly directions on the contrary enhances the probability of dissipation or of non-occurrence of fog.

In the warm air heat flux is downward and causes cooling of the lowest layers and thus the actual temperature reaching the dew point. In cold air the heat flux is inverse, heating and therefore drying the air. Only with very drastic temperature differences between cold air and warm water (approx. 10° C or more) Arctic sea smoke can form developing sometimes into real fog. This cold air fog, however, normally is only shallow and thin compared with dense fog in warm air.

Advection of fog is an important process too, especially near the ice edge, which is particularly susceptible for the formation of fog patches that can be transported by the wind- or crosswind by the ship. The contact of ice and water creates a very complicated structure of fluxes of heat and water vapor and radiation balance giving frequently rise to fog.

The vicinity of fronts is another important factor in fog generation. Here the active process is mixing of different air masses supported by the increase of cyclonic vorticity. In the Arctic fronts are nearly always occluded after a long lifetime in lower latitudes.

The aforementioned processes may be active simultaneously thus enforcing or neutralizing their relative efficiency. The complexity of the problem is the reason, why no plain prognostic rules can be derived. Forecasting fog means estimating the probability of occurrence with a rather wide error rate. For a true physical prediction the knowledge of the fine structure of subscale fields would be necessary that, however, can't be obtained by means of normal routine observations.

From 10 August to 22 August, *Polarstern* operated between an extended complex low over the Norwegian Sea and an anticyclone over the Laptev Sea in a strong easterly to south-easterly moist flow. Here on the southern tip and later in the east of Svalbard dense fog obscured the sky from 10 August, to the morning of 12 August. After half a day of sunshine on Friday, 13 August, fog fell in again. With all the other parameters unvaried the day after brought bright sunshine in spite of fresh southerly wind.

Hence forward fog was the prevailing aspect of sky for more than a week with only a one day interruption when fog rose up to form low stratus. On 23 August, with the wind turning to E and NE drier air was advected. Fog and clouds as well disappeared and *Polarstern* enjoyed one of the very rare sunny days of the cruise. This was the onset of a period of one week with nearly no fog, confirming the rule, that slightly positive difference in temperature between sea surface and adjacent air prevents fog from forming. During that week the pressure fell from high anticyclonic 1034 hPa to 992 hPa toward the end of the month. This cyclonic regime made the wind veer to SSE increasing promptly the occurrence of fog. On 2 September, a coldfront type occlusion crossed the ship's track and with the wind turning to NNW dissipation of fog was to be expected. What happened was just the opposite, the fog became even denser than before. The explanation of this anomalous event was to be found in a small subscale circulation that had formed on this front just south of *Polarstern* and stopped its eastward displacement.

Thus frontal processes cancelled the validity of the interrelation between wind direction and visibility bringing about six mostly foggy days independently from wind direction. Only when the front had finally moved away, the NW-wind caused the fog to disappear. On the other hand, on 8 September, under southerly wind conditions the visibility was unlimited, due to the entrainment of extremely dry air flowing out from a north Siberian anticyclone that made the relative humidity drop to 60 %.

From 9 September to 10 September, a fully developed frontal system crossed the Laptev Sea. The cold sector of the corresponding depression marked the onset of intense advection of cold air from the NW and subsequently a period free of lasting fog. Patches of freezing fog that appeared mainly in the vicinity of leads of open water were only of short duration and low density, but good enough for producing bad helicopter icing. This sort of cold air fog was not to be foreseen from radiosoundings and other predictors. Also the rising of fog to form Arctic stratus or inversely the lowering of stratus to sea level as fog depends on subscale processes and is therefore beyond predictability.

The duration of the observational period is by far too short for a sound statistical treatment of the described phenomena. It should be mentioned, however, that fog of varying endurance occurred on 28 days, i.e. approximately on two thirds of the days in the operational phase of the cruise leg. The duration of cold air fog was less than twelve hours, frontal and warm air fog one or more days. The lower density of freezing fog is obviously a consequence of the lower absolute humidity compared with fog in warm air. Every type of fog could form just on the spot or be advected from a distant waiting position (or reached and entered by the moving ship). From the helicopter the irregular distribution of fog patches sometimes can be seen especially well showing the fortuity of this phenomenon. All these experiences show the difficulties in forecasting and in nowcasting the occurrence of fog. But every new empirical evidence is an additional step toward increased accuracy of prediction. Thus routine forecasting simultaneously merges into meteorological research which on its part acts as feed back on prognosticating skill.

#### 4 REMOTE SENSING OF SEA ICE

The largest continuous areas of sea ice on the globe are located on the Arctic Ocean and the bordering seas. The extent of the sea-ice covered areas changes seasonally. During winter up to 12-13  $10^6$  km<sup>2</sup> are covered with sea ice. This coverage decreases during the summer to one half. Atmospheric and ocean circulation depends on distribution of sea ice and open water in polar regions. The knowledge of the processes in the system ocean-atmosphere-cryosphere are the requirement to get a comprehension of the earth climate system.

The most important sea-ice parameters are: extent, concentration, type, drift, albedo, temperature, floe-size distribution, and locations of leads and polynyas. Ground based observation take much time and the regions are rather inaccessible, therefore only a limited number of samples are practicable. For systematic monitoring, remote sensing technics are applied.

Remote sensing is confined to the use of visible, thermal infrared and active and passive microwave techniques to obtain information about the polar oceans. The combined interpretation of different equipment utilizes the advantages of different spectral ranges and ground resolutions, which are not attainable with one sensor only. This leads to an increase of quantity and accuracy of the derived parameters.

The main focus of the remote sensing part of the present experiment was to obtain improved information on sea-ice extent, concentration, floe size, drift pattern and roughness. Therefore it is necessary to validate the results of interpretations with real ice conditions. The activities of the remote sensing group includes receiving and interpreting of AVHRR satellite images, carrying out sub satellite flights with the INTAARI Side Looking Airborne Radar (SLAR) and a helicopter-mounted line-scan camera. Another part of the activities were to supplement the ice observation from the other groups by measurements of sea ice albedo and emissivity.

##### 4.1 Airborne Radar Surveys (Vladimir Bogdanov, Thomas Martin and Sergey Syrtsov)

In order to estimate ice types and concentrations by microwave radiometers, algorithms have been developed and improved in the past. Major advances have been made in establishing these technics, because microwave radiation penetrates clouds, so that large areas can be monitored nearly independently of atmospheric condition. During ARK-IX/4 expedition the sea-ice distribution was monitored for areas of special interest by the INTAARI airborne radar system in four flight missions. The dual Side Looking Airborne Radar (SLAR) is mounted on board of a long-range aircraft with an operation range up to 5400 km and a total mission time of 11 hours. The data are collected from an operation altitude of 7200 m within two swath of 37.5 km separated by a dead zone of 11.5 km directly underneath the aircraft. SLAR is an active microwave radiometer which obtains surface back scattering information in the X-Band (15 GHz) with a ground resolution of 20 by 40 m. The radar images were processed in real time on board of the aircraft and transmitted to *Polarstern* (Fig. 4.1-1).

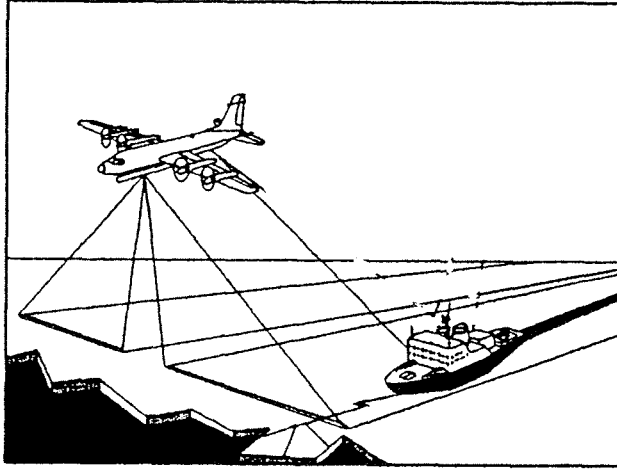


**Fig. 4.1-1:** The radar image of the ice cover is transmitted from the aircraft to *Polarstern* by digital radio link. The satellite navigation system GPS is used for geo-location of the images.

The first two flight missions (12 August and 19 August) were located over the ice of the Barents Sea between Svalbard and Franz Josef Land (Fig. 4.1-2 a and b). The flight pattern was adjusted in accordance with the European Research Satellite (ERS-1) passes to obtain an optimal overlapping with the satellite-borne Synthetic Aperture Radar (SAR). An other task was to generate ice charts to support the ship's navigation. In contrast to all other flight missions, the quantitative output of the first flight mission was less, because of navigation problems on board of the aircraft. But all data of the first two flights provide good coverage for the ERS-1 data.

The remote sensing investigation in the Barents Sea took place under typical summer conditions of melting ice. The measurements represent wet snow and ice surfaces with a large amount of melt puddles (for details of the ice situation see Chapter 6.1). Figure 4.1-3 shows an example of a SLAR image received aboard *Polarstern*. The broken ice floes along the track of *Polarstern* increase the backscattering qualities of the ice, here visible as light line.

Different ice types could be distinguish by thickness, salinity and their snow cover. In radar data the backscattering from multiyear ice is a function of surface and volume scattering, since the low salinity allows penetration into the ice floes, whereas backscattering from snow-free first year ice and open water is determined by scattering from the surface. During summer, melt processes modify the backscattering characteristics of sea ice. The density of the upper portion of the ice sheet is reduced and melt water develops a different surface quality. However, in the last years several groups investigated the backscattering signatures of melting summer sea ice. In any case, the radar signal has not been fully understood. Therefore we plan to compare the ERS-1 data with the results of the radar flights. Furthermore the *in situ* measurements on the ice floes (see chapter 6.3) and the helicopter flight observations (see Chapter 4.3) should give additional information to interpret the radar backscattering signals.

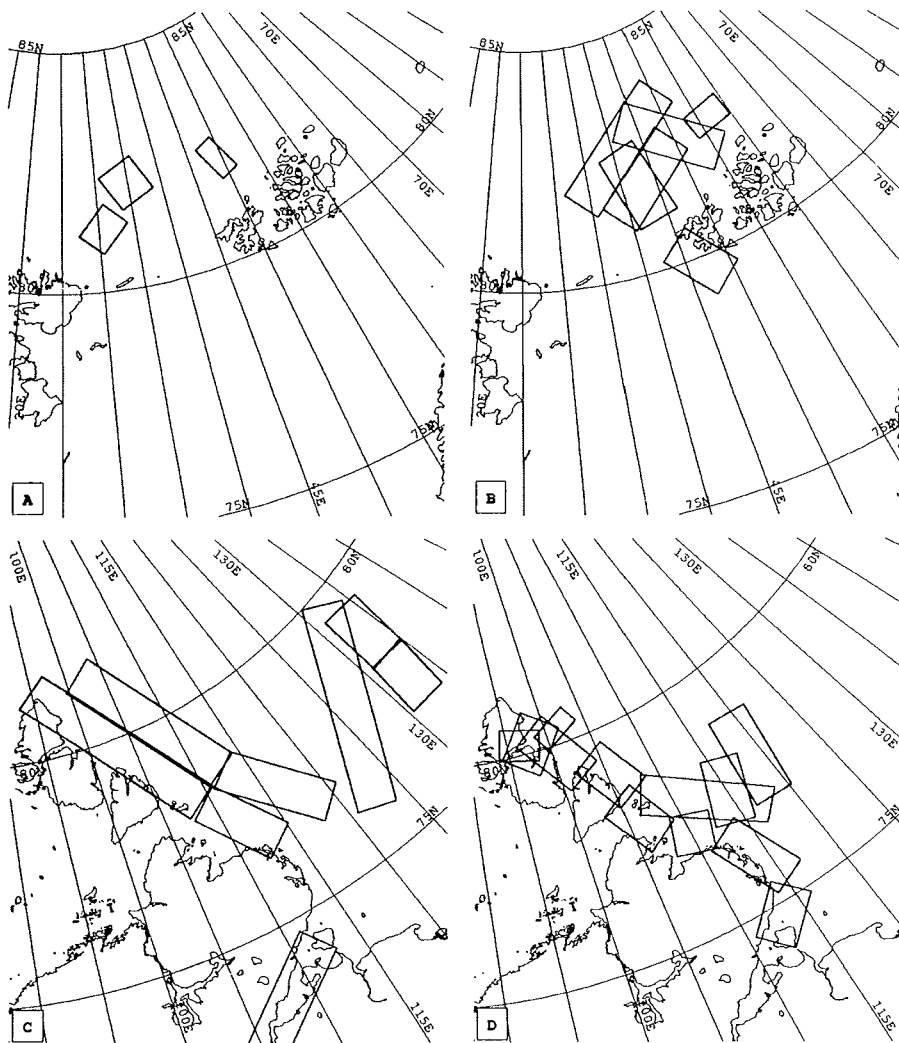


**Figure 4.1-2:** Aerial distribution of the SLAR data for the four flight missions: a) 12 August; b) 19 August; c.) 1 September, and d) 14 September 1993.

The later flight missions in the Laptev Sea (1 September and 14 September), as shown in Figure 4.1-2, are suitable to a lesser extent for comparison with ERS-1 passages, because less satellite data are available for this region. The decreasing surface temperature terminates the melt process and the signature of the ice types changes. The focus of attention in this region is studied on more local phenomena. To get an insight into the mass balance of the Laptev Sea ice regime, the small scale ice velocity field should be determined on the base of the combined INTAARI flight data and ERS-1 images. These data should be compared with the trajectories of ARGOS buoys also deployed in this area (see Chapter 5.4).

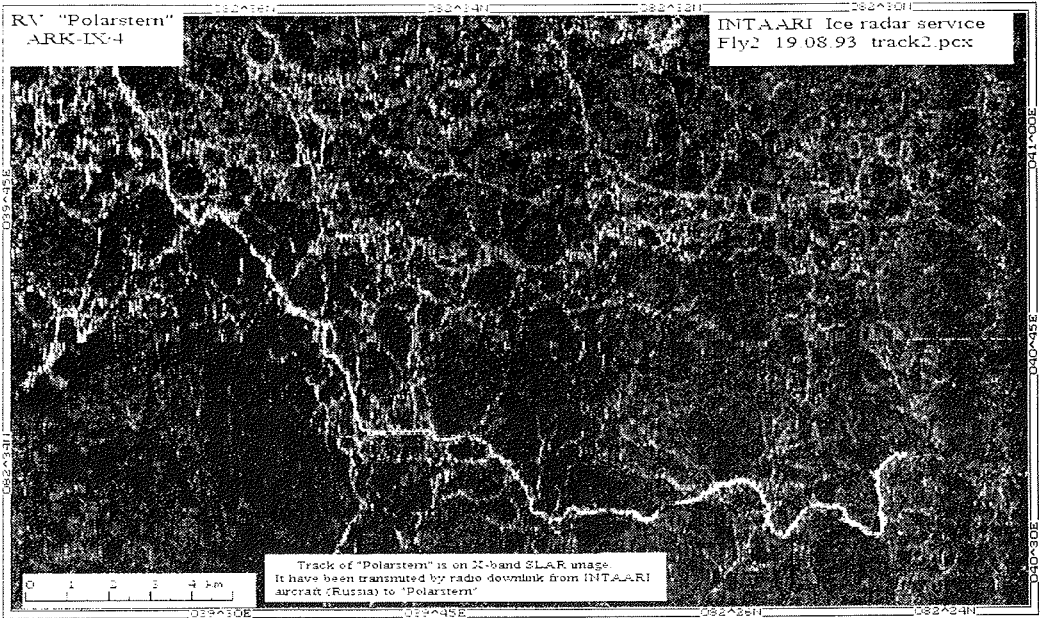


Fig. 4.1-3: SLAR image received on board of *Polarstern* during the second INTAARI flight. The image covers typical summer melt ice. Position of ice station during the flight mission: 82° 23' N, 40° 55' E. The track of *Polarstern* is visible as a light white line.

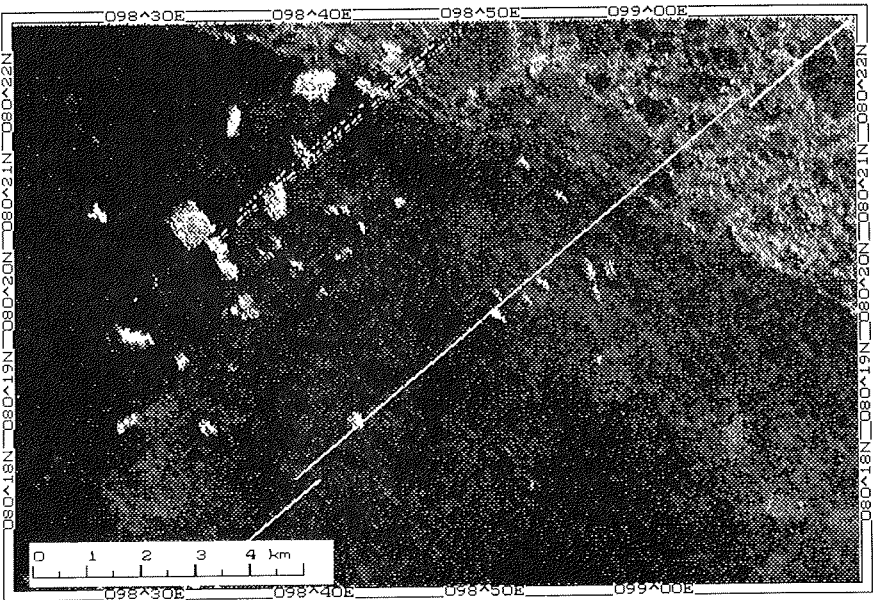


Fig. 4.1-4: Field of numerous icebergs in the western Laptev Sea east of Severnaya Zemlya.

East of Severnaya Zemlya islands numerous icebergs were detected with the radar data (Fig. 4.1-4). Some iceberg positions could be verified during a helicopter flight mission. These iceberg fields could be an important source of iceberg impact to the central Arctic Basin. Our initial observations shall be followed by more extensive investigations to verify the role of the Severnaya Zemlya glaciers for iceberg production. According to our preliminary interpretations during ARK-IX/4 the iceberg drift should also be monitored in this region with ERS-1 images during the second part of the year 1993.

#### 4.2 AVHRR Imaging (Vitali Alexandrov and Thomas Martin)

During ARK-IX/4 expedition more than 200 images of the Advanced Very High Resolution Radiometer (AVHRR) flown on the Television Infrared Observational Satellite (TIROS-N) of the National Oceanic and Atmospheric Administration (NOAA) have been received on board of *Polarstern*. All images passes routines for calibration and rectification into a stereographic grid. The digital data were archived on magnetic tape. For every satellite pass grey scale hardcopies were produced for several areas of interest. According to these pictures the ice distributions were derived for planing the flight activities for the line-scan-camera and the INTAARI SLAR flights, as well as for ship's navigation.

The procedure of sea-ice image interpretations consists of decoding these images and determining sea-ice parameters. Concentration is one of the most important parameter of sea ice in summer. It can be estimated from visual and radar satellite images. During the last years, research has been carried out to derive algorithms of ice concentration estimates from remote sensing data.

After detecting clouds, high resolution images should allow distinguishing two features: ice and water. Ice concentration is determined as a ratio of the number of ice pixels to the total number of pixels in a delineated area. But every pixel of a high resolution image covers an area where both ice and water can be present. We took into account that brightness for every pixel is proportional to ice concentration. Initially the mean brightness for ice-free areas and for areas with 100 % ice cover were determined. Then ice concentration for every pixel was determined by means of linear interpolation between these values. Finally average concentrations for some delineated area were calculated.

Initially we evaluated the brightness stability in test areas for open water and 100 % ice cover. Mean brightness for test areas of open water and 100 % sea ice were found stable and the variability of their values did not exceed 5 %. A larger variability is referred to cloud covered pixels. To compare the levels of the test areas on different images we have to consider the variability of the sun zenith angle. Ice concentration was determined from a series of NOAA AVHRR images (12, 16, 17, and 19 August and 3, 14, and 16 September). Results of ice concentration calculation have been compared with estimates from visual observations by eye. The preliminary analysis showed, that linear interpolation gives a reduced value for ice concentration as compared with visual observations. SLAR surveillance for September 14 covers the areas near the East coast of Severnaya Zemlya, which are cloud free on a NOAA image for September 16. So comparison of ice concentration values for both images can be done. But in spite of their high resolution, it is not always

easy to determine ice concentration from SLAR images. One should determine the threshold between ice and open water, transform an image into a binary one and then calculate ice concentration in delineated areas. Procedures in future efforts of comparison between SLAR and line-scan camera data will be of interest.

#### 4.3 Line-scan Camera Observations (Thomas Martin)

The line-scan camera is a remote sensing instrument which compounds two sensors, one to measure the reflected sun light in the visible spectral range and one to recognize the emitted thermal radiation in the infrared range. Each sensor analyses the signal with 512 picture elements (pixels). The camera is mounted perpendicular to the flight direction on a helicopter. It receives digital images of the sea ice and ocean surface along the flight track. Flying at an altitude of 3000-4000 ft provides a ground resolution of approximately 4 m by 4 m in a swath width of 2600 m. Table 4.3-1 gives an overview of all 20 flight missions.

No.	Date	Start Location		Comments
1	12-08	81° 09'N	30° 02'E	melting summer ice, inside of ERS-1 frame
2	12-08	81° 06'N	29° 29'E	melting summer ice, inside of ERS-1 frame
3	14-08	81° 43'N	30° 20'E	melting summer ice, inside of ERS-1 frame
4	14-08	82° 00'N	30° 00'E	melting summer ice, inside of ERS-1 frame
5	20-08	82° 08'N	40° 28'E	melting summer ice, inside of ERS-1 frame
6	21-08	82° 30'N	42° 00'E	melting summer ice, inside of ERS-1 frame
7	21-08	82° 15'N	40° 00'E	melting summer ice, inside of ERS-1 frame
8	29-08	77° 41'N	107° 02'E	icebergs, ice belt around the islands in front of Bolshevik Island, partly inside of ERS-1 frame
9	30-08	77° 04'N	113° 52'E	fast ice belt in front of Taymyr Peninsula, strong shear zones in the pack ice
10	05-09	78° 10'N	133° 22'E	profile from open water into the ice, inside of ERS-1 frame
11	06-09	78° 12'N	132° 00'E	profile from open water into the ice for intercomparison with AVHRR
12	07-09	77° 02'N	126° 25'E	profile from open water into the ice, inside of ERS-1 frame
13	08-09	77° 51'N	125° 26'E	profile from open water into the ice
14	09-09	77° 08'N	126° 42'E	profile along the ice edge
15	10-09	77° 34'N	126° 52'E	large ice floe, intercomparison with AVHRR and INTAARI
16	15-09	78° 50'N	119° 30'E	intercomparison with INTAARI
17	16-09	77° 53'N	118° 34'E	intercomparison with INTAARI and AVHRR
18	16-09	77° 57'N	118° 51'E	intercomparison with INTAARI and AVHRR
19	19-09	77° 35'N	114° 50'E	profile to the ice edge, increasing portion of nilas and new ice along the flight track
20	20.9	78°16'N	107° 42'E	icebergs, ice belt around the islands in front of Bolshevik Island, inside of ERS-1 frame

**Table 4.3-1:** List of the line-scan flight missions.

The location of the patterns for the first seven flight missions were chosen to correspond with the coverage of the ERS-1 passes. As mentioned in Chapter 4.1, the backscattering characteristics of melting sea ice is still not fully understood. One important factor is the melt puddle portion on the sea ice. High resolution data in different spectral ranges should give additional information.

Flights no. 8 and 20 were located to the east of the Severnaya Zemlya covering the same area with a four week interval. These missions include the *in situ* observations of several iceberg location and sea ice distribution near the small islands east of Bolshevik Island. Both observations should be used to verify the signature of icebergs and fast ice in the ERS-1 images. The measurements of flight no. 9 are located over the fast ice in front of the Taymyr Peninsula. This ice belt was very stable and could be also studied in the AVHRR data during the period of August and September.

The flight missions no. 10-19 give further information to verify AVHRR sea-ice algorithms and provide ground truth for the interpretation of the INTARRI and ERS-1 data.

#### 4.4 Microwave Emissivity of Sea Ice (Alexander N. Darovskikh and Vladimir P. Bogdanov)

##### *Scope*

During ARC-IX/4 cruise passive microwave and infrared emission from sea ice and open water were measured using a 37 GHz dual polarized radiometer and a precision radiation thermometer (PRT-5). The purposes of this investigation were: (i) to continue the study of the processes in the snow cover and ice which determine the microwave emission from sea ice; (ii) to measure emissivities of ice as a functions of incidence angle and polarization, and (iii) to measure emissivities of melt and frozen puddles.

During this cruise we had a unique opportunity to make microwave observations during late summer conditions (air temperatures were positive or zero) and during early autumn (air temperatures were below zero).

##### *Experiments and Methodology*

A microwave radiometer and radiation thermometer were mounted on the port side of the ship, 16.1 m above sea level for measuring emission from open water or thin ice. The angle of incidence could be changed from about 20-25 to 180° by mechanically rotating the radiometer and thermometer. The circular antenna could be rotated together with the microwave radiometer over the range of 180° about its axis in order to find exactly the polarization planes. After this, both horizontal (TBH) and vertical (TBV) brightness temperatures were measured.

The same equipment could also be used directly on the ice while on a station. In this case, it was mounted on a sled, 2.5 m above ice surface, where incidence angle could be changed from 0° (nadir) to 65° by mechanically rotating the radiometer. The construction of the sled permitted changing the angle of incidence while the antenna of the radiometer continues to point at the stationary object.

Figure 4.4-1 shows typical results from the rotation of the radiometer around the antenna axis (incidence angle was 45°). The angle where brightness temperature reaches its maximum value defines the vertical polarization plane, and the horizon-

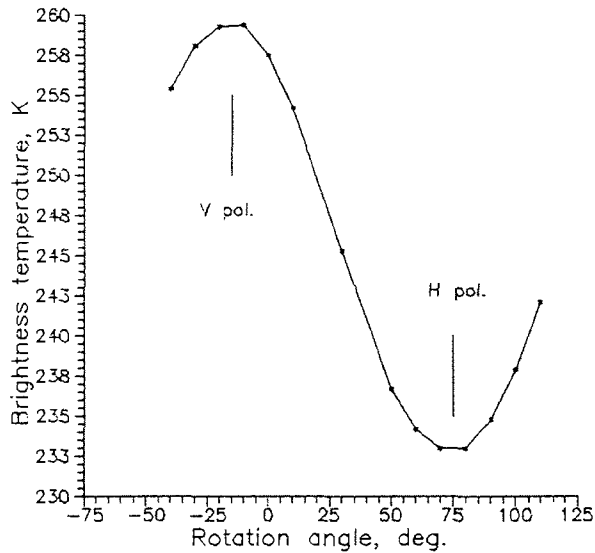


**Fig. 4.4-1:** Brightness temperature as a function of rotation of the radiometer around the antenna axis for the incidence angle 45°. Frozen puddle, ice station on 12 August 1993.

tal polarization plane lies where the brightness temperature reaches its minimum value. The calibration of the microwave radiometer was controlled using the sky as a cold load and a special absorbing material as a hot load. The emissivity of the hot load was approximately 1.

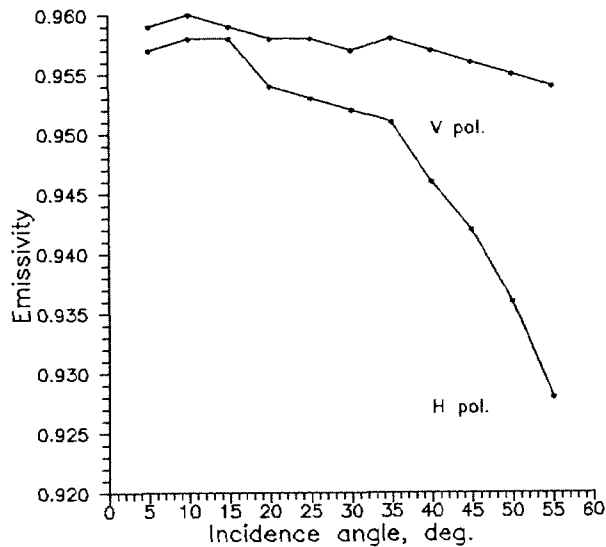
#### Measurements

The microwave measurements can be divided into two groups. The first group includes measurements made from 12 August to 21 August 1993. During this period, air temperatures were above zero. We had summer conditions when brightness temperatures of multi year (MY) and first year (FY) ice are practically equal and the polarization ratios, defined as:

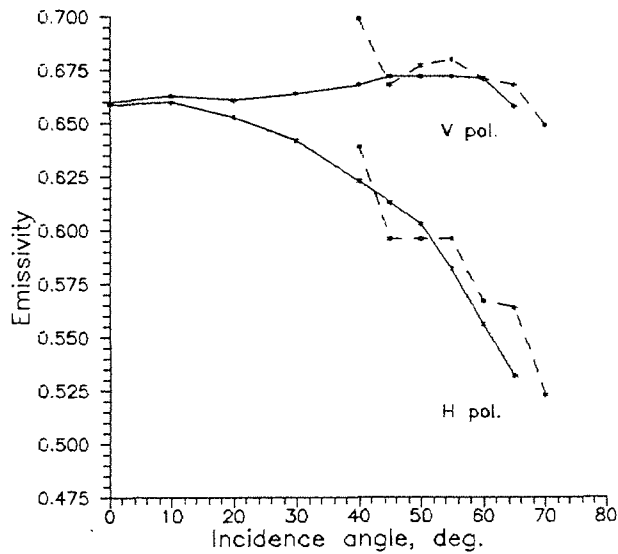
$$PR = (TBV - TBH) / (TBV + TBH) \quad \text{have minimum values.}$$

Figure 4.4-2 shows the dependence of emissivity of MY ice on the angle of incidence. This data were recorded on 18 August (ice station on Julian day 230, air temperature 0.2° C). Emissivity was very high and polarization ratios were less than 0.014. During this period there were many melt puddles on the ice. The emissivities of fresh water under these conditions were estimated as 0.72 and 0.34 for vertical and horizontal polarization, respectively. The polarization ratio is 0.35 for incidence angle 55°.

The second group includes measurements made in the Laptev Sea from 3 September 1993 to 21 September 1993. During this period air temperatures were below



**Fig. 4.4-2:** Emissivity as a function of incidence angle for multi year (MY) ice. Ice station on 18 August 1993)



**Fig. 4.4-3:** Emissivity of multi year ice as compared to RAMSEIER et al. (1991); solid lines - for ice station on 12 August 1993, dashed lines from RAMSEIER (1991).

zero and reached  $-12^{\circ}$  C. The emissivity of MY ice increased to values typical for spring. Figure 4.4-3 demonstrates these relations. Solid lines are data recorded during this expedition and dashed lines are the emissivity recorded in May 1989 by R.O. Ramseier (1991).

As puddles become frozen, their emissivity increased to very high values (Fig. 4.4-4). With increasing ice thickness the emissivity decreases (Figure 4.4-5).

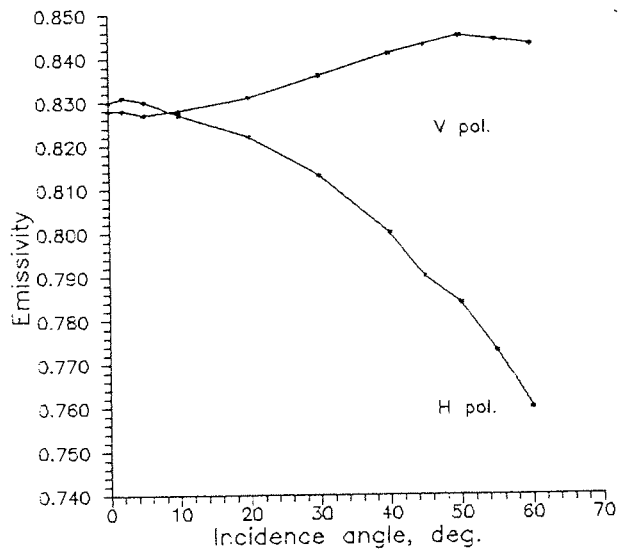


**Fig. 4.4-4:** Emissivity as a function of incidence angle for frozen puddle. Ice station on 12 August 1993.

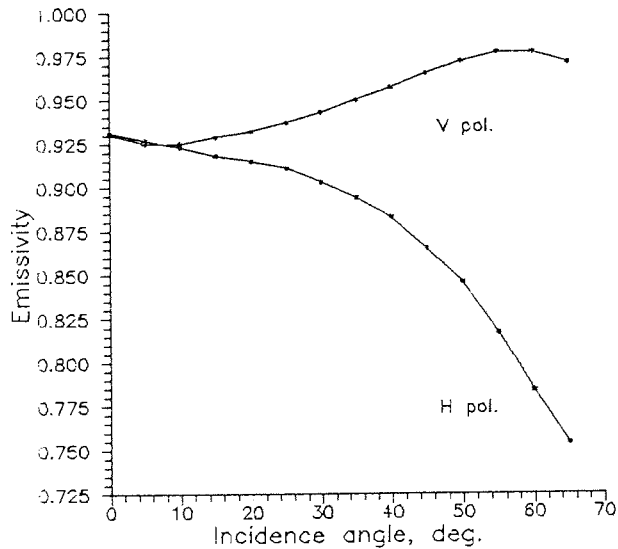


**Fig. 4.4-5:** Emissivity as a function of incidence angle for frozen puddle. Ice station on 12 September 1993.

*Preliminary conclusions*

The measurements made during cruise ARK-IX/4, both from the ship and directly on the ice, can be considered highly successful. Our measurements demonstrate the important influence of puddles in determining the emissivity of multi year ice floes.

## 5 OCEANOGRAPHIC STUDIES

The renewal and stratification of central Arctic Ocean water masses is controlled to a large extent by processes on the shelves. In summer, large amounts of fresh water are discharged by rivers and the ice free water surface allows for heat exchange with the atmosphere. In winter, the areas serve as source regions for ice and dense, brine-enriched waters. The roles of the individual shelf areas depend on the amount of fresh water supply, of input of heat and salt by Atlantic Water, the ice formation rate, the upper ocean currents and the depths of the shelves. ARK-IX/4 cruise had addressed shelf, shelf break and slope conditions of the Barents and Laptev seas. The Barents Sea has a direct inflow of warm saline Atlantic Water, a low river water input and is the deepest among the Eurasian shelf seas, whereas the Laptev Sea is shallower than 100 m in most parts and has a relatively large fresh-water contribution from the Lena River.

Water modified on the wide shelf areas interacts with the waters of the deep basins, which flow as a weak boundary current along the continental slopes.

The oceanographic work during this cruise focussed on the specific roles of the different Eurasian shelf seas in forming surface and subsurface water masses and on quantifying their relative contributions. Furthermore, it was aimed at better understanding shelf-slope exchange mechanisms, the mixing processes involved, and the influence of ventilated water masses on the thermohaline circulation. A special point of interest was the input of dense Shelf Brine Water (SBW), formed in winter by brine release during sea ice production and subsequent mixing with ambient shelf water, to the deep basins. If the production of SBW is high enough, it overflows the shelves and flows along the bottom to the shelf edge, sinks along the continental slope into the central basins, then settles at levels that are determined by their relative densities.

### 5.1 Physical and Chemical Parameters of the Water Column

#### *Methods*

Data for water mass identification were obtained using a Neil Brown Mark III CTD in combination with a General Oceanics rosette water sampler with 24 Niskin bottles of 12.5 litres volume. From the water samples, subsamples have been taken for the determination of various chemical and biological substances which are described below.

CTD salinity measurements were calibrated by measuring the salinity of water samples from the rosette with a Guildline Autosol 8400 B. In shallow water and in the strongly stratified upper ocean, the comparison between salinity of the water samples and the *in situ* CTD measurements of salinity was severely degraded by the strong gradients in temperature and salinity. Therefore only deep water measurements were used for the salinity calibration. The temperature and pressure probes of the CTD are calibrated before and after the cruise.

95 casts were run during 65 stations along all transects and at the mooring positions.

5.1.1 First Results of the CTD-measurements (Ursula Schauer, Bert Rudels, Robin Muench, Leonid Timokhov, Hannelore Witte and Gerrit Lohmann)

The westernmost transect represented conditions close to the inflow of waters entering the Arctic Ocean from the Greenland/Norwegian Sea through Fram Strait. The core of warm, saline Atlantic Water was concentrated within 40 km off the shelf break. Its maximum temperature was more than 3° C at 200 m which was high compared to previous years. The Atlantic Water was subducted below low salinity Arctic surface water from which it was separated by a sharp pycnocline. In the deep water, temperature decreased continuously to -0.93° C at the bottom of the abyss, while salinity showed a deep minimum centered at about 1200 m.

Intrusions of cold, low salinity water were found along the shelf break on all transects (Fig. 5.1.1-1). Most were adjacent to the slope in a depth range between 200-700 m. However, there were also smaller, detached patches found off the slope. These intru-

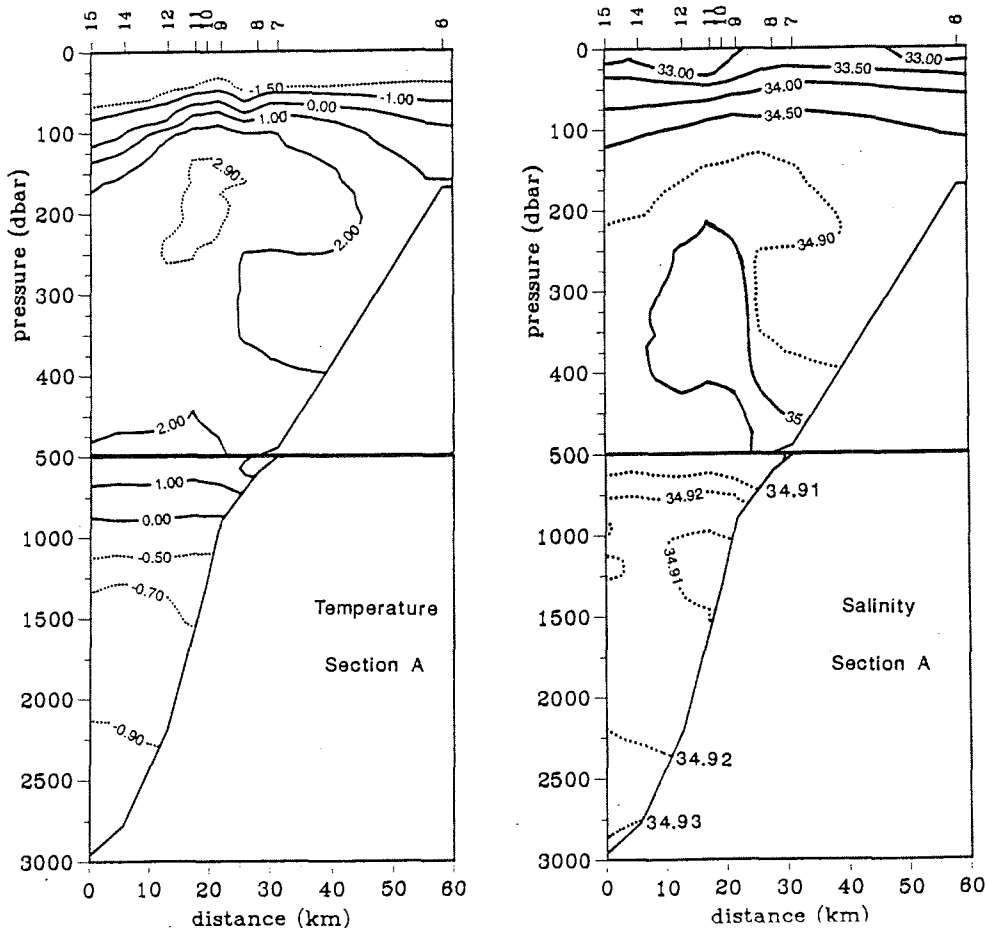
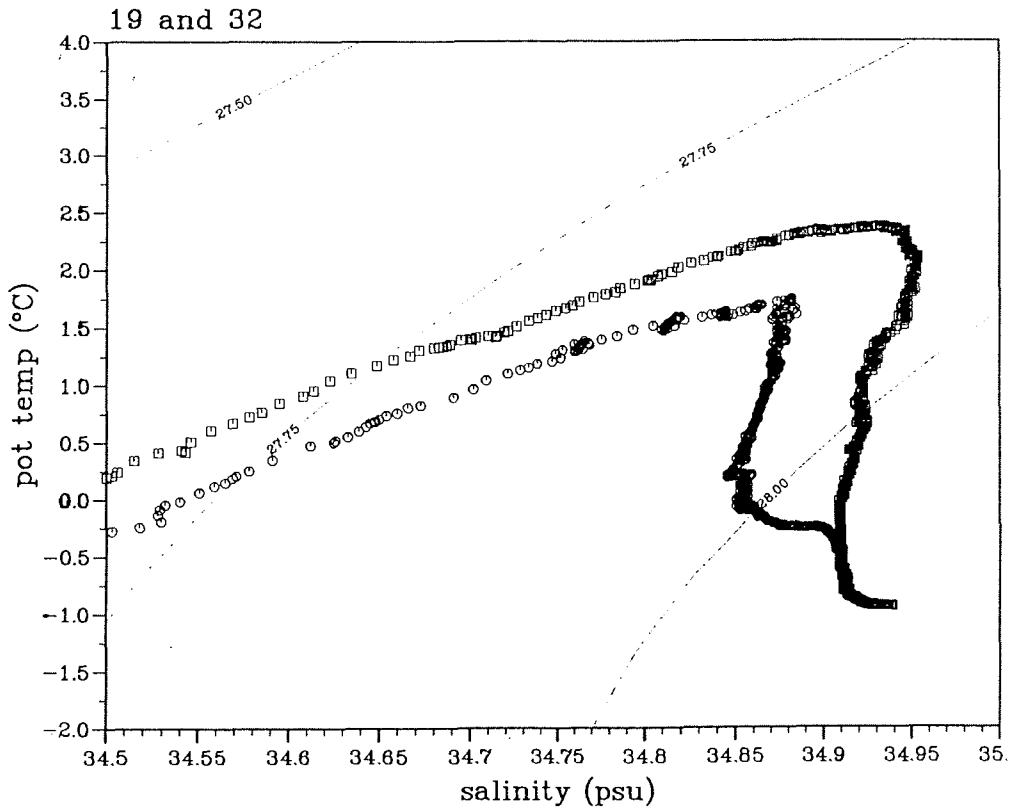


Fig. 5.1.1-1: Temperature (a) and salinity (b) distribution across the continental slope northeast of Svalbard (Transect A).



**Fig. 5.1.1-2:** Potential temperature vs. salinity at Station 19 (squares) northwest of Franz Josef Land and at Station 32 (circles) in the Laptev Sea.

sions appeared to contribute to dilution of the core properties of the Atlantic Water: The core temperature of 3° C in Transect A was already reduced to 2.6° C at Transect C.

Besides these mesoscale intrusions, the transects in the Laptev Sea show that the Atlantic slope water has been replaced by a large volume of colder, less saline water (Fig. 5.1.1-2) extending over a width of hundreds of kilometers. The new water mass extended vertically down to a depth of 1300 m. The intrusion of this water mass depressed the isopycnals and resulted in a zonal density decrease at intermediate levels between Fram Strait and the Laptev Sea.

The upper part of the water column, above the thermocline, was north of Franz Josef Land characterized by water temperatures close to freezing. A 30 m deep low salinity surface layer indicated seasonal ice melt and the winter convection appeared to reach down to 80 m. The salinity was about 33.5 psu at the surface and 34.2 psu on top of the thermocline. Further to the east, the salinity was considerably lower, about 32.5 psu in the surface mixed layer and the layers below showed more stratification (Fig. 5.1.1-3). This suggests an increased importance of advection as compared to local convection and homogenization.

PROFIL ctd 018 ARK XI/4  
82 33.90N 39 21.30E

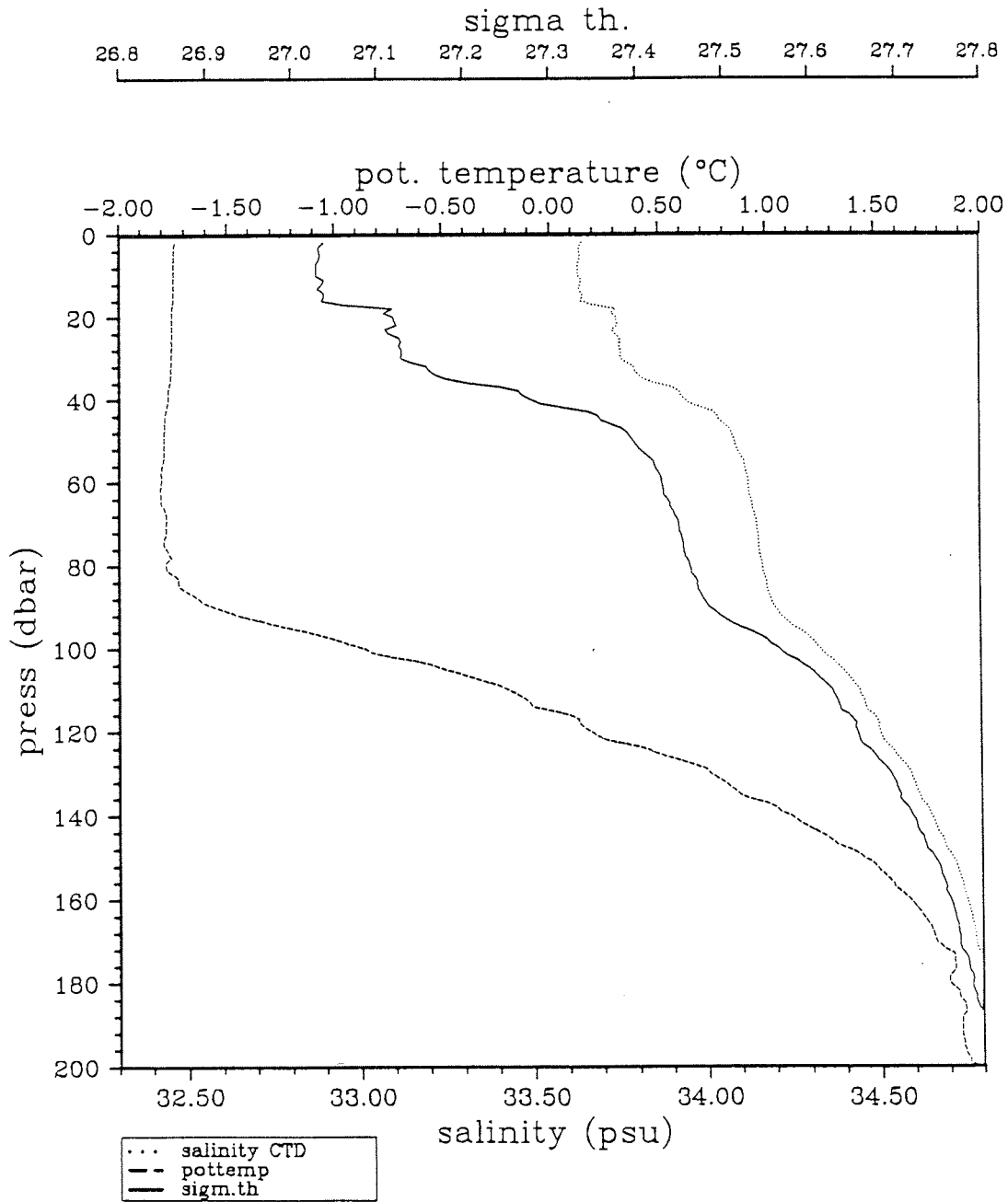


Fig. 5.1.1-3a: Profiles of temperature (dashed), salinity (dotted) and density (solid line) at (a) Station 018 northwest of Franz Josef Land.

PROFIL ctd 035 ARK XI/4  
78 22.70N 133 2.90E

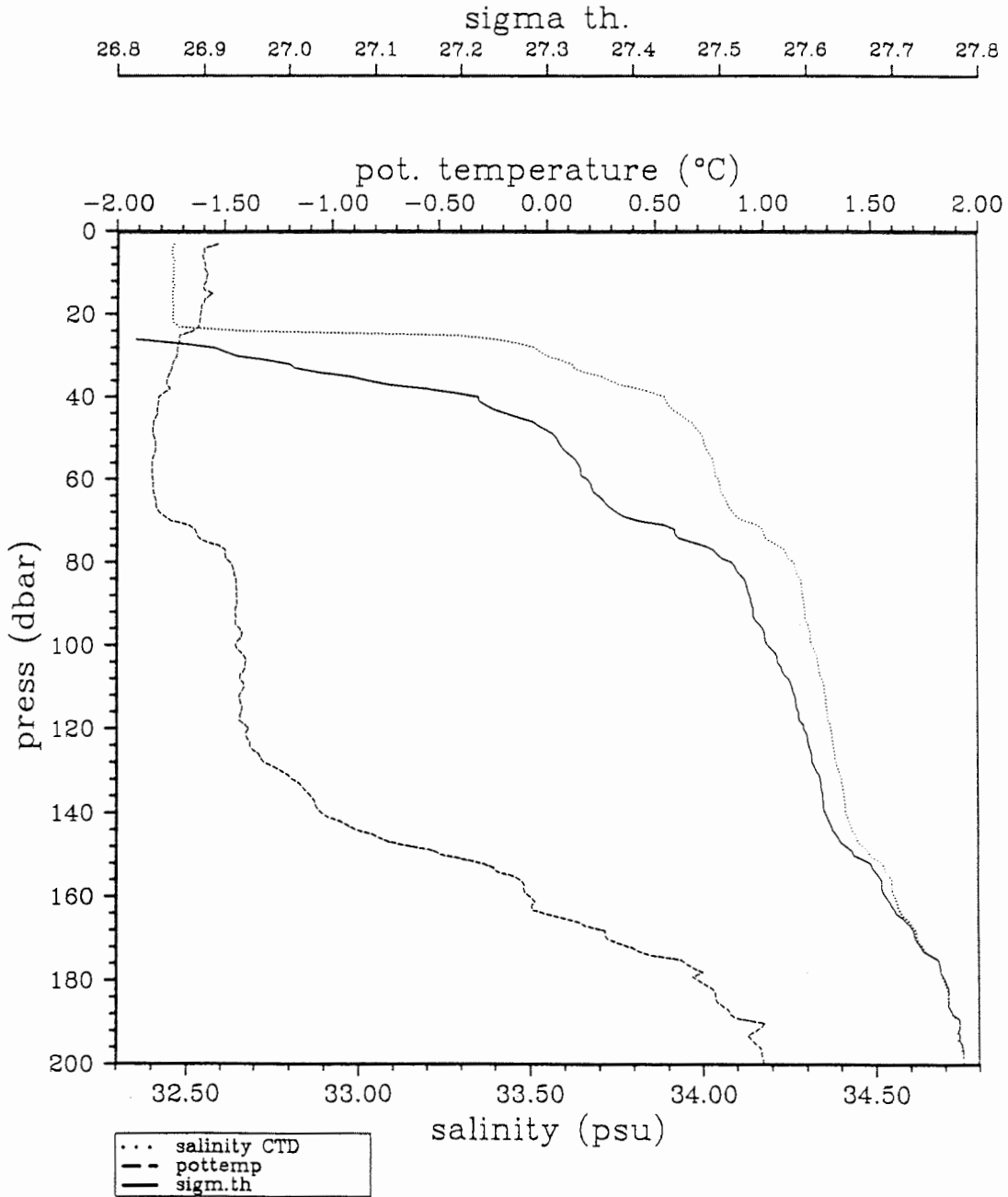


Fig. 5.1.1-3b: Profiles of temperature (dashed), salinity (dotted) and density (solid line) at Station 035 in the eastern Laptev Sea.

The Vilkitski Strait was sampled at two occasions, when entering and when leaving the Laptev Sea. At both times, a section of three stations across the strait was taken. The water column was in all stations well stratified in salinity with  $S < 29$  psu at the surface and  $S > 34.6$  psu at the deepest station. The strongest gradient was found between 30-50 m. The temperature in the upper parts was at the last occasion below  $-1.5^{\circ}\text{C}$ , about  $1^{\circ}\text{C}$  lower than before. The temperature in the deeper, saline part was around  $-1^{\circ}\text{C}$  and almost constant with depth. Close to the bottom, a temperature increase was observed and the bottom water had similar characteristics as those found in the upper part of the Arctic Ocean thermocline.

### 5.1.2 Tracer Measurements

Anthropogenic and natural tracer distributions provide essential information on the circulation, mixing and residence times of water masses in the Arctic ocean. Transient tracers as tritium,  $^3\text{He}$ , CFC's,  $\text{CCl}_4$ ,  $^{14}\text{C}$  and  $^{85}\text{Kr}$  give time informations and are used to investigate renewal times of specific water masses. Stable tracers as  $^{18}\text{O}$  are helpful in determining the mixing ratios between water masses.

#### 5.1.2.1 Sampling for Tritium, Helium, $^{14}\text{C}$ , $^{18}\text{O}$ and $^{85}\text{Kr}$ Analyses (Markus Frank and Guy Mathieu)

Anthropogenic tritium was mainly released to the atmosphere by the nuclear weapon testing during the 1950's and 1960's. In the troposphere, tritium is incorporated in the water molecule and takes part in the natural water cycle. Through water vapor exchange and precipitation it enters the ocean surface waters. Due to its radioactive decay ( $T_{1/2} = 12.43$  y), it can together with its daughter product  $^3\text{He}$  be used for the dating of water masses. At the ocean surface, the helium isotopic ratio is in equilibrium with the atmosphere. Once the water parcel leaves the surface, tritium decay leads to enrichment of  $^3\text{He}$  relative to  $^4\text{He}$ . The combined measurements of tritium and helium allow the calculation of a formal tritium/ $^3\text{He}$ -age. When no mixing occurs, the formal age is identical to the time since the water parcel has left the surface.

$^{14}\text{C}$  is a radioactive isotope of carbon and provides time information due to its radioactive decay ( $T_{1/2} = 5730$  y). Atmospheric nuclear weapon testing increased the total amount of  $^{14}\text{C}$  in the atmosphere by about 90 %.

$^{18}\text{O}$  is a stable isotope of oxygen and is as tritium incorporated in the water molecule. These water molecules are heavier compared to the water molecules containing the more common  $^{16}\text{O}$  and take part in the natural water cycle. The different physical properties cause the water to be enriched or depleted in  $^{18}\text{O}$  each time it undergoes a phase change. Continental rain is depleted in  $^{18}\text{O}$  and river runoff is marked by low  $^{18}\text{O}/^{16}\text{O}$  ratios.

$^{85}\text{Kr}$  is a radioactive inert gas with a half-life of 10.8 years. It forms when uranium and plutonium undergo fission. The sources of  $^{85}\text{Kr}$  to the atmosphere are nuclear weapons testing and nuclear reactors. The specific activity of this radionuclide in the atmosphere, which has been steadily increasing, is well known. Coupled with its

inertness, this makes it an ideal tracer of water masses as they become isolated from the surface.

### *Analytical Methods*

During ARK-IX/4 cruise about 520 samples were collected for tritium, helium and  $^{18}\text{O}$  analyses. About 200 of these samples were collected in the Barents Sea at the Transects A and C. Another 300 samples were collected at the four Transects E, F, G and H in the Laptev Sea. About 20 samples were taken at three CTD-stations in the Vilkitski Strait. The tritium and  $^{18}\text{O}$  samples were stored in 1 litre glass bottles. The samples for helium analyses were stored in copper tubes that were closed at both ends with stainless steel clamps while flowing sample water through.

Further processing and measurement of the samples will be done in Heidelberg at the Institut für Umweltphysik. Prior to the measurement, the helium samples are degassed in a special vacuum extraction system. The helium gas is transferred to a mass spectrometer where the sample is analysed for the  $^4\text{He}$  concentration and  $^3\text{He}/^4\text{He}$  ratio. The precision for the  $^3\text{He}/^4\text{He}$  measurement is about  $\pm 0.2\%$ .

Tritium analyses will be done using the  $^3\text{He}$  ingrowth method. The water sample is degassed and stored in a sealed glass bulb. During the storage time (usually six months),  $^3\text{He}$  will accumulate from tritium decay. The measurement of this small gas amount is performed on the same mass spectrometer used for the helium analyses. Precision of the measurement is about  $\pm 2\%$ .

For the  $^{18}\text{O}$  analyses an aliquot of water is set in isotopic equilibrium with  $\text{CO}_2$ . Thereafter the  $^{18}\text{O}/^{16}\text{O}$  ratio in the  $\text{CO}_2$  is determined by mass spectrometry.

About 30 samples for  $^{14}\text{C}$  analyses were collected on the shelf slope and deep basin north of the Laptev Sea. For each sample one litre of water was transferred from the Niskin bottle into an evacuated glass bulb. In Heidelberg the total inorganic carbon will be converted to carbon dioxide which is then extracted quantitatively from the sample. After reduction, the carbon will be pressed inside a target which can be analyzed for its carbon isotopic ratio via an accelerator mass spectrometer (in cooperation with ETH Zürich, Switzerland).

For  $^{85}\text{Kr}$  analyses all dissolved gases were extracted out of 58 litres of sea water by vacuum degassing. The gases were then stored in pre-evacuated steel tanks. Typically approximately one litre of gases were extracted per sample. Six Niskin bottles would be tripped at the sampling depth and the water transferred into three pre-evacuated 20 liter flint glass bottles.

In the Barents Sea, 11 depths were sampled from surface to bottom over three stations of Transect C. In the Laptev Sea, 12 depths were sampled over three stations of Transect H and three depths at one station of Transect F. In addition, two surface under-way samples were taken, one in the Barents Sea and one in the Laptev Sea, east of the Vilkitski Strait.

#### 5.1.2.2 Chlorofluorocarbons and Carbon Tetrachloride (Guy Mathieu and Markus Frank)

During ARK-IX/4, three different chlorofluorocarbons (CFC's) were measured. They were  $\text{CCl}_3\text{F}$  (F-11),  $\text{CCl}_2\text{F}_2$  (F-12) and  $\text{C}_2\text{Cl}_3\text{F}_3$  (F-113). In addition, 175 water samples were collected in the Laptev Sea for  $\text{CCl}_4$  (carbon tetrachloride). These later samples will be analyzed back at Lamont-Doherty Earth Observatory, they are stored in sealed glass ampules of 60  $\text{cm}^3$  volume each.

CFC's are man-made compounds that are used as refrigerants and in many manufacturing processes (degreasing, etc.). Their concentrations in the atmosphere has been increasing steadily since their introduction in the 1930's.

CFC samples were drawn from the 12 litre Niskin bottles into 100  $\text{cm}^3$  glass syringes with metal caps. For  $\text{CCl}_4$ , the volume of the syringes was 200  $\text{cm}^3$ . The CFC's analysis system consists of a gas stripping system coupled to a gas chromatograph with an electron capture detector. A 35  $\text{cm}^3$  aliquot is drawn into a constant volume sample loop from the 100  $\text{cm}^3$  syringe. The water is then stripped with pure nitrogen and the CFC's removed are trapped on a unibead 2 s trap kept at  $-65^\circ\text{C}$ . The unibead trap is then heated to  $100^\circ\text{C}$  and the contents flushed into the gas chromatograph where the CFC's are separated from other electro-negative compounds and into F-12, F-11 and F-113. The three types of column used are a porasil b precolumn, a mole sieve 5 Å column and an analytical column made of SP2100. Approximately four analyses can be run per hour. The detector is calibrated by injecting known volumes of a standard gas mixture into the trap and transferring the mixture into the gas chromatograph.

#### *Precision of the method as applied here*

For F-12 greater than 1  $\text{pM/kg}$  (picomoles per kilo of sea water) and F-11 greater than 2  $\text{pM/kg}$ , 0.6 %  $\pm 0.5$  based on 37 duplicate analyses. For smaller amounts, the standard deviation for F-12 is 0.01  $\text{pM/kg} \pm 0.01$  and for F-11, 0.02  $\text{pM/kg} \pm 0.04$  based on seven duplicates ranging in F-12 concentration from 0.07-0.7  $\text{pM/kg}$  and in F-11 concentration from 0.1-1.5  $\text{pM/kg}$ .

In the Barents Sea, 16 stations were sampled for CFC's and in the Laptev Sea, 37. We also measured the CFC's concentration at six stations in the Vilkitski Strait. The total number of water samples analysed is approximately 870. Marine air was analysed on six different occasions.

#### *Description of preliminary CFC's results*

The following descriptions are based on very preliminary data:

- In the deep water the concentration of F-12 decreased from west to east. Whereas at the Barents Sea sections F-12 concentrations between 0.05  $\text{pM/kg}$  and 0.1  $\text{pM/kg}$  were encountered in 3000 m water depth, in the Laptev Sea, along all sections, the concentration was below 0.05  $\text{pM/kg}$  at water depth greater than 2700 m.
- Higher surface values were found in the Laptev Sea than in the Barents Sea. The

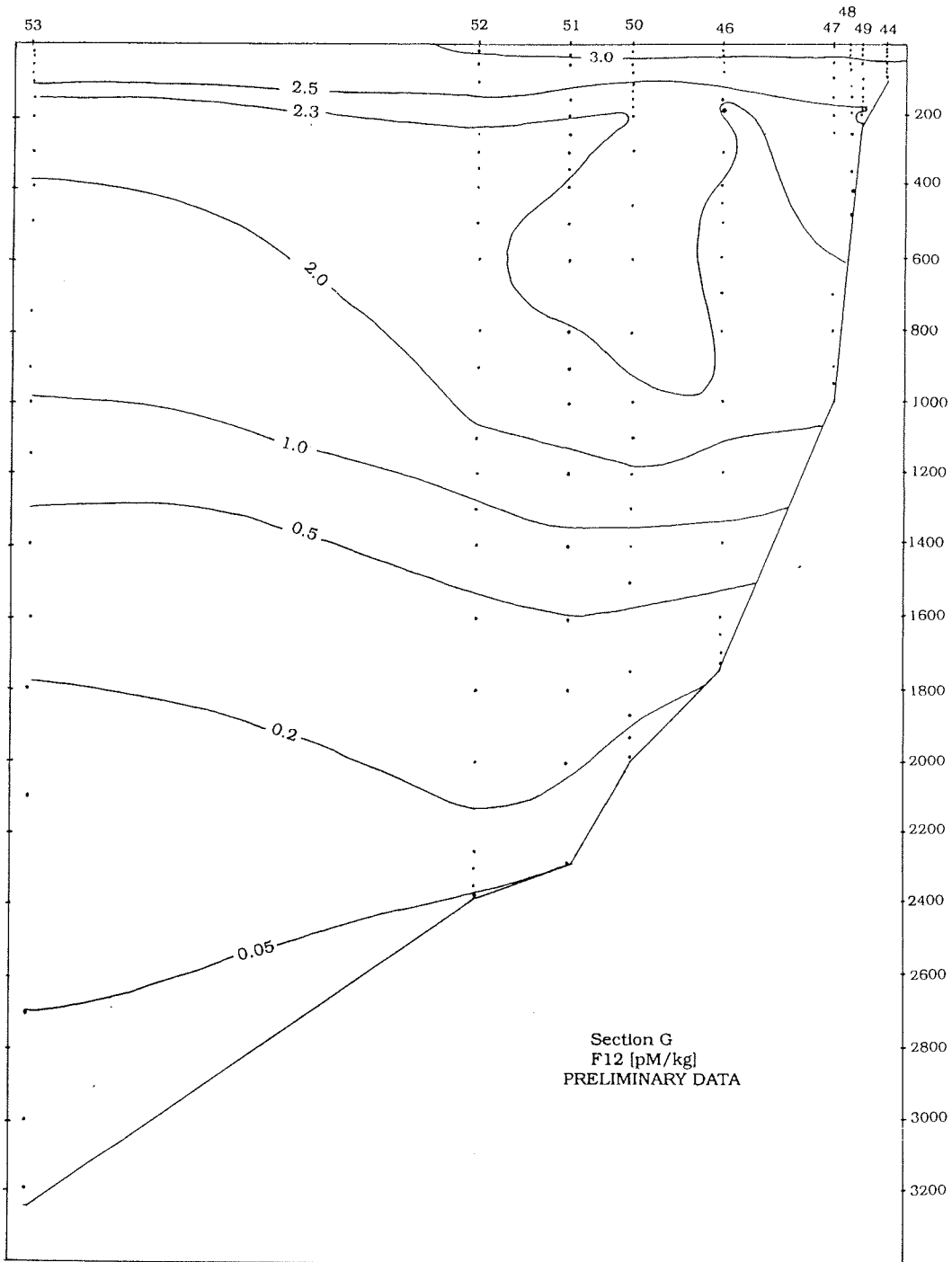


Fig. 5.1.2.2.-1: F-12 (pM/kg) concentration across the continental slope of the northern Laptev Sea at Transect G (preliminary data).

higher concentrations were always found towards the southern end of each transect.

- Higher CFC values were found in the cold, low salinity intrusions seen along the shelf break.
- In the core of warm saline Atlantic Water found at the Barents Sea continental slope, F-12 concentrations ranged from 2.5 pM/kg to 2.3 pM/kg. Below approximately 400 m water depth, a steep decrease was encountered. In the colder and less saline Atlantic waters found near or on the slope of the Laptev Sea (Fig. 5.1.1-3), Freon concentrations above 2.3 pM/kg extended down to about 800-1000 m (Fig. 5.1.2.2-1).

#### 5.1.2.3 Other Tracerwork (Robin Muench, Erk Reimnitz and Ursula Schauer))

In addition to the originally planned tracer work, samples for other tracers were collected on a ship-of-opportunity basis.

##### *Water Sampling for Barium Analyses (Robin Muench for Kelly Falkner)*

More than 1,000 water samples were obtained to be analyzed for Barium content. These samples were obtained at all depths at CTD-rosette stations numbered 10 through 71. They were obtained at the request of, and were provided to, Dr. Kelly Kenison Falkner, Oregon State University, USA, who is carrying out the analyses.

Results of these analyses will contribute to an ongoing multi-year program to track the fate of Arctic river waters using geochemical means. The main objective of this program is to track river waters as they mix into the Arctic through the use of a suite of inorganic minor element tracers which can be readily and precisely determined on small volume samples. It is intended that this multi-tracer approach, which is made possible by recent advances in analytical technology, will complement the nutrient, major and trace element solution and solid phase studies being carried out by other investigators. It is also hoped that our results will improve our understanding of general circulation in the Arctic. Further, these results will provide information relevant to studies of river-borne sediments and pore water fluxes.

This overall program is being conducted in three phases. One phase involves laboratory experiments to test the effects of freezing on the behaviour of a variety of a number of minor and trace elements including Rb, Cs, Ba, Sr, Li, B, F, Br, J, Cd and isotopes of Sr and Li. A second phase is a seasonal study of the relatively accessible MacKenzie River estuary in order to characterize the effects of various natural processes on tracers. Samples are also being obtained from Russian rivers. Finally, sampling is being conducted throughout the Arctic Basin from ships-of-opportunity in order to map the broad-scale distributions of the proposed tracers. Used in combination with other parameters such as temperature, salinity, O<sub>2</sub>, nutrients, etc., the measured distributions will contribute to the effort to deconvolute the effects of riverine input, sea ice formation and ventilation by laterally injected brines.

This cruise has provided a major contribution to the ship-of-opportunity data collection program. It has provided data from an otherwise difficult to access region which is heavily impacted by riverine input.

*Water and Sediment Sampling for additional Radionuclide Analyses (Robin Muench for Lee Cooper)*

24 water samples were collected to be analyzed for  $^{129}\text{J}$  and  $^{99}\text{Tc}$  content. These samples included Laptev Sea shelf water and Arctic Ocean Surface, Atlantic, Deep and Bottom waters. The samples were obtained at the request of, and were provided to, Dr. Lee W. Cooper, Oak Ridge National Laboratory, USA who is carrying out the analyses. In addition to the water samples, 15 bottom sediment samples were obtained from the Laptev Sea shelf, slope and deep basin. These sediment samples will be analyzed by Dr. Cooper for Pu isotopes, Am, Cm,  $^{237}\text{Np}$  and gamma emitters such as  $^{137}\text{Cs}$ .

Results from these radionuclide analyses will be used to address the following specific questions:

- Are the inventories of Pu, Am/Cm and long-lived fission/activation product radionuclides in Arctic sediments consistent with those predicted to occur from accumulated global fallout at these latitudes, or are additional sources suspected?
- Does the isotopic composition of Pu in sediments and biota in the Arctic exhibit isotopic ratios characteristic of integrated global fallout, or do they indicate additional, regional sources of Pu and, if so, can these sources be identified?
- Are atom concentrations of  $^{237}\text{Np}$  in Arctic sediments and biota consistent with a global fallout origin?
- Do Arctic sediments and/or biota show evidence of recent releases of short-lived fission/activation product radionuclides?
- Are atom concentrations of  $^{129}\text{J}$  and  $^{99}\text{Tc}$  in Arctic waters and biota explainable on the basis of their releases from above-ground testing of nuclear devices and fuel reprocessing activities, or do they suggest additional, local sources?
- Over what distances can  $^{129}\text{J}$  atom concentrations be used to characterize water provenance and mixing processes in the Arctic Ocean?

*Methane from sea water (Erk Reimnitz for Keith Kvenholden)*

At each of six oceanographic stations, ranging from the shallowest to the deepest occupied in the Laptev Sea, five water samples were taken for the analysis of methane by Keith Kvenholden, U.S.G.S. in California. The release of methane from sediments at the base of permafrost, where it may be stored in form of gas hydrates, is thought to occur throughout the year. But during winter, the gas exchange between ocean and the atmosphere is reduced by the ice cover. The samples collected here may help to explain the variations in Arctic atmospheric methane concentrations from high levels at summer's end to low levels in winter.

*Trace metals (Ursula Schauer for Chris Measures)*

The goal of this trace element program was to determine to what extent trace elements may be enriched within dense Shelf Brine Water formed as a result of sea ice formation. Evidence from Al distributions in the Fram Strait indicate that dissolved Al concentrations may be considerably enriched in this water and that the excess Al seen in the Greenland and Norwegian seas may have an origin in this process. In

addition there are indications that during the brine production process trace elements may become fractionated.

A total of 114 samples was taken during this cruise distributed over ten stations. To establish that elevated signals are really associated with the brine process two stations have been sampled as "background" information in the deep basins. The samples will be analysed for the content of Be, Al and Se.

### 5.1.3 Chemical Oceanography

#### 5.1.3.1 Nutrients and Oxygen (Anna Luchetta, Paola Poniz and Gennady Ilyin)

Studying the nutrients and dissolved oxygen concentrations in the water masses is useful to contribute either to the investigation of some aspects of the Arctic Ocean circulation, as mentioned in the introduction of the oceanographic studies (5.1), or to investigate the biological activity of phytoplankton in the surface layer of the Arctic Ocean shelves region.

Regarding the first point, it should be briefly reminded that the nitrate, silicate and phosphate content itself can be used as a tracer for identifying different water masses. Actually the nutrients concentration entering the Arctic Ocean through the Bering Strait or through the Fram Strait differ very much. Pacific derived waters tend to have much higher nutrients than the Atlantic derived waters. As a consequence marginal seas as the Barents, Kara and Laptev seas receive waters with relatively low nutrient content when compared with the East Siberian Sea and Chukchi Sea. The derived parameters NO and PO can be used as tracers for the shelf water contribution to the circulation of the Nansen Basin. They can also be used to verify the contribution of the Laptev and Kara seas to the ventilation of the lower Arctic halocline.

Regarding biological activity the correlation between nutrients, their recycling, and primary productivity is of peculiar interest in the shallow Arctic shelves region, where primary productivity has much higher rates than in the polar basins. Primary productivity in the Arctic region is very localized in time and space and it is connected to the presence of the marginal ice zone.

The phosphate, nitrate and nitrite, silicate as well as dissolved oxygen contents in these regions can be influenced by:

- ice formation and ice melting processes, the river runoff, the circulation of Arctic Surface Water and by the biological activity of phytoplankton, in the surface layer;
- spreading of Atlantic Water along the Eurasian continental slope, the eventual ventilation from cold and saline bottom shelf water, the remineralization of dissolved and settling particulate organic matter, in the deep layer, and
- the circulation of cold deep and bottom water, the interaction with sediments, in the deepest layers.

### *Methods*

About 350 samples from the Barents Sea (Transects A and C) and more than 800 samples from the Laptev Sea (Transects H, G, F and E were analyzed on board, directly after the recovery of the rosette sampler, by means of a Technicon I Auto-analyzer according to the method of GRASHOFF (1983). Precision was better than 1.2 % for nitrate and nitrite, 1.7 % for phosphate, and 1.5 % for Si.

Dissolved oxygen was determined on 50 ml aliquots of sample by means of an automatic titration, with a precision within 0,3 %, according to the Winkler method. Ammonia content was determined according to the method of CATALANO (1987).

### *Preliminary Results*

**B a r e n t s   S e a :** Two transects were run from the shallow water across the slope of the Nansen Basin. They appear different with regard to the nutrients and dissolved oxygen content in the surface layer (25 m; Si >4  $\mu\text{M}$ ,  $\text{NO}_3$  >6  $\mu\text{M}$  and  $\text{PO}_4$  >1  $\mu\text{M}$ ,  $\text{O}_2$  <335  $\mu\text{M}$  for Transect C and nutrients depleted,  $\text{O}_2$  >400  $\mu\text{M}$  for Transect A), suggesting the occurrence of biological activity in Transect A at stations 10, 11, and 12, characterized by melt water. Nutrients data are in agreement with the chlorophyll-a data. Below the surficial melt water layer both transects exhibit stratification along the whole water column down to the bottom, with increasing values for the nutrients ( $\text{NO}_3$  >14  $\mu\text{M}$ , Si >11  $\mu\text{M}$ ,  $\text{PO}_4$  >1  $\mu\text{M}$ ) and decreasing values for  $\text{O}_2$  (<290  $\mu\text{M}$ ).

**L a p t e v   S e a :** Four transects (H, G, F, E) almost completely covered by ice were sampled in this region. The two easternmost Transects H and G look like to be biologically influenced (nutrients depleted and  $\text{O}_2$  surface maximum) in the upper 20 m at the southernmost ends (Stations 38-43 and Station 44). A strong gradient occurs in the layer between 75-175 m for all the measured parameters ( $\text{NO}_3$  varied from 6-11  $\mu\text{M}$ , Si from 3-5  $\mu\text{M}$ ,  $\text{O}_2$  from 333-290  $\mu\text{M}$  in both sections) after that a weaker stratification was evident down to the bottom ( $\text{NO}_3$  >12  $\mu\text{M}$ , Si >11  $\mu\text{M}$ ,  $\text{O}_2$  <320  $\mu\text{M}$ ).

Transects E and F don't show any biological activity in the surface layer (concentration value >3  $\mu\text{M}$  for nitrate, Si >3  $\mu\text{M}$ ). The profiles were similar to those of the previous transects and do not show any other peculiar characteristics different from the strong gradient between 75-175 m (values similar to those of Transects H and G). Transects F and E show an intrusion of fresh water (silicate content >3.5  $\mu\text{M}$ ) from the shelf into the slope region, extending to the Stations 59 and 71.

#### 5.1.3.2 Total Carbonate (Kristina Olsson)

One of the main aim in chemical oceanography during ARK-IX/4 expedition has been to trace the fresh water distribution from the shelf region out towards the deeper basins in the Eurasian part of the Arctic Ocean. To distinguish the origin of the fresh water component and to investigate the input of shelf water to the subsurface water masses in the central basins were other aspects of interest.

Total carbonate measurements give means to distinguish between melt water from sea ice and river run-off as fresh water sources. As a result of biological productivity and decay on the tundra, the Siberian rivers carry inorganic and organic carbon to the Arctic Ocean. The resulting elevated total carbonate concentrations allow for the tracing of riverine input throughout the Eurasian Arctic Ocean.

Ice free conditions in the summer period enhance biological primary production on the shelf regions. This in turn induces uptake of atmospheric carbon dioxide by increasing the difference in partial pressure over the atmosphere-sea interface. Knowing the total carbonate concentrations in the source waters, mixing processes transformation of carbon within the Arctic Ocean can be described. An understanding of the present circulation paths and budgets is necessary for predicting possible responses to climatic variability.

#### *Sampling and Analysis*

About 1000 samples were obtained and analyzed during the cruise of which about 300 samples were sampled in the Barent Sea (Transects A and C), about 50 in the Vilkitski Strait and approximately 650 in the Laptev Sea (Transects H, G, F and E).

The samples for total carbonate analysis were drawn from 12.5 l Niskin bottles (General Oceanic) into 250 ml pyrex glass bottles with airtight plastic caps. Analysis was carried out on board directly after sampling using gas extraction followed by coulometric titration (JOHNSON 1985). The sea water sample is first acidified and sparged of its carbon dioxide content by an inert carrier gas (nitrogen). In the cell solution the evolved carbon dioxide reacts and forms a titratable acid which decreases the pH in the solution. Spectrophotometric detection then automatically generates a back titration to the original pH (absorbance), thus relating the amount of coulombs utilized with the amount of carbon dioxide in the sample. The precision was  $\pm 0.05-0.1$  % and the accuracy was set by analyses of carbon dioxide reference water samples (Dr. A. Dickson, SIO).

#### *Preliminary Results*

In the Barents Sea low total carbonate concentrations in the surface layer indicate the freshwater source to be sea-ice melt-water. Below this layer, the concentration increases towards the bottom. However, a small decrease is seen in the bottom layer.

The eastern transect in the Laptev Sea (Transect H) has high surface concentrations, which indicate river run-off stretching throughout the whole section. In this freshwater tongue decreasing total carbonate values in some shallow stations is believed to be related to biological activity. A similar, but much less pronounced, biological signal is seen at a few shallow stations on Transect G. In Transects F and G a front is found where the freshwater source, due to lower total carbonate concentrations, is believed to be more influenced by sea-ice melt-water. In the Vilkitski Strait elevated concentrations of total carbonate suggest that the origin of this freshwater is riverine input which is also seen in the surface layer in Transect E.

## 5.2 Acoustic Doppler Current Profiler - ADCP - Observations (Robin Muench)

Extensive use was made during this cruise of the hull-mounted Acoustic Doppler Current Profiler (ADCP). This instrument uses beams of high frequency sound to measure water currents beneath the ship down to a depth of about 350 m or to the bottom, whichever is shallower. It can sample as rapidly as one complete vertical profile each second, but the sampling intervals used during this cruise were either one or three minutes, depending on the specific information desired, to obtain maximum measurement accuracy and minimize the volume of data.

The ADCP was used in two modes during ARK-IX/4 cruise. One mode was to measure instantaneous currents along transects while the ship was underway. It is possible in this way to map out the currents over a region, although in shallow shelf regions such as the Barents and Laptev seas a good knowledge of the tidal currents is necessary in order to fully utilize the ADCP data because the tidal currents are typically sufficiently large that they dominate other shelf currents. Such transects were obtained during the ship's transit from the Bjørnøya region to the working area northeast of Svalbard, and across the Laptev Sea shelf between the oceanographic sections.

A second mode was to measure currents over periods of time at fixed locations, in particular when the ship was stopped at an oceanographic station. The resulting current time series allow identification of vertical shear in the currents, which can be important to upper layer oceanographic processes, and can allow detection of internal waves which are known to influence ocean mixing processes. Several time series were obtained which exceeded 12 hours in length.

The ADCP current measurement program had several specific goals:

- To detect the presence of, and estimate the magnitudes of, regional oceanographic current features. As an example, data obtained from the oceanographic stations in Vilkitski Strait should be adequate to estimate currents there at a site which presumably is representative of the summer shelf current system in the Laptev Sea.
- To detect mesoscale current features, i.e., those having scales of several tens of kilometers, which can be associated with bathymetric features such as banks and with shelf and slope frontal systems or with eddies. The temperature and salinity data which are collected continuously from the ship's systems while underway are essential supporting data to address this goal, since they allow detection of horizontal temperature and salinity gradients which are generally associated with such oceanographic features.
- To measure the time-averaged vertical variations in horizontal currents, or vertical shear, in the upper ocean so that these can be related to the observed temperature and salinity features and to the physical processes which control them. Shear associated with the Arctic Ocean halocline or Atlantic Water layers was of particular interest, and the warm Atlantic Water core fell, at a depth of about 300 m, well within the 350 m maximum profiling range of the ADCP. Very preliminary analyses of several of the time series data sets have revealed significant shear associated with the halocline, which was particularly well

developed in the Laptev Sea region as compared with that north of the Barents Sea.

- To detect internal waves which might be present in the upper ocean, inasmuch as these features can exert a significant influence over ocean mixing and can help to explain the observed distributions of temperature and salinity. Preliminary analyses have suggested that semidiurnal period internal waves were present in the very sharp Arctic Ocean halocline. The data also suggested that higher frequency features were present, although conclusions away rigorous treatment using spectral analysis routines.

The ADCP system was not used when the ship was making way through heavy pack ice or at relatively greater speed through medium pack. In these circumstances, bits of ice and air bubbles interfere with the acoustic signal and degrade the resulting data so that it is not useful. Experience has shown this problem to be common to all ADCP systems which have so far been used in sea ice. Given these constraints, the system performed well and provided data which should be useful when analyzed in connection with the other oceanographic data obtained during this program.

### 5.3 Moorings (Ursula Schauer)

Four moorings were deployed south of Svalbard in continuation of a program that was started in the northwestern Barents Sea in summer 1991. The aim of this program is to study the outflow of dense Shelf Brine Water during its production time in winter and the mixing of outflowing water with ambient water on its way to the deep basin. Two moorings were deployed at the southern entrance of the Storfjord (Station 3 and 4) where earlier measurements have revealed a strong outflow of Shelf Brine Water. Two other moorings were deployed downstream of the outflow at the western shelf edge of the Barents Sea (Station 2 and 3). The moorings are equipped with current meters, CTDs, thermistors chains and a sediment trap. It is planned to recover the moorings after one year during *Polarstern* cruise ARK-X/1, 1994.

In summer 1991, two moorings were deployed northeast of Svalbard on the continental slope. They were designed to measure the flow of Atlantic Water and deep water and the possible intrusion of dense shelf waters spreading as a plume along the slope. Ice conditions at the mooring sites were extremely heavy, and recovery was not possible. A further approach to recover them on another cruise has to be considered.

### 5.4 Meteorological Buoys (Ursula Schauer for Christoph Kottmeier)

In the framework of the "International Arctic Buoy Program" two meteorological buoys were deployed on ice floes in the northern Laptev Sea at 79° 53.32' N / 125° 54.0' E (Buoy No. 3312) and 78° 04.4' N / 125° 1.8' E (Buoy No. 3311). On these buoys, air temperature, pressure, wind speed and wind direction are measured. These data, as well as the position of the buoys, are transmitted to shore based receiving stations via the Argos satellite system. The buoys were deployed in a sparsely sampled region and will fill gaps in the meteorological and ice drift data coverage.

## 6 SEA-ICE STUDIES AND SAMPLING

### 6.1 Sea-ice Conditions along the Cruise Track (Hajo Eicken, Thomas Martin and Erk Reimnitz)

While the ship was travelling within the sea-ice zone, observations of ice conditions were conducted at regular (1-2 h) intervals from the ship's bridge by an observation team consisting of Vitali Alexandrov, Andrei Darovskikh, Hajo Eicken, Christine Friedrich, Rolf Gradinger, Hinrich Hanssen, Boris Ivanov, Thomas Martin, Regina Pác, Michael Poltermann, Erk Reimnitz, Leonid Timokhov and Jürgen Weissenberger. Observations recorded routinely include standard parameters such as position, meteorological conditions along with concentration and characteristics of the ice types observed, with notes on the amount and distribution of sediment inclusions and ice algae. Even though observations are somewhat subjective and only valid for a limited area, they can be of use in validating remote-sensing data obtained from airplane, helicopter and satellite, allow for a generalization of conclusions to be drawn from ice sampling and water column sampling carried out at individual stations, possibly to further our understanding of the sea-ice system in the Barents and Laptev Seas. The two sections below provide some general information on the ice conditions observed along the cruise track from generalizations of the ice observation log as well as additional observations made from the ship and during helicopter reconnaissance flights.

#### 6.1.1 Ice Conditions in the Svalbard and Franz Josef Land Area

During the morning hours of August 11 (0730 UTC), *Polarstern* entered the ice at 77°30' N / 24°42' E. Open patches and ice fields with concentrations ranging mostly below 7/10 extended along the southeastern coast of Spitsbergen, as evident from the NOAA AVHRR image shown in Figure 6.1.1-1. The closed pack-ice zone was entered on August 12 (0600 UTC) at roughly 81°03' N / 30°22' E. Until leaving the ice southwest of Franz Josef Land on August 23, the ship operated in heavy ice of more than 9/10 concentration (average ice concentration from 96 ship observations 9.3/10 ±0.5/10) with the northernmost position reached on August 19 at 82°45'N, 40°18' E. Upon entering the closed pack, level-ice thickness increased from <1.5 m to 2-3 m north of roughly 81°20' N and floe sizes ranged between few hundred meters to >1 km in size. Generally, the ice displayed the rolling topography typical of multi-year ice, where hummocks account for <10 % of the surface. Melt puddles were ubiquitous, covering between 20 and 50 % of the ice surface. Core and thickness drilling at six stations also indicated ice thicknesses mostly between 2.5-3 m. Detailed stratigraphic analysis of ice cores indicates the thicker ice to be two to three years of age (see chapter 6.3).

In the area northwest of Franz Josef Land east of 42° E, a larger fraction of presumably first-year ice with thicknesses less than 1-1.5 m was observed. In some of these floes, patches of turbid ice (evenly dispersed sediment inclusions with aggregate sizes <10 mm) were found. West of Prinz Georg Land (80°15'N / 45° E) we noted floes with extremely high surface sediment concentrations, suggesting a history of perhaps more than one summer of surface melting. However, sea birds feeding on the ice surface in some regions of turbid ice indicate that the ice was no older than the previous winter. Sediments collected from the ice generally consisted

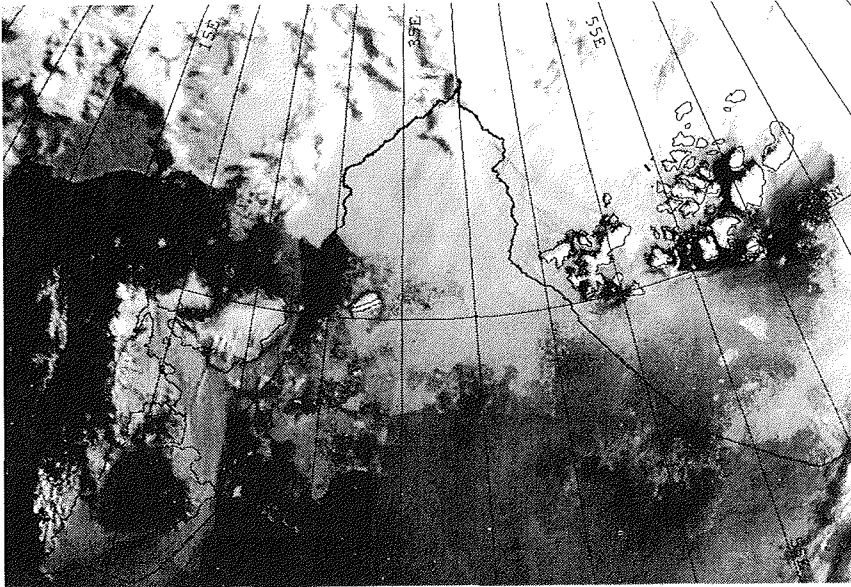


**Fig. 6.1.1-1:** Satellite image (NOAA 11, channel 1) of Svalbard and Franz Josef Land area of August 13, 1993. Cruise track of *Polarstern* is shown as solid line.

of silt and clay, with a small admixture of fine sand (see chapter 6.5). No pebbles, shells, or kelp with holdfasts were observed, although they are difficult to make out from a moving vessel. However, 30-cm-diameter, straight logs, and smaller pieces of wood, were commonly noted. One dirty floe sampled, carrying only clean, fine sand, presents an enigma. With relatively little experience, a diffuse, reddish-brown discoloration of the basal part of ice floes is readily distinguished from greyish-brown turbid ice in the upper section as algal growth. Such algal discoloration was widespread over tens of kilometers of shipboard observations, commonly associated with the production of turbid water by the action of breaking the ice.

Winds from southerly quadrants resulted in considerable compaction of pack ice between Svalbard and Franz Josef Land during the second half of August, as is evident on the satellite picture in Figure 6.1.1-2. Navigation in the ice became increasingly difficult with ice concentrations approaching 10/10. Cracks opened periodically, presumably driven by tidal effects. At roughly  $80^{\circ}10' \text{ N} / 46^{\circ}10' \text{ E}$ , off Gray Bay (Franz Josef Land) ice concentrations decreased southward to 8/10. The compact ice edge, which is clearly visible in Figure 6.1.1-2, was crossed at  $79^{\circ} 51' \text{ N} / 46^{\circ} 50' \text{ E}$  on August 23 (0320 UTC). In this area a number of both grounded and freely drifting icebergs, bergy bits and growlers, probably originating from Prinz Georg Georg Land, were sighted (see chapter 6.7).

#### 6.1.2 Ice Conditions in the Laptev Sea

The NOAA AVHRR satellite images shown in Figures 6.1.2-1 to -3 characterize the temporal evolution of the ice conditions found in the Laptev Sea from the middle of

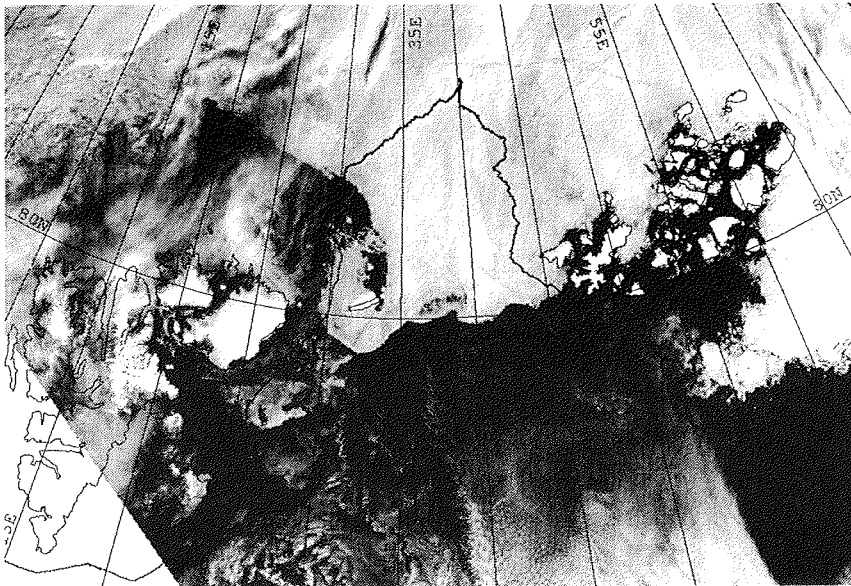


**Fig. 6.1.1-2:** Satellite image (NOAA 12, channel 1, visible) of the Svalbard and Franz Josef Land area of August 28, 1993. Cruise track of *Polarstern* is shown as solid line. Note the compact ice edge as compared to Figure 6.1.1-1.

August until late September 1993. In early to mid-August, the entrance to Vilkitski Strait was ice-free on both, the western and the eastern side. Open fields of pack ice extended along the northeastern tip of the Taymyr Peninsula (Fig. 6.1.2-1). The fast ice belt along the peninsula remained intact over a width of roughly 10-50 km as observed on satellite images received until the end of September, while in Vilkitski Strait little to no fast ice remained. By the time of *Polarstern's* arrival at Cape Cheluskina on August 25, persistent easterly winds had shifted and compacted the entire pack towards the western edge of the Laptev Sea, rendering the passage towards the planned eastermost profile location extremely difficult (Fig. 6.1.2-2). Vilkitski Strait was covered by ice of less than 5/10 concentration up to roughly 119° E, east of which ice concentrations were rarely below 10/10. A helicopter flight towards the North along the coast of Bolshevik Island, the southernmost of the Severnaya Zemlya group, proved this area to be highly deformed, with ridges accounting for up to 50 % of the surface. Several well-delineated shear zones of several kilometers length were found to the northwest of the Maly Taymyr Island group at roughly 77°30' N / 108° E. The positions of icebergs grounded in the area and originating from the two northern Severnaya Zemlya islands as well as the wakes on the southeastern and ice pile-up on the northwestern sides of some of these bergs indicate that ice drift was directed towards the Southeast. As described by BARNETT (1991), sea ice thus follows the setting of the East Taymyr current.

During mid-September, winds veering to southwesterly direction shifted the entire pack to the East and created long stretches of open water along the Severnaya Zemlya Coast (Fig. 6.1.2-3). Within this polynya, extensive new-ice formation with thicknesses up to 0.25 m by the end of September was observed. On September 20,

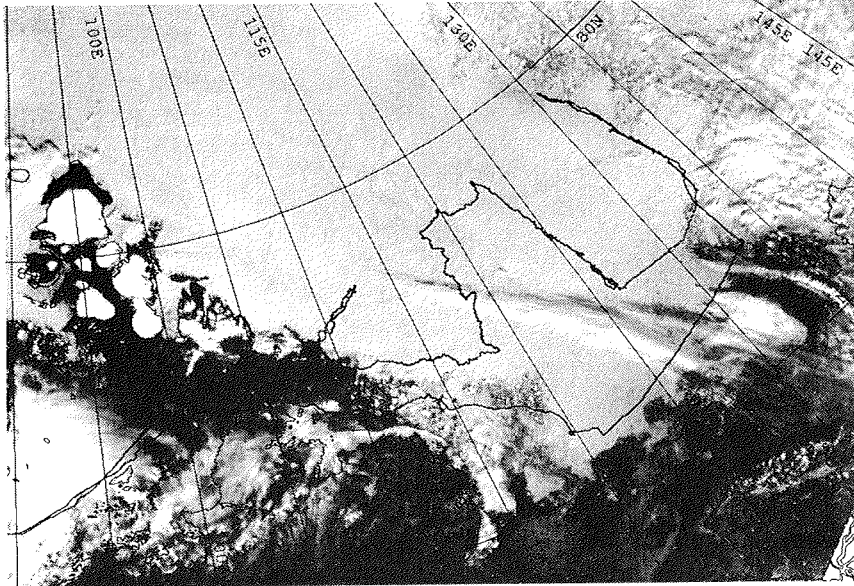


**Fig. 6.1.2-1:** Satellite image (NOAA 11, channel 1, visible) of Laptev Sea, August 16, 1993. *Polarstern* cruise track shown as solid line. Vilkitski Strait is ice-free with open pack ice fields along northeastern part of the Taymyr Peninsula. Note pack-ice belt along the Taymyr Peninsula and the ice caps on Severnaya Zemlya.

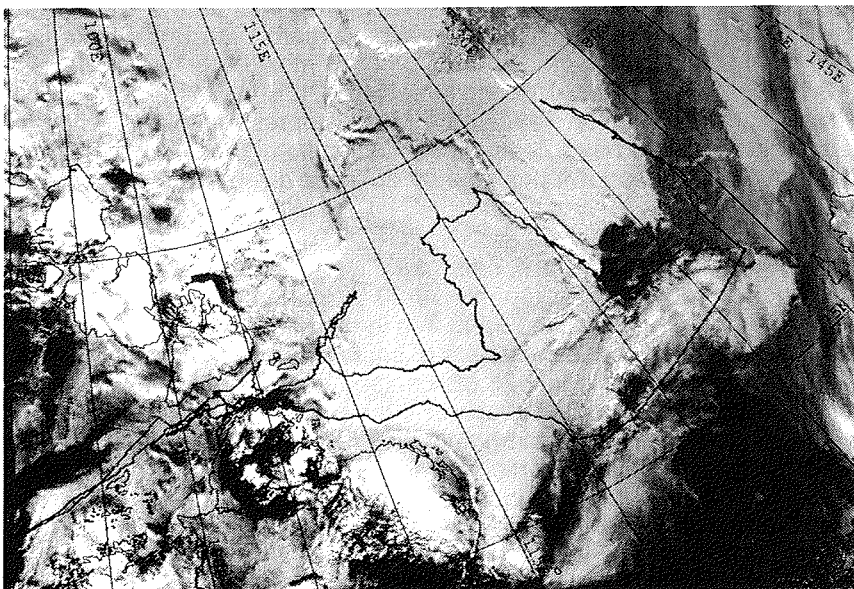


**Fig. 6.1.2-2:** Satellite image (NOAA 11, channel 1, visible) of Laptev Sea, September 6, 1993. *Polarstern* cruise track shown as solid line. Ice is covering Vilkitski Strait and bordering against Taymyr coast, half-moon shaped fast-ice belt still discernible.

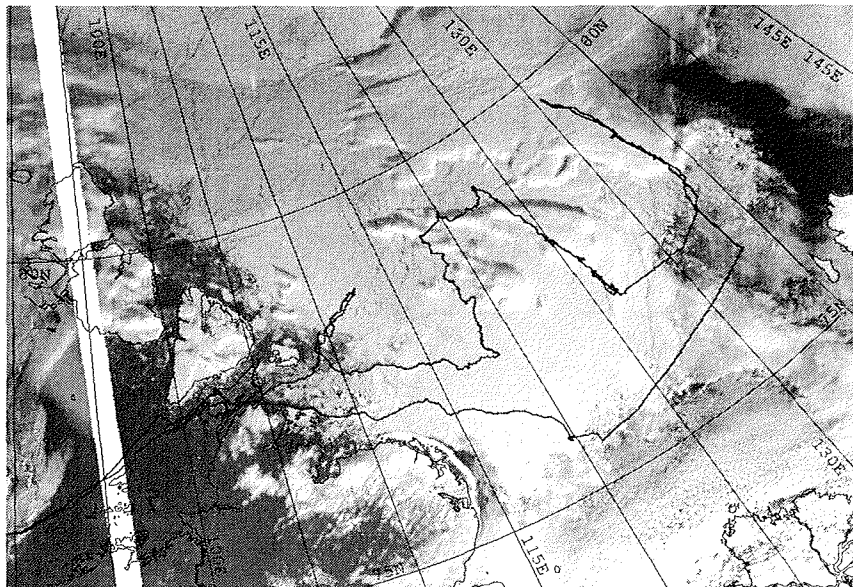


**Fig. 6.1.2-3:** Satellite image (NOAA 11, channel 1, visible) of Laptev Sea, September 20, 1993. *Polarstern* cruise track shown as solid line. Southwestern Laptev Sea covered by open pack-ice fields; open water stretches along eastern coast of Severnaya Zemlya.

the compact ice edge was crossed at roughly 78°20' N / 110°20' E for the north-western Laptev Sea profile. Here ice observations as well as the coring and drilling work indicate the ice to be rather thick (reaching more than 3 m thickness in level areas) and highly deformed. Some cores are in fact most likely two years of age (see Chapter 6.3, Fig. 6.3-1). In accordance with BARNETT's (1991) report, these results demonstrate that the so-called Taymyr Ice Massif represents older, recirculating ice pressed against the Severnaya Zemlya coast. Despite high ice concentrations in the area, tidal movement eased the passage by episodic divergence with the opening of leads.

The central and eastern Laptev Sea pack ice appeared less deformed, with weathered ridges accounting for roughly 10-20 % of the surface and ice thicknesses ranging between <1 in the east and up to 2 m in the Mid-West (see chapter 6.3). Melt puddles were covered by few centimeters of snow when work commenced in Vilkitski Strait. The first snowfall on August 25 also helped to conceal puddles. Nevertheless, puddles in this region covered as much or even more of the ice surface than in the Barents Sea, in particular in the marginal ice zone of the East, where 50 % or more of floe areas were affected. Episodic snowfalls increased snow depths to 0.05-0.15 m during the course of the expedition. Puddles were covered by more than 0.2 m of ice towards the end of September. Leads were mostly covered by dark to light nilas.

As described in chapter 6.5, net snow accumulation on the ice after entering the Laptev Sea made detection of dirty ice increasingly difficult. Turbid ice and surface sediment accumulations, however, were observed, and some very large samples of mud with 5-10 % of sand admixtures were collected on helicopter flights. A number of floes sampled were devoid of sediment. Because of the increasing snow cover, a

realistic comparison of percentages of dirty ice in the Laptev and Barents Sea can not be made.

## 6.2 Albedo of the Ice Cover during Late Summer Time and Energy Exchange Processes (Boris Ivanov and Vitali Alexandrov)

The sea ice cover plays an important role in the climate system. The distribution of drifting ice, especially its surface condition during summer and autumn have a pronounced influence on the energy exchange processes in the surface layer of the atmosphere. The most important sea ice variables relevant for energy exchange and melting are concentration, thickness, surface temperature and albedo. To our mind, albedo plays the main role, because turbulent fluxes and the long-wave radiation balance (average daily estimates) in this period are near zero. This situation causes that ice surface and air temperature are very close to one another, but compact cloudiness (10/10 Stcu or St) limits the minimum values of the long-wave radiation balance during late summer to not more than 10-20 W/m<sup>2</sup>. Therefore the total heat balance of the ice surface as well as melting processes are determined by incoming short-wave solar radiation and reflected radiation, i.e. albedo.

At present several simple summer albedo parametrisations are being used in thermodynamic ice models. These parametrisations are based on the connection of albedo and ice/snow thickness or relative area of puddles. But this information does not suffice. Our ground truth observations revealed a big variation of ice surface types (i.e. wet snow, dirty and bare ice, puddles and others) during late summer. The determination of integral albedo through calculation of the contribution of all types of ice surface helps to improve estimates of energy exchange and variability of ice thickness and concentration.

The energy exchange work during this expedition included the following projects:

- Estimation of total incoming short-wave radiation.
- Measurements of long-wave emitted from the ice surface and atmospheric counter radiation.
- Measurements of albedo and ice/snow temperature.
- Calculations of energy exchange characteristics with the help of special algorithms developed at AARI.

### *Instruments and Sensors*

Surface temperature was measured with an infrared radiometer with a sensitivity in the range of 0.8-14 microns. The opening angle was 45°. The response time was not more than 10 sec. The radiometer had an absolute accuracy of ±0.5° C, with a resolution of 0.055 mv/C. The temperature of the radiometer body was measured by a semiconductor thermistor MMT-4 and computed according to:

$$T_b = B \cdot \ln(R) + A - 273.15$$

where  $A = 5.44060 \cdot 100$ ,  $B = -3.09178 \cdot 10$  and  $R = R(T)$  - the resistance at temperature  $T^\circ \text{C}$ , standard deviation = ±0.16275° C.

The temperature of the surface was computed according to:

$$T_s = T_b + K \cdot U$$

where  $K = 18.1820^\circ \text{C/mV}$  - sensitivity coefficient,  $U$  - registered signal (mV).

**Long-wave radiation balance:** Upward and downward looking pyranometers and pyrgeometers were mounted on the bridge desk. The pyrgeometers consist of thermopile shielded by a germanium hemisphere.

**Albedo** was measured by hand-held pyranometers PP-1 with spectral range of 0.39-0.78 microns and sensitivity coefficient  $-81.02 \text{ mV}/(\text{kW/m}^2)$ . The horizontal position of the sensor was ensured by a special cardan system.

### *Sensor Calibration*

All sensors were calibrated before the expedition at the Main Geophysical Observatory in St. Petersburg. The calibration of the infrared radiometer was controlled with the help of a portable black-body radiator of AARI during expedition.

### *Preliminary results*

During our field activities to the Northwest of Franz Josef Land, we had very constant weather and ice conditions as listed in Table 6.2.3-1.

$T_{\text{air}}$	( $^\circ\text{C}$ )	0.4	$T_s$	( $^\circ\text{C}$ )	0-0.6
$W$	(m/s)	4.0	puddles	(%)	30
$h$	(%)	98	dirty ice	(%)	15-20
$H$	(ft)	300	bare ice	(%)	5-10
clouds	(type)	Stcu/10	ice thickness	(m)	2-3
$Q$	( $\text{W/m}^2$ )	80-150			

**Table 6.2.3-1:** Weather and ice conditions north of Franz Josef Land.

It was a typical situation for late summer time in this region. On average, the surface ice temperature was near zero or slightly below. Melting processes were predominated by the ice cover. Turbulent (sensible and latent) fluxes lay in the range of  $-5$  to  $+10 \text{ W/m}^2$ . After a detailed analysis of the ice surface we distinguish four main types of ice surface: puddles, wet snow, bare ice, dirty ice. Mean values of albedo are presented in Table 6.2.3-2.

Based on these measurements we can obtain a new parameterisation for integral albedo a larger ice covered area:

$$A = A_1 \cdot S_1 + A_2 \cdot S_2 + A_3 \cdot S_3 + A_4 \cdot S_4$$

where  $A_{1,2,3,4}$  = albedo of wet snow, bare ice, dirty ice and puddles.  $S_{1,2,3,4}$  = areal fraction of different types of ice cover. Computation of the integral albedo requires further data on the areal fraction of different ice surfaces obtained from Line-Scan-Camera flights. Then we can calculate the values of total heat balance according to:

$$B = Q \cdot (1-A)$$

and to use this estimate in thermodynamic models for the determination of ice concentration and thickness.

Albedo of puddles (without sediments on the bottom and ice rind)	
z < 20 cm	A = 30 ±5 %
20 cm < z < 30 cm	A = 30 ±5 %
30 cm < z < 50 cm	A = 26 ±3 %
Albedo of puddles with ice rind on surface	
h = 5 mm	A = 34 ±5 %
h = 10 mm	A = 38 ±6 %
Albedo of puddles with sediments on the bottom (patches, cryoconites, thaw holes)	
	A = 14 ±6 %
Albedo of wet snow	
blue ( h < 3 cm )	A = 64 ±8 %
white ( 3 cm < h < 5 cm )	A = 68 ±2 %
white ( 10 cm < h < 15 cm)	A = 70 ±4 %
fresh dry snow (h < 1 cm)	A = 78 ±8 %
average value	A = 67 ±3 %
Albedo of bare ice	
blue	A = 56 ±6 %
white	A = 64 ±3 %
average value	A = 59 ±7 %
Albedo of dirty ice	
slightly	A = 55 ±6 %
medium	A = 34 ±9 %
dark	A = 14 ±2 %
average value	A = 45 ±14 %

**Table 6.2.3-2:** Sea ice albedo, obtained during August 12 through 21, 1993.

We met more difficult situation for analysis in the Laptev Sea due to the start of autumn conditions. Air temperature varied from 0 to -10° C. We had fresh snow after snowfall and short time periods with thaw. During many days the sky was cloudless and incoming shortwave radiation exceeded 300 W/m<sup>2</sup>, but during nights the long-wave balance amounted to more than 70 W/m<sup>2</sup>. Therefore, during the day we had radiation melting on the surface, during the night radiation freezing. Ice-cover albedo is a complicated function of this process. As an example of that we show a time series of snow and puddle albedos during our observations in the Laptev region (September 03 through 21) in Figure 6.2.3-1. The difference between puddle and snow albedo was practically constant (20-30%) during Julian days 246-258. In this period, we had short time intervals with snowfall and thaws, with radiation melting and freezing, but the reaction of snow and puddle surfaces to these variations was not the same. To our mind that was connected with peculiarities of snow and puddle surfaces. For example, we had three colours of ice puddles (white, grey, blue), puddles with fresh and frozen wet snow, light puddles without snow cover, puddles with different ice thickness Table 6.2.3-3).

The same is true for the snow surface - fresh and frozen wet snow of different thickness and density (hard snow-crust, crumbly snow). We obtained very interesting information about the albedo of young ice, shown in Figure 6.2.3-2. The main conclu-

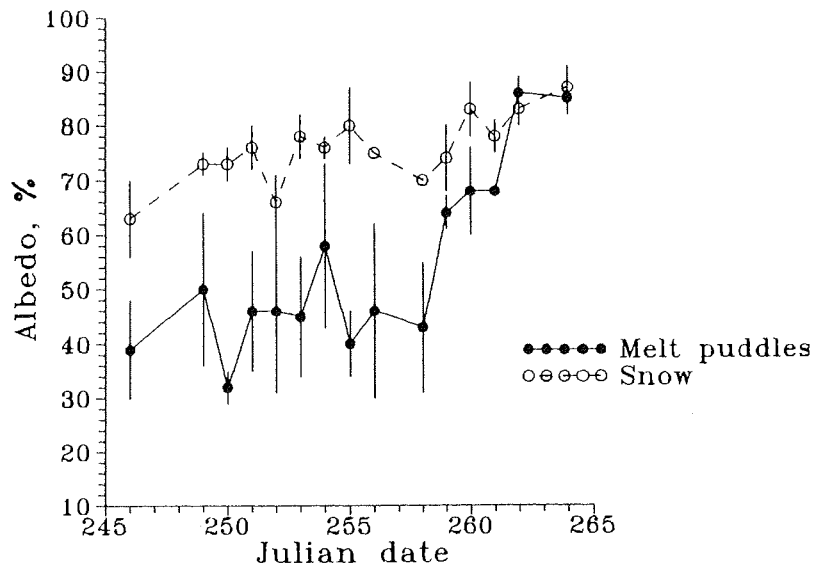


Fig. 6.2.3-1: Time series of snow and puddle albedos during our observations in the Laptev Sea (September 03 through 21, 1993).

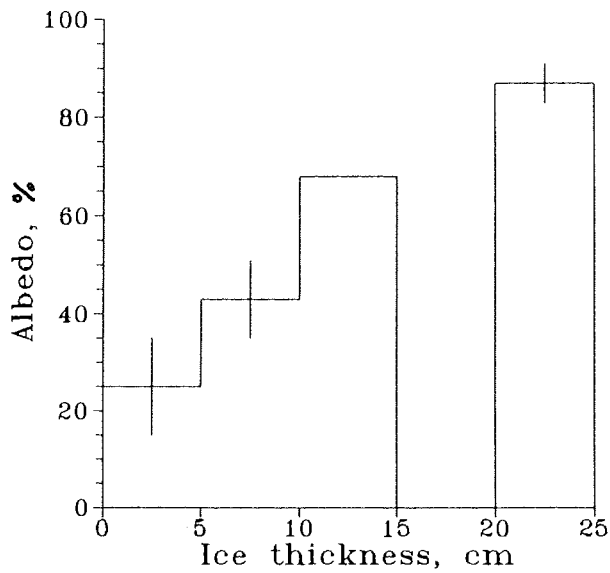


Fig. 6.2.3-2: Albedo of young ice of different thickness. Vertical bars indicate standard deviation.

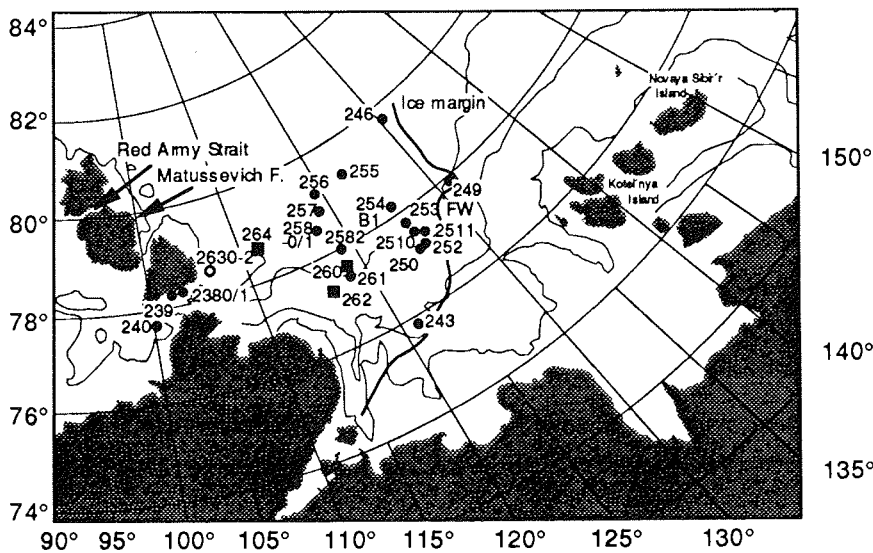
Date	13.09	15.09	16.09	17.09	18.09	21.09
Puddle ice thickness (cm)	13.6	17.2	20.4	22.0	23.0	26.0
Standard deviation	2.6	1.4	3.0	3.0	2.0	2.0

Table 6.2.3-3: Variation of puddle ice thickness with time.

sion is that albedos of all types of ice surface (puddles, snow, young ice) were the same at the end of our observations, ranging between 85-87 % (Fig. 6.2.3-1). This is a very important conclusion for ice cover modeling. Because now we know the approximate period, during which a special albedo parametrisation has to be applied (as shown above), and for which period we can assume albedos of snow, puddle surfaces and surface of young (grey-white) ice to be equal.

### 6.3 Thickness, Structure and Properties of Sea Ice (Hajo Eicken and Regina Pác)

Roughly half of the area covered perennially by sea ice in the Arctic is affected by the Transpolar Drift, resulting in a large-scale transport of sea ice from the Eurasian shelves across the North Pole into the Nordic Seas, mainly Fram Strait. Within this drift pattern the Laptev Sea acts as one of the major source areas as shown by drifting buoys and analysis of sediments transported by the ice in the Transpolar Drift. One of the aims of the sea-ice program during ARK-IX/4 was to obtain insight into the growth processes of sea ice in the Laptev Sea. Furthermore, we studied the structure and properties of the ice in order to better understand the transformations undergone by first- and second-year ice as it is fed into the Transpolar Drift Stream at the end of summer. Station locations for ice-coring in the Laptev Sea are shown in Figure 6.3-1. The work carried out in the Barents Sea provided us with further data on the structure and properties of multi-year sea ice. In collaboration with the ice biology group, these data will be analysed with respect to evidence of annual layering in sea ice.



**Fig. 6.3-1:** Map of ice-coring locations in the Laptev Sea. Open circles mark sampling sites in the fast ice off Starokadomskogo Island. Squares indicate locations of older, possibly second-year ice.

### Ice Thickness Measurements

At a total of 12 stations (11 in the Laptev Sea) thickness measurements were carried out at 2 m spacing along profiles ranging in length between 50 and 110 m (100 m at eight stations). Holes were drilled with a mechanical 5 cm auger for measurements of ice thickness, freeboard, surface elevation and snow depth. Profiles were mainly drilled in level ice to learn more about the evolution of undeformed ice in combination with ice-core stratigraphies. The distribution of level ice thicknesses in the Laptev Sea based on thickness profiles and ice-core drilling is plotted against longitude in Figure 6.3-2. It is clearly evident that away from the ice edge towards the western Laptev Sea the average ice thickness as well as its variance are increasing. Sea-ice observations carried out during the cruise confirm this trend (see Chapter 6.1). As marked in the station map, some of the thicker floes sampled in the western areas were most likely two years of age. Ice core stratigraphies suggest, however, that dynamic growth processes may induce rapid thickening of first-year level ice in the Laptev Sea. The average thickness of level ice based on 419 measurements along 11 profiles amounts to  $1.64 \pm 0.59$  m, the mean thickness obtained for averaging core lengths and profile results at all stations visited is  $1.62 \pm 0.56$  m.

Drill-hole measurements of ice thickness are time-consuming and do not allow for acquisition of larger data bases. Yet, apart from submarine sonar measurements, no operational technique for remote sensing of ice thickness has been implemented as of yet. One promising method involves active-inductive electromagnetic thickness soundings (KOVACS & MOREY 1991, for a detailed description of the method). In short, the technique is based on the induction of eddy currents at the ice-water interface with an electromagnetic transmitter coil. The secondary field generated by these currents (and others induced in half-space beneath the measurement site) is

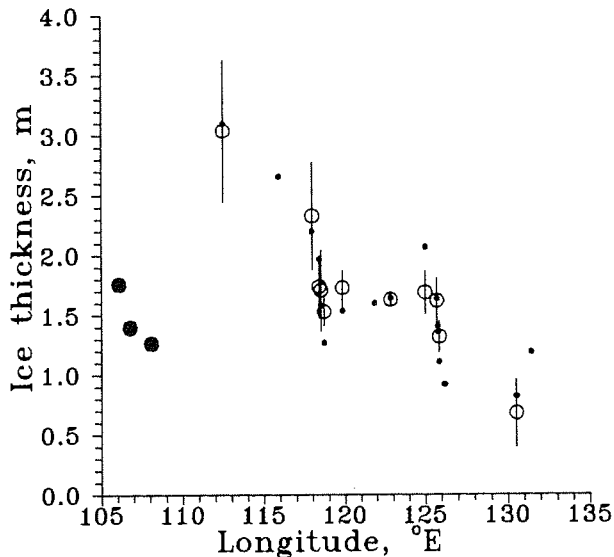


Fig. 6.3-2: Longitude plot of level ice thicknesses derived from thickness profiles (circles with bars indicating standard deviation) and ice cores (small dots). Large dots at the left indicate thickness of fast ice off Starokadomskogo Island.

urement site) is received by the instrument and translated into an apparent conductivity. With the aid of a two-layer conductivity model ice thickness can then be computed. This technique using a Geonics EM-31 has been applied successfully in cold, multi-year ice during the ARK-IX/1a cruise in late winter 1993. During ARK-IX/4, measurements were carried out along all thickness profiles at 4 m spacing in order to assess the reliability of the instrument during conditions of severe summer melt. Results even look promising for those measurements carried out in spots where the ice surface was covered by melt puddles up to 0.3 m deep. A more detailed analysis will comprise joint evaluation of all profile data along with measurements carried out at different instrument heights in order to further evaluate the conductivity-depth dependence for routine measurements.

#### *Ice-core Studies*

Sets of two to six ice cores were drilled through the entire thickness of floes at six locations in the Svalbard and Franz Josef Land area and 23 stations in the Laptev Sea by the multi-disciplinary sea-ice group. At eight additional locations, surface cores were obtained for detailed studies of sediment inclusions in relation to structure and properties of the ice. Sampling locations are shown in Figure 6.3-1. Along with other environmental parameters, ice temperature was measured on the site (see chapter 6.4). After drilling, two cores were transferred to the ship and stored at  $-30^{\circ}\text{C}$ . From one of these, thick sections were produced over the entire length of the core. Based on examination in ordinary light and between crossed polarizers a textural core stratigraphy was produced, with detailed observations on the distribution, sizes and shapes of pores and grains. From each core, several subsamples were taken back to the Alfred Wegener Institute for the production of horizontal and vertical thin sections for quantitative textural studies employing image-processing techniques. Based on the stratigraphy, cores were sectioned into pieces of 0.05-0.15 m length. These were melted at  $4^{\circ}\text{C}$  in the dark. After determination of salinity and subsampling for later nutrient analysis, samples were filtered over GF/C filters for determination of chlorophyll-a. Further samples for isotope and biogeochemical analysis were cut and stored at  $-30^{\circ}\text{C}$ .

First results from the analysis are shown in Table 6.3-1. The average fraction of columnar ice within cores, grown through congelation of seawater at the underside of an ice floe, is an indicator of the contribution of thermodynamic growth to the thickening of level (i.e. unridged) ice. This fraction is significantly smaller for ice from the Laptev than for that from the Barents Sea, indicating the importance of dynamic growth processes in ice cover thickening in the Laptev Sea. This is also suggested by a qualitative estimation of grain sizes and shapes in columnar ice. Yet, validation of these preliminary findings requires further study of the ice texture and associated parameters.

One important process affecting ice entering into the Transpolar Drift is surface melting during the summer months. Part of this meltwater can be found in melt puddles (Chapter 6.6), part percolates through the ice column, strongly affecting sea-ice salinity and associated chemical parameters. At this preliminary stage, requiring more detailed analysis of individual cores by drawing on other measurements such as stable isotopes, there is strong evidence that surface ablation in the Laptev Sea can be so severe as to reduce salinities of first-year ice by end of the summer to values

		Svalbard/Franz Josef Land		Laptev Sea	
		Mean	Std. dev.	Mean	Std. dev.
Length	(m)	2.49	0.39	1.58	0.54
Columnar ice in core	(%)	82	15	59	27
Core salinity	(‰)	2.0	0.5	1.3	0.7

**Table 6.3-1:** Average ice-core parameters.

within or below the range of ordinary multi-year ice. This is evident from the average salinity values shown for Laptev Sea and Barents Sea ice in Table 6.3-1. A further illustration is given in Figure 6.3-3 showing a plot of average integrated core salinity vs. core length. The ARK-IX/4 data fall within the same range or even below that found in multi-year ice of the central Arctic in 1991.

Future work will focus on a detailed analysis of the entire suite of parameters determined on the ice cores, in particular in relation to measurements from other years and other areas. Detailed textural studies may shed some light on processes of sediment incorporation and relocation in Laptev Sea ice. Colonization of sea ice in the source areas of the Laptev Sea should also depend to a considerable degree on processes of ice growth and transformation. Clearly, more field data, augmented by laboratory and model results are needed to further our understanding of the role of sea ice in the system Laptev Sea - Transpolar Drift.

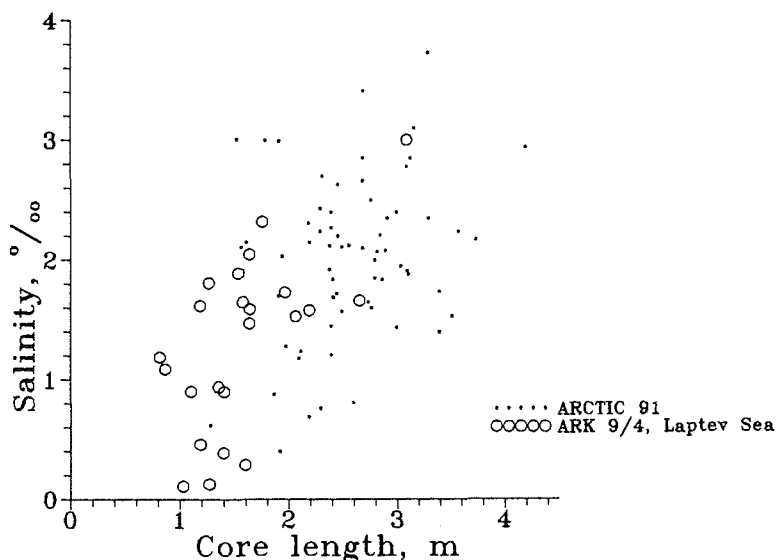


**Fig. 6.3-3:** Average integrated ice-core salinity plotted against core length. Large, open circles represent measurements from the Laptev Sea during ARK-IX/4, small dots are data from the international ARCTIC'91 cruise to the central Arctic in 1991.

### *Snow Studies and Sampling in the Laptev Sea*

Data on the precipitation and accumulation patterns are notoriously sparse in the central Arctic. The atmospheric freshwater flux represents an important component of the mass-balance of Arctic sea ice, however. Studies of the distribution of stable isotopes, namely  $^{18}\text{O}$ , are important sources of information in this respect. Thus, the study of surface ablation (Chapter 6.6.) also requires such data for freshly fallen snow. Of similar importance is the question whether atmospheric input of particulate material (and associated anthropogenic pollutants) contributes significantly to the load of particulate and dissolved material in sea ice.

In an attempt to address some of these issues, snow studies and sampling was carried out at 12 stations in the Laptev Sea. Sites and sampling techniques were chosen such as to minimise contamination problems. Measurements in the field comprised depth, density, temperature and structure of the snow. Samples of different stratigraphic units were taken onboard and melted for determination of electrolytical conductivity. At the Alfred Wegener Institute mass-spectrometric measurements will be carried out for determination of  $^{18}\text{O}$ . Larger sample volumes (ca. 2-4 l) have been taken at the sites for later determination of heavy metal concentrations at the Alfred Wegener Institute. Furthermore, it is planned to study composition, sizes and types of micro-particles found in freshly fallen snow.

## 6.4 Sea-ice Biology

The sea ice cover of the Arctic Seas serves as an habitat for a diverse community of organisms of various size and taxonomic classes ranging from bacteria below  $1\ \mu\text{m}$  in size up to metazoans of more than  $500\ \mu\text{m}$  body length. During the ARK-IX/4 expedition we investigated the abundance of organisms in sea ice samples taken from the Barents Sea and Laptev Sea. Experimental studies gave insights into the food web structure and dynamics. Special attention was given to the under ice fauna as one factor controlling the biological coupling processes between sea ice and pelagial.

### 6.4.1 Abundance of the Sea Ice Organisms (Christine Friedrich and Rolf Gradinger)

In the Barents Sea a total of 19 ice cores was taken at seven sampling sites, and in the Laptev Sea a total of 33 cores was taken at 19 sites with a three inch ice corer. Ice floe thickness ranged from 10-280 cm. The ice cores were cut into 2-20 cm long segments directly after coring. These segments were melted in an excess of  $0.2\ \mu\text{m}$  filtered seawater at  $4^\circ\text{C}$  to avoid osmotic stress to the organisms. After complete melting of the sample, a subsample of 100 ml was fixed with 0.5 % formaline end concentration. This subsample was filtered onto  $0.2\ \mu\text{m}$  Nuclepore filters and stained with Diamidinophenylindol. Bacteria, auto- and heterotrophic flagellates and diatoms were counted on the filter using an epifluorescence microscope equipped with UV and blue light excitation. The rest of the melted sample was concentrated over a  $20\ \mu\text{m}$  gaze and organisms larger than  $60\ \mu\text{m}$  were counted and sorted alive under a dissecting microscope. For further taxonomical studies the samples were fixed in 1 % formaline, except for turbellarians and ciliates, which were fixed in Bouin fluid.

Most of the filters prepared for epifluorescence counting of bacteria, flagellates and diatoms were deep frozen for further analysis on land. Fig. 6.4.1-1 shows a first result of the abundance of bacteria in core AR9422403 taken in the Barents Sea. The highest concentration of bacteria was found in the lowermost 2 cm, reaching up to more than  $1 \cdot 10^6$  bacteria  $\text{ml}^{-1}$ . Similar data will be available for all other sampled cores for the taxa mentioned above.

On board the ship four cores from the Barents Sea and three cores from the Laptev Sea could so far be investigated with regard to main taxa of larger ice organisms. Highest organism densities of up to 1148 specimens/l were observed in the lowermost cm of the ice floes, intermediate concentrations of 15-522 specimens/l occurred in the layers 40-110 cm above and only single specimens of turbellarians, ciliates and rotifers were found in the upper layers of the ice cores (Fig. 6. 4.1-2 to 8). The diversity of organisms also increased towards the bottom of the ice core. These findings are in accordance to earlier investigations (GRADINGER & HÄRTLING 1992) during the ARCTIC'91 expedition, except for one core from a deep water station (AR94225) northeast of Spitsbergen, which had up to three times higher organism densities in the 60 cm above the bottom than in the lowermost 2 cm.

Of special interest was the comparison between the meiofauna community of shallow and deep water stations, since earlier investigations (HORNER 1989) revealed that nematodes followed by copepods were the dominant taxa. GRADINGER & HÄRTLING (1992) suggested upon their own findings from the Barents Sea and the deep central Arctic Ocean that this community type is restricted to the shelf areas, while the meiofauna community of the deep stations was dominated by ciliates and turbellaria. In contrast to these results the ice community of the shelf and deep water northeast of Spitsbergen was dominated by nematodes with a much lower total abundance of organisms in the deep water station (AR94225) and a higher diversity in the shelf

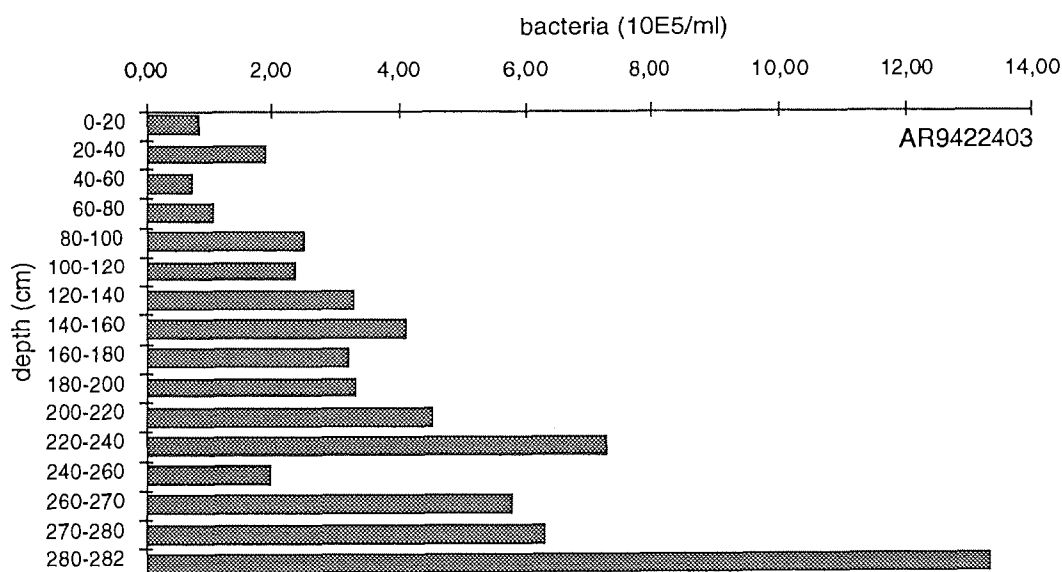


Fig. 6.4.1-1: Abundance of bacteria in core AR9422403.

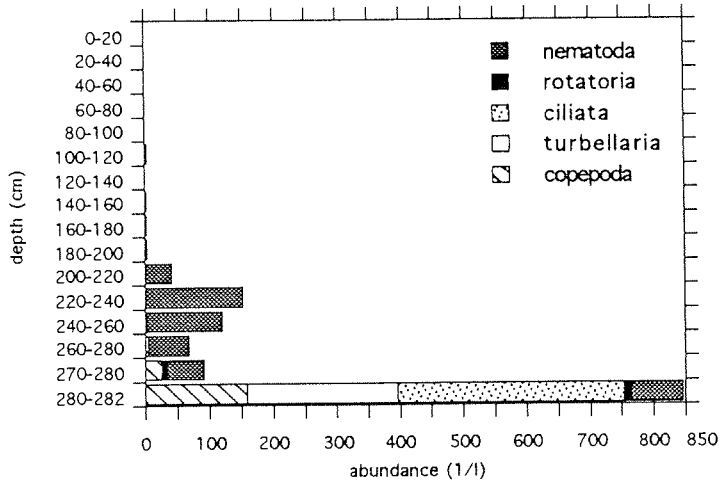


Fig. 6.4.1-2: Abundance of meiofauna organisms in the Barents Sea, core AR9422403, depth 188.5m.

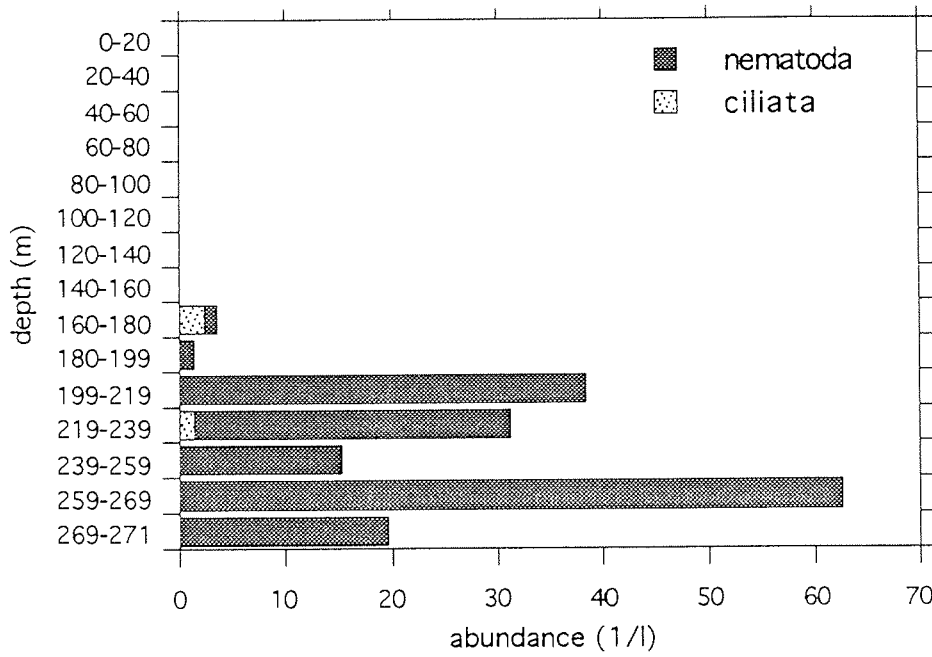
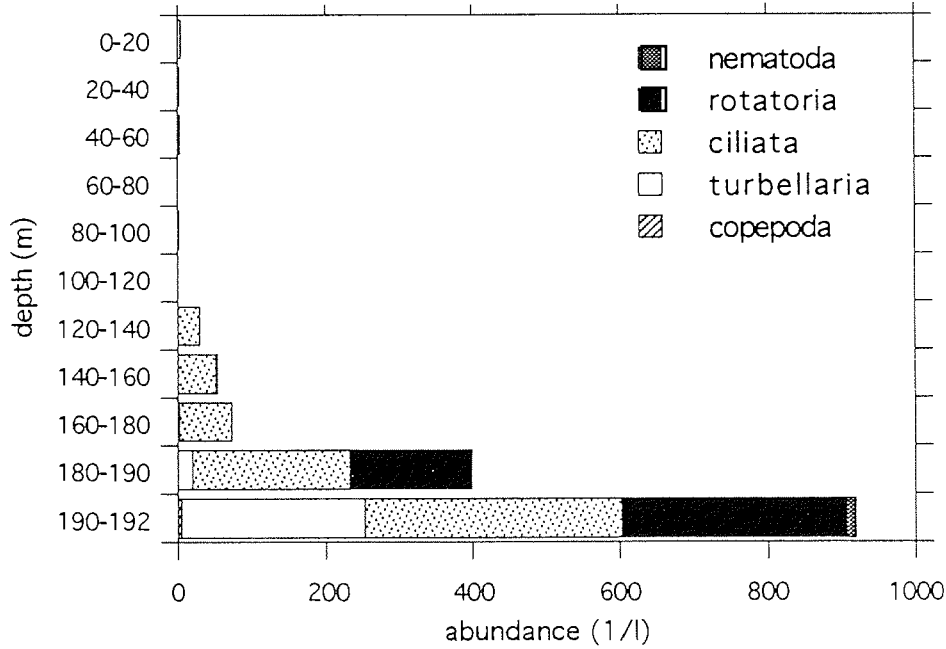
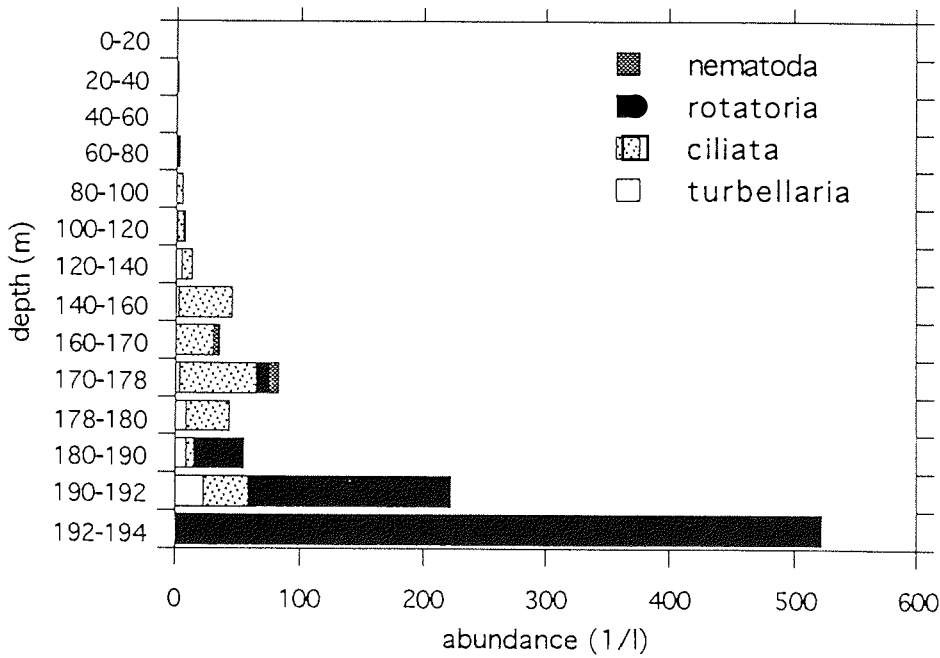


Fig. 6.4.1-3: Abundance of meiofauna organisms in the Barents Sea, Core AR9422503, 2762 m.



**Fig. 6.4.1-4:** Abundance of meiofauna organisms in the Barents Sea, Core AR9423003, depth 3001 m.



**Fig. 6.4.1-5:** Abundance of meiofauna organisms in the Barents Sea, Core AR9423303, depth 289 m.

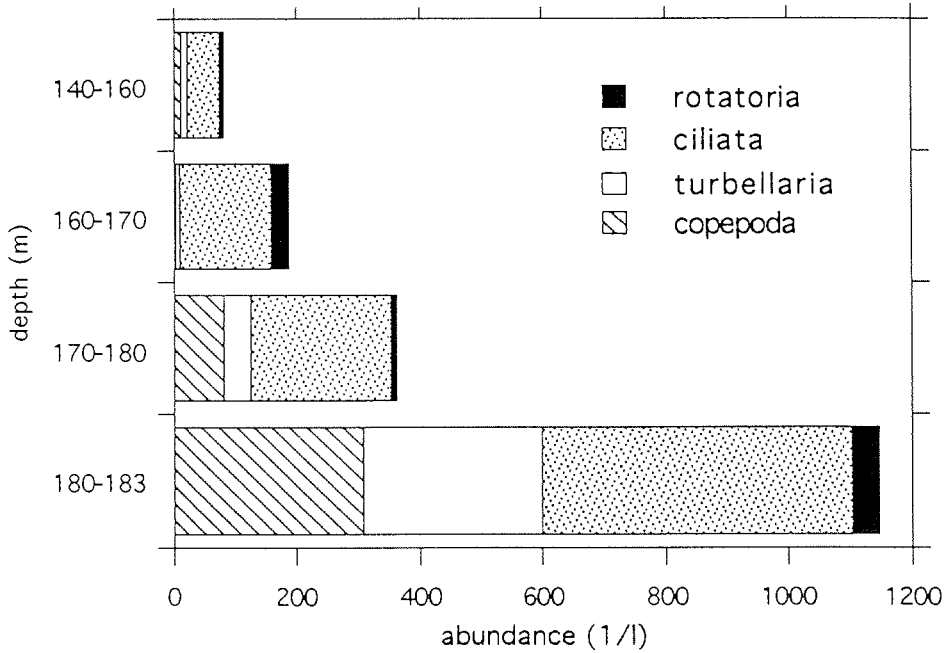


**Fig. 6.4.1-6:** Abundance of meiofauna organisms in the Laptev Sea, Core AR9424003, depth shallow.

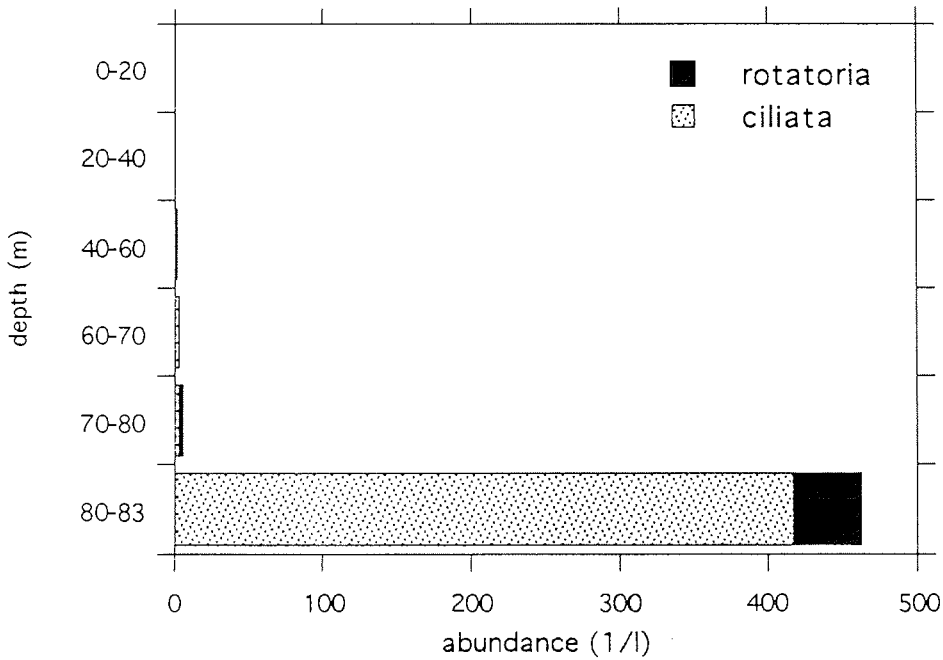


**Fig. 6.4.1-7:** Abundance of meiofauna organisms in the Laptev Sea, Core AR9424603, depth 3426 m.

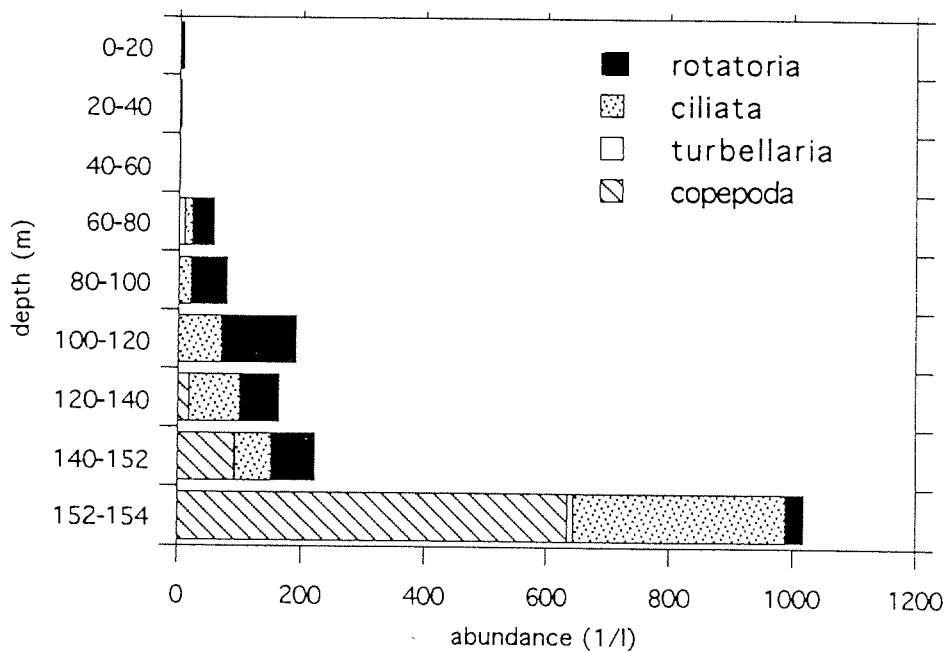


Fig. 6.4.1-8: Abundance of meiofauna organisms in the Laptev Sea, Core AR9425004, depth 1735 m.

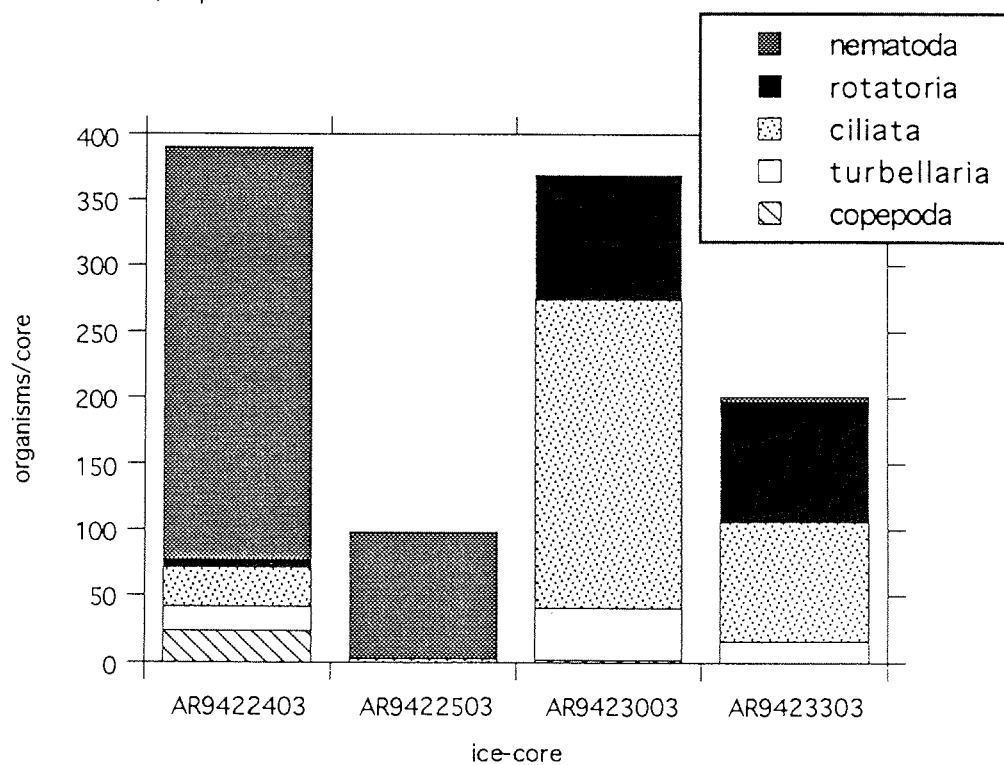
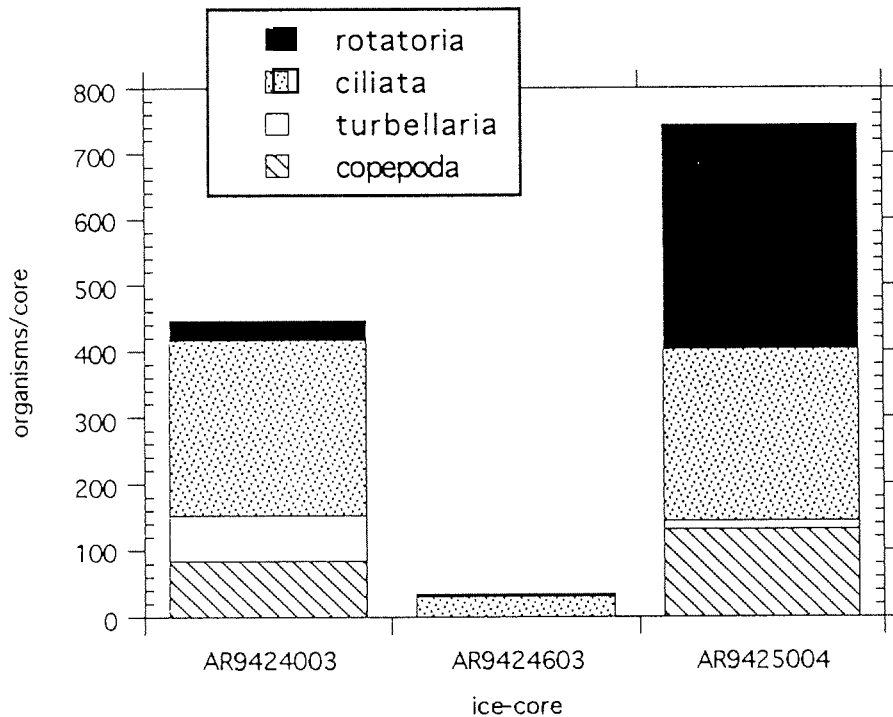


Fig. 6.4.1-9: Total number of meiofauna organisms per core in the Barents Sea.



**Fig. 6.4.1-10:** Total number of meiofauna organisms/core in the Laptev Sea (core AR9424003 only the bottom 43 cm of the ice floe sampled).

area station (see AR94224, Fig. 6.4.1-9). The community structure of the sea ice samples taken in the northwest of Franz Josef Land showed a totally different pattern. The sea-ice community of the deep station (AR94230) was dominated by ciliates, followed by rotifers, while only a lower number of turbellarians were found and the total number of organisms/core was higher than in the shallow water station (AR94233). The sea ice of the shallow water station was dominated by rotifers and ciliates.

In the Laptev Sea the sea ice of the deep water stations was dominated by rotifers and ciliates, followed in one core (AR9425004) by harpacticoid copepods, their copepodids and nauplii (Fig. 6.4.1-9). The bottom 43 cm of a core taken over shallow water (AR9424003) were dominated by ciliates, followed by copepods and turbellarians. Females of harpacticoid copepods with egg sacks as well as copepodids and nauplii were found in the ice of the Laptev Sea from the end of August on. Copepods in the Barents Sea and the Laptev Sea were mainly harpacticoids, presumably belonging to the families Tisbidae and Ectinosomatidae. Besides this only a few cyclopoid copepods were found.

Specimens of all main meiofauna taxa are kept in cultures for life observations and experiments in our home laboratory. By studies on their behaviour and reproduction cycles as well as experiments on temperature and salinity tolerance we hope to get a better understanding of the biology of the sea ice organisms. During this cruise

hatching of nauplii of three female harpacticoids could already be observed, which gives us the opportunity to study the different stages of development.

#### 6.4.2 Structure and Dynamics of Sea-ice Food Web (Rolf Grading)

Information on interactions between the various groups of sea-ice organisms are very scarce both from Arctic and Antarctic areas. Our present knowledge is based on investigations on fecal pellets formed by metazoans or by direct studies on their gut contents. Quantitative information on fluxes of organic carbon are restricted to measurements of total production by algae and bacteria using radioactive tracers. During the expedition ARK-IX/4 a series of four experiments was conducted using the so-called serial dilution technique according to LANDRY & HASSET (1982) using brine samples collected on three ice floes. The dilution leads to a proportional reduction of the probability that a potential grazer hits a prey particle, and, thus, to a proportional reduction of the grazing rate, while the growth rate remains unaffected. Plotting the apparent growth rates of the various dilution steps against the dilution itself allows the estimation of both growth and grazing rates under natural conditions. Four sets of dilution steps (1, 0.5, 0.2, 0.1), made with brine and 0.2 µm filtered brine, with three triplicates each, were incubated in an incubator at +1° C and a light to dark cycle of 18 to 4 hours. Subsamples were taken every 48 hours

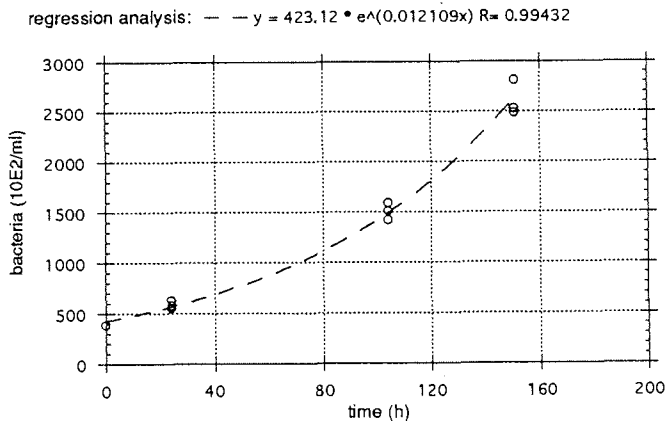


**Fig. 6.4.2-1:** Changes in the abundance of bacteria in serial dilution experiment 1 in dilution step 0.2.

and counted with an epifluorescence microscope after DAPI staining (see above). The apparent growth rates of bacteria, auto- and heterotrophic flagellates and diatoms were calculated for each dilution step using an exponential curve fit model:

$$N_t = N_0 \cdot e^{(\mu-g) \cdot t}$$

where  $N_{t/0}$  = abundance of organism group at time t/0,  $\mu$  = growth rate,  $g$  = grazing rate and  $t$  = time (hours).

Figure 6.4.2-1 shows an example of the growth of bacteria during experiment 1 in the dilution 0.2. During the incubation time of 154 hours the changes in the abundance of bacteria followed the expected pattern with  $(\mu-g) = 0.012$  with a doubling time of the bacterial population of 58 hours under these condition. Calculation based on the in-

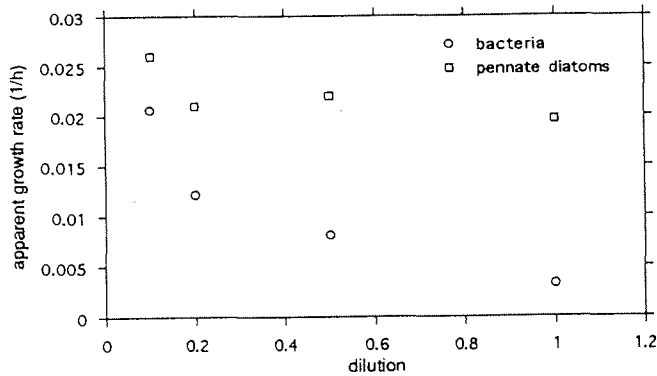


**Fig. 6.4.2.-2:** Relation between apparent growth rate ( $\mu$ -g) and dilution for bacteria and diatoms during serial dilution experiment 1.

formation shown in Figure 6.4.2-2 showed that the bacterial population had a generation time of 41 hours but was also completely grazed during 46 hours and remains therefore nearly constant in the sea ice. Similar calculations done for diatoms resulted in mean generation times of 30 hours, while the grazing pressure was relatively low (140 hours to graze the entire population). These first preliminary results indicate, that the bacterial population is controlled in its development by grazers, most likely protozoans, while the development of diatoms was controlled by their own growth potentials under the environmental conditions.

#### 6.4.3 Study of the Under-ice Fauna (Michael Poltermann)

Organisms are found not only living inside the sea-ice floes but also at the lower ice surface. The inhomogeneous structure of this surface gives the under-ice fauna favourable life conditions like high quantity of food, shelter from predators and strong water currents, and a nursing ground.

Several studies were conducted on the species composition of the under-ice fauna but information on their biology and ecology is still very scarce. Thus, the main topic during this expedition was (i) to sample under-ice macro fauna, especially amphipods, with baited traps and hand nets; (ii) to observe these species with an under water video system called "ELSE" under natural conditions. The video material allowed both estimations of species distribution patterns as well as behavioural observations.

Several hundred amphipods were caught during the entire cruise in the Barents and Laptev Seas. Mainly three species were present in the baited traps and in the hand net: *Gammarus wilkitzkii*, *Onisimus (Pseudalibrotus) spp.* and *Apherusa glacialis*, which are known to dominate the under-ice macro fauna in other Arctic sea areas too. Most of the specimens caught were immediately deep frozen for gut content analysis by scanning electron microscopy and population dynamical studies. Living

animals from *G. wilkitzkii* and *Onisimus* spp. will be used for investigations of behaviour, reproduction and ecophysiology (temperature and salinity resistance).

All three species were observed in their natural environment using the video equipment. All animals were very active. Most of them were observed near patches of ice algae, which could also be detected with the video system. Differences in the behaviour could be seen. *Gammarus wilkitzkii* and *Onisimus* spp. were the two most abundant species. *G. wilkitzkii*, like *Apherusa glacialis*, was mostly observed using small cracks and holes to rest. *G. wilkitzkii* walked directly at the under surface of the ice floes using its spiny legs. Several females of this species contained eggs in their marsupium showing that the reproduction period of *G. wilkitzkii* starts in August. The other two species were much better swimmers. *Onisimus* was mostly observed hanging at the underside of the ice floes, while *A. glacialis* showed its highest densities on vertically orientated edges of the individual ice floes. Further analysis of the video-material will include detailed description of behavioural patterns of these animals.

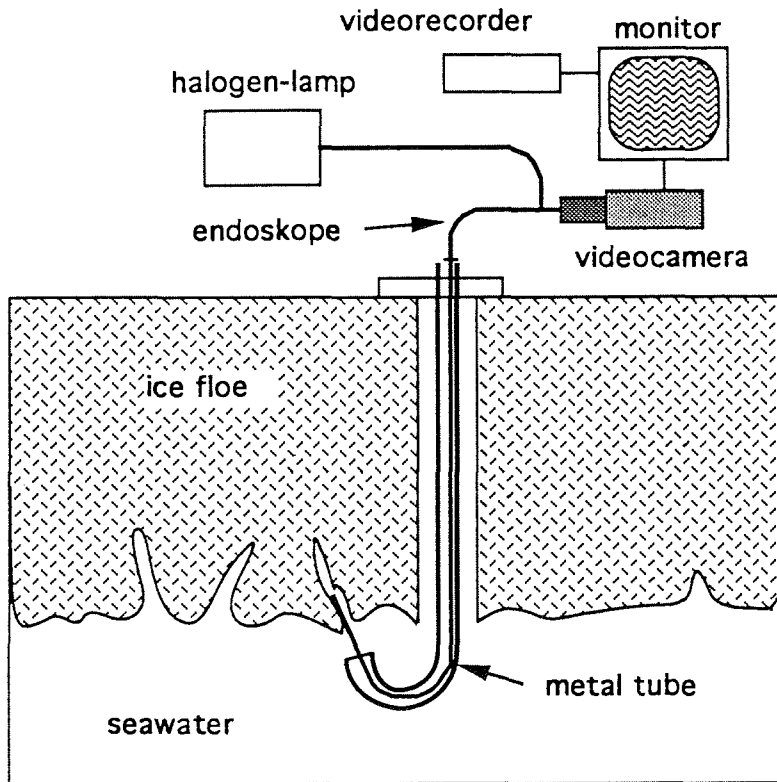
It should be mentioned that not the total under-ice fauna could be collected with the techniques used during this expedition. During icebreaking of RV *Polarstern*, many fishes, mainly polar cod (*Boreogadus saida*), were observed, but no adequate techniques for collection of fishes could be used in the relatively short time available on station during this cruise. Thus, further investigations should include, e.g., diving as a method to make direct *in situ* observations on the distribution of the under-ice macro fauna as well as to collect quantitative samples for species composition analysis.

#### 6.4.4 Observations of Sea-Ice Organisms in the Field Using an Endoscope (Jürgen Weissenberger)

In sea ice the interstitial system of brine channels and pockets is the habitat of sea-ice organisms. The frequencies of brine channels and pockets per unit of volume and their dimensions depend on the history of the ice floe and the actual temperature and salinity. We are not able to visualize and observe the organisms in their habitat, because extraction of ice and the following changes of temperature and hydrostatic pressure destroy more or less the original habitat. Even smaller temperature changes cause dramatical changes of pore volume.

On this cruise we tried to use an endoscope for observations of sea ice organisms. It was the first use of an endoscope for this purposes under the harsh conditions of the Arctic. At first we had to adapt the technical equipment for optimal use in the field. The endoscope was an ELTROTEC MKF fibrescope with a working length of 4 m and a diameter of 1 mm together with a 150 W halogen lamp, a special lens and an JVC video camera with monitor and video recorder. The principal arrangement of the equipment is shown in Figure 6.4.4-1. The angle of view of the endoscope was 70°, the depth of focus 2-40 mm. A metal tube of 3 mm internal diameter was placed as a liner in an core hole. Thereafter the endoscope was introduced into the tube. The end of the endoscope was placed in a brine channel or at the undersurface of the ice. It was helpful to use the "ELSE" under-water video system to control the place where the endoscope looked in. A total of 30 hours observation was recorded in different habitats. We obtained images from the *in situ* microstructure of the ice-water interface as well as those from algae and animals living there. The smallest

structures visible in our records were about 100  $\mu\text{m}$ , but the visibility of details strongly depends on the contrast. The contrast in the ice, e.g. in small brine channels, was very poor, better contrast was found on the under surface of the ice with open water in the background. The video observations will be analysed at the AWI in detail.



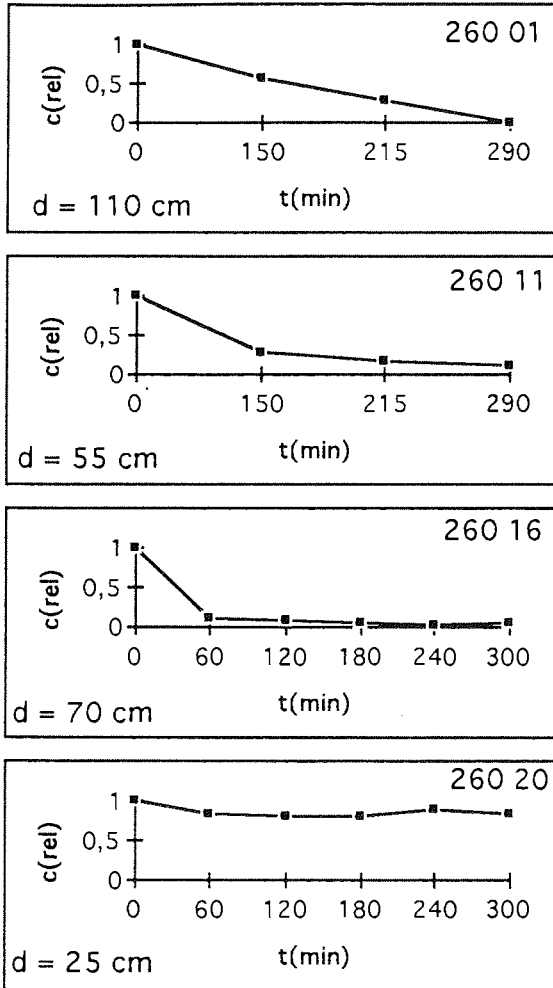
6.4.4-1: Schematic arrangement of the endoscope and recording equipment used.

#### 6.4.5 Stain Dilution Experiments (Jürgen Weissenberger)

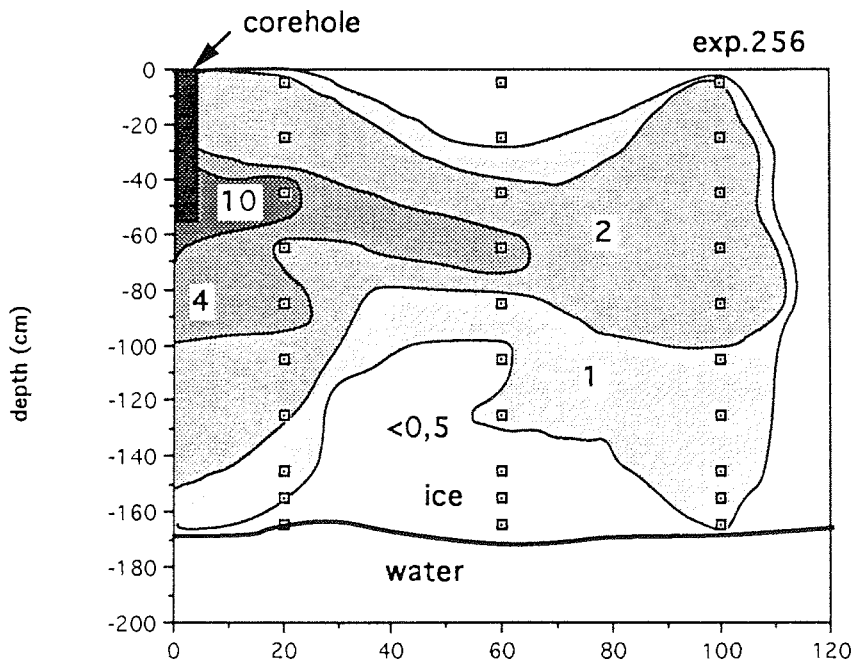
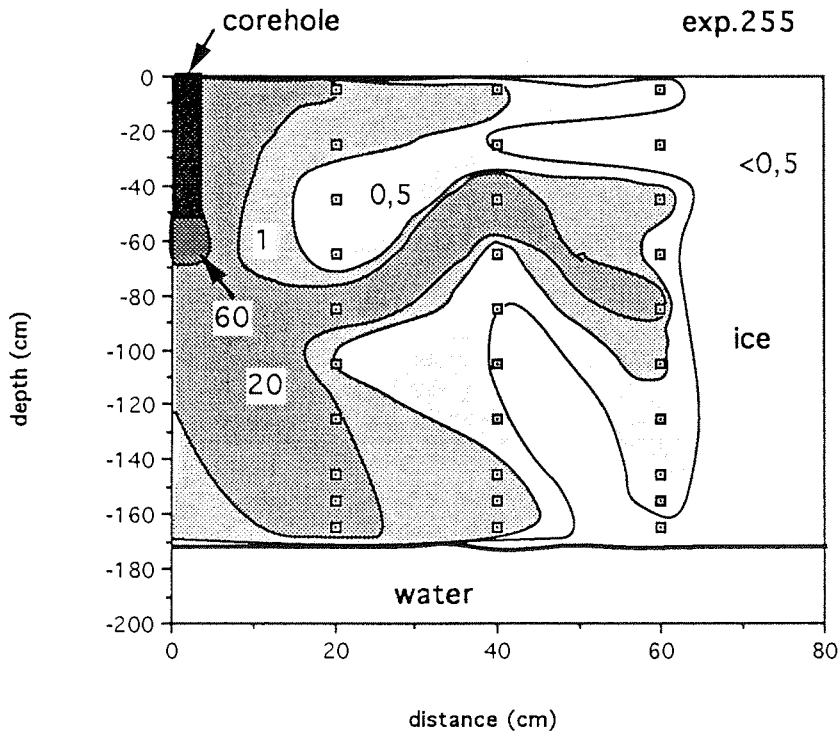
A total of 35 stain dilution experiments was carried out to estimate the motion of brine in an ice floe on five different ice floes. Surface ice holes were drilled with depths of 10-110 cm. 5 ml of saturated Rhodamin solution was added to the brine and stirred immediately. After 15 min stained brine was sampled using small plastic bottles (60 ml). Every 60-90 min the brine was stirred again and a new sample was taken. The stain concentration in each brine sample was measured with a photometer (Nanocolor 100 D) at 540 nm wavelength in 1, 2 and 5 cm kuvettes. In some surface holes the stain concentration was constant during the observation time (up to 6 h) in other holes the stain disappeared in 2-3 hours completely (Fig. 6.4.5-1).

Three experiments were carried out to measure Rhodamin concentration in the ice near the stained surface hole. Ice cores were drilled in distances of 20, 40 and 60 cm from the center of the stained surface core hole 5 to 7 hours after the beginning of

the experiment and cut into pieces of 10 cm each. Rhodamin concentrations were measured after melting the ice samples. (Fig. 6.4.5-2).



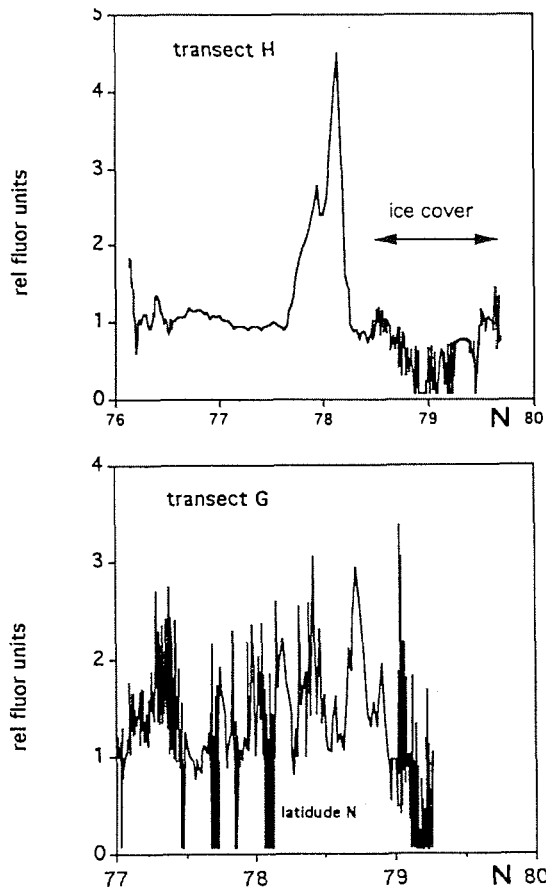
6.4.5-1: Dilution of Rhodamin concentration (c rel) in four surface core holes at Station 260; d = depth of the core hole.



6.4.5-2: Distribution of stain in the ice after 5.5 hours (Exp. 255) and nine hours (Exp. 256). The numbers indicate the percentage of stain concentration in the ice. Square dot indicate sample points.

#### 6.4.6 Continuous Chlorophyll Measurements (Jürgen Weissenberger)

From August 8 until September 30 a continuous flow fluorometer was connected to the sea water pump system of RV *Polarstern*. The fluorescence signal was recorded as 10 min averages. 1000 ml sea water from the same water flowing through the fluorometer were filtered over Whatman GF/C filters twice a day to calibrate the fluorescence signal. Figure 6.4.6-1 shows the fluorometer signal recorded along the Transects H and G. On Transect H, the ship was steaming in open water most of the time, the signal was a continuing line. In opposite of that the signal at Transect G was highly interrupted and discontinuous due to the ice breaking activities. We assume that most algae causing the fluorescence signal during ice breaking activities may be washed out from the broken ice floes. The lowest values of fluorescence units on Transect G highly corresponds with station times when the ship wasn't moving. After processing of the chlorophyll filters at the Alfred Wegener Institute these data will be analyzed in detail.



6.4.6-1: Fluorescence signal in relative fluorescence units along Transects H and G recorded with a continuous flow fluorometer plotted against latitude. Note phytoplankton bloom at 78° N.

## 6.5 Sediments in Sea Ice (Erk Reimnitz)

Observations and measurements of sediment in sea ice were carried out during the *Polarstern* expedition ARK-IX/4 between Svalbard and the New Siberian Islands (Fig. 2-2). These studies cover the Siberian Branch of the Transpolar Drift, which originates on wide, shallow Siberian shelves, including as an important component the Laptev Sea. The Laptev Sea is considered a major ice factory for the Arctic Ocean, where sedimentary particles along with other foreign substances are entrained into newly forming ice. The stream of pack ice then carries such substances across the Arctic Ocean through Fram Strait into the North Atlantic, where they are released by ice melt. Knowledge about the mechanism of modern ice rafting, covering a three-year period from entrainment to ultimate melting, is necessary for:

- understanding the high rates of Arctic coastal retreat and shelf erosion,
- interpreting the polar deep-sea sedimentary record,
- assessing the total sediment budget of the Arctic Ocean, and
- learning about dispersal of hazardous substances in the Arctic.

"Dirty ice", as observed near its source, is mainly in the form of turbid ice. Turbid ice contains individual particles dispersed rather evenly throughout an ice layer ranging from decimeters to one or more meters in thickness. The formation of turbid ice by suspension freezing is now believed to be the principal entrainment mechanism, but there are others. Wind transport of fine sediments from the Siberian continent onto ice, flooding by river waters, and slumping from coastal cliffs all would be recognizable as distinct surface layers or mounds on first-year ice. Bottom adfreezing on very shallow shelf regions would be revealed by basal sediment accumulations, while the formation of grounded pressure ridges would incorporate internal sediment pockets. During transit, the ice undergoes changes that affect the mode in which sediments are carried. These changes gradually mask the original entrainment mechanism to the point where its recognition is impossible.

One half meter of seasonal surface melting, greatly enhanced by dark foreign substances, results in the formation of irregular sediment layers on top of the ice and on floors of melt puddles. Various surface processes combine fine particles and biogenic substances into millimeter-size pellets, which become increasingly cohesive with aging through several melt seasons. With slightly acidic conditions prevailing on ice surfaces during summers, calcareous micro-fossils may dissolve with time, making the recognition of sediment entrainment environments increasingly difficult. Not all sediment is retained on ice floes, as some turbid meltwater flows into the sea.

Near ice source regions, the pack carries sand and coarser grains, in the Central Arctic and Fram Strait mainly fines have been found, suggesting that coarse grains are lost preferentially. Winter wind-ablation mobilizes exposed sedimentary particles and redistributes them throughout snow drifts. More sediment is lost to open cracks and leads by eolian transport on the ice in winter.

ARK-IX/4 reached to the very heart of Siberian ice production areas. Because of the above described metamorphosis of the sediment-ice mixture with age and drift distance, the expedition provided an unique opportunity to learn about original entrainment mechanisms, and the fate of sediment in ice.

### *Objectives*

The list of objectives pursued during the expedition includes the following:

- observe and document the mode of sediment occurrence in ice;
- compare local observations with those of other parts of the Arctic Ocean;
- assess likely methods of sediment incorporation, and attempt to evaluate the time or distance from the source region;
- use regional sediment distribution to evaluate ice dispersal patterns in the Arctic Ocean;
- collect and process suitable ice samples for sediment load and transport quantification;
- make albedo measurements at sites where the sediment load is quantified;
- collect sediment bulk samples for determination of grain-size, clay mineralogy, sand lithology, microfossils, organic carbon, total carbon content, etc.;
- help establish criteria for the recognition of interglacial (sea-ice rafted) layers in deep-sea sediment cores.

### *Methods of Investigation*

Personal observations, focused on specific objectives listed above, are combined with hourly shipboard ice observations in an attempt to achieve a regional understanding of ice drift patterns and potential sediment sources (see Chapter 6.1). All opportunities for actual sample collection were used. These include 19 ice stations directly from the ship, and 13 helicopter sorties (see table), depending on flight conditions. Where sediment concentrations on the ice permitted, bulk samples were collected by use of spoon, spatula, slurper (when below water), or by chopping and scraping with a spade. Any ice shavings included with sediments were melted and the water decanted. Excessive amounts of mud were condensed aboard ship by panning and sieving, and the residues dried in an oven at 60° C. One-meter long ice cores were commonly taken next to other cores taken for ice biology and physical properties studies. Where cores looked clean, they were split into upper and lower halves, melted, and vacuum filtered through pre-weighed 0.4 µm filter papers. Where they contained distinct, sediment-rich layers, these were often sampled, melted, and filtered separately. Filters and condensed/dried residues were inspected under a binocular microscope. The filters with sediments will be re-weighed in a laboratory in Kiel. Spectral radiation measurements in the visible parts of the spectrum were made, before snow accumulations or low sun angles prevented this, on surfaces of discolored ice or snow. At these sites, ice- or snow-samples of the upper 2-3 cm were also taken, melted, and filtered for later comparisons of sediment content and albedo values. Whenever possible, separate sediment samples were taken with pre-cleaned tools and stored frozen in specially rinsed petri-dishes for studies of anthropogenic pollutants (PCB, DDT, etc.). Small subsamples were also collected for clay-mineralogical studies.

### *Preliminary Results*

Sample analyses can not be performed aboard ship, and therefore the following presents only some general impressions and discusses the types of data collected during the cruise.

With the small footprint of individual ice observations shifting slowly along the cruise track (Fig. 2-2) relative to the rapid advance of the summer melt cycle, a synoptic view of dirty ice is not achieved. In fact, ten short days observing Barents Sea ice during the climax of the surface melt season, followed by a long period of observations in the Laptev Sea with a thickening snow cover, provide a distorted or unrealistic view of relative sediment load in the large study area. In the Barents Sea, observers commonly reported 30 % of the ice as dirty. In the Laptev Sea, with frozen melt puddles and a complete snow cover, observed areas of dirty ice were reduced to only a few percent. Yet, when dirty ice was identified by low-flying helicopter, the volumes of sediment collected per site were relatively large in the Laptev Sea.

At 19 stations, sediments in sea ice were studied by walking onto the ice directly from the ship. Another 13 ice stations were chosen from the helicopter. The ship-board stations are somewhat random, since they are chosen largely by water depth, while helicopter stations can be more selective, thereby improving the chances for collecting sediment bulk samples. Sixteen such samples, ranging to as large as 1 kg per site, were collected. At 10 of these sites, separate samples for PCB analyses were also taken. At 31 sites, a total of 105 ice samples were taken for quantification of the sediment load by melting and filtration. Usually at least two such samples, but ranging to as many as 14 per station, were processed aboard ship (Table 6.5-1). At stations, where numerous samples were processed, these were done for the purpose of comparisons with parallel studies of ice physical properties, such as ice crystal fabric. Albedo measurements were made at 10 stations, usually on several different sites per floe, with emphasis on areas discolored by sediments. At numerous sites, duplicate readings were made with different techniques for comparisons (see Chapter 6.2). These readings will later be related to sediment concentrations per liter of meltwater. Only two sets of measurements were made after August 21 because of the new snow cover.

From ca. 100 ml cuts of numerous sediment bulk samples, a tablespoon-size sand-fraction was condensed by washing and sieving. Under a binocular microscope, these coarse fractions were found to consist of apparently well sorted, fine quartz sand. There were no individual coarser clasts. Most quartz grains were angular to subangular in shape. Some diatoms were seen in these coarse fractions on cursory examination, but neither foraminifera nor ostracodes.

### *Discussion*

The untrained human eye can rather easily recognize dirty ice without snow cover, and satellites recording in the visible part of the spectrum allow delineations of dirty ice on scales of over thirty thousand square kilometers per scene. The observations carried out aboard RV *Polarstern* are not supported by such large scale, synoptic views, because LANDSAT-4 unfortunately was shut down several months before the cruise, while LANDSAT-6 is still not operational. In this writer's opinion, future studies of dirty ice should no longer be carried out without the aid by synoptic views from satellites, because an accurate distribution of sediments can not be obtained.

The search of clues for sediment entrainment mechanisms revealed the following. A thin, even surface dust cover was not observed on first-year ice, not even at the three coastal sites visited, indicating that eolian transport from land to sea is

Station	Filtered samples	Bulk samples	Clay minerals	PCB	Alb.	Notes
2241	2	x	x	x	x	
2251	4	x	-	-	-	
2271	3	x	x	x	x	
2281	8	x	x	x	x	
2291	14	x	x	x	x	
2301	1	-	-	-	x	
2311	3	x	x	-	x	
2321	4	x	x	-	-	
2332	3	x	x	x	x	helo
2381	2	-	-	-	-	helo
2391	3	-	-	-	-	helo
2401	3	x	x	x	x	helo
2461	3	-	-	-	-	
2491	5	-	-	-	-	helo
2501	3	x	-	-	-	helo
2511	2	-	-	-	-	
2512	2	x	x	x	-	helo
2521	3	-	-	-	-	helo
2531	2	x	x	x	x	
2541	2	-	-	-	-	
2551	2	-	-	-	-	
2552	-	-	-	-	-	
2561	2	-	-	-	-	
2571	2	x	-	-	-	
2581	10	x	x	x	-	helo
2582	4	x	x	-	-	helo
2583	2	-	-	-	-	
2601	2	-	-	-	-	
2611	9	x	x	x	-	helo
2631	2	-	-	-	-	helo
2641	2	-	-	-	-	

**Table 6.5-1:** Station list of samples for "dirty ice" investigations; x = sample collected or present, helo = helicopter station.

insignificant overall. No evidence was seen in the dirty ice for bottom adfreezing of sediment in shallow water, or for slumping from coastal sites. Most important for the Laptev Sea, dominated by water and sediment supply from several large rivers, is the fact that no distinct layers that can be attributed to deposition by flood waters, were seen on first-

year ice. In particular, the easily identifiable freshwater ice mapped off the eastern Lena Delta by the 1992 ESARE study was not seen during the present expedition. This suggests that the ice that may become flooded by the river melts in place before incorporation into the Transpolar Drift. However, ample evidence for suspension freezing in form of turbid ice was seen. Strata of turbid ice sometimes occurred in complex patterns of short layers intersecting at acute angles, where individual layers had been partly condensed by surface melting. Such sediment occurrences therefore

indicate that the ice had survived one melt season and then was compressed into ridges.

The stations with enough sediment for collecting bulk samples generally contained a mixture of silt and clay. Except for wooden logs, no clasts coarser than fine sand were found in careful searches of ice floes. One 200x300 m diameter floe was an exception. This undulating floe was discolored in patches of several meter diameter, occurring both adjacent to as well as on the floors of meltwater ponds. Sampling at five sites on this floe, including pond floors, clean, medium-grained sand was collected, without any admixture of finer particles. The meltwater from ice scrapings and the sediment/water mixture sucked off puddle floors was clear. We have presently no explanation of the setting nor of the mechanism of entrainment for this clean sand. All samples will have to be studied carefully for any microfossils that give clues as to the environment of entrainment.

#### 6.6 Distribution, Structure and Hydrography of Surface Melt Puddles (Hajo Eicken, Vitali Alexandrov, Rolf Gradinger, Gennady Ilyin, Boris Ivanov, Anna Luchetta, Thomas Martin, Kristina Olsson, Erk Reimnitz, Regina Pác, Paola Poniz and Jürgen Weissenberger)

During the summer months, a large fraction of the Arctic sea-ice surface is covered by meltwater pools. These melt puddles are of importance because they

- greatly affect the surface energy balance, due to the significant lowering of the albedo and the storage of latent heat which delays growth of the multi-year ice cover during fall freeze-up;
- influence the mass- and freshwater-balance of Arctic sea ice, as they trap low-salinity meltwater originating in part from melted snow;
- modify the surface roughness of multi-year sea ice by redistributing mass into topographic depressions and by deepening these;
- may represent a previously disregarded biological habitat, with unique abiotic conditions regarding salinity and irradiance, and
- modify the sea-ice signature as observed from remote sensing instruments on-board satellites.

Despite their importance, melt puddles have not been studied in any detail as of yet, excepting some work carried out on the mass balance of puddles at drifting stations and interpretation of remote-sensing data. Investigations made during the ARCTIC'91 cruise prompted us to carry out comprehensive measurements on puddles, mainly before freeze-up in the area off Svalbard and Franz Josef Land.

In total 44 puddles were studied during the cruise (eight in the Laptev Sea). Field measurements included depth profiles at 0.5 m spacing, augmented by thickness drilling and coring of the underlying ice in selected cases. At several sites, temperature and salinity profiles were obtained in order to obtain information about the stratification of puddles. Later during the season, the thickness of the puddle-ice cover was measured. Furthermore, total albedo was measured as a function of puddle depth and other parameters at a larger number of sites (see Chapter 6.2). At selected sites, spectral albedos were obtained with two different instruments.

Water samples were obtained from different depths and were analysed onboard for salinity, pH, nutrients, total carbonate and oxygen (for methodology of the latter three parameters refer to Chapter 5.2). Furthermore, samples were filtered for determination of chlorophyll-a, augmented by cell counts. Additional samples were taken for stable isotope analysis ( $^{18}\text{O}$ ) at the Alfred Wegener Institute. Sediment samples were obtained from cryoconite holes and bottom layers in puddles where present.

To obtain an estimate of distribution, areal coverage and sizes of melt puddles, a video camera was mounted on the helicopter looking vertically downward. A total of six flights carried out in combination with Line-Scan-Camera recordings (see Chapter 4.3) will be suited for analysis, comprising digitizing of frames obtained along the flight track with subsequent application of semi-automated image-processing techniques.

The results of the depth measurements (total of 427 data points) are shown in Figure 6.6-1. Here, a distinction has been made between clean puddles and those with a sediment-covered floor or with cryoconite holes. Clean puddles have an average depth of 0.22 m (standard deviation 0.12 m), while for dirty puddles this amounts to 0.44 m (standard deviation 0.18 m). This discrepancy in puddle depth is also evident from the frequency distribution of depths shown in Figure 6.6-1. Further data analysis in conjunction with thermodynamic modelling studies will have to establish whether these depth differences are due the different amounts of heat absorbed by clean and dirty ice within one summer season, or whether these are a result of sequential deepening during successive years. Remarkable is the low

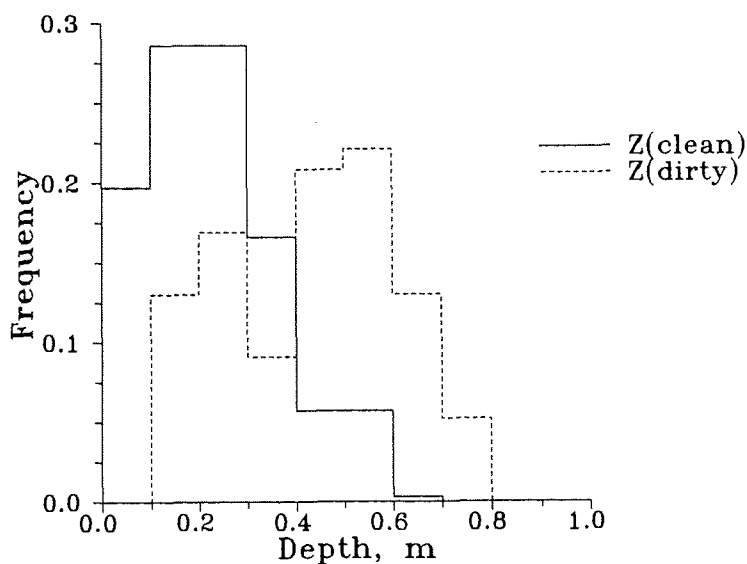


**Fig. 6.6-1:** Frequency distribution of measured melt puddle depths. Solid line for 350 measurements in clean puddle areas; dashed line for 77 measurements in dirty puddles and cryoconite holes.

standard deviation exhibited by depth measurements made within individual puddles and associated cryoconite holes, indicating the importance of solar radiation in controlling puddle depths. Analysis of ice thickness profiles (see Chapter 6.3) and airborne video imagery will provide additional information on the genesis and evolution of puddles. In this context the albedo measurements for puddles of different depths are also of importance.

A summary of hydrochemical measurements relating to melt puddles is given in Table 6.6-1. While salinities mostly range below 1 ‰, maximum values are close to

Depth	(m)	0.25
Salinity	(‰)	2.9
pH		7.0
Total carbonate	( $\mu\text{mol/kg-seawater}$ )	48 (computed from all measurements for an average salinity of 2.9 ‰)
Dissolved oxygen	(ml/l)	9.58
Nitrate	( $\mu\text{mol/l}$ )	0.43
Phosphate	( $\mu\text{mol/l}$ )	0.13
Silicate	( $\mu\text{mol/l}$ )	2.0

**Table 6.6-1:** Average parameters determined for melt puddles

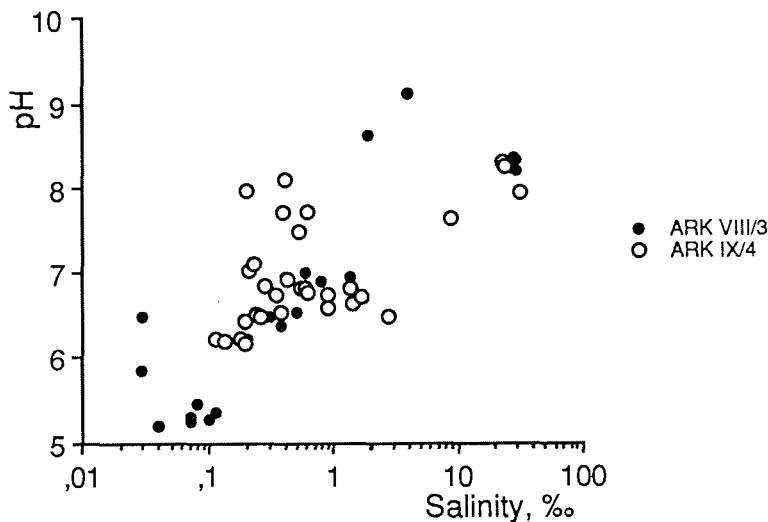


**Figure 6.6-2:** Scatterplot of salinity vs. pH of water samples drawn from melt puddles. Circles are measurements made during ARK-IX/4, dots are measurements from ARK-VIII/3 (ARCTIC'91).

those for seawater. The pH-salinity scatterplot shown in Figure 6.6-2 illustrates that "pure" meltwater puddles display salinities near 0.1 ‰ and are acidic in nature. With increasing fractions of brine or entrained seawater data points extend further towards the other end member with salinities around 30 ‰ and a pH of roughly 8.2. Salinity

and temperature profiles of saline puddles in the Franz Joseph Land area indicate a pronounced stratification, with temperatures mostly few tenths above 0° C. Nutrient concentrations (determined according to the methods outlined in chapter 5.1.3) in puddle water are low, yet not as low as to be expected for simple dilution of seawater. Silica in particular appears to be remineralized partly from frustules, partly from sediment inclusions. A preliminary analysis of total carbonate measurements (for measurement technique refer to chapter 5.1.3) indicates that for most samples total carbonate increases in proportion with salinity, with maximum values just above 2000  $\mu$  mole / kg seawater. Oxygen is essentially at or close to saturation levels.

Regarding the biological studies, first qualitative microscopical observations indicate that bacteria and auto- and heterotrophic flagellates occurred in melt puddles with salinities below 3 ‰. Detailed analyses will include determination of species abundances and taxonomic studies of the plankton species found within puddles.

Further data analysis will focus on determination of areal coverage for better estimates of the role of puddles for the surface energy balance and to obtain puddle volumes as an important parameter in the mass balance of sea ice. The assessment of the ecological importance of melt puddles also requires a more thorough characterisation of the environmental parameters and a biological inventory of puddles.

#### 6.7 Iceberg Observations (Hajo Eicken, Vitali Alexandrov, Vladimir Bogdanov, Thomas Martin, Erk Reimnitz and Sergey Syrtsov)

Greenland and several islands of the high Arctic are covered by ice caps or extended mountain glaciers. Areas where these reach sealevel may be a source of icebergs that calve and subsequently drift within the Arctic Basin and the Nordic Seas. Iceberg production is of utmost importance in the mass-balance of polar ice caps as a major loss term next to surface melting. The geological importance of icebergs derives from the inclusion and dispersal of coarser clastic material, strongly affecting sediment lithologies of glacial periods. Furthermore, the sediments on the shallow shelf are reworked intensively as a result of iceberg plowing and scouring (see Chapter 8.1). While mass-balance data of glaciers and ice caps in the North American Arctic, Greenland, Svalbard and Franz Josef Land have been collected for some time, comparatively little is known about the glaciology of Siberian Islands, in particular the Severnaya Zemlya islands. Consequently, observations on the distribution of icebergs in the Franz Josef Land area and the Laptev Sea were carried out during cruise ARK-IX/4 from ship and helicopter with additional, most valuable data provided by the INTAARI side-looking airborne radar (SLAR) surveys.

The first icebergs were observed off the coast of Prinz Georg Land (Franz Josef Land) on August 23. All bergs counted were identified both visually and with the ship's radar. In total, 50 bergs, bergy bits and growlers could be identified. Maximum diameters (determined by radar and goniometer) ranged below 100 m, with maximum freeboard less than 10 m. Most bergs appeared to be grounded in shallow water, originating from Peary Glacier and other more southerly outlets. While some bergs displayed flat surfaces, most appeared with eroded or slanted tops and steep sidewalls.

During the transect to the Laptev Sea a tabular iceberg was observed in ice-free waters on August 24 at 77° 08' N / 75° 42' E. Radar and sextant measurements indicated a diameter of 150 m across and 15 m height above sealevel. The top appeared completely flat, no sediment or other conspicuous features were evident. Based on a Russian bathymetric chart, the berg might have been grounded on the flank of a shoal rising to 90 m waterdepth.

In the Laptev Sea the first icebergs and bergy bits were observed during a helicopter flight east of Vilkitski Strait on August 29. This group of 15 bergs appeared to be grounded in waterdepths between 50 to 20 m northeast of Maly Taymyr Island. These bergs are thought to have drifted from source areas to the North and subsequently grounded with decreasing water depth. Most bergs ranged between 30 and 100 m in diameter, with two roughly 150 and 250 m across. Measurements aided by the helicopter radar altimeter indicated maximum heights of 15 to 20 m above sealevel. While some smaller bergs appeared to have partially capsized and eroded to some degree, the larger ones displayed a flat shape, with rounded pinnacles rising few meters above the average height. The larger bergs exhibited a wake of smaller floes and open water to the southeast, with ice piling up on some bergs at the northwestern end. Sediment inclusions were visible neither at the top surface nor within the side walls.

A second group of six bergs and bergy bits was observed at 79°10.73' N / 123° 05.03' E on September 12 from the ship and was visited by helicopter for ground observations and sampling. The largest berg was roughly 40-50 m in diameter, with a cliff of 9 m height. Two bergy bits were of intermediate size (5-7 m height, 25-30 m diameter), the other three were 20 m in diameter at maximum. Three bergs were of caldera-type with a meltwater puddle in the center. The three bergs visited showed a distinct stratification, with darker layers of few cm thickness separating brighter layers. Layer thicknesses were roughly 0.2 m. All bergs were firmly engulfed by sea ice with no evidence of strong pressure on any one particular side. In some places a moat with a frozen fresh or seawater puddle was developed. In the largest berg, a core was drilled to approximately 3 m depth in a location where solar heating of the ice was suspected to be minimal due to shading. As in all other bergs, the surface at this location was covered by firn of several decimeters thickness. Sediment or other particulate inclusions were not found anywhere on the bergs. Two more bergy bits were sighted within 70 km of this location. Further iceberg sightings were reported by the *Ivan Kireyev* from the southern and southeastern Laptev Sea (KASSENS pers. comm.).

In order to obtain a better estimate of the distribution and size of bergs, INTAARI SLAR flights No.3 and 4 were routed so as to achieve maximum coverage in the likely source areas on the eastern side of the Severnaya Zemlya islands (see also chapter 4.1). Evaluation of the radar flights allowed for identification of two major source areas of icebergs in the archipelago. The first is an ice tongue extending into Matussevich Fiord on October Revolution Island, which has been described in earlier reports by Russian and international researchers (see Figure 6.3-1 for location). In addition, an ice stream ending as an ice tongue in Red Army Strait separating the northernmost Komsomolets Island from October Revolution Island could be identified. First estimates indicate that large tabular icebergs of several hundred meters to more than 1 km diameter are produced at these two sites.

An evaluation of radarflight No.3 covering the eastern coast of the archipelago with a resolution of 20 by 40 m demonstrated that icebergs down to roughly 75-100 m diameter can be identified in the radar images. The distinguishing characteristics were size and shape, high radar backscatter as compared to wet, puddled sea ice, and a distinct high return from the steep, high side wall facing the radar beam with a corresponding shadow on the opposite side (a typical radar image of a group of bergs is shown in Chapter 4.1, Fig. 4.1-4). Two large bergs of more than 100 m diameter seen during a helicopter flight could also be identified on the radar images as a means of cross-checking. Along the entire track of flight No.3, a total of 259 ice

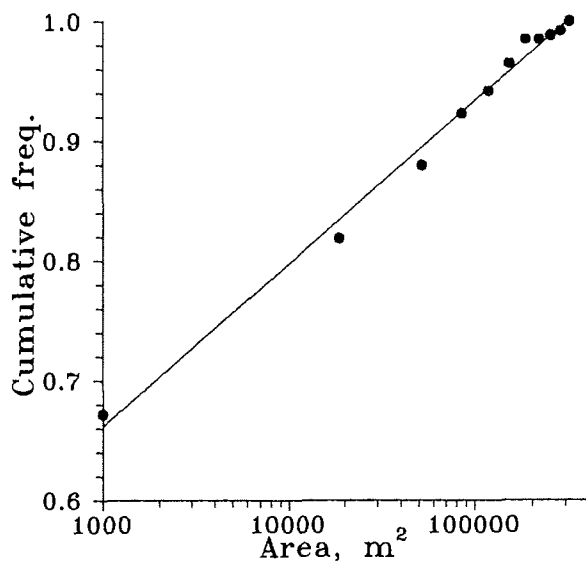


**Figure 6.7-1:** Size distribution of icebergs identified in INTAARI flight No.3 along the eastern coast of the Severnaya Zemlya islands.

bergs could be identified to a high degree of confidence. On average these bergs were 25,000 m<sup>2</sup> in size (standard deviation 53,000 m<sup>2</sup>). The largest bergs observed outside of the Strait and Fjord areas were roughly 800 m in diameter. Figure 6.7-1 shows the frequency distribution of iceberg sizes on a semi-logarithmic plot. At this preliminary stage there is some indication that berg sizes are exponentially distributed, as to be expected in theory for a set of sequentially fractured objects. Most bergs observed during this flight were located in an area between 80° 25' N / 98° 20' E and 80° 10' N / 100° 40' E.

Future work will focus on the observation of iceberg drift patterns as compared to sea-ice drift aided through analysis of ERS-1 satellite imagery. Possibly synthetic aperture radar data along with AVHRR imagery can also be used to obtain a better estimate of the present-day glaciological status of the Severnaya Zemlya ice caps. The importance of icebergs for the reworking of surface sediments and shallow seafloor morphology requires a combined study of iceberg-distribution data and (sub)-bottom profiling.

## 7 BIOLOGICAL INVESTIGATIONS

The Arctic Ocean with its deep basins is to a large extent permanently ice-covered. Accordingly, its deep-sea biota are dependent on lateral import of organic matter. The vast marginal seas surrounding the basins, including the terrestrial river discharge, are regarded the main sources of this importation. Other sources may be the water masses advected from the North Atlantic. An until now unknown amount of organic material may be derived by ice-related algae.

The investigation of sources, fluxes and effects of organic matter in the strong depths gradients of the continental slope areas form a main guideline of our research. Therefore, we planned and realized our sampling program mainly along transects in the transitional zones from the offshore parts of the shelves down the continental slopes to the deep sea. By comparison of the Barents shelf slope, strongly influenced by Atlantic water, and the more continentally impacted Laptev shelf slope, a first evaluation of the relative contributions of these very differing marginal seas for the life and the actual sedimentary regime in the central Arctic Ocean will be attempted.

Thus, processes and structures related to the intensity of the (direct) pelago-benthic coupling and to the significance of lateral advection of organic matter form important targets of the biological work during ARK-IX/4.

The Arctic ecosystems are regarded to be very sensitive to the assumed man-induced climatic changes. After the melting of the glacial ice shields, the comparatively deep Barents Sea allowed a quick biological colonization and "stabilization" of its biocenoses under the favourable Atlantic water influences. The Laptev Sea ecosystem, however, seems until now still to be in an immature, unbalanced stage of development, for which the existence of submarine bottom and the ongoing coastal and shelf floor erosion are indicators. During the major part of the year, this sea is almost totally covered by pack and fast ice. The flora and fauna of such an environment are expected to be very variable. Biological control will be less important than the strong physical impact.

Therefore, biological research during ARK-IX/4 will contribute not only to the understanding of the above mentioned ecological processes (fluxes of organic matter), but also of the biogeographical differences between Barents and Laptev Seas. The planned description of structural features of plankton and benthos communities, together with the identification of the now existing distribution limits of populations, will provide baselines for the understanding and prediction of possible future ecosystem changes.

### 7.1 Phytoplankton and Particle Flux (Karin Springer)

The main topic of the phytoplankton programme during ARK-IX/4 was the investigation of the distribution of phytoplankton and its relation to hydrographical, chemical and other environmental conditions on the Eurasian shelves. In its major aspects this programme continues the investigations in the northwestern Barents Sea in 1991 (*Polarstern* cruise ARK-VIII/2).

The major questions of interest were the investigation of:

- processes of the benthic-pelagic coupling, i.e. the export of particulate organic matter from the euphotic zone to the benthos. Sedimentation patterns together with the results of microbial activity measurements on the respective sediments will give additional information about variations on a longer time scale;
- regional trends in the sources of particulate organic matter, its fluxes on the continental shelves and down the slopes and a comparison between the Barents Sea, which is influenced by Atlantic water and the Laptev Sea, influenced by important riverine input;
- community analyses, i.e. the investigation of species abundances and community composition in the Arctic Ocean;
- kryo-pelagic coupling, i.e. the exchange of organic matter between ice and water.

Chlorophyll-a *in vivo* fluorescence was measured continuously by a flow-through fluorometer, which was connected to the ship's seawater pumping system with the intake pipe located approximately 9 m below the sea surface. The data were recorded on the POLDEV/POLDAT (POLArstern DATen) System.

Water was sampled with the rosette sampling system attached to the CTD (Neil Brown). Subsamples were obtained from the surface layer (5-10 m) at around 10 different depths down to 300 m water depth at almost every ship's station for the following parameters:

- Species abundance: Watersamples (ca. 200 ml) were fixed with buffered formalin (Hexamethylenetetramin) at a final concentration of about 1 % and stored in brown glass bottles. The composition of species and their identifications will be carried out in the home laboratory by Utermöhl microscopy.
- Chlorophyll-a and phaeopigments: 3 l of water were filtered on Whatman GF/C glass-fibre filters. The concentrations of chlorophyll-a and phaeopigments were measured on board with a Turner fluorometer.
- Particulate organic carbon and nitrogen: 3-4 l of water were filtered on precombusted Whatman GF/C glass-fibre filters and stored deepfrozen for later analyses in the home laboratory.

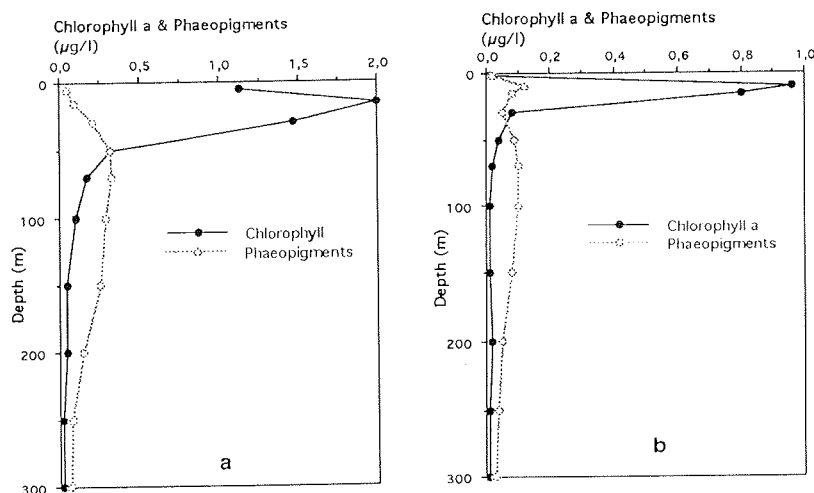


**Fig. 7.1-1:** Vertical distribution of plant pigments. (a) Station 11 (Transect A, 1566 m); (b) Station 25 (Transect C, 514 m).

- Biogenic silica: 2 l of water were filtered on Millipore cellulose acetate filters and stored deepfrozen for later analyses in the home laboratory.
- Seston: approx. 2 l of water were filtered on preweighed GF/C filters and stored deepfrozen for later analyses in the home laboratory.

Light attenuation was measured as Secchi depth at every station when weather and light conditions allowed meaningful estimations.

### *Preliminary Results*

**Northern Barents Sea:** The intensity of ice coverage along the Transects A and C varied between 8/10 and 10/10. Mean chlorophyll-a values of the 5 m surface layer were  $0.76 \mu\text{g l}^{-1}$  and  $0.41 \mu\text{g l}^{-1}$ , respectively. A maximum of  $2.0 \mu\text{g l}^{-1}$  was observed at Station 11 (Transect A, 1566 m) in 15 m water depth (Fig. 7.1-1a). At all other stations of both transects chlorophyll-a was less than  $1.0 \mu\text{g l}^{-1}$ . At Station 25 (Transect C, 514 m) the chlorophyll-a maximum was  $0.96 \mu\text{g l}^{-1}$  in 10 m water depth (Fig. 7.1-1b). At most stations higher phaeopigments than chlorophyll-a concentrations were measured below the 30-50 m layer, indicating degraded plant material.

**Laptev Sea:** The easternmost Transect H was situated in open water, close to the ice edge in about 5 nm distance. Chlorophyll values were comparatively high to all other transects, which were ice-covered during the cruise. The highest chlorophyll-a concentration of all stations was measured at Station 38 (Transect H, 960 m) with a maximum of  $4.25 \mu\text{g l}^{-1}$  in a depth of 20 m (Fig. 7.1-2a). Also at stations 39 (536 m), 40 (223 m) and 42 (61 m) of Transect H chlorophyll-a concentrations in the surface layer (2-20 m) reached values higher than  $1.3 \mu\text{g l}^{-1}$  and decreased sharply below the maximum to values less than  $0.5 \mu\text{g l}^{-1}$ .

In these layers, especially at Station 38, nutrients ( $\text{NO}_3$ ,  $\text{PO}_4$ ) were totally depleted (see chapter 5.2.1), indicating a bloom event. The concentrations of phaeopigments never exceeded those of chlorophyll-a at all water depths.

On Transect G the highest chlorophyll-a values were measured at Stations 47 (996 m) and 48 (516 m) with a maximum of  $1.03 \mu\text{g l}^{-1}$  at a water depth of 10 m at Station 48 (Fig. 7.1-2b). No other station on the Transects G, F and E reached chlorophyll-a values higher than  $1 \mu\text{g l}^{-1}$ .

Both western Transects F and E of the Laptev Sea show a very low level of chlorophyll-a concentration with mean values of  $0.1 \mu\text{g l}^{-1}$  in the 10 m surface layer. On both transects the ice coverage was about 9/10 to 10/10. The concentrations of phaeopigments were often slightly higher than those of chlorophyll-a below the depth of about 30-50 m. Typical profiles of each of the Transects F and E are given in the Figures 7.1-3a and -3b. An overview of the distribution of chlorophyll-a along the four Transects E, F, G and H in the Laptev Sea is given in Figure 7.1-4.

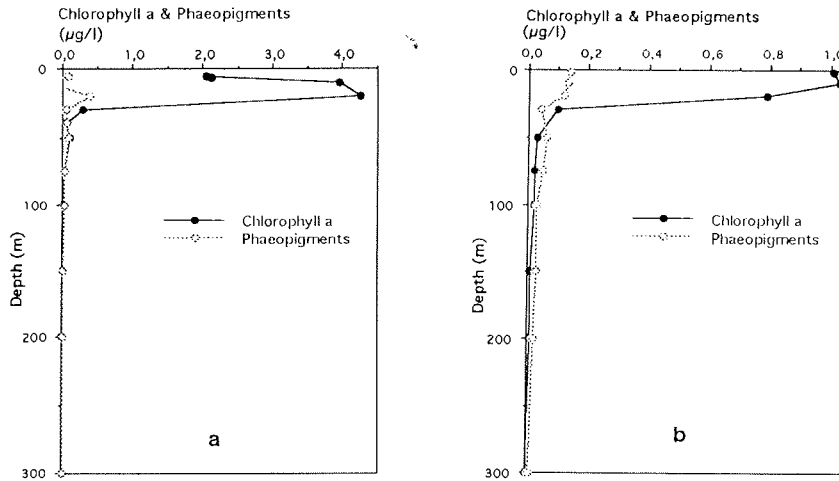


Fig. 7.1-2: Vertical distribution of plant pigments. (a) Station 38 (Transect H, 960 m) with highest chlorophyll-a concentration of all stations during ARK-IX/4. (b) Station 48 (Transect G, 516 m) with highest chlorophyll-a concentrations of Transect G.

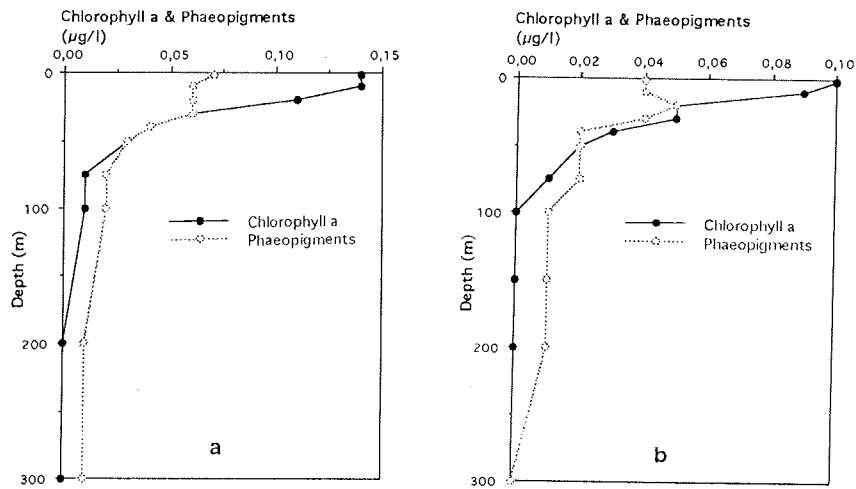
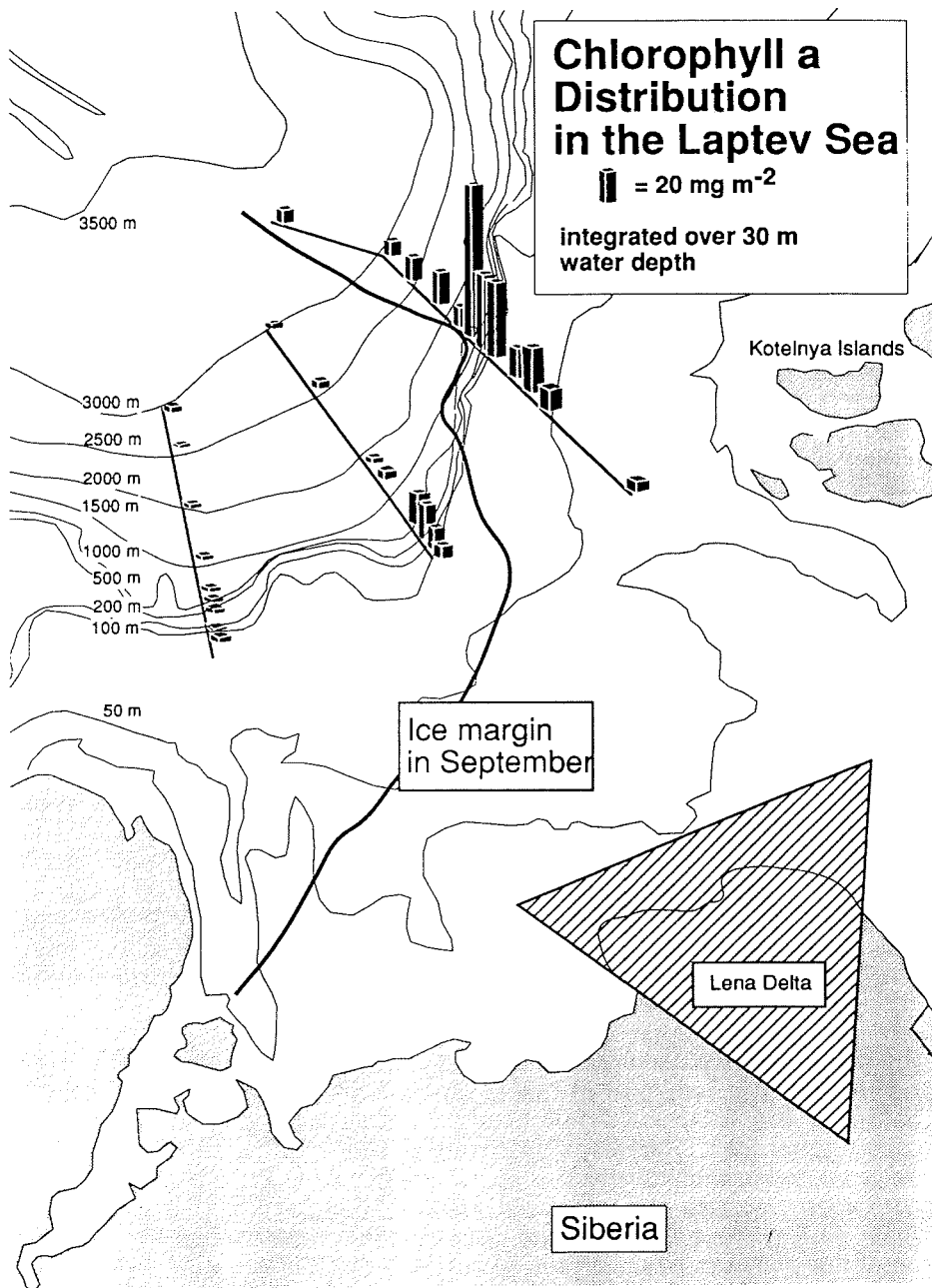


Fig. 7.1-3: Vertical distribution of plant pigments. (a) Station 62 (Transect F, 545 m). (b) Station 69 (Transect E, 529 m).



**Fig. 7.1-4:** Concentration of chlorophyll-a along Transects E, F, G and H in the Laptev Sea. The values given in mg m<sup>-2</sup> were integrated over the upper 30 m water depth.

#### 7.1.1 Mooring of Sediment Trap (Antje Boetius)

Organic matter that settles from the euphotic zone is the main energy source for the abyss. In order to estimate the flux of particles to the seafloor with its seasonal variabilities in quality and quantity, a sediment trap was deployed for one year at a mooring south of Spitsbergen at 76° 20' N and 15° E at 300 m water depth (see section 5.1.4). The trap was programmed for a time resolution of 2-4 weeks and positioned at a depth of 150 m. This continues the investigations of EPOS II (ARK-VIII/2 in 1991), studying the different hydrographic areas of the Barents Sea shelf and continental slope.

#### 7.2 Distribution of Zooplankton and Community Structure (Hinrich Hanssen and Sergey Timofeev)

Ice drift stations carried out since the 1930's showed that zooplankton development in the central Arctic Ocean is restricted mainly to the short period of primary production during the Arctic summer. During this time most of the plankton is concentrated in the upper 200 m of the water column, while in winter biomass values decrease and, after several species descended to greater depth for overwintering, the zooplankton standing stock is distributed more uniformly over a greater depth range.

The employment of ice breaking research vessels permits the investigation of spacial variability in zooplankton biomass and species composition over large areas of the Arctic Ocean in relatively short time.

A severe decrease in zooplankton biomass and increasing importance of bathypelagic species near the surface to the north of the Nansen Basin were the most striking features of the zooplankton investigations carried out during ARK-VII/2 with the RV *Polarstern* in 1987 which covered the entire Nansen Basin from the continental slope to its northern boundary, the Gakkel Ridge.

The international Arctic Ocean expedition ARCTIC'91 which was carried out jointly by the Swedish ice breaker *Oden*, the U.S. Coast Guard icebreaker *Polar Star* and RV *Polarstern* extended across the north pole and the Lomonosov Ridge into the Makarov Basin and revealed a sharp decrease of zooplankton abundances in the upper 100 m from the continental slope to the north.

The ARK-IX/4 expedition extends the area of investigation to the eastern Barents Sea and the Laptev Sea, one of the large Siberian shelf seas, and allows the comparison of the Atlanticity influenced Barents Sea and the continentally influenced Laptev Sea. The plankton fauna of this area is poorly investigated. Previous planktological studies in this region were mainly restricted to the shallow near shore area. Because of the Organic matter that settles from the euphotic zone, is the main energy input to the central position of the Laptev Sea and its shallow topography the plankton fauna of this region is expected to be influenced less by Atlantic and Pacific waters but by the huge fresh water discharge especially from the Lena River. For these reasons different community structures are expected compared e.g. to the Barents Sea, which is mainly influenced by Atlantic waters.

In recent studies the under-ice habitat appeared to be important for several planktic species in the Arctic, e.g. some abundant copepod species occur in large numbers in the water layer beneath the ice at least by times and are supposed to feed on ice algae. Since it cannot be sampled with the ordinary sampling gear, this habitat is poorly investigated. Also the pelago-benthic coupling in the Laptev Sea is studied, which is supposed to be strong in this extended shallow area.

### Methods

For the investigation of species composition and depth distribution of zooplankton multi-net samples (mesh size 150  $\mu\text{m}$ ) in vertical hauls to a maximum depth of 1500 m were taken on 39 stations (see station list in annex). Bongo nets (200 and 500  $\mu\text{m}$  mesh size) were employed on 37 stations to sample zooplankton from the upper 100 m for investigation of species composition, biomass, grazing rates and for collecting animals for measurements of *in situ* egg production.

A pumping system was used on 16 ice stations to sample the under-ice fauna in two size fractions ( $>200 \mu\text{m}$  and  $>20 \mu\text{m}$ ). For comparison of under-ice and pelagic fauna additional plankton samples of the upper 30 m were taken using a handnet (mesh size 20  $\mu\text{m}$ ) on 29 stations.

The multi-net samples as well as the under-ice and handnet samples were preserved with formalin for further processing (sorting and community analysis) after the cruise. The 200  $\mu\text{m}$  bongo net samples were splitted. One half of each sample was frozen for biomass determination, the other half was preserved in formalin for analysis of species composition.

Specimens of the dominant copepod species were taken out of the 500  $\mu\text{m}$  bongo net samples and used for egg production measurements carried out on board. Additional specimens of the large copepod species were frozen for gut fluorescence measurements that will be done after the cruise.

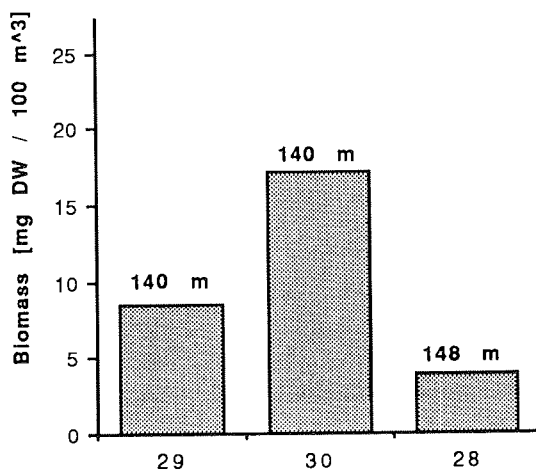


**Fig. 7.2-1:** Zooplankton biomass in Vilkitski Strait at Stations 27/028, 27/029 and 27/030, calculated by determination of displacement volume.

### *Biomass*

While biomass measurements (ash-free dry weight) will be performed after the cruise, a first rough estimation has been made on board by determination of displacement volume calculating wet weight as 1g per ml and dry weight as 10 % of wet weight.

This calculation shows generally low biomass values of 5-10 g 100 m<sup>-3</sup> in the entire area investigated. Only at one station in the centre of Vilkitski Strait (Fig. 7.2-1) and at the shallow stations of the easternmost section in the Laptev Sea (Fig. 7.2-2) higher values of 15-30 g 100 m<sup>-3</sup> were obtained. On this section a sharp decrease of biomass from Station 27/041 (72 m) to Station 27/040 (240 m) was observed while chlorophyll-a content was highest further north on Station 27/038 (982 m).

### *Community Structure with Special Reference to Meroplankton*

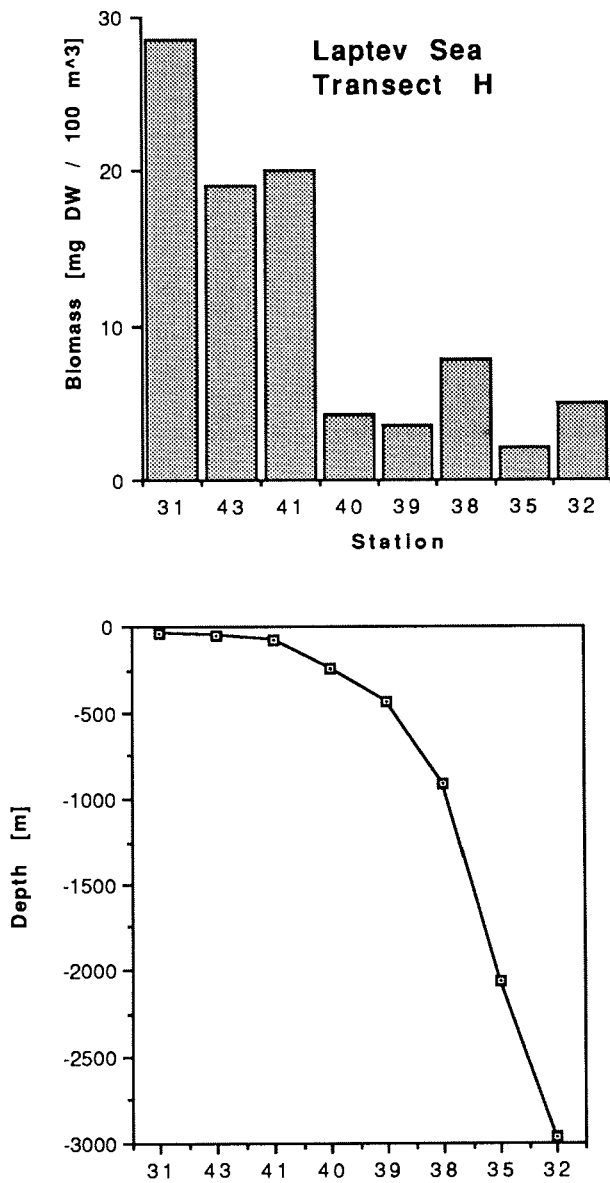
At the biological stations vertical hauls were made using a bongo net with 200 µm mesh gauze from 100 m to the surface. To study the community structure of zooplankton and population structure of the chaetognaths, a total of 36 bongo net hauls were taken in this region.

Copepods were dominant at all stations. Echinoderm larvae, especially ophioplutei, were subdominant at all stations also. The eggs and bipinnaria of the sea stars (asteroidea) were found at the Stations 27/027, 27/028, 27/029, 27/030 and 27/062 only. There is an increase in abundance of the polychaete larvae towards shelf water. But this is valid for the larvae of the families Spionidae and Aphroditidae only, whereas for the larvae of Oweniidae we can see an opposite distribution. In the decapod larvae the late stages of the shrimps *Sabinea septemcarinata* (27/027) and *Pandalus* sp. (27/029) were present (see Chapter 7.4).

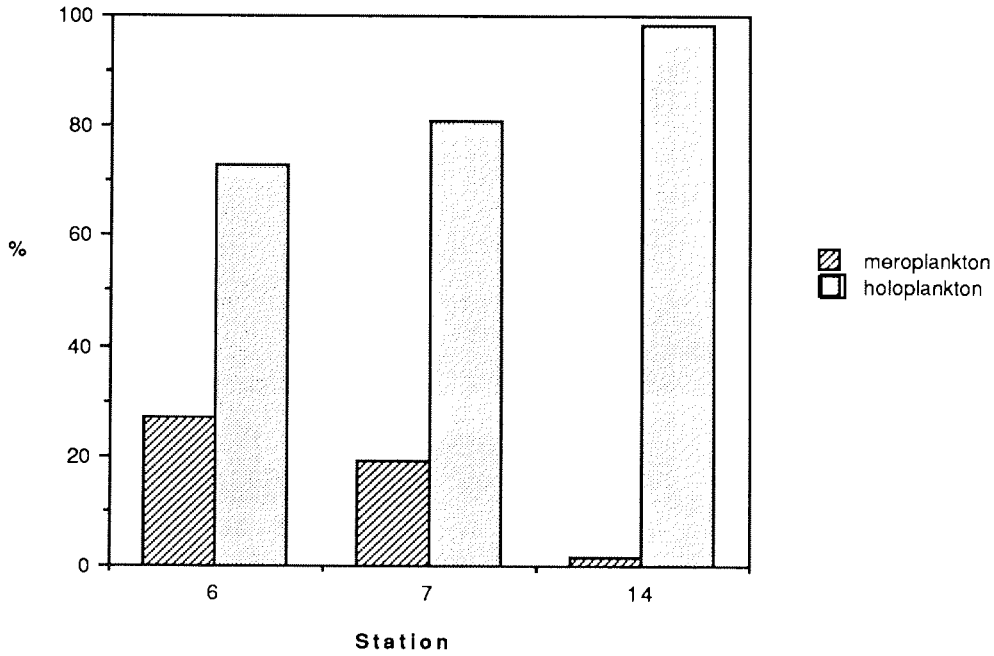
The relative abundance (%) of the holo- and meroplanktonic animals is not constant at the different stations. The greatest significance of the meroplankton was observed at the shelf stations (Fig. 7.2-3). In the Laptev Sea meroplankton was not abundant.

Herbivorous and omnivorous planktonic animals were dominant at all stations, with exception of Station 27/006 where eggs of various animals were most abundant (56 %).

At the Stations 27/006, 27/007, 27/014, 27/027 and in the Vilkitski Strait the nauplii of the parasitic cirripedian crustacean *Peltogaster* spp. (Cirripedia, Rhizocephala) were found. This finding is a prolongation of the area of these animals to the east. The north-easternmost points of their distribution up to now have been off northwestern Spitsbergen and the Murman Coast. By the occurrence of such animals as the euphausiid crustaceans *Meganyctiphanes norvegica*, *Thysanoessa longicaudata*, *Thysanoessa inermis*, the pelagic polychaetes *Tomopteris* spp. and copepods which are infected by the parasitic dinoflagellates *Ellobiopsis* spp., it is confirmed that there is an inflow of Atlantic Water into the Franz Josef Land region, Vilkitski Strait and Laptev Sea.

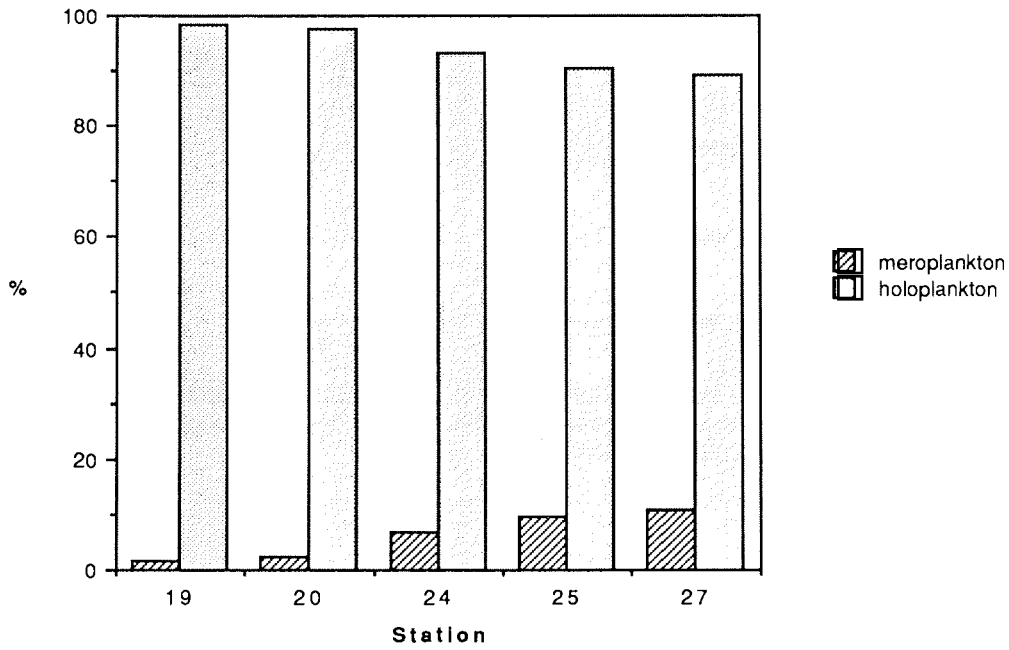


**Fig.7.2-2:** Zooplankton biomass in the eastern Laptev Sea, Transect H, calculated by determination of displacement volume (station numbers are according to the last digits of the complete station number).



**Fig. 7.2-3a:** Relative contribution of holo- and meroplankton to total zooplankton numbers [%]; Transect A, northeast of Svalbard.

**Fig. 7.2-3b:** Relative contribution of holo- and meroplankton to total zooplankton numbers [%]; Transect C, northwest of Franz Josef Land.



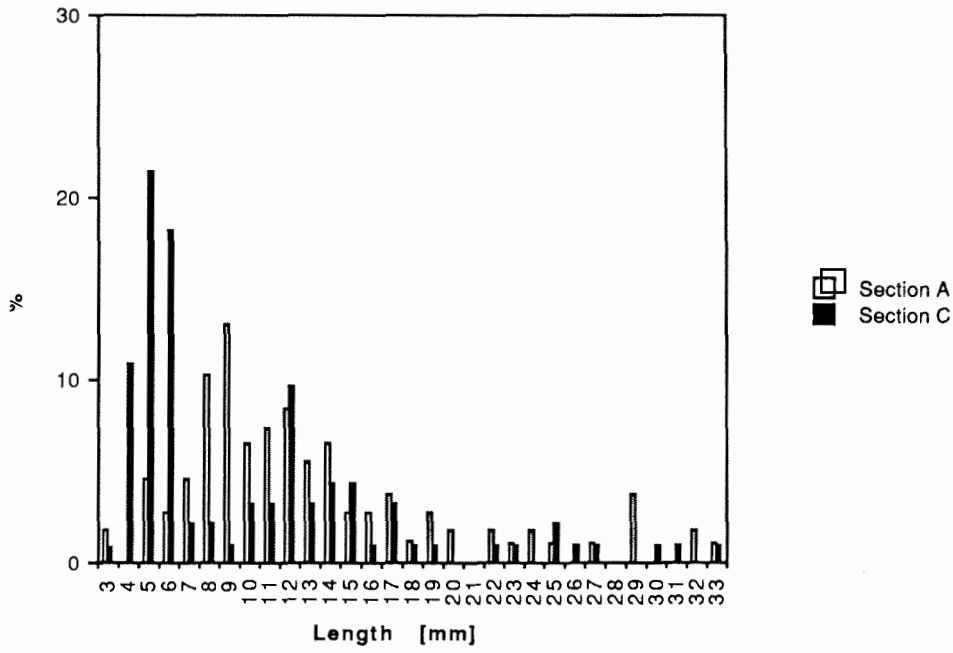
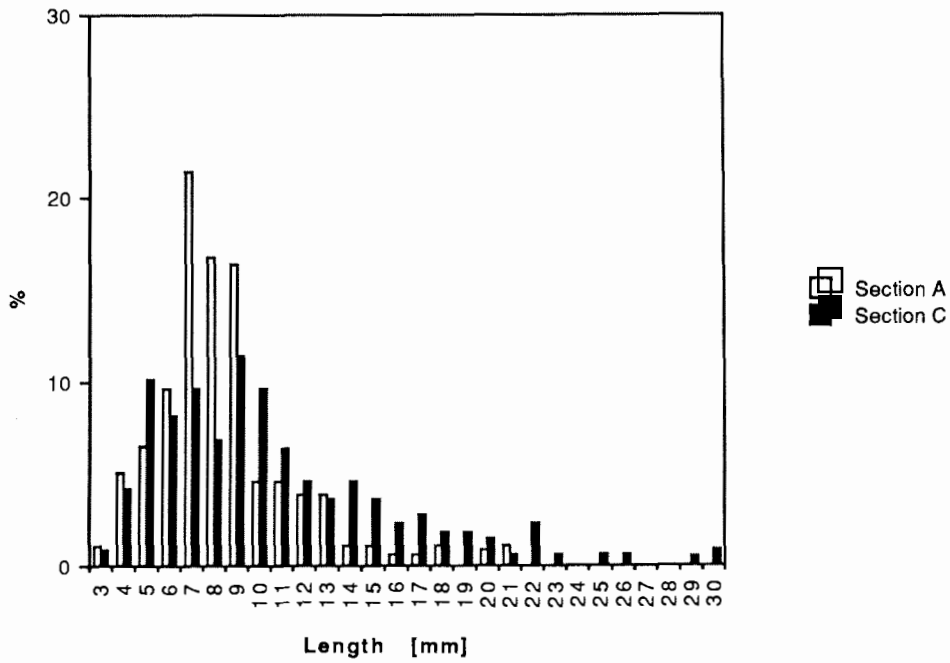


Fig. 7.2-4: Size structure of *Sagitta elegans* in Transect A, off northeast Svalbard and Transect C, northwest of Franz Josef Land.

Fig. 7.2.5: Size structure of *Eukrohnia hamata* in Transect A, off northeast Svalbard and Transect C, northwest of Franz Josef Land.



There are two species of chaetognaths in the investigation area, *Sagitta elegans* and *Eukrohnia hamata*. *Eukrohnia hamata* was dominant at the majority of the stations, but its abundance decreased from the open sea towards the shelf waters. *Sagitta elegans* was discovered in the Vilkitski Strait only. There are differences in the size spectra of these both species of chaetognaths in the different regions. Along the continental slope east of Svalbard only an unimodal size distribution was found. On the continental slope northwest of Franz Josef Land the size structure was more complicated and included two modal classes (Fig. 7.2-4). In the Vilkitski Strait the population of *Sagitta elegans* was dominated of animals with body length of 5 and 20 to 23 mm.

To study the morphological variations of the chaetognaths from the different sea regions 1140 individuals (432 individuals of *Sagitta elegans* and 708 individuals of *Eukrohnia hamata*), were analyzed during this cruise. Both species have no morphological differences in different parts of the Arctic.

### 7.3 Egg Production of the Dominant Copepod Species (Ksenia Kosobokova)

Herbivorous calanoid copepods play a central role in the Arctic marine food web as predominant consumers of phytoplankton. Ecological studies aimed at the investigation of their production require a detailed knowledge of their distribution pattern and life cycle strategies. Studies of egg production will contribute to a better understanding of reproductive physiology, relationship between intensity of spawning and food conditions and to a better understanding of the life cycles of dominant copepod species in whole. Moreover, the egg production is used as a direct measure of secondary production of adult copepods.

#### Methods

Zooplankton for egg production experiments was collected from the upper 100 m water layer by bongo net (mesh size 500  $\mu\text{m}$ ). Egg production experiments were carried out with four copepod species: *Calanus finmarchicus*, *C. glacialis*, *C. hyperboreus* and *Metridia longa*. 25-30 females of each species were sorted out from the samples immediately after capture and were placed in two litre plexiglass cylinders having a mesh (300  $\mu\text{m}$ ) false bottom to separate eggs from females. These were then suspended in 3 l TPX jars containing filtered sea water. Egg production during the first 24 hours was used as a measure of the actual rate in the field (*in situ* egg production rate).

Actual egg production rate was measured at nine stations on the continental slope of the north eastern Barents Sea, at three stations in the Vilkitski Strait, and at 25 stations in the Laptev Sea.

The effect of starvation upon egg laying was studied in *C. glacialis* and *M. longa* for 7 and 10 days. Starvation experiments with *C. glacialis* were carried out in groups of 25-30 females and on individual females. The effect of starvation in *M. longa* was studied on groups of females.

*Preliminary Results*

In the area of the northern continental slope of the Barents Sea the copepods *Calanus finmarchicus* and *C. hyperboreus* dominated in terms of biomass. *Metridia longa* was less abundant. Only a few individuals of *C. glacialis* were found.

*C. hyperboreus* and *C. finmarchicus* did not lay eggs during this study. The state of gonadal maturation of *C. hyperboreus* indicated that all females were unripe. On Transect A, to the northeast of Svalbard, *in situ* egg production of *C. glacialis* was the highest at the Station 27/006 in the shelf area (Fig. 7.3-1 ). At the section C, to the northwest of Franz Josef Land, only *Metridia longa* was laying eggs.

In the Laptev Sea *Calanus glacialis* and *M. longa* dominated the copepod biomass. The biomass of *C. hyperboreus* and *C. finmarchicus* was considerably low compared to the northern slope of the Barents Sea. *C. glacialis* produced eggs at relatively low rates at most stations of the eastern Transect H (Fig. 7.3-2 ) and only at one station of the Transect G. Egg production in *C. glacialis* was clearly positively related to availability of phytoplankton (Fig. 7.3-2). Egg laying of *M. longa* was observed at most stations of Transects H and G located deeper than 100 m (Fig. 7.3-2). All data on egg production of this species both in the area of the northern slope of the Barents Sea and in the Laptev Sea demonstrated low activity of spawning during the studied period. Neither *C. hyperboreus* nor *C. finmarchicus* laid eggs in the Laptev Sea during our study.

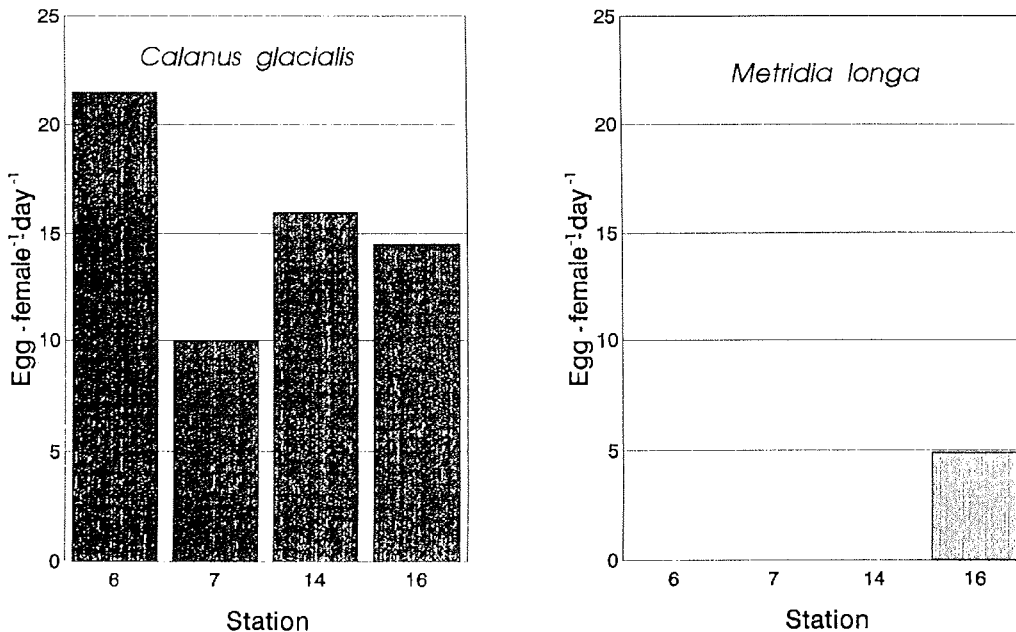


**Fig. 7.3-1:** Transect A, northeast of Svalbard; *in situ* egg production rates of *Calanus glacialis* and *Metridia longa*.

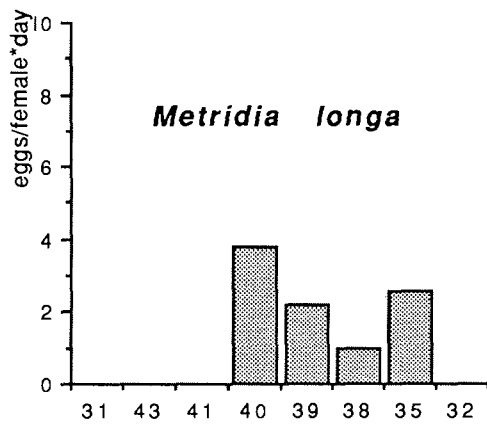
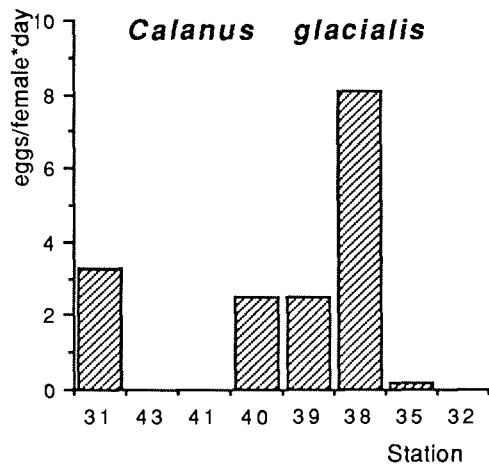
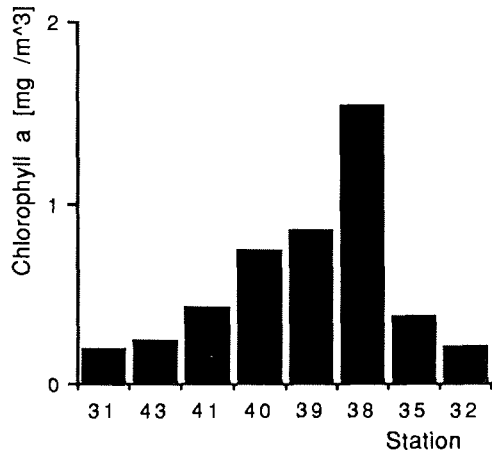


**Fig. 7.3-2:** Laptev Sea, Transect H; Chlorophyll-a content in the upper 50 m water layer and *in situ* egg production rates of *Calanus glacialis* and *Metridia longa*.

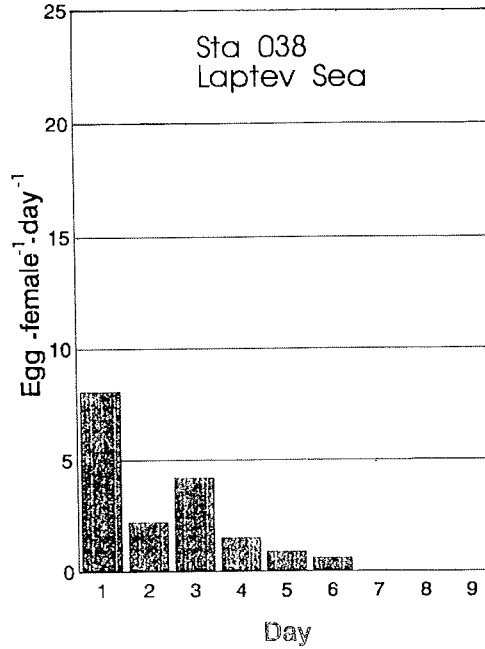
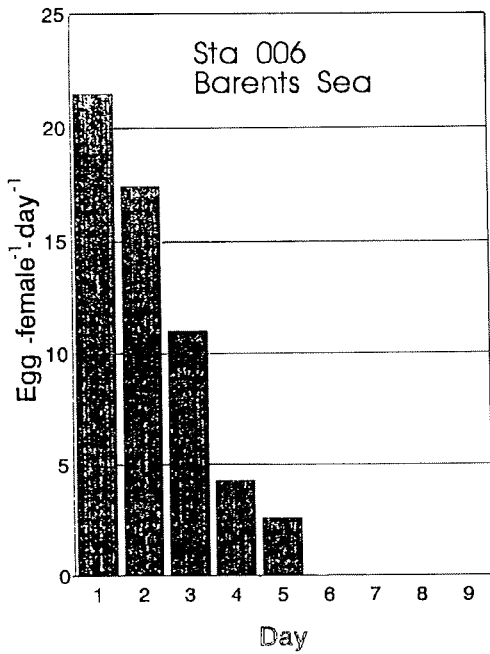
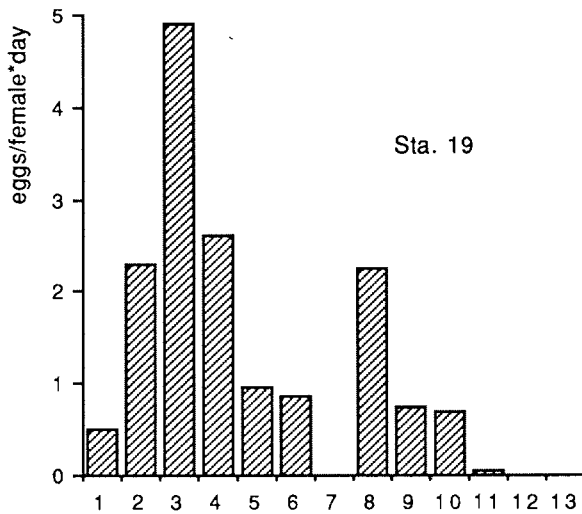


Fig. 7.3-3: Egg production rate of *Calanus glacialis* under starvation conditions.

Fig. 7.3-4: Egg production rate of *Metridia longa* under starvation conditions.



#### Starvation Experiments

An obvious decreasing of egg production rates was observed in *C. glacialis* under starvation conditions. Egg laying ceased completely after 6-7 days of starvation (Fig. 7.3-3). On the contrary *M. longa* demonstrated an increasing of egg production rate during the first days of starvation (Fig. 7.3-4). In most experiments it was at

maximum by the third day before decreasing again. The low levels of egg production during the first days might be due to stress caused by capturing the animals.

#### 7.4 Zoobenthos (Eike Rachor)

Zoobenthos research during ARK-IX/4 comprised meiofauna and macrofauna as well as fishes. Macrofauna, in this case, is defined as those animals which can be retained on a 0.5 mm mesh, when the bottom substrate is sieved. Meiofauna animals, as a rule, are smaller, and include also late larval and other young stages of the macrofauna (temporary meiofauna).

While the macrofauna of inshore and not ice-covered parts of the Eurasian marginal seas has been studied quite extensively especially by Russian scientists, meiofauna research was restricted to very limited areas (like the White Sea). The more offshore, deeper areas of the Laptev Sea, which are normally badly accessible due to nearly permanent pack ice coverage, until now, have been insufficiently studied.

During the discussions between Russian and German biologists preceding the final plannings of ARK-IX/4, it was very much stressed that these insufficiently investigated ice-covered areas deserve a strong research effort as they are of significant importance for the understanding of the relationships of the central Arctic Ocean and its Siberian marginal seas (see HUBERTEN et al. 1993).

During the 1991 expeditions of RV *Polarstern* to the northern Barents Sea continental slope (ARK-VIII/2, EPOS-2) and the central Arctic basins (ARK-VIII/3, ARCTIC'93), macro- and meiofauna were sampled extensively. The macrofauna of the basins appeared to be very poor regarding densities and species numbers (KRÖNCKE 1991). ARK-IX/4 allowed us to continue this kind of research and compare the benthic fauna sampled in 1991 with the fauna at the continental slopes northwest of Franz Josef Land and in the northern Laptev Sea. Moreover, by the zoobenthos sampling on board RV *Ivan Kireev* in the shallower parts of the Laptev Sea, the whole shelf was covered quasi-synoptically, which will allow a better understanding of relationships between the inshore and the very remote deep slope communities.

##### 7.4.1 Meiofauna (Pedro Martinez)

The meiofaunal biocenosis was studied along five transects (two in the Barents Sea and three in the Laptev Sea), in different depths from the shallow water to the deep sea, and also in the Vilkitski Strait. The samples were taken with the Multicorer (BARNETT et al. 1984) at 30 stations (see Annex 10.2). As a rule, four cores with a diameter of 6 cm, were used for a detailed quantitative analysis of meiofaunal abundances and for biomass estimation. For this, a subsample was taken from each core using a minicore that was inserted about 10 cm into the sediment and covered an area of 1.5 cm<sup>2</sup> (e.g. HERMAN & DAHMS 1992). The rest of the each core was collected and fixed separately. A fifth core was not subsampled, but was fixed completely. This core will be used to estimate the meiofaunal diversity of the different stations of the Barents and Laptev Seas and its changes along the transects. At several stations, two additional cores were fixed completely for the special study of young macrofauna in the sediment. Qualitative samples for taxonomical studies were

also taken routinely from a giant box corer, using the uppermost 6 cm sediment of an area of about 1400 cm<sup>2</sup>. For the same purpose, some samples were taken from the multi-box corer and from the remaining sediment of some Agassiz trawls.

All samples were fixed with formol at a final concentration of about 4 %. A subsample of the qualitative samples was kept in a cooling container, at about 0° C, for live observations.

The results will be an approach to understand the poorly known species composition and distribution of Arctic communities. It is also intended to elaborate data about the total biomass of the meiofauna fraction. The use of multivariate analyses will allow to study which biotic and abiotic parameters may influence the species composition and the abundances of species.

Several new species are expected to be found. Detailed descriptions of the new species and phylogenetical analyses of some representative groups will be done. Distribution analyses will allow a better understanding of the zoogeographic regions in the Arctic and to come to some hypotheses about the origin of the Arctic meiofauna.

#### *Preliminary Results*

The meiofauna communities are dominated by Nematoda and Copepoda (Harpacticoida); other taxa as the Plathelminthes, Kinorhyncha, Ostracoda and Tanaidacea play an important role. Amphipoda, Isopoda and temporary meiofauna were also found especially in the shallow water stations. Taxa like the Copepoda Poecilostomatoida and Cyclopoida play a subordinate role. Table 7.4.1-1 shows the total abundances of taxa found at two stations of Transect H in the eastern Laptev Sea, one in shallow waters, the other one in the deep sea. In these stations Nematoda is the most important taxon, with similar abundances in both depths. The total abundances of harpacticoid copepods and of the other found taxa decrease with the depth. This correlates with the decreases of other biotic parameters, e.g., that there is only half the chlorophyll concentration at the deep station as in the shallow

Date:	September 01, 1993	September 03, 1993
Depth:	38 m	3428 m
	Station	Station
Nematoda:	150,000	130,000
Copepoda:	140,000	14,000
Plathelminthes:	9,500	1,500
Kinorhyncha:	8,500	1,700
Ostracoda:	7,500	1,000
Tanaidacea:	1,800	350
Trochophora:	1,400	0
Amphipoda:	700	0

**Table 7.4.1-1:** Abundances of meiofauna taxa (numbers of individuals per m<sup>2</sup>) at two stations of Transect H in the Laptev Sea.

water station. Protein concentration is only 1/8, and the activity of bacteria decreases to 1/10 (Boetius, pers. comm.).

*Harpacticoida (Copepoda) in the Arctic*

There are 47 known harpacticoid families. At least 17 families are present in the samples taken during the ARK-IX/4 expedition. The families Tisbidae (comprising the genera *Zosime*, *Idyella* and *Tisbella*), Orthopsyllidae and Paranannopidae (*Nannopus* and *Paranannopus*), Huntemannidae and Ectinosomatidae play an important role in terms of diversity and biomass in the Arctic harpacticoid biocenosis. Other common families in the study area are Cerviniidae (*Cervinia* and *Herdmannia*), Cletodidae (*Mesocletodes*), Tachidiidae (*Danielsenia*), Harpacticidae (*Harpacticus*) and Canuellidae. Diosaccidae (*Stenhelia*), Laophontidae (*Platychelipus*), Paramesochridae, Ancorabolidae and Ameiridae (Stenocopiinae) were also found. *Malacopsyllus fragilis* Sars 1911 was re-discovered after over 80 years. This species, originally described from shallow waters of Norway (Korshavn) was found in the Laptev Sea at 3400 m depth. Although there are a great distance and a great difference in depths between these two findings, the Laptev Sea individuals seem to be identical with the holotype.

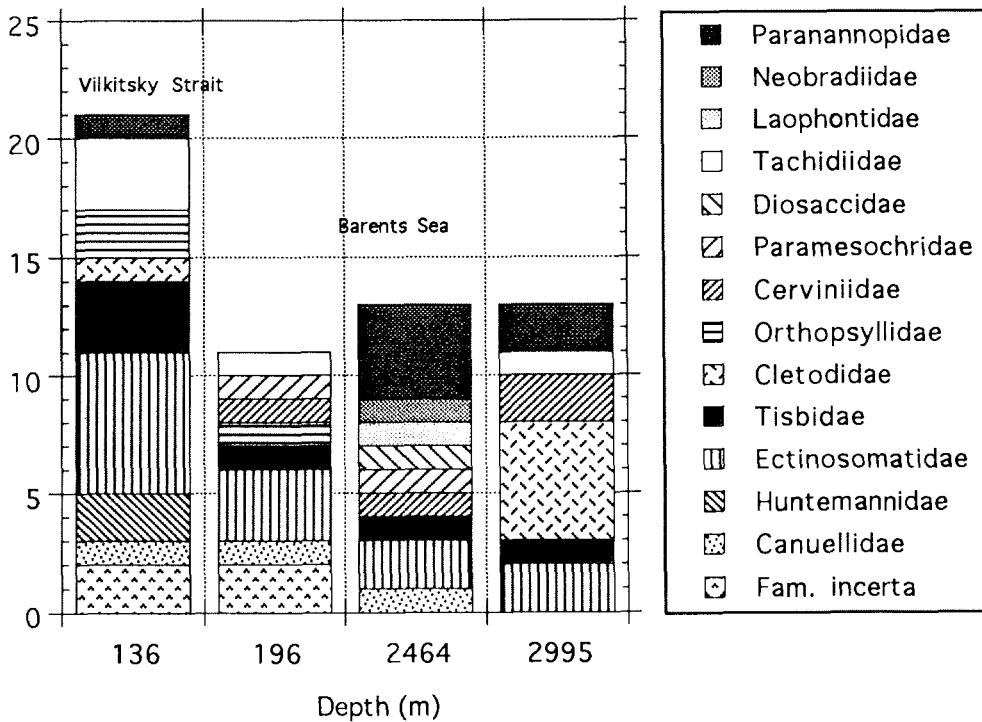


Fig. 7.4.1-1: Species numbers and family composition of harpacticoid copepods in different water depths in the Vilkitski Strait and Barents Sea.

Preliminary patterns of distribution of few species seem to show a relation between the Barents and Kara Seas. Severnaya Zemlya seems to be a zoogeographic border that separates the Laptev Sea from these two western Eurasian seas.

Figure 7.4.1-1 shows the species numbers and family composition at two shallow and two deep stations. The samples were taken from a large box grab (GKG) covering a large area. There seems to be no important decrease of species number with depths, if a sufficiently large area is sampled; however, as a rule, the abundances are lower in the deep as evidenced above.

Live observations have shown that most of the families including Cletodidae, Orthopsyllidae and Tisbidae live in the sediment and not on the sediment surface. A real epibenthic Harpacticoid found was *Harpacticus sp.* (Harpacticidae), that is present in nearly all the Laptev Sea samples, in shallow waters as well as in the deep sea.

The sex ratios of some families are dominated by the females. Especially in the deep stations no males of the present species of Cletodidae were found. This harpacticoids may develop other reproductive strategies, such as parthenogenesis (?), as it is known from a few fresh-water harpacticoids.

#### 7.4.2 Macrofauna (Eike Rachor, Katja Hinz and Boris Sirenko)

Benthic macrofauna communities are not only indicators of the sedimentary and nutritional conditions of their habitat, but also of the hydrological-climatological regimes of the environment. The individuals of several species are often long-lived, and, accordingly, integrating indicators of the long-term variability of their life conditions.

The endofauna can easily be sampled quantitatively, often allowing more detailed analyses of community structures, dynamics and production than the normally not quantitatively sampled epifauna. Quantitative population and community data are also most helpful for reliable numerical analyses of the relationships with e.g., environmental parameters or in comparative studies.

Deeper water epifauna is mainly sampled by trawls or described by imaging methods (like video or photography). Accordingly, we can receive larger scale overviews along sections and avoid deficiencies, e.g., in the sampled species spectrum of an investigated site due to small scale patchiness and low densities. Therefore, macrofauna research during ARK-IX/4 covered both, endo- and epifauna, for which a set of different sampling gears were used.

The biogeography of the marine macrofauna is well developed, and the shelf fauna of the Eurasian Arctic is sufficiently known especially due to Russian investigations. Therefore, studies comparing the fauna along a large-scale west-to-east gradient as from the Barents Sea to the Laptev Sea, are promising and will allow to explain recent and future changes in the distribution patterns of populations. Nevertheless, since the pack-ice covered Siberian continental slope areas have been badly accessible, it is expected that also new zoogeographical insights can be extracted from the samples taken in these areas. The interesting question, whether and where

there is a continuation on the deeper slope of the biogeographical provinces meeting in the Laptev Sea shelf, may be answered after working up the material collected.

Our work on the benthic macrofauna during and after the expedition is tackling the following main questions:

- How strong are the gradients in diversity and density of macrofauna from the shelves down the slopes to the deep Arctic basins?
- Is the macrofauna distribution along these gradients related to the different water masses found at the continental slopes? How strong is the Atlantic water mass influence in the northern Laptev Sea?
- How different are the macrofauna communities at the slopes of the Laptev and Barents Seas? Are there principal differences between both seas?
- To what extent does the macrofauna mirror the pelagic productivity and the consumption processes near the sampling site?
- What is the role of lateral advection of organic matter, especially when reaching greater depth under the pack-ice?
- How strong are the relations between the sedimentary/substrate conditions and the macrofauna community structures?

By cooperation with the various disciplines like physical and chemical oceanography, sedimentology and glaciology on board it is expected to answer also the question about the origin and the transport processes involved in the lateral advection of organic matter. For this, especially the possible influence of the material imported by the Lena river, the samples taken on board *Ivan Kireev* will be very helpful. Additional information is expected from the parallel expedition of RV *D. Mendeleev* of the Shirshov-Institute of Oceanology in Moscow to the Kara Sea. This will at least allow to fill some gaps in the zoogeographical research done in the northern Barents Sea and the Laptev Sea.

#### *Sampling Methods and Sample Treatment*

Samples for quantitative infauna estimates were taken mainly with the multi-box corer (Mehrfach-Kastengreifer, MG; GERDES 1990), in a few cases also as sub-samples from the giant box grab (Großkastengreifer, GKG). Each box (or sub-sample) covered an area of 230 cm<sup>2</sup>; and each haul with the MG provided up to nine boxes. Additional material for qualitative studies were taken from sediments adhering outside the MG boxes or found in the GKG boxes routinely taken for geological purposes.

Sediments and fauna were sucked by help of a flexible plastic tube and adding sea water from the top of each box down to a sediment depths of 6-10 cm, depending on the sediments. The remaining deeper sediments were then taken out of the boxes and examined for deep-living macrofauna by visual inspection. The separation of animals and fine sediments was done by sieving on screens of 0.5 mm; in some cases the top 1.5 cm sediment layer was sieved through a 0.2 mm screen.

Animals and sediment remainders were fixed and preserved in borax-buffered 4 % formaldehyde. A few samples were transferred to 70 % ethanol after at least several hours fixation in formaldehyde to preserve fine calcareous structures. The fauna of only a small number of all samples were already sorted, identified and counted on

board. All the remaining samples will be studied extensively in the home laboratories. The material will then be available for taxonomic studies.

The epibenthic animals were sampled with a variety of gears, Agassiz-trawl (AGT), epibenthic sledge (EBS), giant box grab (GKG) and multi-box corer (MG) in order to get a qualitative and more or less quantitative overview of the benthic epifauna communities with their small and large scale distribution patterns and to analyse community structures. The Agassiz-trawls were used to get information about areas of several hundred meters. With an opening of 3 m by 1.10 m and a mesh size of 1 cm it supplies us with reliable information about the larger benthic organisms. Smaller animals are only semi-quantitatively caught due to the mesh-size.

The collected sediment was divided in two parts, one quantitative part for species and community analyses and the other for qualitative taxonomic and zoogeographic studies. Each part was washed through a sieve cascade with screens of 10 mm, 2 mm and 1mm. The remaining organisms and sediment fractions were preserved with 4 % borax-buffered formaldehyde or, in case they had calcareous structures, with 70 % ethanol after a pre-fixation with formaldehyde. The large fraction of the qualitative part was directly sorted into different taxa and as far as possible identified on board.

A selection of representative bottom animals including fishes were taken from several Laptev Sea Agassiz trawls and frozen at -30° C. This material will be analysed by AWI chemists to study the degree of contamination with halogenated organic compounds.

For assessments of animals living above the sea floor, a nektobenthic net was attached to the trawl, fixed in a height of 0.75 m. Its frame opening measured 1 m by 0.25 m, and its net had a mesh size of 0.5 mm. It was used at ten selected stations.

The material collected from the AGT was often damaged during the trawling procedure by overload of mud or stones in the trawl. Therefore, and to complete the species inventory in the station area, the epibenthic sledge was used in addition. It has an opening of 1.0 by 0.3 m and a net with 0.5 mm meshes, which allows to catch the smaller fauna. This sledge supplied us with well preserved material in good conditions for taxonomic determinations and experimental work.

While these gears provide semi-quantitative benthos data of a larger area, quantitative data are obtained with giant box grabs (GKG) and multi-box corer (MG, see above). Both corers provide undisturbed sediment surfaces. The GKG covers an area of 50 by 50 cm. The sediment surface was subsampled quantitatively with a rectangular frame of 25 by 25 cm. The material of the uppermost centimeter were sieved through a 0.2 mm screen, the next 5 centimeters through 0.5 mm. The remaining undisturbed part of the GKG was used for qualitative macro- and meiofauna-samples or endofauna sub-samples.

The samples from the multi-box grab were taken in the same way as for endobenthos analyses, but the uppermost layer of 1 cm was always sieved through a 0.2 mm screen. Because of the relative small size of the MG boxes (19 by 12 cm), three were taken from the first haul at each station.

For direct and further autecological and behavioural studies of animals collected with the mentioned gears, a cooling container with 42 aquaria was used, allowing to keep the animals at 0-1° C.

### *Preliminary Results*

The locations and other station data of benthos work are presented in the Annex 10.2. Altogether, quantitative infauna samples were taken at 38 stations (32 with MG-sampling and additional six stations with only GKG-subsamples).

The majority of the sampling sites especially in the Laptev Sea were characterized by soft muddy sediments. More detailed information may be taken from the geological descriptions of parallel samples taken at the same sites.

First quantitative infauna evaluations show the expected decreases of species numbers and abundances (individuals per m<sup>2</sup>) with depths along the continental slope transects. However, species numbers and densities at the deepest stations seem to be higher when compared with the data provided by KRÖNCKE (1991) in the ARCTIC'91 cruise report for the deep central basin fauna (Figs. 7.4.2-1 and -2). From the existing data on Laptev Sea animal diversity it was assumed that species numbers would be low in our samples. This is not found in our evaluations: infauna species numbers are relatively high, in the central Laptev Sea (Transect G) not lower than in the Franz Josef Land (Transect C; Fig. 7.4.2-3). When comparing the deepest stations (see Fig. 7.4.2-1), the easternmost station even appears to be the richest one. This overall tendency is also found in the Agassiz-trawl samples (see Chapter 7.5).

Compared with the investigated fauna of the Barents Sea continental slope, suspension feeders, especially sponges and bryozoans, seem to be of lower importance in the northern Laptev Sea. Instead, infaunal polychaetes like the Maldanidae seem to be dominants. Accordingly, deposition feeding may be of greater importance than in the Barents Sea. This is in accordance with the predominance of muddy sediments in the Laptev Sea.

Compared to the endofauna, epibenthos was sampled along all seven transects with a total of 21 Agassiz-trawl, 10 epibenthic sledge, 23 giant box grab and 29 multi-box corer stations, most of them in the Laptev Sea.

Trawling was carried out even at stations with more than 8/10 ice coverage. Thus, especially the very deep trawls at Stations 27/032, 27/050 and 27/054 provided exceptional deep sea fauna material never collected in the Eurasian Basins so far.

The on-board evaluation of the larger trawl fauna has already shown seven species new for the Laptev Sea: the crab *Chionoecetes opilio* (Station 27/040, Pacific species), the shrimp *Pandalus borealis* (Station 27/049, Atlantic species), the octopodids *Bathypolypus arcticus* (Station 27/049) and *Benthoctopus* sp. (Station 27/032), a crinoid of the genus *Bathycrinus* (Station 27/054), and, may be, a sea cucumber of the genus *Elpidia* (Station 27/032, 050, 054). In the central northern Laptev Sea (Transect G) a snail of the gastropod family Turridae was found, presumably new for science.

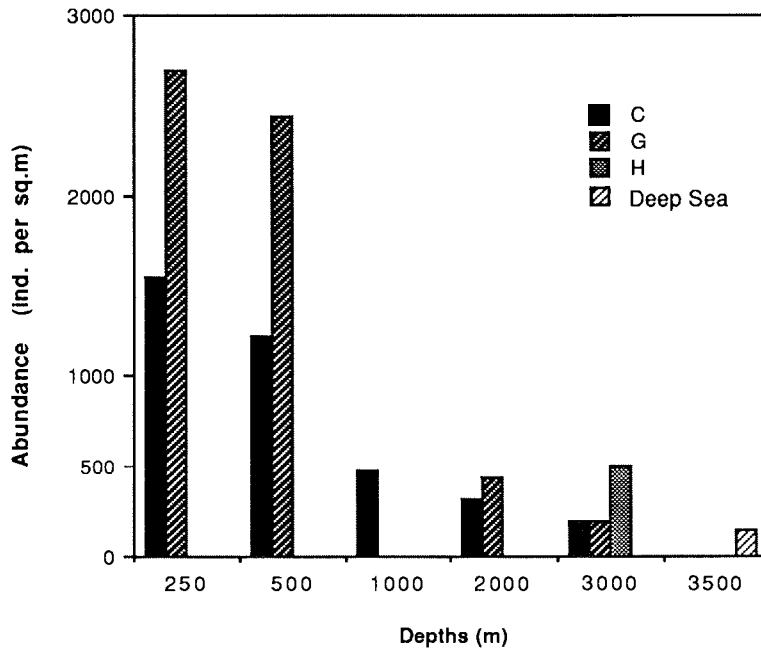
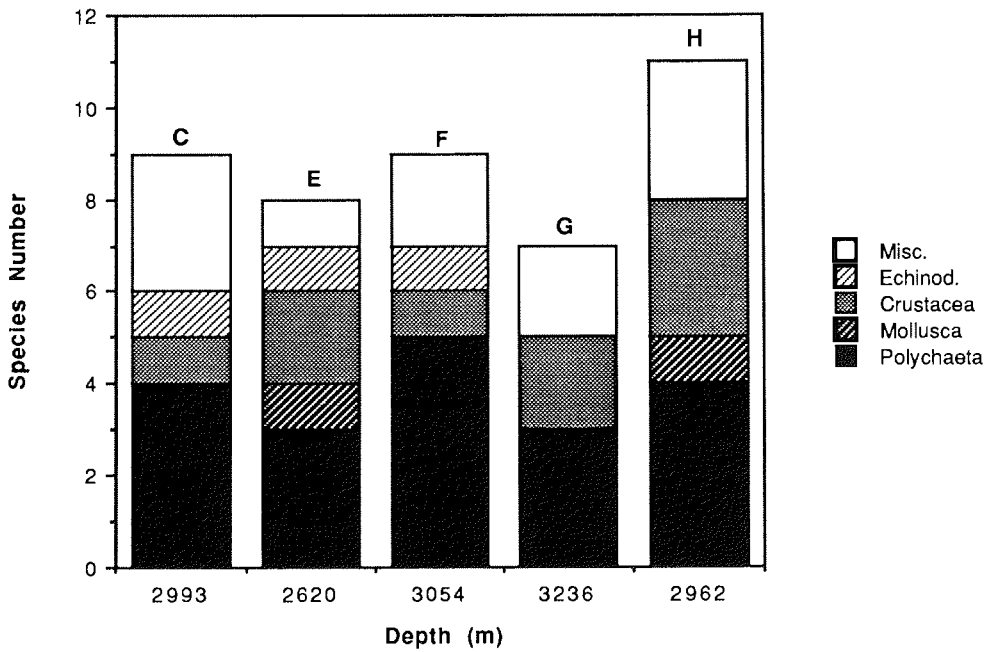


Fig. 7.4.2-1: Species numbers of macrofauna at the deepest stations (from West to East) of different transects in the Barents Sea and Laptev Sea; preliminary data from two boxes of the MG at each station.

Fig. 7.4.2-2: Macrofauna densities with decreasing depth along selected transects in the Barents Sea (Transect C) and Laptev Sea (Transects G and H) compared with Arctic deep-sea data of KRÖNCKE (1991); preliminary data from two boxes of the MG at each station.



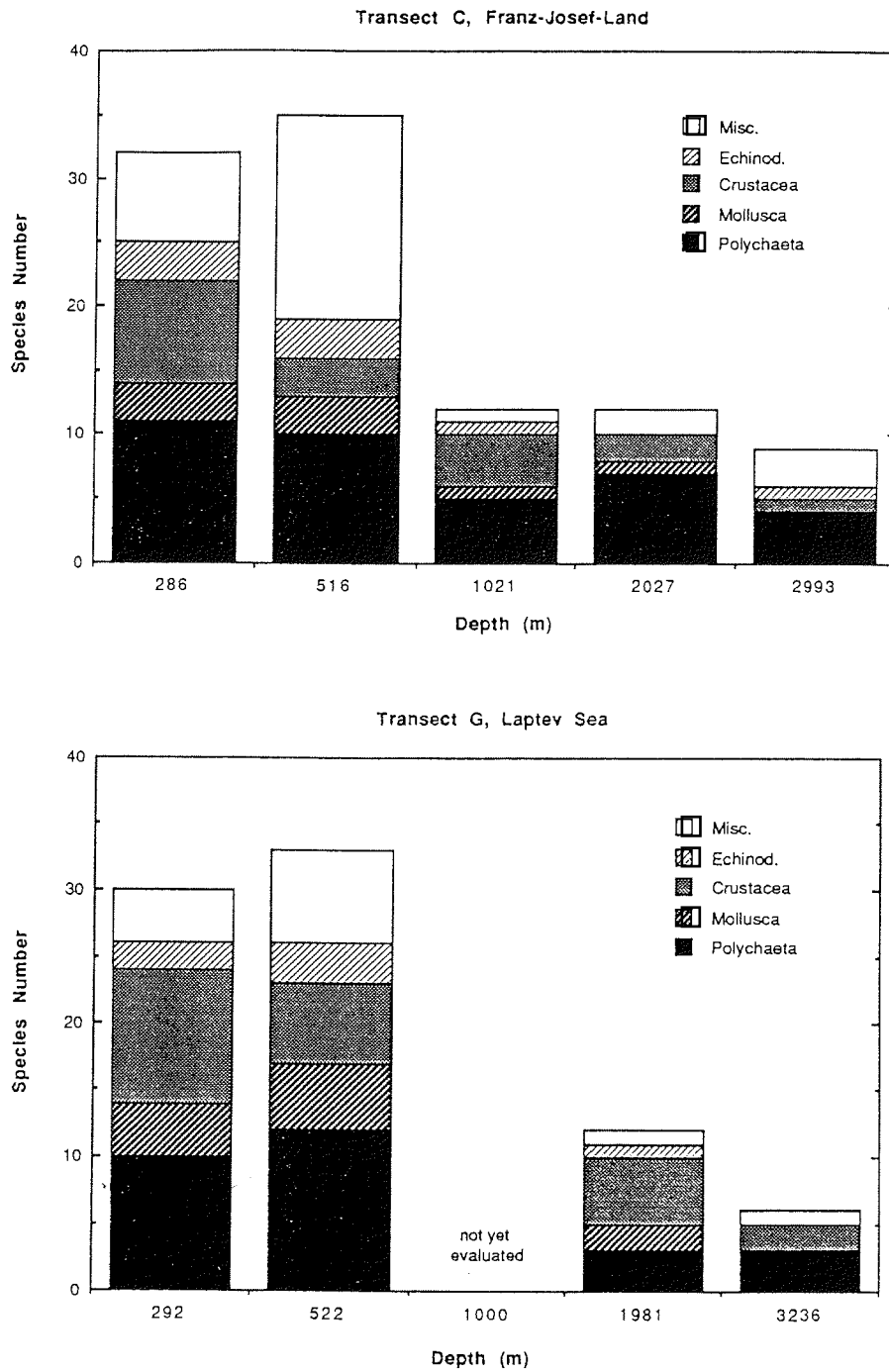
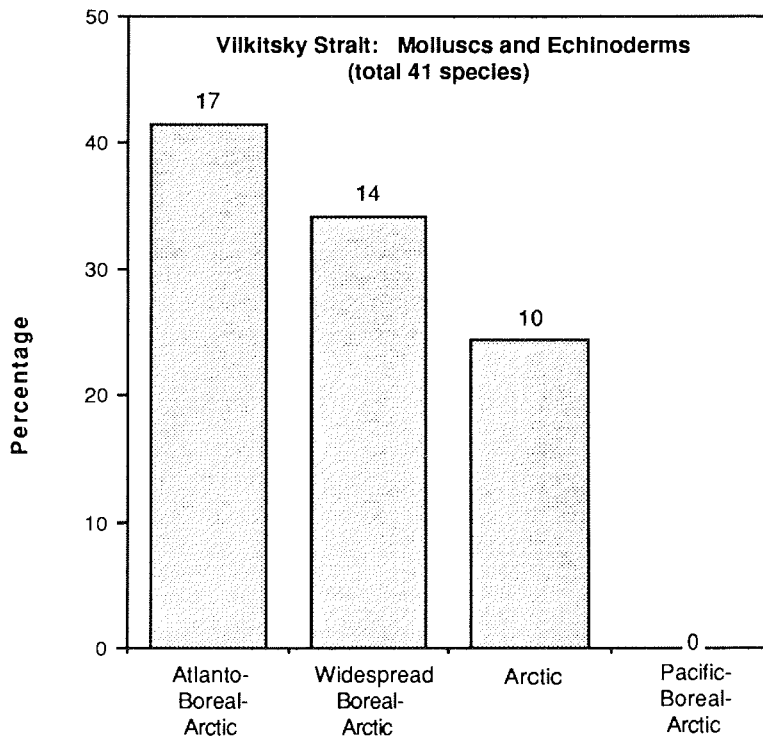


Fig. 7.4.2-3: Comparison of macrofauna species numbers along transects in the Barents Sea (Transect C, Franz Josef Land) and Laptev Sea (Transect G); preliminary data from two boxes of the MG at each station.

In the Vilkitski Strait, the existing literature on zoogeography allowed an analysis of 41 identified mollusc and echinoderm species (MG and AGT samples) with respect to their known distribution. This analysis shows that the fauna of Vilkitski Strait, in addition to the Arctic elements, is exclusively dominated by Atlantic species, while the Pacific elements are totally lacking (Fig. 7.4.2-4). This finding is in accordance with the oceanographic characterization of the Vilkitski Strait bottom water. Altogether, the Pacific elements seem to be in the minority in the investigated Laptev Sea bottom communities.

First qualitative results (Fig. 7.4.2-5) from AGT-samples in the Laptev Sea show the already mentioned gradients in species numbers occurring from the shelf down the slope to the deep sea.

Along the depth gradient of the Laptev Sea continental slope three depth related belts (zones) of macrozoobenthos assemblages were identified by their most apparent and dominating larger species (Figs. 7.4.2-6 and -7). From the shallow water stations to a depth of about 550 m brittle stars were most abundant (*Ophiopleura borealis*, *Ophiacantha bidentata* and *Ophiocten sericeum*) together with a few molluscs and polychaetes. The next zone comprises deeper slope-stations down to 2600 m with dominances of maldanid polychaetes and of *Spiochaetopterus* together with ophiuroids, isopods and actinaria. Station 27/050 at a depth of 1981 m



**Fig. 7.4.2-4:** Allocation of mollusc and echinoderm species from the Vilkitski Strait to zoogeographical regions.

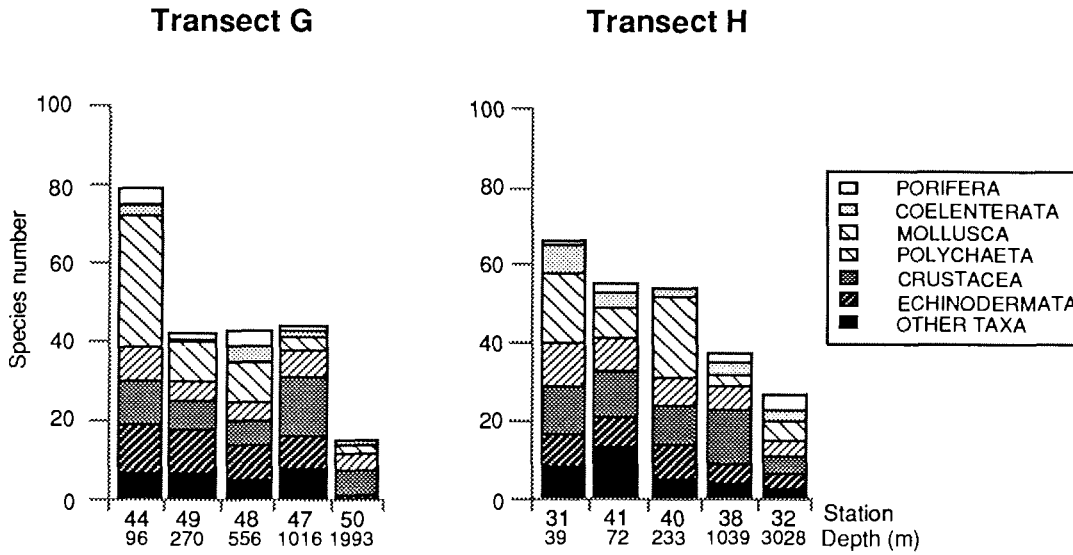
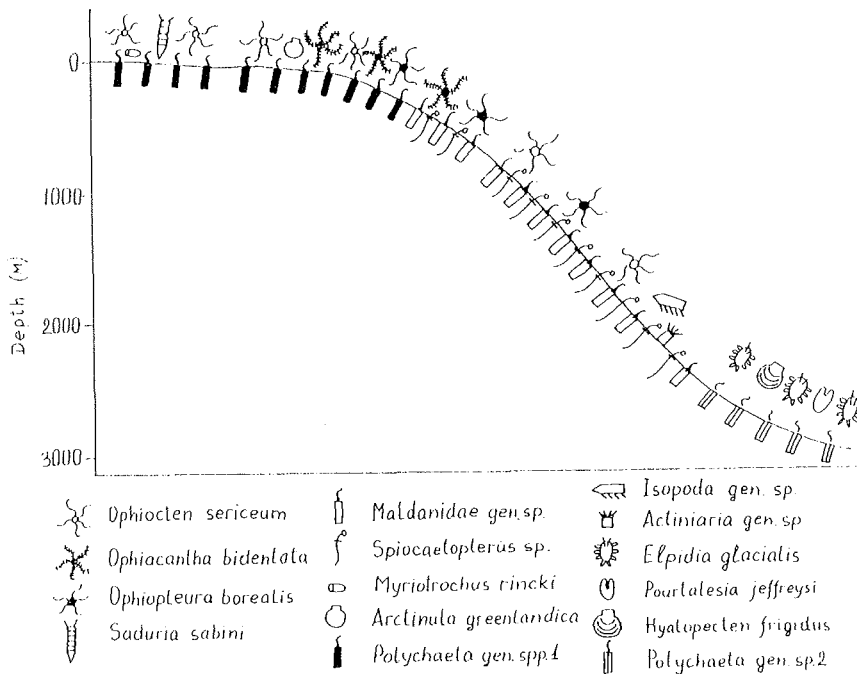


Fig. 7.4.2-5: Species numbers from the AGT-samples along the Transects G and H in the central and eastern Laptev Sea, according to main taxa.

Fig. 7.4.2-6: Zonation of apparent and dominant species assemblages along Transect H in the eastern Laptev Sea from the shallow shelf down to the deep sea (B. Sirenko).



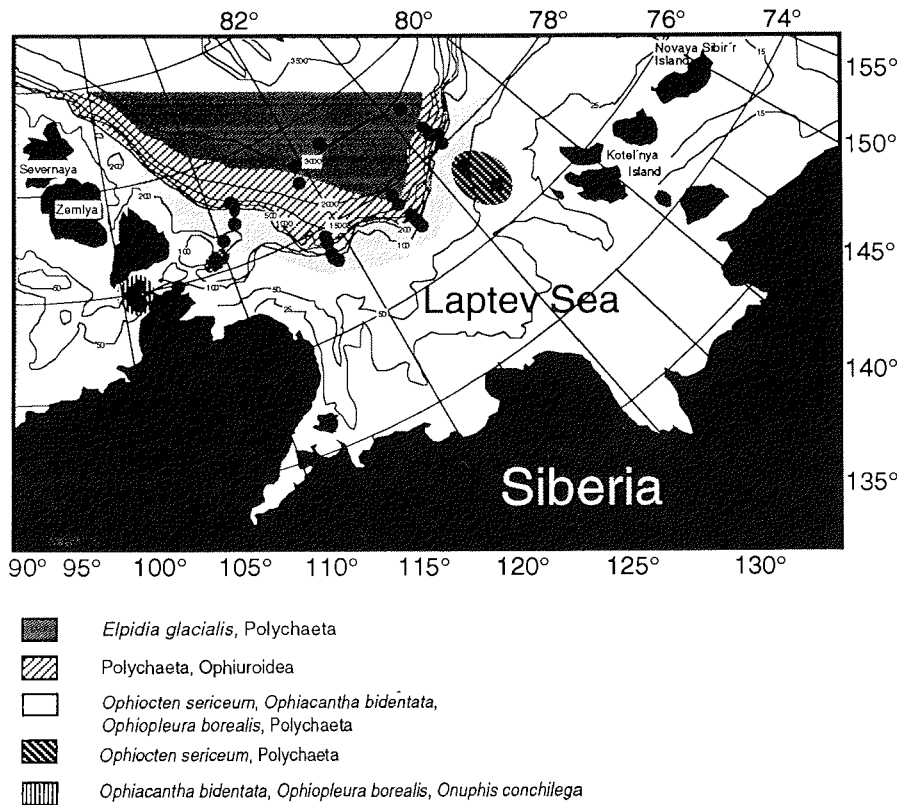


Fig. 7.4.2-7: Distribution of apparent and dominant species assemblages in the northern Laptev Sea combined from AGT, MG and GKG samples (according to Boris Sirenko).

differs in species numbers and composition from the others at similar depths. It is dominated by the same animals that are characteristic at the very deep stations, the sea cucumber *Elpidia glacialis*, some polychaetes and sponges, the sea urchin *Pourtalesia jeffresi* and the bivalve *Hyalopecten frigidus*. In the Agassiz-trawl sample of this station dead bivalve remainders were found which may be indicators of a (subfossil) hydrothermal activity. The presented zonation scheme is to be regarded as a first working hypothesis until a more detailed numerical community analyses is available.

The eastern and western parts of the Laptev Sea seem to have some differences in their species inventories. At some western Laptev Sea stations with sandy and stony sediments, filter-feeding organisms were more apparent than at the muddy central and eastern transects. A similar difference, but on a larger scale, was found comparing the Barents Sea and the majority of Laptev Sea stations. For example, at a station near Franz Josef Land with very coarse and stony bottom deposits, large amounts of the filter-feeding sponges and bryozoans covered the sample surfaces entirely. Such assemblages were never met in the Laptev Sea.

### *Conclusions and Perspectives*

The animal bottom communities in the northern Laptev Sea appeared to be richer in species numbers and abundance than presumed before the cruise. Regarding densities (of the infauna), the assemblages investigated so far in the Laptev Sea were even richer than those of the Barents shelf and slope. This is also valid for the deepest stations of the slope transects, the fauna of which belongs already to the deep basin assemblage. However, more detailed studies, especially of the macrofauna size structure, and analyses of the macro- and meiofauna biomass, are necessary, before final conclusions can be made. In the deep sea samples analysed until now, small individuals (of intermediate size between meio- and macrofauna) are predominant.

Altogether, there seems to be a considerable input of organic matter by lateral advection from the Laptev Sea shelf down into the adjacent deep sea. More detailed sedimentological and geological analyses will enable us to describe the main sources of the organic matter transported to the deep sea. It will be very important to understand the role of physical sediment perturbations (erosion and resuspension, including the effects of ploughing icebergs) in these processes and their significance for the structure and state of maturity of the benthos communities.

#### 7.5 Benthic Microbial Ecology (Antje Boetius)

During *Polarstern* expedition ARK-IX/4 sediments were sampled along the shelves and slopes of the Barents and Laptev Seas to investigate regional differences in the input of organic matter and the related variations in microbial biomass and activity.

This program was mainly focused to the following questions:

- Is there a trend in the quantitative and qualitative distribution of organic matter in the sediments of the Arctic shelves and slopes?
- Can the regional distribution of organic matter be related to other features of the investigated areas like the productivity in the euphotic zone, hydrography of the water masses and/or the geochemical characteristics?
- What is the relation between the quantity and quality of organic material in the Arctic sediments and the potential activity in its degradation by benthic microbes?
- How are these activities coupled to the distribution of benthic microbes within the sediments?
- What is the contribution of the microbenthos to the total benthic biomass of all size classes?

The microbiological investigations included sampling for several parameters: various organic compounds, the biomass and distribution of the microbial communities along the continental slope and within the sediments as well as the microbial enzymatic activity in the degradation of organic polymers. Eight stations along the Transects A and C in the Barents Sea and 30 stations along the Transects E, F, G, and H in the Laptev Sea were sampled with the multiple corer (MUC). The sediment cores were sliced to 1 cm layers from 0-5 cm sediment depth with additional layers taken from 6-7 and 9-10 cm depth. Sediment from several cores of one MUC were combined to subsample a surface of 50-300 cm<sup>2</sup> per station with 3-5 replicates per analysis.

The following parameters were measured on board (o.b.) or prepared for later analysis in the home laboratories (h.l.):

- Determination of numbers and sizes of bacterial cells (h.l.).
- Estimation of the biomass of the total sediment infauna by phospholipid measurement (h.l.).
- Estimation of the active biomass by measuring adenylates (ATP, ADP, AMP; h.l.).
- Investigation of the potential heterotrophic activity of the microbenthos using different artificial substrates for extracellular hydrolytic enzymes (FDA, MUF- $\alpha$ - and MUF- $\beta$ -glucosides, MUF-N-acetylglucosamine, MUF-stearate, MCA-leucine; o.b.).
- Measurement of chloroplastic pigments (CPE) as a tracer of the input by sedimentation of plant detritus (o.b.).
- Determination of protein compounds in the sediments (globuline equivalents; o.b.).
- Determination of carbohydrates and chitinous materials in the sediments (h.l.).

The content of plant pigments showed a maximum at sediment surface at all stations. A good correlation between pigment content and the activity of the saccharidases was found, both decreasing with sediment depth (Fig. 7.5-1). The measurement of the total heterotrophic potential (FDA hydrolyzation by esterases) also showed surface maxima at slope stations but often subsurface maxima at shelf stations.

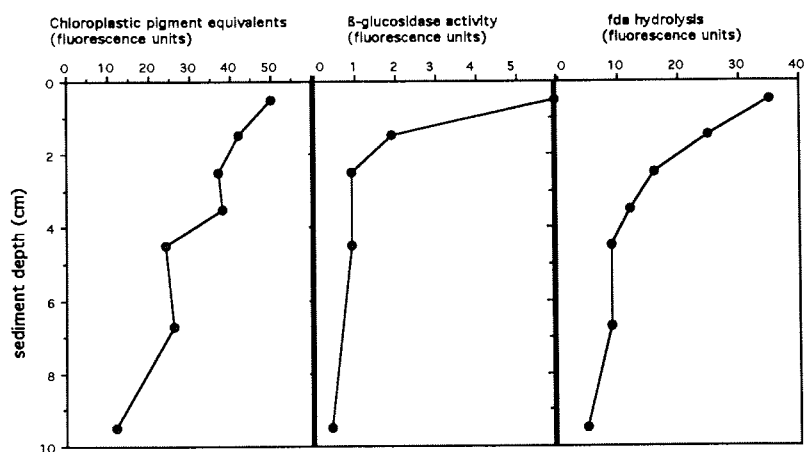


Fig. 7.5-1: Station 27/038 at 800 m water depth (Laptev Sea, Transect H). Mean values of five replicates per analysis are given in relative fluorescence units.

At most of the slope stations the maximum in protein content within the sediment was measured at 2-4 cm sediment depth. Those cores from the shelves with strong gradients in oxygenation showed high accumulation of protein in the deeper, oxygen depleted sediment layers.

Comparing the sediment surfaces at different water depths, a strong decrease in pigment content was observed, as well as a decrease in protein content (Fig. 7.5-2). Corresponding to this distribution the potential of hydrolytic activity of enzymes degrading chitinous and cellulose materials decreased down the slope (Fig. 7.5-3).

Also the total heterotrophic potential (FDA-measurements) at the sediment surface and its extent into the sediment decreased from the shelf to the deep stations.

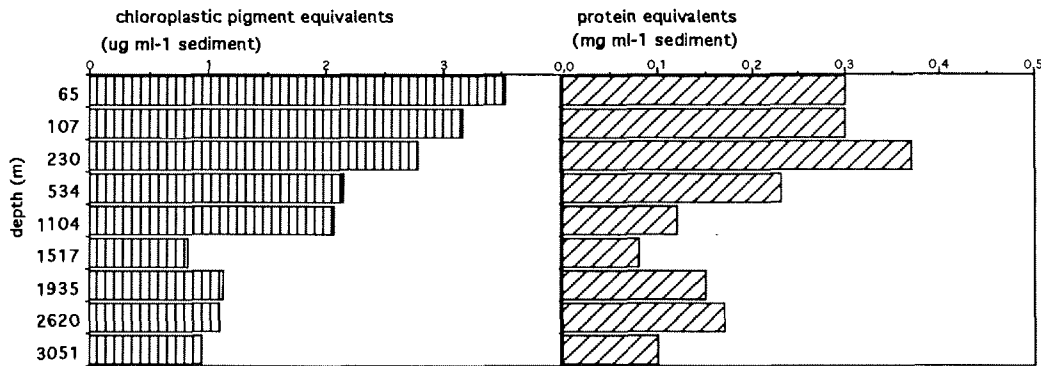


Fig. 7.5-2: Distribution of plant pigments and protein along the shelf and slope of western Laptev Sea (Transect F). Mean values of five replicates from the top sediment layer (0-1 cm).

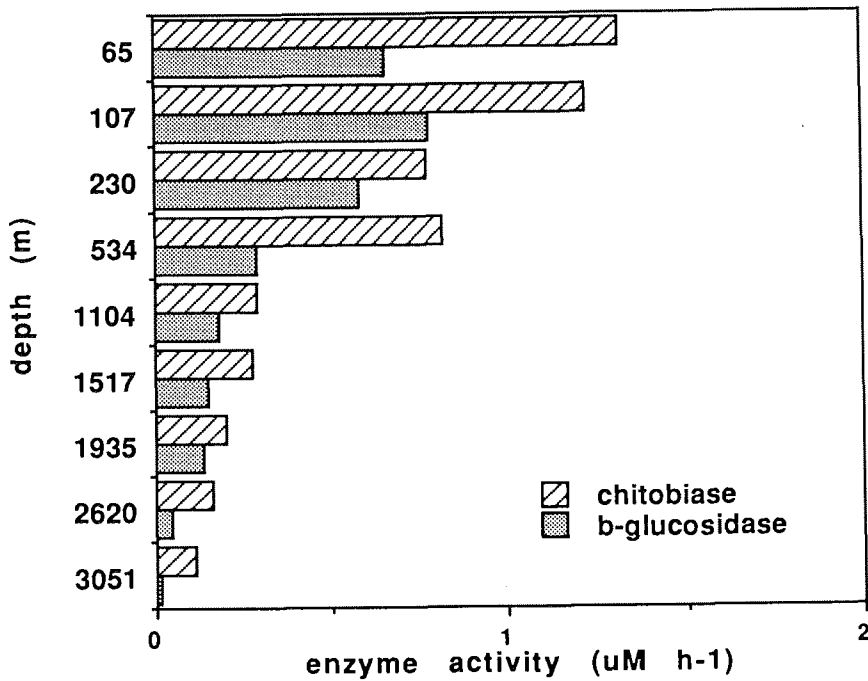


Fig. 7.5-3: Distribution of the exoenzymes chitinase and  $\beta$ -glucosidase that hydrolyze chitin and cellulose subunits (Laptev Sea, Transect F). Enzyme activities were measured in the top sediment layer (0-1 cm).

A striking feature of the Barents and Laptev Seas continental slopes was the strong change in the relative activities of the investigated hydrolytic enzymes: with increasing water depth the potential of all enzymes decreased besides the activity of aminopeptidase, that was found to be increasing (Fig. 7.5-4). This is presumably caused by the diminishing availability of labile substrates down the slope.

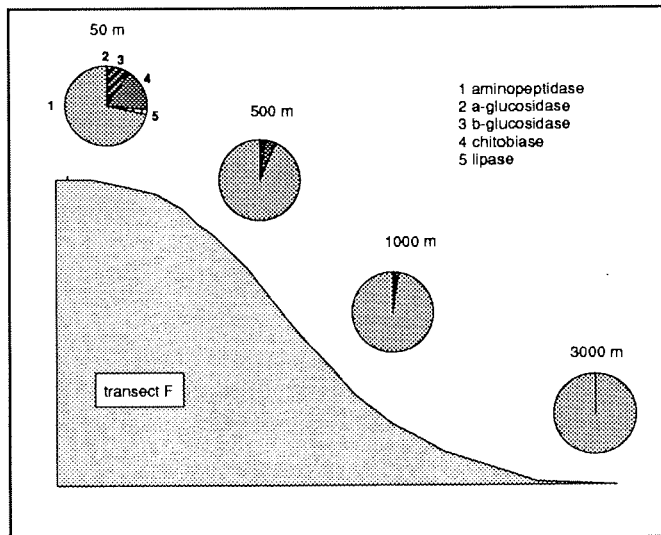
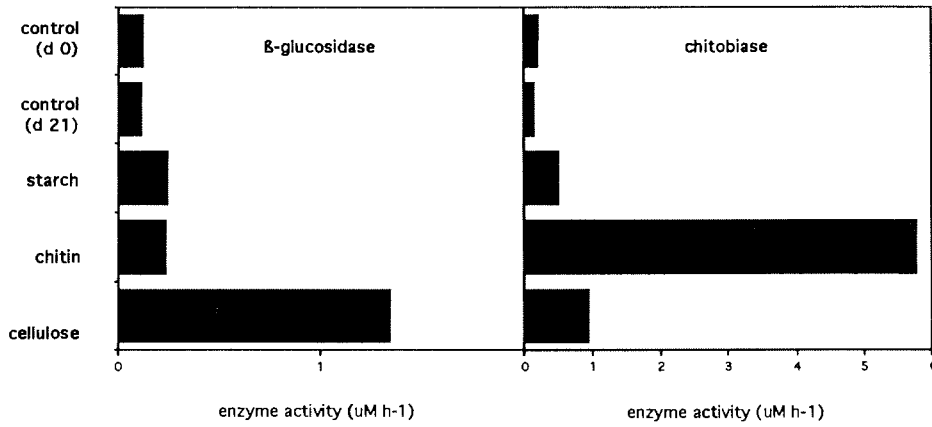


Fig. 7.5-4: Spectrum of relative enzyme activities measured in the top sediment layer at four stations along Transect F, Laptev Sea.

Comparing the different transects in the Laptev Sea, a general decrease in organic content and microbial activity from the East to the West was found in the sediments. The highest values were measured at the shelf stations of Transect H, possibly due to the influence of the river Lena discharge. Also the deeper stations of Transect H must have had a higher input of organic material compared to the other stations of equal water depth. Transect H was situated in open water close to the ice margin, so that a higher surface productivity and flux of organic material to the sediment at the ice-covered transects can be expected. This is also supported by the Chlorophyll-a data from the water column (see Chapter 7.1). The stations along Transects A and C in the Barents Sea were also under 80-100 % ice-cover and show values comparable to the stations of equal water depth of Transects G and F in the Laptev Sea.

In addition to the measurements executed on samples from the transects, feeding experiments were set up with sediments from Station 27/024 (1013 m water depth) to test the microbial reactivity to distinct inputs of different organic substrates under close to *in situ* conditions. Approximately 20 mM C in the form of aminoacids, cellulose, chitin, glucose, lipid, protein and starch were supplied to the sediments. Activities of the different enzymes were measured over 40 days and samples for microbial biomass were taken to investigate growth rates. Sediment without supply of organic matter served as control incubation. The substrates caused very different reactions in the new production of the investigated extracellular hydrolytic enzymes

(Fig. 7.5-5). These first results show that the hydrolytic potentials of the microbial communities mirror not only the quantitative but also the qualitative availability of organic matter.



**Fig. 7.5-5:** Enzyme activities in enriched sediments after incubation of 29 days. Measurements of the control incubations at day 0 and 21 are shown for comparison.

8 GEOLOGICAL INVESTIGATIONS (Ellen Damm, Frank Niessen, Nils Nörgaard, Dirk Nürnberg, Carsten Schubert, Robert Spielhagen and Monika Wahsner)

The marine geology program aboard RV *Polarstern* focussed on the investigation of sediments from the Eurasian continental margin. Research objectives basically referred to the reconstruction of the depositional environment and its change through time. Especially, the evolution and spatial variability of the Arctic sea-ice cover during glacial/interglacial changes, the influence of North Atlantic water masses entering the Arctic Ocean via Fram Strait, the impact of the large Siberian river systems transporting sediments onto the shelf areas and down to the deep sea, and biogenic productivity changes are presumably reflected in the sediments.

During ARK-IX/4 cruise, sediments from different areas of the Eurasian continental slope and adjacent shelf areas were obtained (see Fig. 2-1 and 2-2). First sedimentological and geophysical investigations were already performed during the expedition. However, detailed analyses using a wide variety of stratigraphical, sedimentological, geochemical and mineralogical methods will be performed in the home laboratories.

8.1 Sediment Echography and High Resolution Sub-bottom Profiling

The ship-mounted PARASOUND high resolution sediment echosounding system was in continuous operation along all cruise tracks between the departure and arrival at Murmansk. Bottom and sub-bottom reflection patterns of the uppermost sediments received by the system document sedimentary features. They can be used to characterize sedimentary environments and their changes in space and time. During ARK-IX/4 the aims of the sediment profiling were:

- to select coring locations for gravity and box coring,
- to identify and interpret lateral differences in sedimentary facies along shelf-slope transects and between the Barents and Laptev Seas and,
- to evaluate major stratigraphic features indicative for past environmental changes, in particular glacial-interglacial transitions.

*Methods*

The PARASOUND system designed by Atlas Electronics (Bremen, Germany) generates two primary frequencies between 18 and 23.5 kHz transmitting in a narrow beam of 4°. As a result of interaction of the primary frequencies in the water column known as the parametric effect, a secondary frequency between 2.5 and 5.5 kHz is created. The latter is suitable for sub-bottom profiling of the upper sediment layers. Along the tracks of ARK-IX/4 the secondary frequency was set to 4 kHz resulting in sediment penetration of up to 100 m with a vertical resolution of about 20 cm. Recorded echograms were independently digitized by two different systems:

- by the PARASOUND system for simultaneous printing on a chart recorder (Atlas Deso 25) and
- by the PARADIGMA system (V.Spiess, University of Bremen) for tape storage and later seismic processing on land. The terminology and interpretation of the echograms given in this report follows largely the approach of DAMUTH (1980).

### *The Shelf and Continental Slope of the Barents Sea*

At the beginning of the cruise, echosounding across the Barents shelf to Svalbard basically reproduced features already intensively studied during Norwegian surveys. Penetration of PARASOUND was poor (mostly a few meters) resulting in single distinct or prolonged surface reflectors, often carved by numerous small channels. These findings are interpreted as glacially consolidated sediments which were subsequently incised by meltwater channels during deglaciation. It has been suggested that during the last glacial large areas (if not all) of the Barents shelf were covered by an ice sheet.

Holocene sediments are very thin or absent on the shelf. There are two exceptions:

- In the Bear Island Trough penetration was up to 30 m suggesting insufficient sediment consolidation by former ice loads and/or higher post-glacial sedimentation rates.
- Along the northeastern flank of Spitsbergen Bank some sediment pockets were found (Fig. 8.1-1). They contain fills up to 15 m thick which appear to comprise undisturbed deposits of the latest Pleistocene and Holocene overlying consolidated Pleistocene sediments.

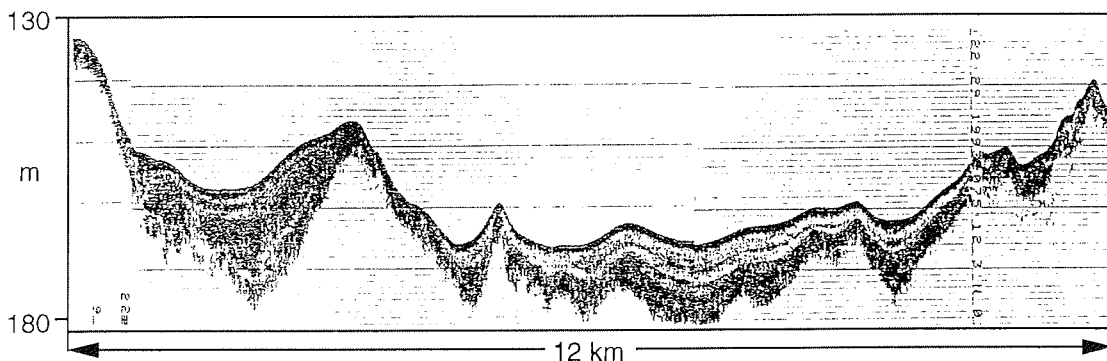


**Fig. 8.1-1:** PARASOUND profile showing sediment pockets west of Spitzbergen Bank between 75° 00' N / 17° 58' E and 75° 13' N / 17° 44' E.

In the area around Svalbard and Franz Josef Land the shelf is covered by numerous push moraines identified by their typical steep slopes which face the former glacier fronts. These moraines are either exposed on the ocean floor or, in places, draped by about 1-2 m thick sediments. The latter are probably of Holocene age. The northernmost locations at which moraine ridges were recorded are northeast of Svalbard at 80° 53' N / 29° 47' E and west of Franz Josef Land at 80° 50' N / 43° 07' E. A similar moraine-ridge topography was also observed along the entire transect between the above location at Franz Josef Land and Novaya Zemlya up to 76° 24' N / 66° 50' E. There, seismic evidence for push moraines ceased.

Along the continental slope the quality of the PARASOUND records strongly suffered from the heavy ice conditions. Many profiles recorded along steam courses are practically unreadable. This is due to secondary noises from ice breaking, recording

failure due to ice and air bubbles under the transmitter and/or receiver units as well as geometric effects due to ice ramming of the vessel. Nevertheless, sections of reasonable quality were recorded during station time when the vessel drifted with the ice.

Between Svalbard and Franz Josef Land, seismograms from the continental slope show penetration between 30-50 m (for example at sampling stations of Cores PS2444 and PS2445, respectively, Fig. 8.1-2). For both locations the top of the sediments down to 1.5-2 m are characterized by distinct and parallel reflectors suggesting a dominantly undisturbed pelagic or hemipelagic character of these deposits. Below, there is a series of thick transparent layers subdivided by distinct reflection bands. At the western location, these deposits have lenticular geometries and show truncation of beds at the top. The observed depositional pattern is associated with strong lateral movement of sediments by debris and/or turbidity flows. It may indicate a marginal facies of the relatively large shelf-basin oriented channel which is located east of Svalbard and west of Franz Josef Land. Since the sediments cored from the transparent layers (Cores PS2444 and PS2445) are diamictic, the lower part of the seismic sequence may represent glacial conditions and high sedimentation rates during either the last or earlier glaciations on the Barents Sea shelf. Indeed, slump structures were commonly observed in the transparent layers along steam tracks on the Svalbard to Franz Josef Land slope. The lower series of the eastern location, however, has more subparallel reflectors. This suggests that relatively undisturbed and complete records of the whole sequence may occur in places. It also implies that it is difficult to correlate cores from different locations, in particular with respect to the deposits below 1.5 m sediment depth.

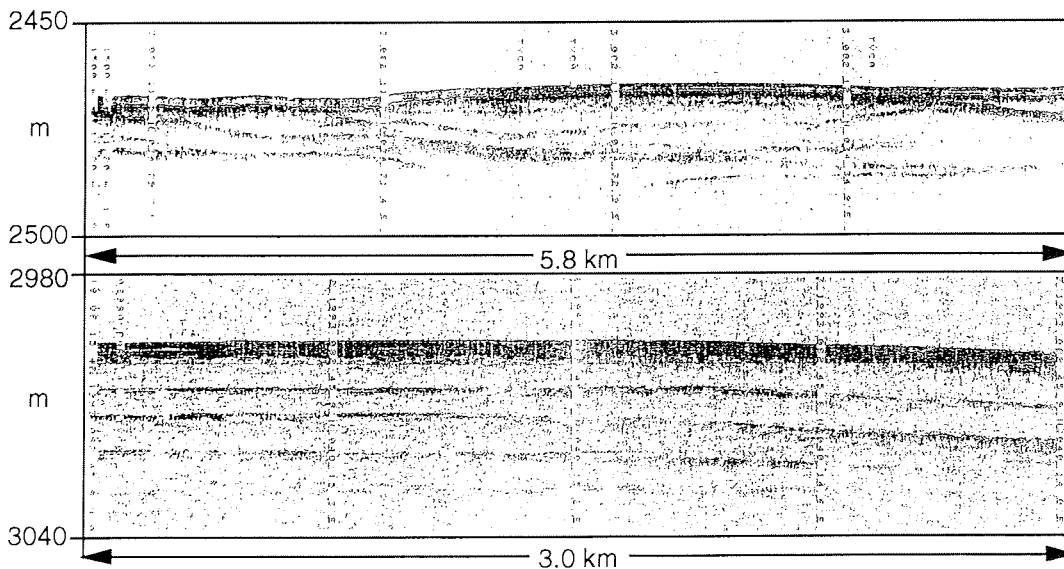


**Fig. 8.1-2: PARASOUND profiles near coring stations on the Svalbard to Franz Josef Land continental slope. Top: between 82° 12' N / 34° 29' E and 82° 12' N / 34° 37' E. Bottom: between 82° 45' N / 40° 16' E and 82° 46' N / 40° 14' E.**

*The Shelf and Continental Margin of the Laptev Sea*

There are in total four PARASOUND transects with seismic information from the Laptev Sea shelf: one west to east profile across the central part of the Laptev Sea between Vilkitski Strait and the sampling Transect H in the east, two east to west profiles near the shelf edge between the sampling Transects H-G and F-E, and a short profile linking the shelf edge at Transect E back to the slope of the Vilkitski Strait.

In contrast to large areas of the Barents Sea, the Laptev Shelf is characterized by a flat surface. There are no moraines which would give any direct evidence for a glaciated history of this area. PARASOUND penetration was limited to mostly a few metres which locally increased up to 20 m. Subsurface reflectors have subparallel geometries, which appear in places slightly deformed or "folded" (Fig.8.1-3). Locally a dip of the strata was observed with an angle of a few degrees toward the east. Subsurface reflectors are often cut unconformably at the top and are overlain by a horizontal bed, mostly only a few meters thick (e.g. Fig. 8.1-3). The latter is interpreted to represent Holocene deposits.

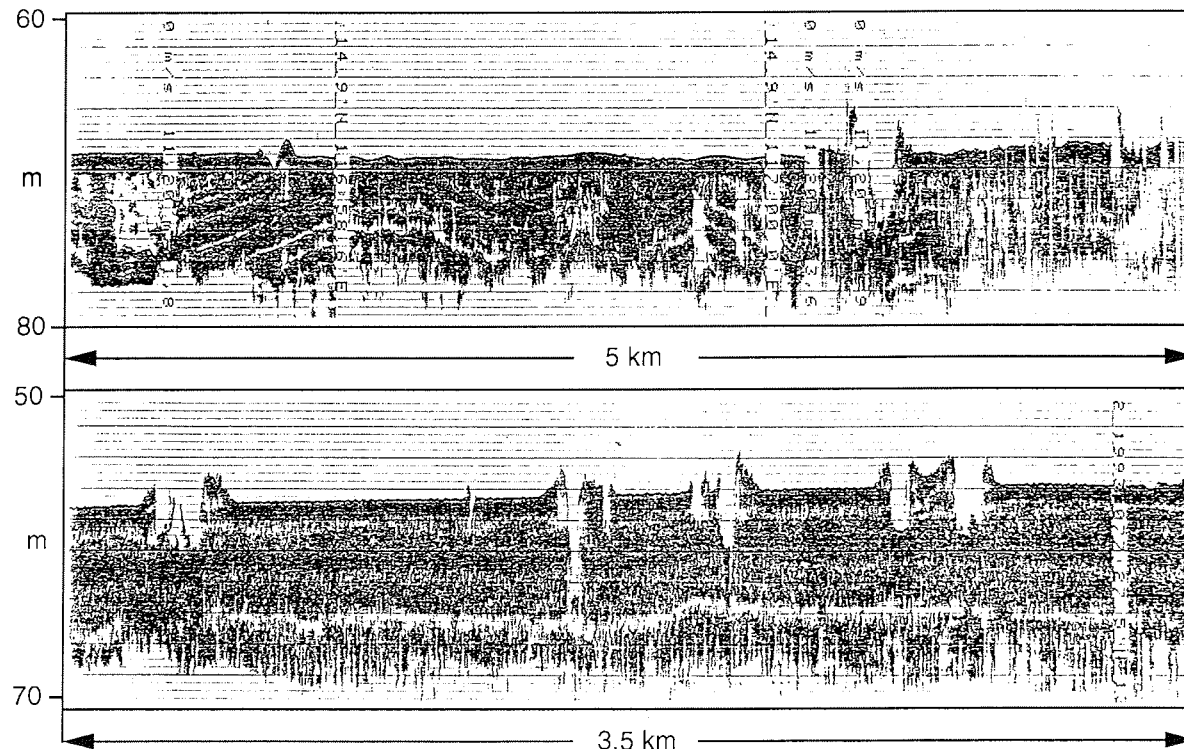


**Fig. 8.1-3:** PARASOUND profiles from the central and eastern part of the Laptev Sea shelf. Top: between 77° 15' N / 116° 58' E and 77° 14' N / 116° 54' E, Bottom: between 77° 30' N / 133° 37' E and 77° 27' N / 133° 37' E.

There are two features which are of particular importance with respect to the history of the shelf area and with respect to recent shelf processes:

- the presence of Pleistocene river channels cut into the shelf and,
- the abundance of ice gouges in surface sediments due to recent ploughing of sediments by icebergs and/or ice-pressure ridges.

Several incised river channels were recorded on profiles near the shelf edge. The widths of the channels are on the order of a few kilometers, the depth are about 10 to 15 meters (Fig. 8.1-4). All channels are filled with acoustically transparent sediments. These channels are related to Pleistocene drainage of the large Siberian rivers, such as the Lena (Fig. 8.1-4) and were cut into the shelf during times of lower sea level. This occurred most likely during the last glacial when the sea level was supposed to be 120 m below that of today, and the coast line was located north of the shelf region near the present shelf to slope boundary. It implies that considerable freshwater drainage occurred during Glacial times from the Eurasian continent into the Arctic Ocean. Furthermore, these findings cause difficulties to believe that a large ice sheet has covered the entire area of the Laptev Sea during the last glacial maximum as has been suggested by GROSSWALD (1990).

In certain areas of the Laptev Sea a large number of ice gouges were observed (order of magnitude  $10^3$  numbers in total). There are abundant findings near the coast of Severnaya Zemlya and the Taimyr Peninsula as well as near the New Siberian Islands. The characteristic features of the gouges are incisions between 1-10 m deep, flanked by walls on just one or both sides. The total widths are on the order of a few tens of metres. Generally it appears that the sediment accumulated in the walls would fill the scars. The relatively small total width of the features compared to their total relief make them clearly distinguishable from drainage channels flanked by levee deposits. Also, the occurrence of gouges is strictly limited to a certain range of water depth between 30-90 m water, which was not observed for erosional channels elsewhere during the cruise. Observations and simulations with respect to formation and filling of ice gouges from the Alaskan Beaufort Sea suggest that ice gouges are short-lived and filled in a few years (BARNES et al. 1985). The abundance of gouges observed in the Laptev Sea would then suggest that ice erosion is presently an important shelf process. It may induce resuspension of sediment and thus forth lateral sediment transport over the shelf. Furthermore, ice gouges may provide information about clustering of grounded ice (icebergs or pressure ridges) in certain areas. This could then be used for identification of ice drift patterns. A statistical evaluation of the observed gouge features is planned in order to test these possibilities. Also, the effect of ice gouging on subsurface strata has to be examined in more detail. In some areas, ice gouging has the effect that some of the subsurface deposits were homogenized down to about 10 m sediments, whereas in other places the strata of older deposits below 1.5 m are still intact (Fig. 8.1-3). Moreover, it has to be tested whether gouging becomes so prominent in certain areas (such as near the New Siberian Island) that a post-sedimentary reflection pattern may be created by the ice load during grounding (Fig. 8.1-3).

In total five profiles were recorded on the continental slope perpendicular to the shelf edge. Except for the Transect H in the eastern Laptev Sea, all sections along sampling profiles suffered from the partly heavy ice conditions. This led to limited data quality similar to the situation described for the continental slope of the Barents Sea. There are three different facies which can be identified in the seismic profiles:

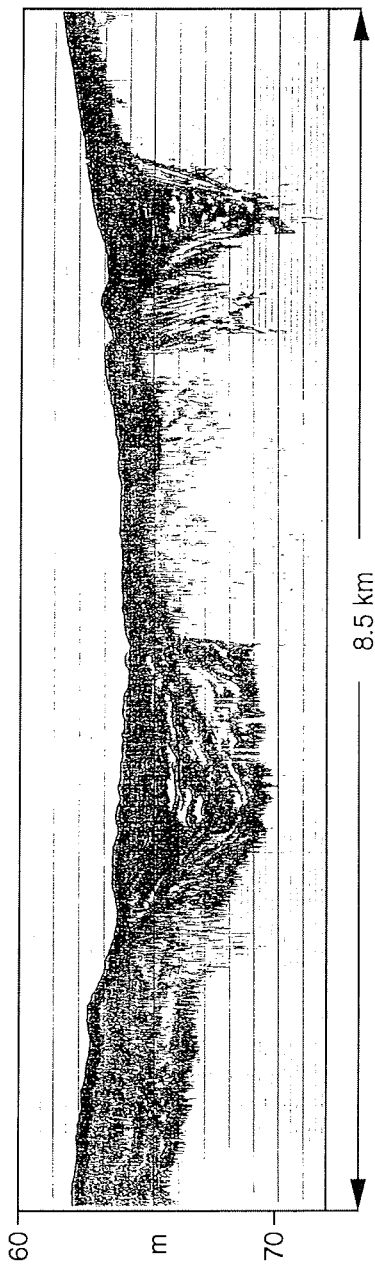


Fig. 8.1-4: PARASOUND profile from the centre of the Laptev Sea near the continental slope between 77° 03' N / 131° 06' E and 77° 02' N / 130° 48' E.

- slumps,
- channels flanked by levee deposits, and
- undisturbed slope deposits.

The slope in the central part of the Laptev Sea (Transect G) is characterized by reflection patterns of slumps down to waterdepths of approximately 2000 m followed by channel and levee deposits to the deepest point at 3200 m. Channels have distinct or prolonged reflection character. Some channels show truncation of older beds. In places, thick undisturbed sections were found. They comprise subparallel reflectors which drape underground topographies. Penetration was down to 50 m sediment thickness. The transparent sediments are interpreted as levee facies. In general, these deposits are typical for submarine fans. Since incised river channels of the Lena drainage system were found on the continental shelf, the fan facies observed below 2000 m water depth may have formed mainly during the last Glacial, when the riverine transport of continental debris was to the edge of the present slope/shelf boundary.

Thick mostly undisturbed slope deposits were recorded along Transects H and F. Reflections are mostly multiple distinct down to about 100 m sediment depth. The deposits drape topographies. Only in the lowest part of Transect H (deeper than 3000 m) a major slump was identified (Fig. 8.1-5). Distinct reflectors correlate over long distances and show a pronounced thickening of the layers towards the shelf (Fig. 8.1-6). In relatively shallow water below the shelf edge down to about 400 m water depth, downlaps are observed which build up sigmoidal sediment bodies. This is typical for prograding slopes during times of high sedimentation. Since there is no major change in stratigraphy, neither with respect to the reflection geometry nor in the lithology of the cores drilled along the transect, it is speculated that these deposits are of Holocene age. If correct this would suggest high sedimentation rates near the shelf edge probably caused by strong lateral transport of debris on the shelf in off-shore direction. The sigmoidal geometry of reflections on the upper continental slope was reproduced along a steam course from the western Laptev Sea shelf through the Katanga-Vilkitski Strait channel (Fig. 8.1-7).

#### *The Vilkitski Strait*

The sediments of the Vilkitski Strait are different compared to all other locations described above. Packages were penetrated down to sediment depths of 100 m. This is surprisingly thick for near coastal shelf sediments. Two profiles are presented here: a longitudinal section from the centre of the Vilkitski Strait extending to the east into the westernmost part of the Laptev Sea (Katanga-Vilkitski Channel), and a north to south cross profile from the western area of the Vilkitski Strait.

In the centre of the strait, the sequence is built up by relatively thick transparent sediment lenses overlain by several series of multiple distinct reflectors. The latter show lateral variation of thicknesses, and in places truncation of older strata (e.g. near the western end of the profile shown in Fig. 8.1-8). The seismic transparency of the fill suggests relatively fine grained unconsolidated sediments. The geometry im-

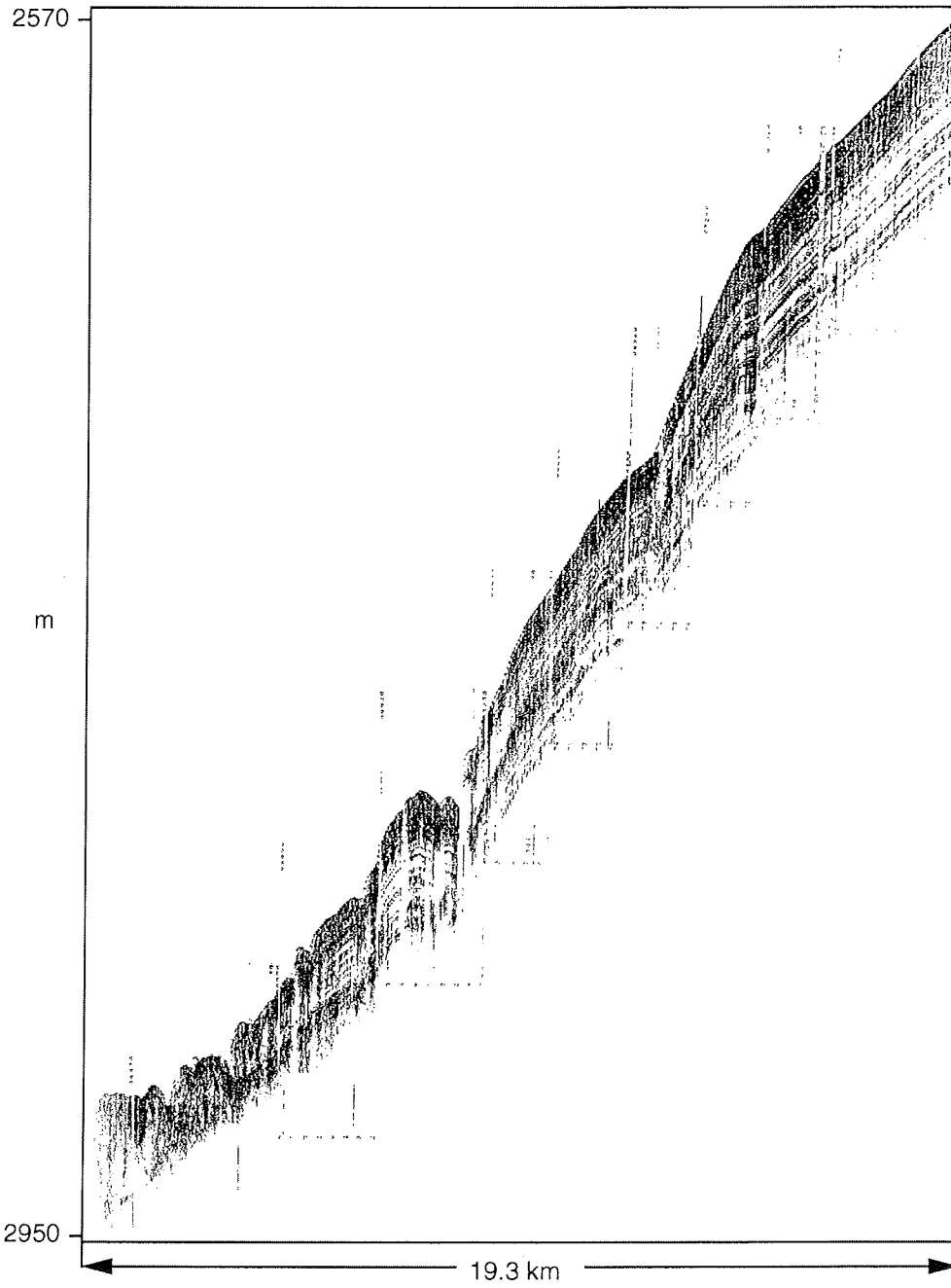


**Fig. 8.1-5:** PARASOUND profile from the lower part of the continental slope along Transect H between 78° 41' N / 132° 41' E and 78° 31' N / 132° 51' E.

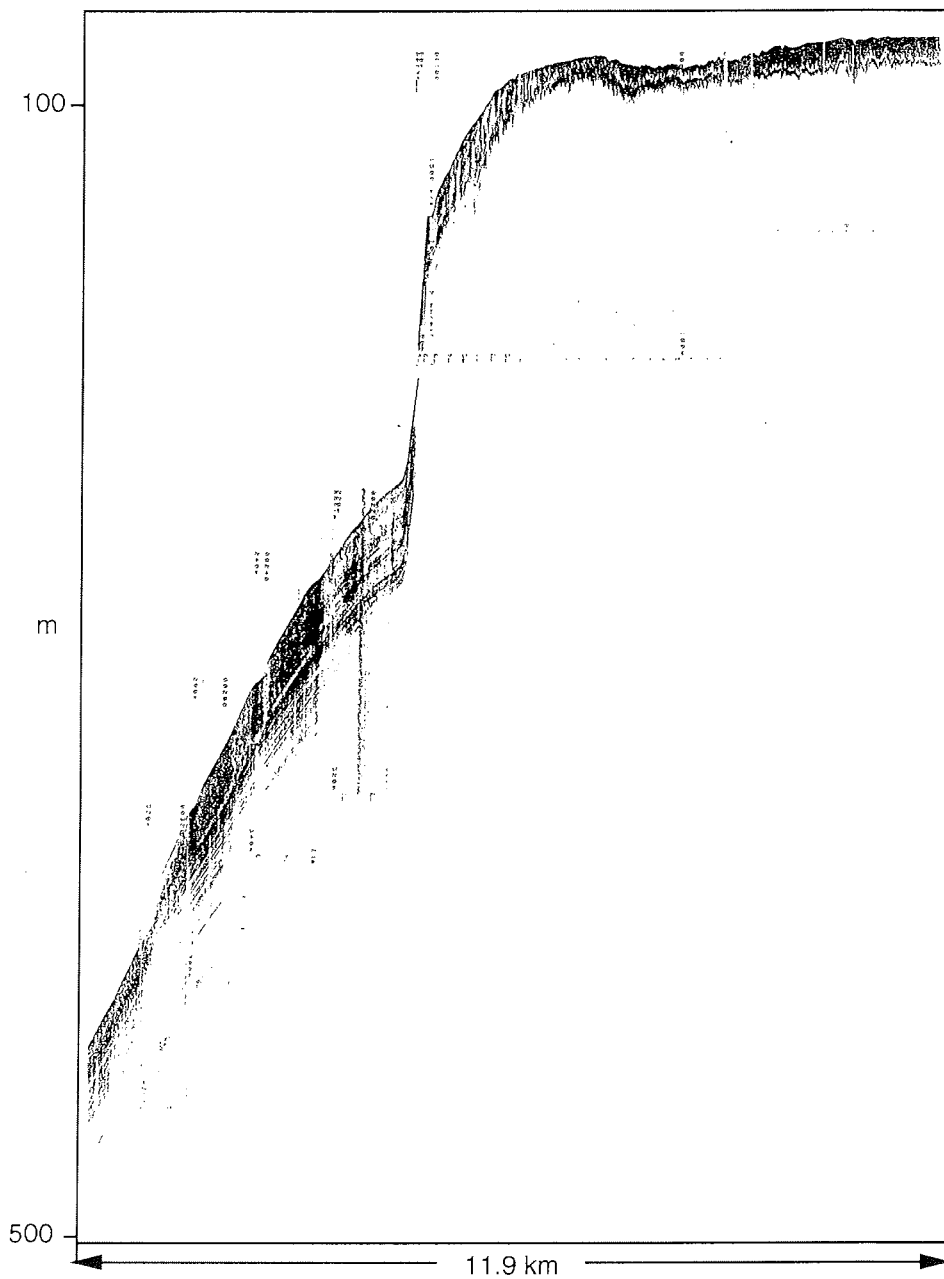


**Fig. 8.1-6:** PARASOUND profile from the upper part of the continental slope along Transect H between 78° 06' N / 133° 34' E and 78° 00' N / 138° 39' E.

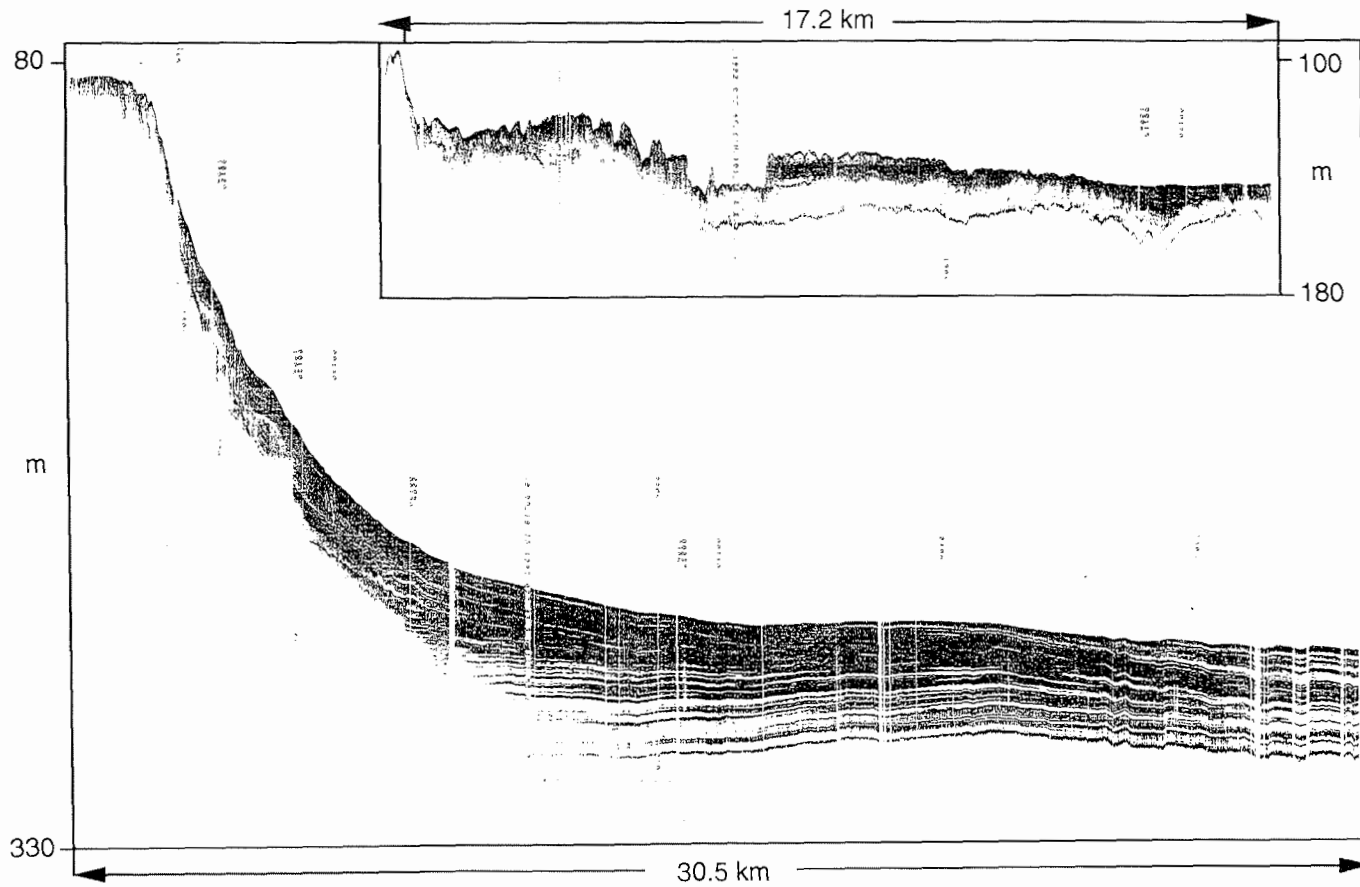


**Fig.8.1-7:** PARASOUND profiles from a transect between the Laptev Sea shelf and the central part of the Katanga-Vilkitski channel (bottom), between 77° 42' N, 112° 22' E and 77° 42', 111° 05' E. and across the western area of the Vilkitski Strait (top), between 77° 43' N / 101° 43' E and 77° 51' N / 101° 48' E.

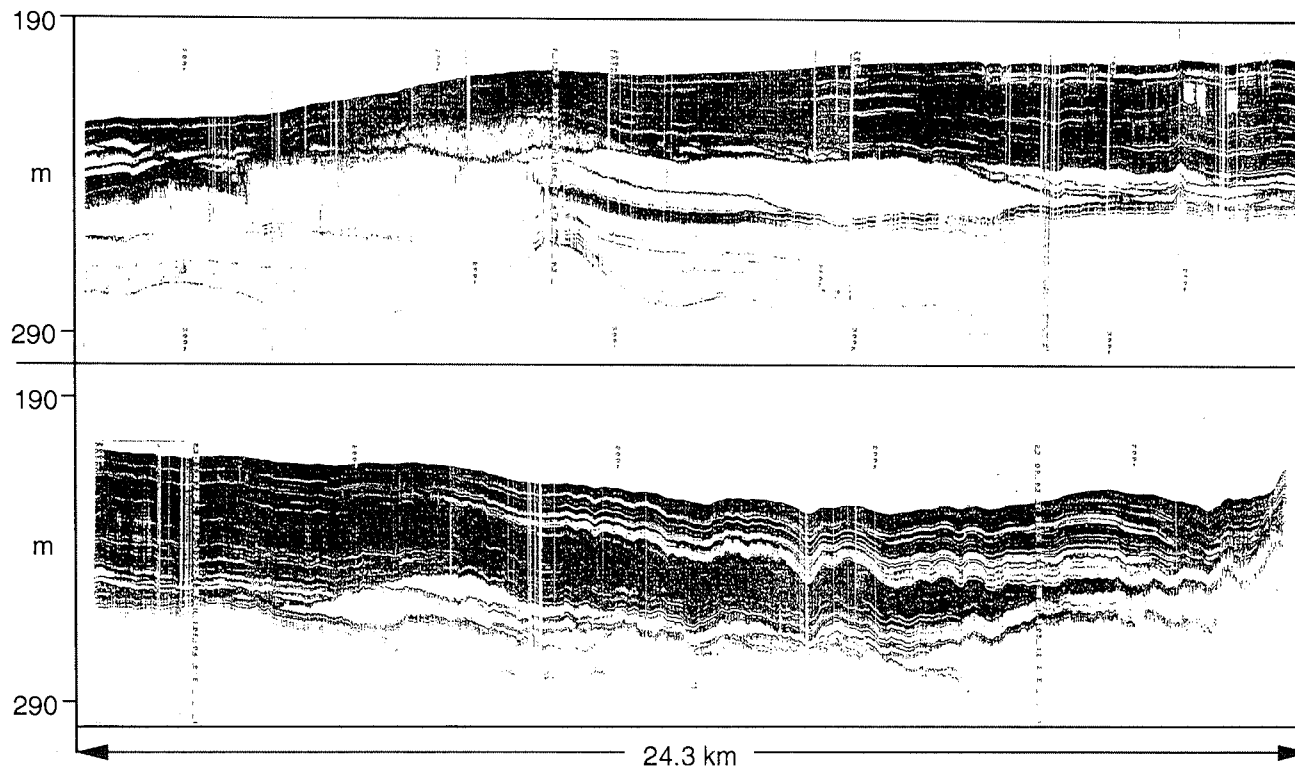


**Fig. 8.1-8:** PARASOUND profile along the axis of the Vilkitski Strait between 77° 52' N, 107° 20' E (western Laptev Sea) and 77° 49', 105° 15' E (centre of Vilkitski Strait).

plies debris flows for the formation of lenticular features in the lower part of the sequence and turbidity flows for generating lateral changes in thickness in the upper part. There is direct evidence for such currents in Fig. 8.1-7, where a major channel is exposed at the surface. The channel is flanked by levee deposits which were subsequently cut by minor channels. This pattern has the character of more proximal facies than the deposits in the central parts of the strait, where only little evidence for erosion is documented. Generally, this implies an environment with relatively high transport and deposition rates. It also suggests that the direction of suspension flows through the strait was mainly west to east except for the debris flows which may be of local origin derived from the northern flank of the strait. It is interesting to note that different to the other profiles in the Laptev Sea, there is an onlap sequence at the top of the seismic profile in the Katanga-Vilkitski Channel off the continental slope. These deposits are probably turbidites and may form the distal part of the Vilkitski Strait deposits (Fig. 8.1-7).

Since there is presently no major river system delivering debris into the Vilkitski Strait, it is difficult to explain the above findings by recent processes. A reasonable interpretation can be given if the deposits are of latest Glacial and/or early Holocene age, and if they are derived from local and/or large scale deglaciation. For example, if a relatively fast meltdown of parts of the ice caps and glaciers of the Severnaya Zemlya archipelago and of past glaciers on the Taimyr Peninsula occurred, then high input rates of freshwater suspension flows are expected. This implies that the Vilkitski Strait functioned as a large melt-water channel and was not covered by a glacier by that time. Indeed, there is no evidence for a presence of a glacier in the Vilkitski Strait since the sediments are not consolidated (see Chapter 8.4.3) and there is no clear indication for moraines at the boundary of the strait to the western Laptev Sea. However, this hypothesis has to be tested by further analysis of the core material as well as more investigations in the field.

## 8.2 Sediment Sampling and Description

Geological sampling and coring was one of the topics during RV *Polarstern* cruise ARK-IX/4. There had been two major aspects, first to recover undisturbed surface and near surface samples for biological, paleocological and geochemical investigations and second to recover undisturbed and long sediment sequences for the various stratigraphic (stable isotope and AMS<sup>14</sup>C stratigraphy, biostratigraphy etc.), paleoenvironmental, geochemical and sedimentological investigations (e.g. coarse fraction, clay mineralogy, organic carbon and carbonate contents as well as heavy-mineral distribution or alkenone-measurements, etc.).

Geological coring and sampling stations were performed mainly over the continental margin of the Barents Sea and Laptev Sea. Transects A and C on the continental slope northwest of Svalbard comprise about 10 stations (Fig. 8.2-1). Transects E, F, G and H from the shelf to the deep sea in the Laptev Sea region consist of 30 stations (Fig. 8.2-2). Five geological stations had been performed in the Vilkitski Strait (Fig. 8.2-2).

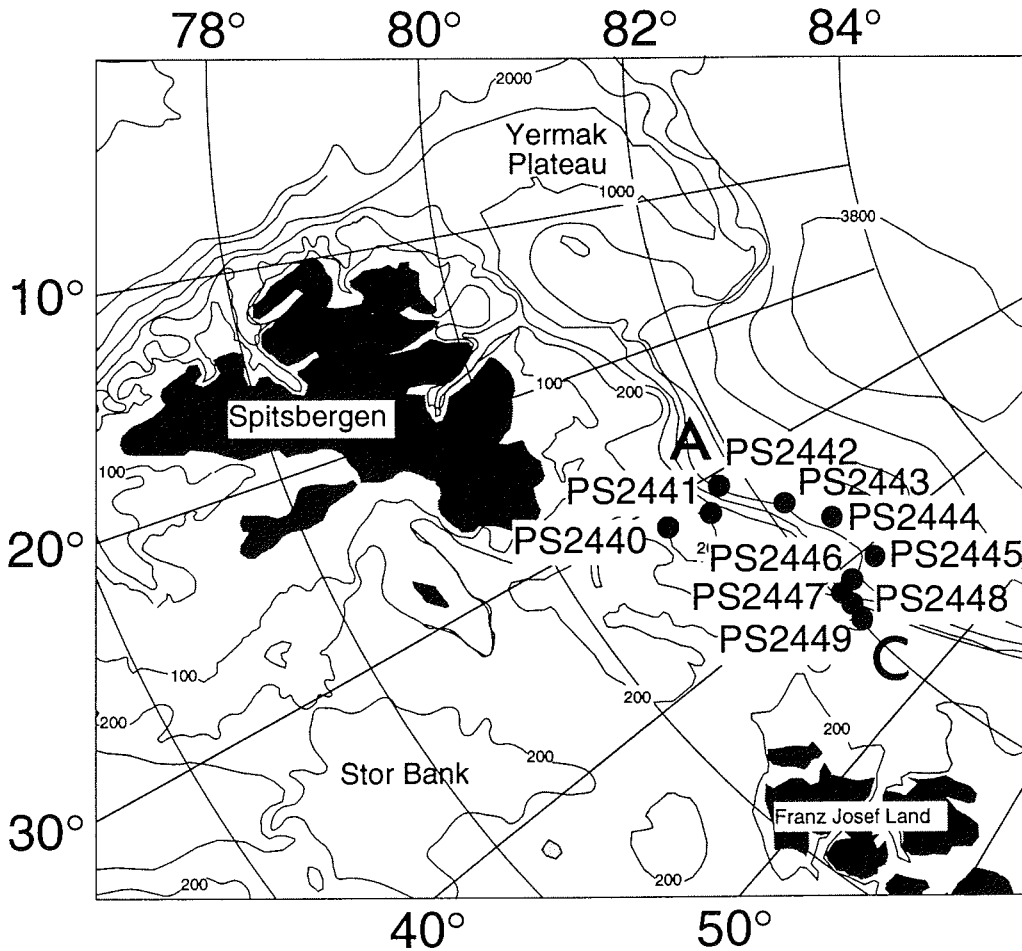


**Fig. 8.2-1:** Bathymetric chart of the Barents Sea shelf and continental slope showing sample locations.

#### *Sampling of Near-surface Sediments*

In order to recover undisturbed near-surface sediments the giant box corer (GKG) and the multicorer (MUC) were used. In addition to high quality sediment sampling the giant box corer also samples the bottom water directly overlaying the sediment surface.

**Multicorer (MUC):** The standard 12-tubes-version multicorer (manufactured by Fa. Wuttke, Henstedt-Ulzburg, Germany) with a tube diameter of 6 cm was used. The penetration weight was up to 250 kg. On 42 out of 47 geological stations the MUC was run, of which 40 recovered sedimentary sequences with an average thickness of about 30 cm; only two times the multicorer did not trigger due to freezing.

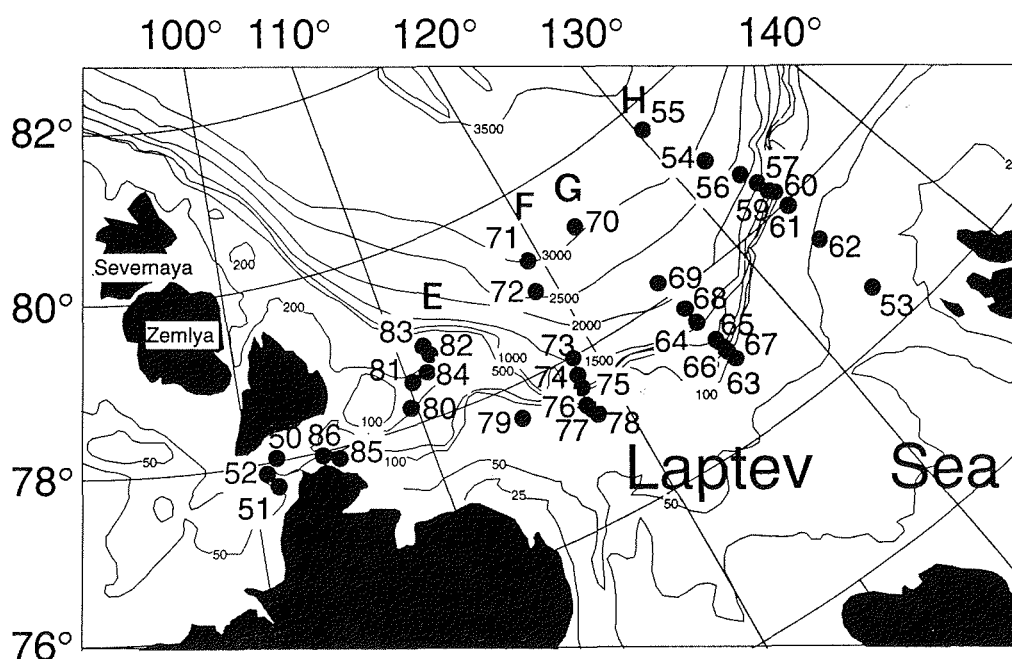


Fig. 8.2-2: Bathymetric chart of the Vilkitski Strait and the Laptev Sea shelf and continental slope showing sample locations.

Multicorers were sampled according to the following scheme depending on the numbers of cores filled with sediments:

- 4-5 cores for the investigations of benthic foraminifers and stable isotopes. Sediment samples were taken at 0-1, 1-2, 2-3, 3-4, 4-5, 7-8, 10-11, 14-15 cm and subsequently mixed with bengal-rosa-methanol-solution to stain living organisms.
- 2-3 cores for sedimentological investigations (organic carbon and carbonate content, clay and coarse fraction analyses). Samples were taken every centimeter.
- One core for organic geochemical investigations (n-alkanes, long chain alkenones, etc.). Samples were taken every centimeter and deep-frozen at -30° C.
- 1-3 cores for pore-water analysis.
- Up to 2 cores for the investigation of biological activity (enzymes and bacteria) in the upper part of the cores.

**Giant box corer (GKG):** Sampling with the giant box corer (50 by 50 by 60 cm) was carried out routinely on all geological stations. In total, 45 box cores were run, of which 42 recovered surface and near-surface sediments with an average thickness of about 37 cm. Only three box core casts failed due to technical problems.

The sediment surface of large box cores was sampled as follows:

- 100 ml plastic vial for stable isotopes in foraminifers;
- 20 by 10 cm surface sample for sedimentological and geochemical investigations;
- 10 by 10 cm surface sample for anorganic geochemical investigations;
- 10 by 10 cm surface sample for specific investigations at GEOMAR, Kiel;
- 100 ml vial for investigations on ostracodes.

The sediment column gained by large box corer was sampled as follows:

- 3 plastic boxes (7.5 by 15 by 27.5 cm) covering a complete sediment sequence for sedimentological and stable isotope investigations;
- 100 ml plastic vials every 5 or 10 cm for the investigation of ostracodes;
- 3 plastic tubes (12 cm in diameter) covering the entire profile for archiving at AWI;
- 1 plastic tube for radioisotopes (stored at AARI, St. Petersburg)

*Coring of long sediment cores*

Besides the near-surface sampling one of the major aim was to get undisturbed sediment cores as long as possible. For this purpose the gravity corer (SL) and the kastenlot (KAL) were in progress.

Gravity corer (SL): The gravity corer has a penetration weight of 1.5 t and a core barrel segment of 5.00 m in length and 120 mm in diameter. During ARK-IX/4 core barrels with a length of 5 or 10 m were used. The gravity corer had been performed on 33 stations and penetrated sediment sequences with an average length of 470 cm. The longest core recovered about 921 cm of sediment. Six times the cores were empty or only very short sediment sequences were recovered because of too stiff or hard seabottom.

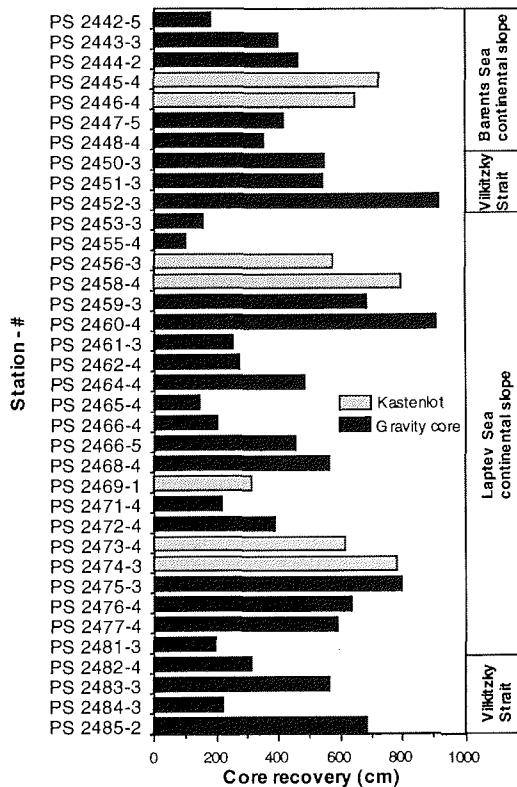


Fig. 8.2-3: Core recovery of long gravity corer.

Long sediment cores (SL and KAL) were sampled according to the following scheme: SL-cores were sampled in 10 cm interval:

- Sample for water content and wet-bulk density (5 ml in pre-weighted glas vials);
- Sample for sedimentological investigations (10 ml for grain size distribution and clay mineralogy);
- Sample (20 ml) for coarse fraction analyses, stable isotope measurements and organic carbon and carbonate contents.

**Kastenlot (KAL):** The Kastenlot (KÖGLER 1963) has a rectangular cross section of 30 by 30 cm and a length of corebarrel of 575 cm (manufactured by Hydrowerkstätten Kiel, Germany). The penetration weight is 3.5 t. Because of the relative large diameter area (900 cm<sup>2</sup>) and the small wall-thickness, the quality of the sediment cores was generally excellent i.e. very low sediment-disturbance due to shear-stress occurred. The length of the core boxes used on ARK-IX/4 was 5.75 m, 11.50 m or 14.50 m plus 35 cm for the core catcher.

On the cruise eight kastenlot-stations had been carried out, from which seven attempts recovered sediment sequences with a maximum length of 784 cm. Average sediment thickness was about 630 cm. Only one time the core catcher did not trigger and no sediment was recovered.

Sampling of KAL-cores was according the following procedure:

- 1 cm slices every 5 or 10 cm in 100 ml plastic vials;
- 3 plastic boxes (100 by 16 by 7.5 cm) covering the entire core (AWI Archive, AWI geochemistry and GEOMAR, Kiel)
- 1 plastic box (100 by 9 by 7.5 cm) over the entire length of the core for organic geochemical investigations. Samples were immediately deep-frozen at -30° C.

#### *Sediment Description and Characterization*

**Visual description:** The sediment cores obtained during this expedition and opened on board *Polarstern* (Tab. 8.2-1) have been routinely photographed, described in detail and graphically displayed (see Appendix). Sediment colours were identified according to the "Munsell Soil Color Chart" (Kollmorgen Instruments Corp., Newburgh, USA). Samples were coded by the PS-initials, an AWI number code, and an abbreviation for the sampling gear (e.g. PS2460-3 SL).

**Coarse grain analysis:** Bulk sediment samples of selected sediment cores were washed through a 63 µm mesh, dried, and analyzed for the coarse fraction composition under a binocular.

**Radiographs:** X-ray radiographs have been prepared for all short and long sediment cores, which have been opened during the cruise. Therefore, sediment slabs of ca. 0.5 cm thickness were taken continuously downcore in order to elucidate sedimentary and biogenic structures. Processing of images is still in progress.

**Smear slide investigations:** Smear slides provide an excellent tool to quickly characterize the sediment. Estimations of grain size distribution and distribution pattern of main sediment components have been proved to reflect actual circumstances. For all discernable lithological units, thus, smear slides were prepar-

GKG	SL	KAL
2485-1		
2484-3		
2483-2	2483-3	
2482-2		
2481-2		
2480-2		
2478-3		
2477-3		
2476-3	2476-4	
2475-1		
2474-2		2474-3
2473-3		2473-4
2472-2		
2471-3	2471-4	
2470-4		
2469-3		2469-1
2468-3		
2467-3		
2466-3		
2465-3	2465-4	
2464-2		
2463-3		
2462-3		
2461-2		
2460-3	2460-4	
2459-2		
2458-3		2458-4
2456-2		2456-3
2455-3		
2453-2	2453-3	
2452-2		
2451-2	2451-3	
2450-2	2450-3	
2449-3		
2448-3	2448-4	
2447-4	2447-5	
2446-3		2446-4
2445-3		2445-4
2444-1	2444-2	
2443-2		
2442-4		
2441-3		
2440-4		
2439-2		

**Tab. 8.2-1:** List of sediment cores opened, described and samples aboard RV *Polarstern*. during ARK-IX/4.

ed (Annex 10.3). Smear slides were analyzed under a microscope in order to establish a rough biostratigraphical zonation for selected sediment cores (e.g. PS2445-4, PS2446-4, PS2471-4). Abundance of coccoliths could easily be determined under crossed nicols, and thus, provide a preliminary time constraint. A minimum of four transects crossing each smear slide were considered to be representative for the entire sample. The occurrence of coccoliths has been documented by applying following systematics: 0 = barren, 1 = present, 2 = rare, 3 = common, 4 = abundant, 5 = rich (see Fig. 8.4.1-6).

### 8.3 Physical properties

#### *Shear Strength*

A vane shear instrument (HAAKE viscometer, RV 3) was used to measure undrained shear strength of undisturbed box and kastenlot cores and selected gravity cores. A 20 x 8.8 mm vane was used with this instrument, inserted 1 cm deep into the sediment and rotated at a speed of four rotations per minute (24°/sec). The measurement interval ranged from 2.5-12 cm. At each depth interval 2 to 4 measurements were taken in order to determine the scatter associated with sediment inhomogenities, such as bioturbation. Shear strength was measured at peak failure, and some tests were allowed to run to a constant post peak value (residual strength). All values are reported in kPa.

#### *Wet Bulk Density*

From the index properties water content and bulk density, sediment phase relationships as dry density, porosity and void ratio can be derived. The index properties can be determined from the direct measurement of the total mass of the sample ( $M_t$ ), the dry mass of the sample ( $M_d$ ) and the total volume of the saturated sample ( $V_t$ ).

To compensate for ship's motion, mass was determined using a technique of differential counterbalancing on twin top loading electronic balances (CHILDRESS & MICKEL, 1980) The computerized precision electronic balance system used during this cruise was kindly provided by GEOMAR Technologie GMBH, Kiel.

A constant volume sampling tube of 10 cm<sup>3</sup> was used. The tube was carefully pushed into the sediment, then cut out, trimmed and weighed. After determination of the total (wet) mass and volumen, samples were stored for later freeze drying and determination of water content and dry mass in the home laboratory.

Bulk density ( $M_w$ ) is the density of the total sample, including pore fluid or:

$$M_w = M_t/V_t$$

Units are reported in Mg m<sup>-3</sup> which is numerically equivalent to g cm<sup>-3</sup>.

In addition to being one of the most basic measurements for determining material properties, bulk density is also one of the two variables required for calculation of sediment accumulation rates.

### *Magnetic susceptibility*

Detailed descriptions of the applied equipment and methods for magnetic susceptibility measurements are given in NOWACZYK (1991) and FÜTTERER (1992). In this context, only a brief outline is given.

The relation between a magnetic field  $H$  and an induced magnetization of a sample  $J_i$  exposed to this magnetic field is quantified by the magnetic susceptibility  $k$ :

$$k = H J_i$$

In general, the magnetic susceptibility reflects the content of magnetite in the sediments investigated, since the ferrimagnetic magnetite exhibits quite high susceptibilities ( $k = +10^{-2}$  SI) in contrast to all other rock-forming minerals with weak diamagnetic ( $k = -10^{-6}$  SI) or paramagnetic ( $k = +10^{-6}$  SI) characteristics.

Different source areas can be differentiated, which lead to the influx of magnetic minerals into ocean sediments (THOMPSON & OLDFIELD 1986). The role of biogenic magnetite produced by bacteria (CHANG & KIRSCHVINK 1989) is not sufficiently investigated for Arctic sediments. However, submarine volcanism along active spreading zones may provide magnetic carrier-minerals.

Measurements were performed by a Bartington susceptibility control unit M.S. 2 in conjunction with two different sensors, one for measurements of entire core segments, the other for paleomagnetic standard samples with volumes up to  $10 \text{ cm}^3$ . During the analyses, the sample within the sensor is subjected to a weak magnetic field ( $0.5 \text{ mT}$ ,  $f = 565 \text{ Hz}$  or  $f = 460 \text{ Hz}$ ). The sensor is part of a loop, the frequency of which will be changed by the entering sample. The frequency change is directly proportional to the magnetic susceptibility and will be transferred to a digital unit presented in magnetic susceptibility logs. Logging was done in steps of ca.  $2 \text{ cm}$  with zero reading at the beginning and ending of single core segment measurements

## 8.4 Sediment Characteristics and Lithostratigraphy

### 8.4.1 *Sediments from the Barents Sea Continental Slope between Svalbard and Franz Josef Land*

**Lithological description:** The study of the terrigenous sediment supply and identification of the different transportation processes, bringing the material from the Eurasian shelf into the deep basins of the Arctic Ocean, and their changes through the late Quaternary are major topics of the sedimentological investigations in the Barents Sea. The studied area of the continental slope of the northern Barents Sea was chosen to get more information about the sediment composition and stratigraphy and to carry out a better interpretation and correlation of the shelf sediments and the deep-sea sediments sampled in the adjacent Nansen Basin during the ARCTIC'91 cruise (FÜTTERER 1992). One question for example is, whether mineralogical changes in the sediment cores of the Nansen Basin are related to different supply mechanisms from the shelf and whether Spitsbergen, Franz Josef Land or the shelf in between are possible source areas of the sediment material. A correlation of sediment cores in an area as the Barents Sea slope, where high energy mass flows depending on the local topography and environment occur,

is in most cases very difficult, because of lenticular sediment layers due to erosional processes, channellization and local depositional centers.

One station in the Bear Island Trough (southwestern Barents Sea), two transects (A and C) perpendicular to the continental slope and a number of stations parallel to the lower slope (Figs. 8.2-1, 8.4.1-1, 8.4.1-2) were sampled in the Nansen Basin. 11 GKGs (about 45 cm length), 9 MUCs (about 30 cm length) and seven longer cores (up to 6.45 m length) from water depths between 180 and 2988 m were obtained in this area. Thus, the profiles cover the shelf, the continental slope and the transition to the deep abyssal plain in front of the slope. Transect C is located beside a local channel system, which makes intercore correlation difficult.

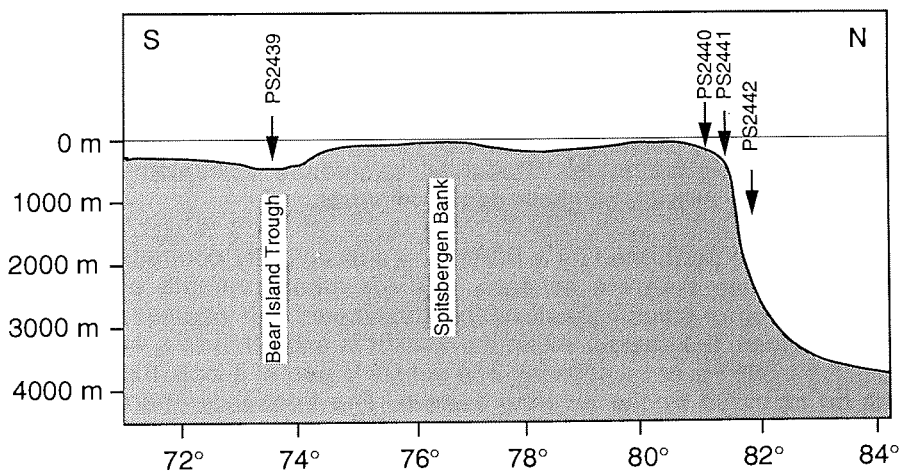


**Fig. 8.4.1-1:** Schematic cross section of the Barents Sea continental slope showing the core stations of Transect A, northeast of Nordaustland, Svalbard.

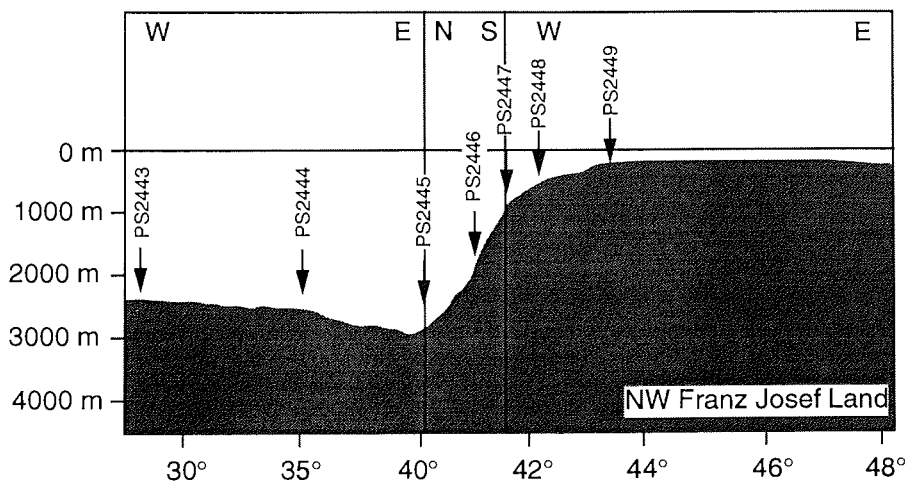


**Fig. 8.4.1-2:** Schematic cross section of the Barents Sea continental slope along Transect C showing site locations; note changes in transect direction.

The sediment surfaces, as observed in the box cores, generally consist of dark brown silty clay and show, mainly in shallower water depth down to 1000 m, a high activity of benthic life. In most of the cores from the Barents Sea continental slope planktic and benthic calcareous foraminifers occur in the surface and near-surface sediments. The uppermost, brownish coloured, oxidized layer of silty clay shows different thicknesses along the slope. In the shallow cores down to 1000 m waterdepth this layer is from a few centimetres to about 25 cm in thickness. In the cores from deeper waters this layer exhibits thicknesses of up to 70 cm (e.g. Core PS2445-4). One exception is Core PS2442-5 in a water depth of 2900 m, which has an oxidized layer of only 10 cm thickness.

The transition from this brownish oxidized layer to the underlying, more reducing olive to gray sediment units is characterized in the deeper cores by a 2-5 cm thick layer of reddish-brownish, very stiff and laminated sediment. This diagenetically altered horizon, with a probable strong enrichment of Fe and Mn, sometimes contains centimetre thick layers of dark brownish to black coloured, strongly cemented sediment. In more shallower cores from shallower water depths the transition zone between these different oxidation environments is more gradual and often a mottled structure occurs.

The sediment sequence underneath is varying from core to core, but consists in general of an olive to gray silty clay followed by thin sandy turbidites or turbidites enriched in mud clasts. In Cores PS2445-4 and PS2446-4, which can be correlated at least in parts, a characteristic sequence of olive and brown coloured, bioturbated, fine-grained sediments rich in planktic foraminifers is found. In PS2446-4, a deformed slump unit occurs between 180 and 300 cm.

A typical sediment, which occurs in all sampled cores from the Barents Sea continental slope, is a muddy, unsorted, sandy silty clay, which was found also in core PS2157 sampled on the Barents Sea slope during the ARCTIC'91 cruise of RV *Polarstern* (FÜTTERER 1992). This diamicton is gray to dark gray and contains outsized pebbles, stones (up to 15 cm) and mud clasts. Bioturbation is absent. In the PARASOUND subbottom records, this diamicton is visible as acoustically transparent layers intercalated between distinct reflectors (see Chapter 8.1). The geometry of the reflection pattern is characterized by lenticular shapes and, in places, truncation.

The structure of the above described sediment units is clearly visible in the radiographic prints of the sediments. They show in more detail very thin sand layers, the internal layering of certain units, the shape of dropstones and mudclasts, and the shape of the boundaries between different sediment layers. Also, the grading upwards in some turbidites and the occurrence of small mud clasts can only be identified in the radiographic prints.

An example of correlation of four cores along Transect C is shown in Figure 8.4.1-3. A good correlation of several units in Cores PS2445-4 and PS2446-4 could be obtained with the help of the structure and colour of sediments. In all four cores, an uppermost brownish unit exists. A characteristic sequence of a thin pinkish layer, an underlying unit with abundant mudclasts, followed by a thin sandy layer occurs in Cores PS2445-4 and PS2446-4. An intercalated sediment package of about 55 cm in Core PS2446-4 makes this sequence apparent in deeper parts of the core. Two addi-

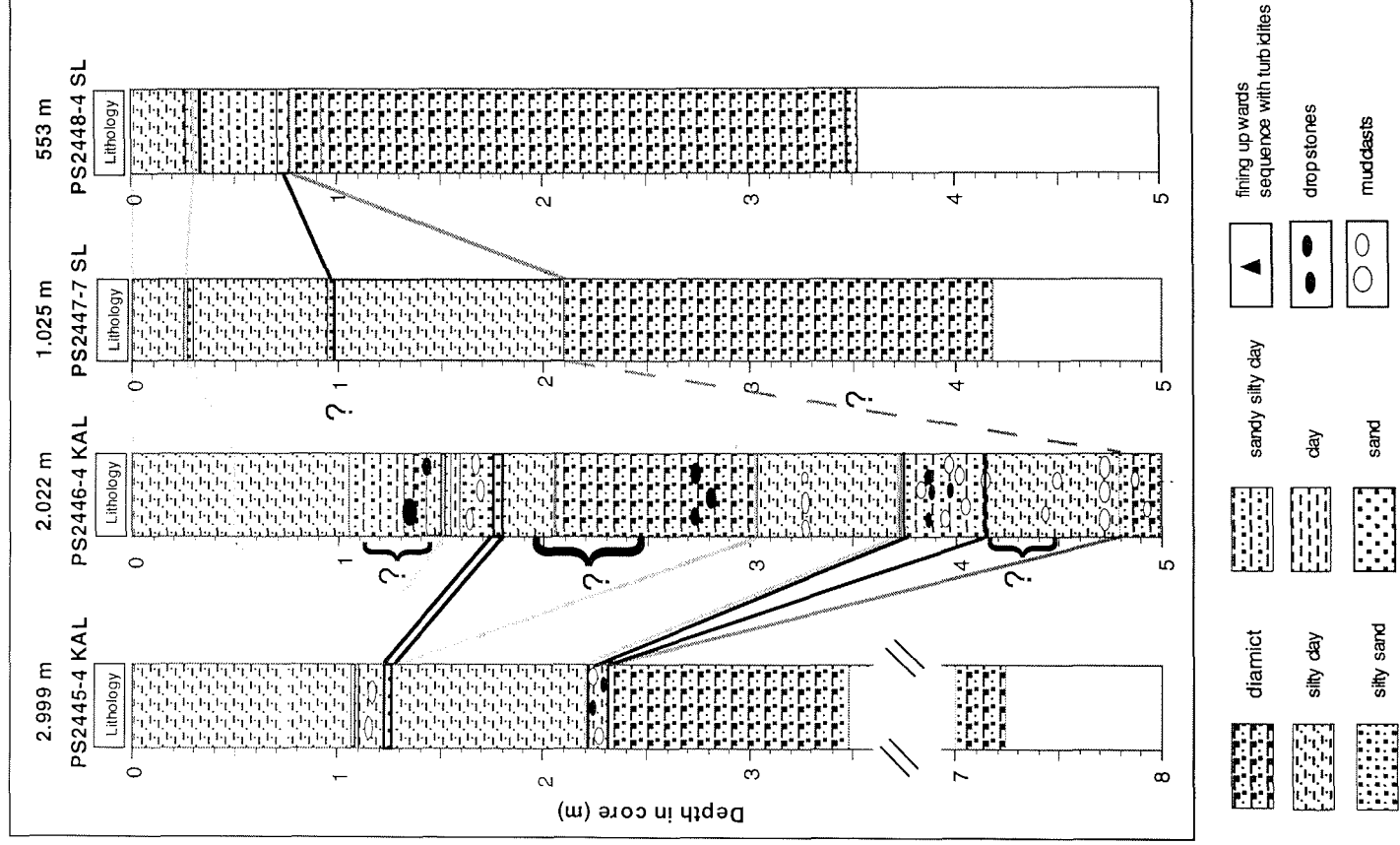


**Fig. 8.4.1-3:** Lithological core description of four sediment cores from the Barents Sea continental slope along Transect C, northwest of Franz Josef Land.

tional sediment sequences intercalated in Core PS2446-4 are visible, which correspond to local depositional events and can not be correlated with the other three cores. These intercalated sequences cause the grayish diamict to end in a core depth of 480 cm. The upper boundaries of the diamictos are situated in a depth between 230 (deepest Core PS2445-4) and 80 cm (shallowest Core PS2448-4).

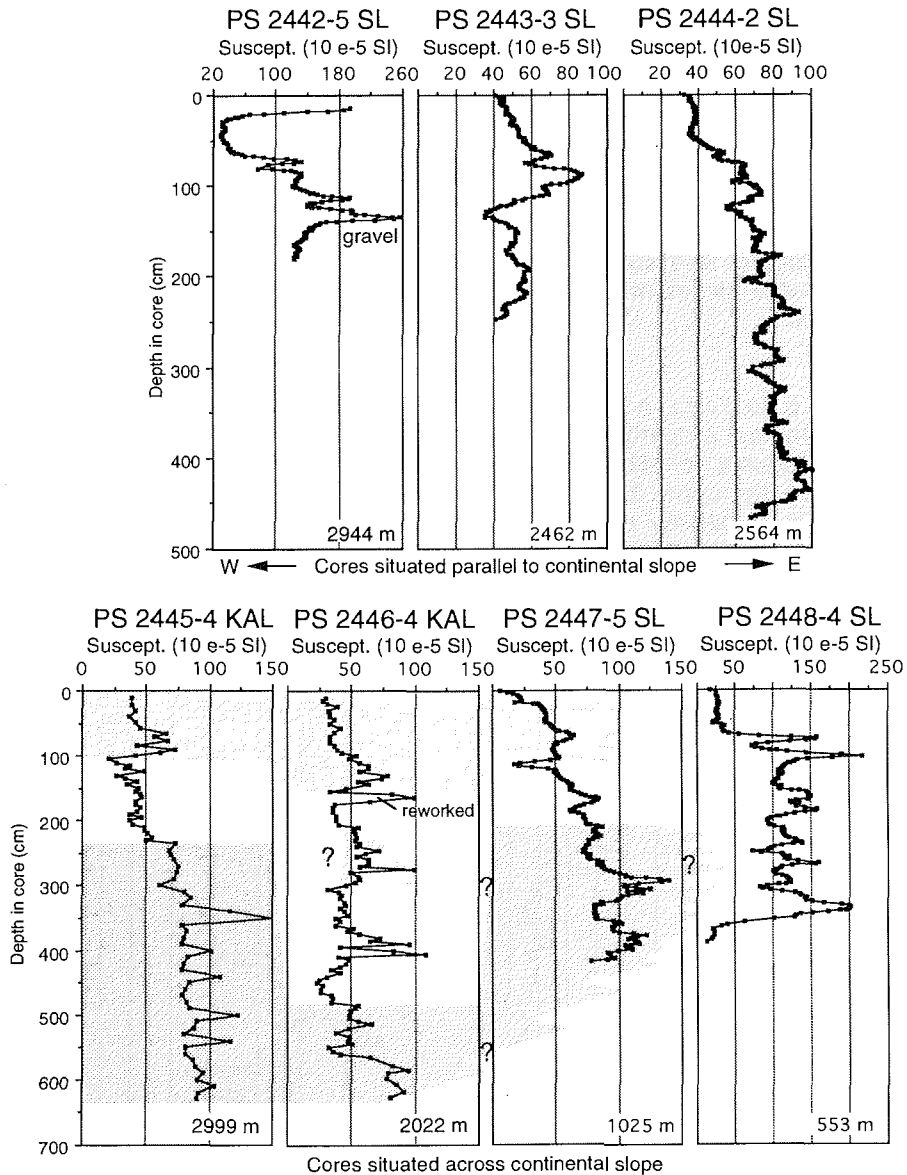


**Fig. 8.4.1-4:** Magnetic susceptibility logs of seven longer cores recovered from the Barents Sea continental slope.

Magnetic susceptibilities within cores PS2443-3 and PS2444-2 from approximately 2500 m water depths along the lower continental slope range generally between  $40-80 \cdot 10^{-5}$  SI (Fig. 8.4.1-4). A quite speculative core correlation in the upper sediment sections (shaded area in Fig. 8.4.1-4) cannot be extrapolated further west to core PS2442-5. Here, very high magnetic susceptibilities of up to  $260 \cdot 10^{-5}$  SI are closely related to the occurrence of well-sorted gravel in approximately 3000 m water depth (80-180 cm core depth).

Transect C crossing the continental slope northwest of Franz Josef Land allows the correlation of magnetic susceptibility records at least for the upper sediment sequences (Fig. 8.4.1-4). Sediments from the shallowest coring site at approximately 553 m water depth have highest magnetic susceptibilities of mainly  $100-150 \cdot 10^{-5}$  SI with maxima around  $200 \cdot 10^{-5}$  SI. Downslope, magnetic susceptibilities decrease below  $100 \cdot 10^{-5}$  SI. A correlation of magnetic susceptibilities of Cores PS2445-4 and PS2446-4, at the first glance, is problematic. However, when comparing the lithological and susceptibility records, it becomes obvious that in Core PS2446-4 a large sediment package is intercalated, which cannot be identified in adjacent cores.

Physical properties: The cores collected from the Barents Sea continental slope show physical property variations which are a reflection of the wide grain size and sediment source variations (Fig. 8.4.1-5). In Core PS2445-4 (KAL), retrieved at the lower slope, the upper 2.3 m of the sediment sequence has very variable shear strength and bulk density curves showing characteristic peaks corresponding to layers rich in mud clasts (? turbidites) and more silty intervals. From 2.3 m to the

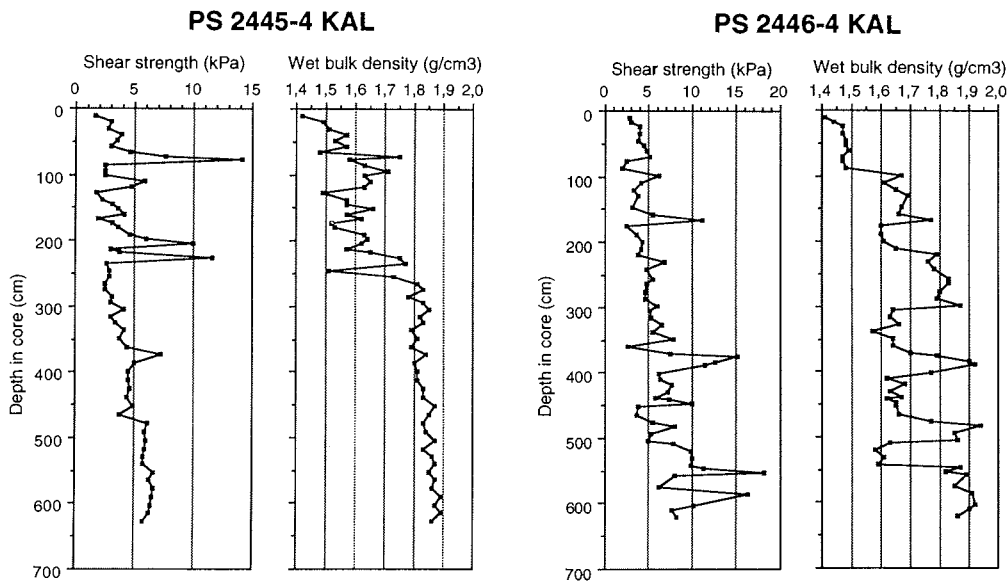
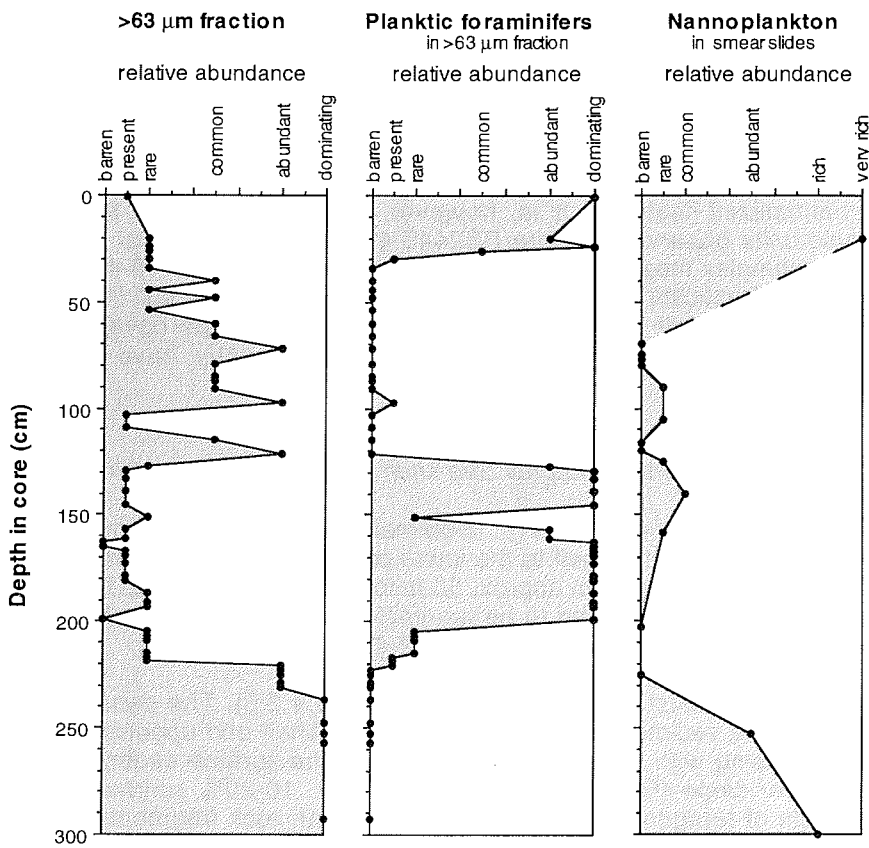


Fig. 8.4.1-5: Physical properties (shear strength and wet bulk density) of Cores PS2445-4 KAL and PS2446-4 KAL located on the continental slope northwest of Franz Josef Land (Transect C).

base of the core (6.3 m), a sandy diamicton shows rather low shear strength and high bulk density, supporting that the unit represents the upper part of a larger mass flow. Core PS2446-4 (KAL), taken at the middle part of the slope, has quite variable physical properties throughout the core length, reflecting the occurrence of intimately bedded lithological units. In general, shear strength increases with depth at a rate of less than 1 kPa/m. The characteristic pattern of the bulk density curve is reflecting the presence of two depositional types. Intervals with low densities (1.4-1.7 kPa/m) are supposedly hemipelagic sediments, whereas coarser-grained intervals with densities of 1.7-1.9 kPa/m are interpreted as rapidly deposited mass flows.

**Depositional environment:** The sediment cores sampled on the Barents Sea continental slope consist in general of two different depositional types: (i) fine-grained hemipelagic deposits and (ii) coarser-grained mass-flow deposits. The variability of the core sections is reflecting the dynamic depositional environment on a relatively steep continental slope, which during glacial times was a potential depocenter for glacier-eroded material from the Barents Sea shelf. Local channelliza-



**Fig. 8.4.1-6:** Comparison of the abundance of the >63 μm grain fraction and abundances of planktic foraminifers and nannoplankton in sediment Core PS2445-4 (KAL) from the Barents Sea continental slope (Transect C).

tion, erosion/deposition of mass flows, as well as slide/slump redeposition of sediment units can explain the observed variability.

The upper 1-2 m of the sequence can be correlated among most of the longer cores. The uppermost, brownish silty clay with abundant planktic foraminifers and nannoplankton (Fig. 8.4.1-6) is of hemipelagic origin and most probably of Holocene age. In most of the cores, a greyish clay with scattered mud clasts and occasionally thin sandy turbidites, barren of planktic foraminifers follows below. It seems possible that these sediments are of last glacial age. In Core PS2445-4 KAL, which presumably presents a relative complete sequence, follows an about 0.8 m thick unit of olive and brown-coloured hemipelagic sediment rich in planktic foraminifers and nannoplankton. This unit may represent the last interglacial age. However, detailed stratigraphical investigations including stable isotope stratigraphy are necessary to confirm this anticipation.

A homogeneous diamictic sediment is found in the middle to lower part of all longer cores. The lithological character as compared to the PARASOUND records (see Fig. 8.1.2-1) and physical properties (see Fig. 8.4.1-5) suggests that this represents a large lenticular debris flow lobe, having a maximum thickness of about 7-8 m on the lower slope. Large debris flows were supposedly deposited in a glacial-deglacial phase, where glaciers from the wide Barents Sea shelf were capable of dumping large amounts of unsorted sediment directly on the shelf break and/or upper slope. The diamictic sediment was subsequently transported downslope as extensive debris flow units, which occasionally may have developed into turbidity currents. Two of the cores, PS2442-5 and PS2446-4, deviate from this general pattern and may represent locally channelized features. It is, however, interesting to note that the same hemipelagic units observed in Core PS2445-4 in the depth interval 1.3-2.1 m are found in the complex mass-flow dominated section of Core PS2446-4 between 3.0-3.7 m. This might indicate that channels were inactive during the last interglacial high sea level stand, so that a relative uniform hemipelagic drape covered the entire slope. Local erosion and slide/slumps may subsequently have modified the distribution.

#### 8.4.2 *Sediments from the Laptev Sea shelf and continental margin*

**Lithological description:** Sediment cores were obtained along four sampling transects from the shelf to the lower continental slope. Transects F, G and H covered the depth range from approx. 50 m to  $\geq 3000$  m (Fig. 8.4.2-1 to -3). Coring operations along Transect E had to be terminated at a water depth of approx. 1200 m due to unfavorable ice conditions (Fig. 8.4.2-4).

All box core tops consist of soft brown mud (Fig. 8.4.2-5). The density of benthic populations on the sediment surface is high on the shelf and uppermost slope, but strongly decreasing with increasing water depth. The surface sediments from the shelf and upper slope (50-1000 m) contain approx. 10-20% sand-sized material, which consists of terrigenous grains (quartz, feldspar, rock fragments). Ostracods, small bivalves, calcareous and agglutinated benthic foraminifers are common, whereas planktic foraminifers are absent to rare. Sand content of the surface sediments decreases strongly with water depth. In samples from  $>3000$  m water depth, it is  $<1\%$  and consists almost entirely of planktic foraminifers.

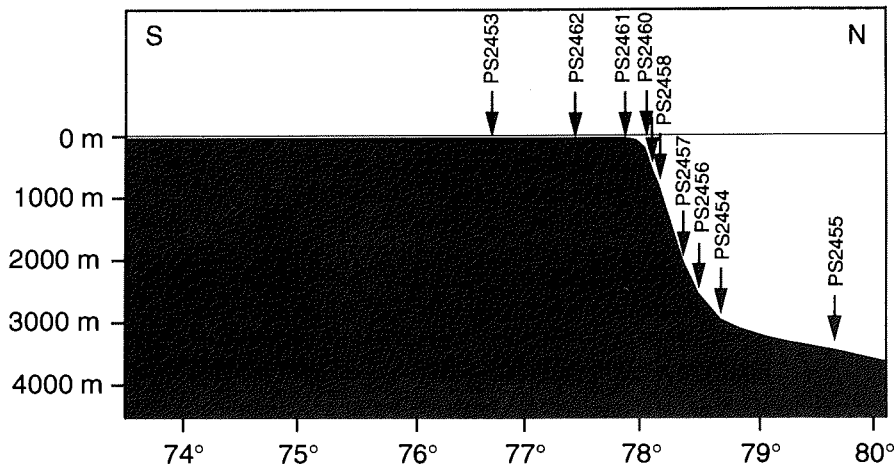


**Fig. 8.4.2-1:** Schematic cross section of the Laptev Sea continental slope showing stations of Transect H.

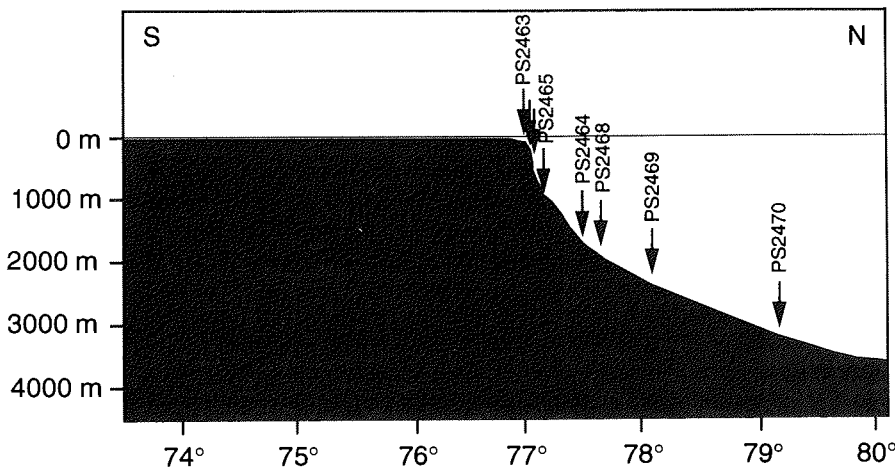


**Fig. 8.4.2-2:** Schematic cross section of the Laptev Sea continental slope showing stations of Transect G.

The thickness of the uppermost, brown lithologic unit of the sediment cores is highest in the cores from the lower slope showing approximately up to 60 cm in thickness, and decreasing to 3-10 cm to the upper slope and shelf. The lithology of this unit always resembles the sediment surface. The sediments are strongly bioturbated.

On the shelf and upper continental slope, the underlying sediments consist entirely of dark gray, sandy, silty clays with abundant black spots (Fig. 8.4.2-5). Again, bioturbation is very strong. The sediments contain relatively high amounts of terrigenous organic matter (plant fibers) and the sediment colour is determined by black aggregates of biogenic origin. They resemble worm tubes and remains of other

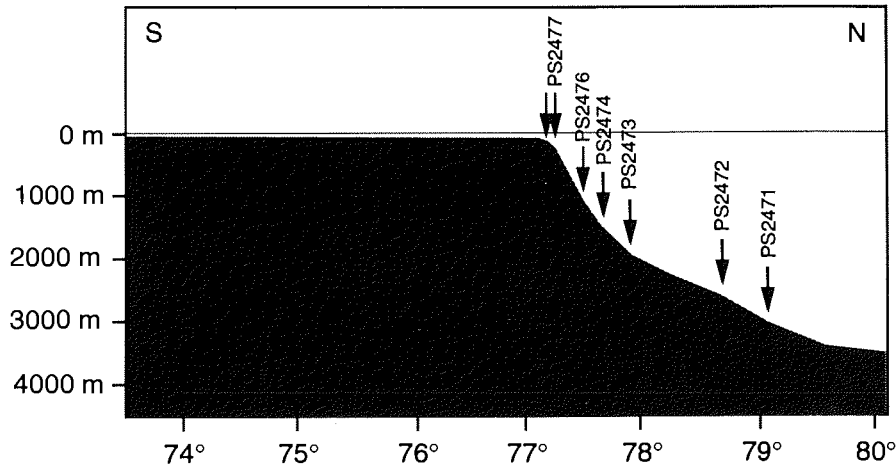


Fig. 8.4.2-3: Schematic cross section of the Laptev Sea continental slope showing stations of Transect F.

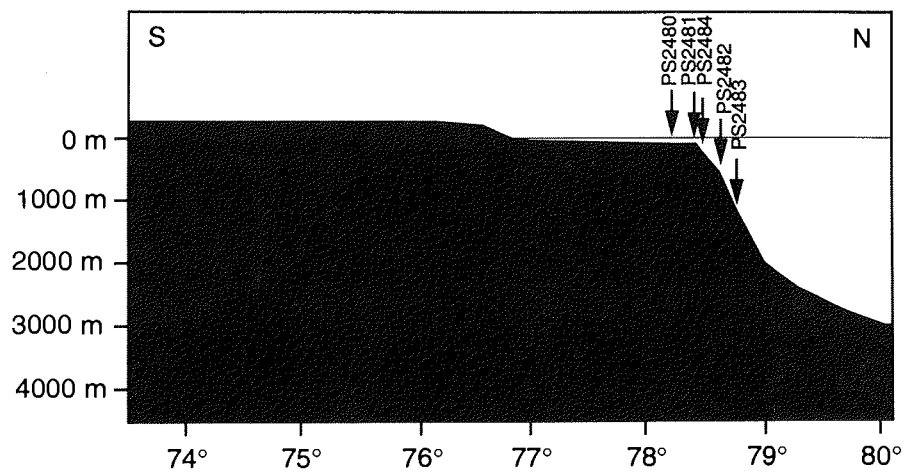
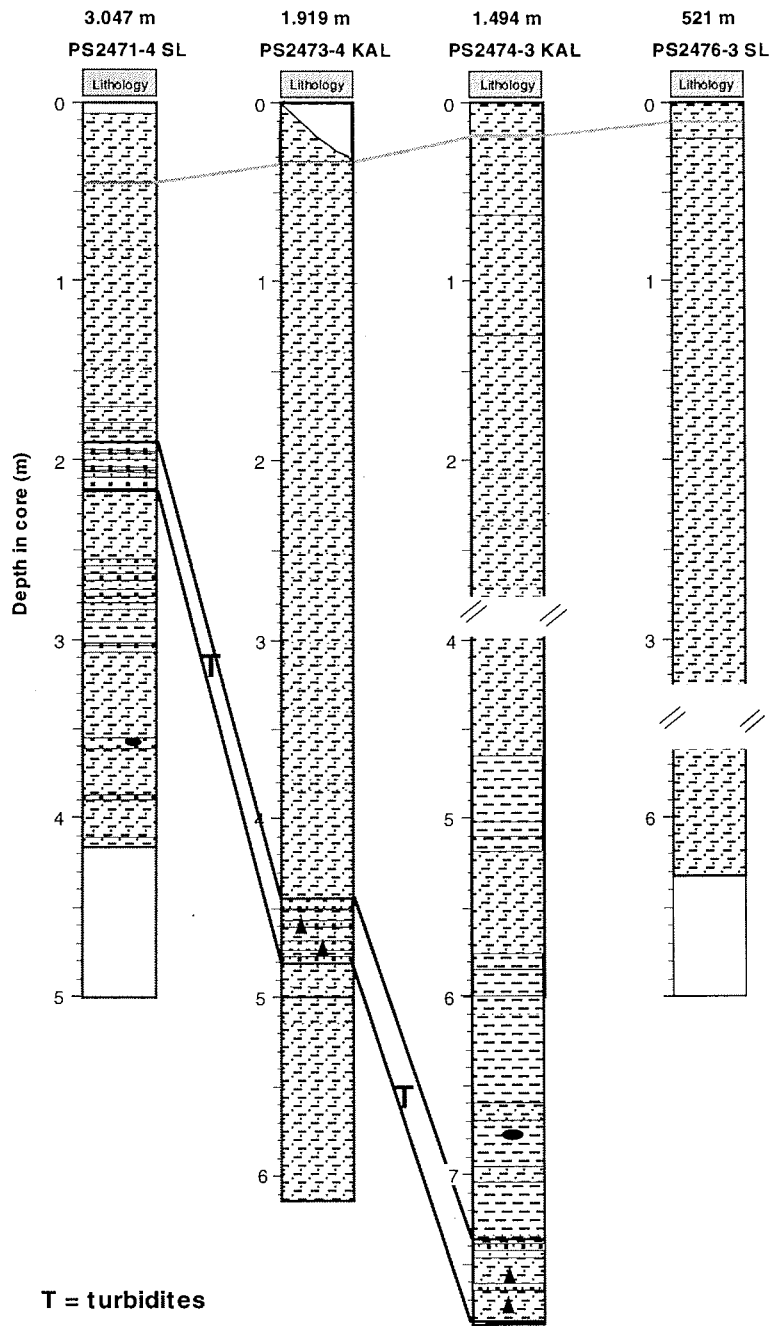


Fig. 8.4.2-4: Schematic cross section of the Laptev Sea continental slope showing stations of Transect E.

burrowing organisms, but are converted to iron-manganese sulphides. Apart from some variability in the density of black spots, the sediments look very similar in all cores. As soon as the dark gray sediments described above were exposed to the atmosphere for a sufficient time (12-48 hours), one could observe a surficial colour change to brownish and olive greenish colours. Obviously, the Fe-Mn sulphides at the exposed sediment surface were oxidized, revealing the "normal" colours of the bulk of the terrigenous sediment components.

In the eastern Laptev Sea (Transects G and H), the subsurface-sediments from the middle and lower slope (water depth >1000 m) resemble very much those of the up-



**Fig. 8.4.2-5:** Lithological core description of four sediment cores from the Laptev Sea continental slope along Transect F.

per slope. The amount of coarse grained material ( $>63 \mu\text{m}$ ) is lower than in cores from shallower depths. Occasionally, thin sandy layers (turbidites) are intercalated, especially in the lower parts of the sediment cores. In the western Laptev Sea (Transects E and F) however, the subsurface-sediments from the middle and lower slope contain mostly silty clays of brownish to olive greenish colours. Again, thin turbidites are intercalated.

**Magnetic susceptibility:** For nearly all short (GKG) and long sediment cores (KAL, SL) collected from the Laptev Sea shelf and continental slope, magnetic susceptibility records have been produced aboard RV *Polarstern*. In this report, however, only gravity core and kastenlot logs are presented (Fig. 8.4.2-6 to -9).

Sediments recovered from the Laptev Sea continental slope and shelf are typically characterized by magnetic susceptibilities of approximately  $40\text{-}250 \cdot 10^{-5}$  SI. These values are significantly higher than values previously published for central Arctic Ocean sediments. Cores recovered during the ARCTIC'91 expedition of RV *Polarstern* exhibit magnetic susceptibilities of approximately  $25\text{-}50 \cdot 10^{-5}$  SI in Amundsen and Nansen Basin, and  $15\text{-}30 \cdot 10^{-5}$  SI on Gakkel and Lomonosov Ridge respectively (FÜTTERER 1992).

Cores obtained during this expedition generally show decreasing magnetic susceptibilities downslope. Shelf and upper slope sediments down to approximately 500 m water depth are commonly characterized by magnetic susceptibilities larger than  $60 \cdot 10^{-5}$  SI, mainly ranging around  $100 \cdot 10^{-5}$  SI with extremes up to  $250 \cdot 10^{-5}$  SI. Below approx. 500 m water depth, magnetic susceptibility values mainly decrease to  $20\text{-}60 \cdot 10^{-5}$ . The decrease of magnetic susceptibilities from shelf to continental slope and further on to central Arctic deep-sea and mid-ocean ridge sediments presumably reflects a constant, density-dependant loss of heavy, magnetized minerals like magnetite during long-range transport.

Though most cores from Laptev Sea continental slope do not show any significant lithological change, thus preventing visual core correlation, magnetic susceptibility provides an excellent tool for core correlation and, in addition, for determination of relative sedimentation rates. Transect F (Fig. 8.4.2-7), comprising seven magnetic susceptibility logs, clearly elucidates distinct deposition patterns along the continental slope. The susceptibility record of Core PS2471-4, which has been recovered from the deepest location at 3047 m water depth, unambiguously correlates with all other cores located across the slope. Distinct peaks in the records, become more and more pronounced when approaching the upper slope at 187 m water depth (indicated by light shading in Fig. 8.4.2-7). Here, high sedimentation rates generate an approximately 6 m thick homogenous sediment sequence. The downslope wedging-out of sediment layers to finally approximately 50 cm thickness is also indicated in the corresponding PARASOUND echosounding record (see Chapter 8.1). The gradual decrease of magnetic susceptibilities below the uppermost maxima in Cores PS2471-4, PS2472-4, PS2473-4, PS2474-3, and PS2475-3 is also reflected by decreasing wet bulk densities in cores PS2473-4 and PS2474-3.

In general, the magnetic susceptibility record of Core PS2471-4 can be correlated to Core PS2483-3, which is the deepest site on Transect E in approximately 1200 m water depth. Comparable values up to approximately  $70 \cdot 10^{-5}$  SI appear in the uppermost metre of sediment, decreasing gradually. It culminates again in three peaks

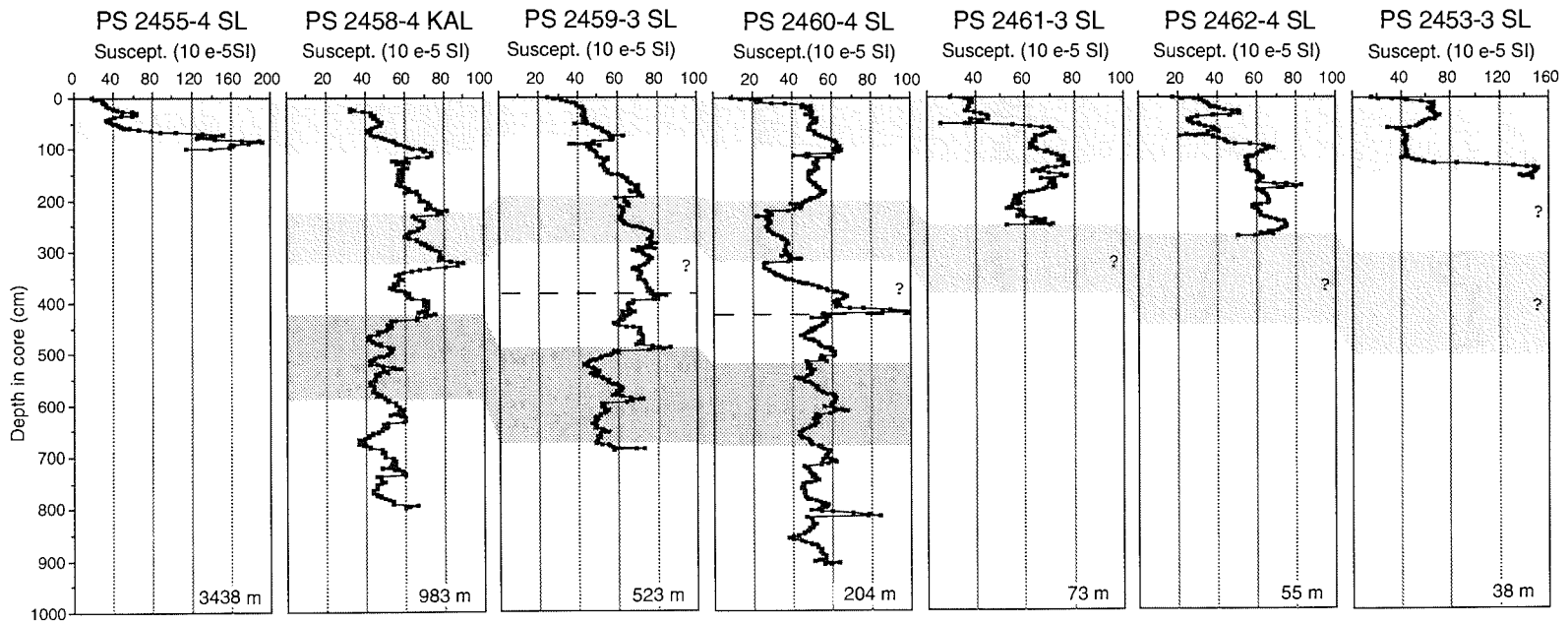


Fig. 8.4.2-6: Magnetic susceptibility logs of cores located across the Laptev Sea continental slope (Transect H).

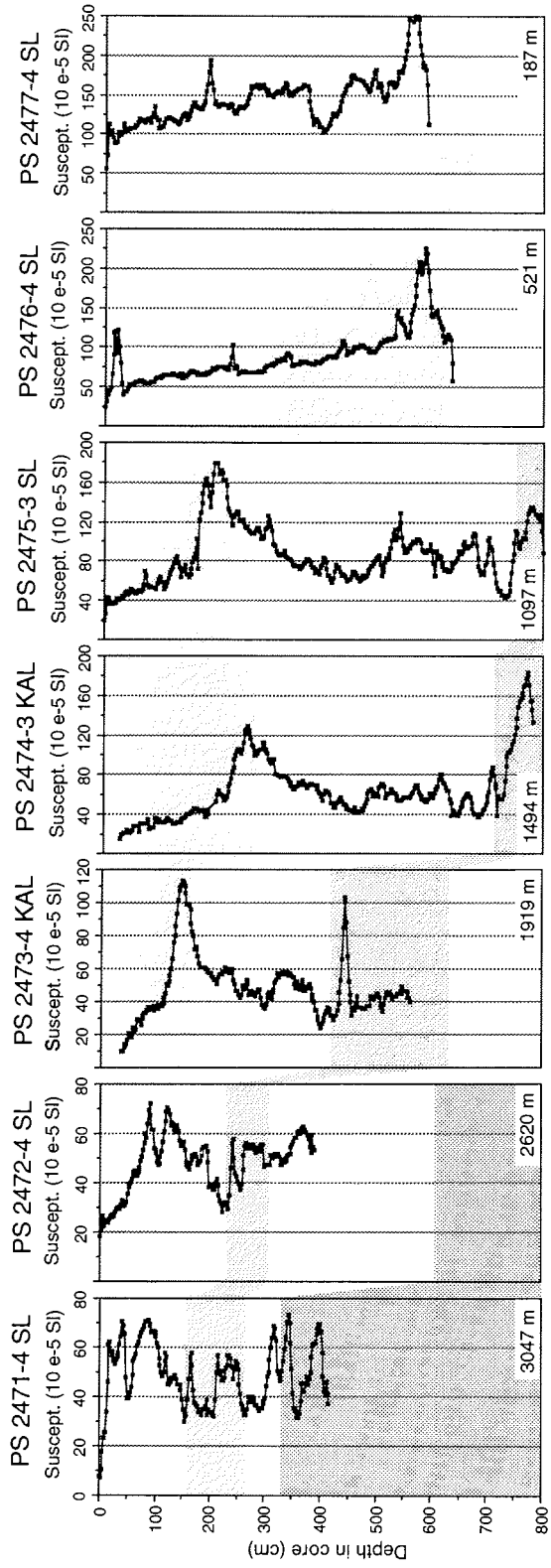
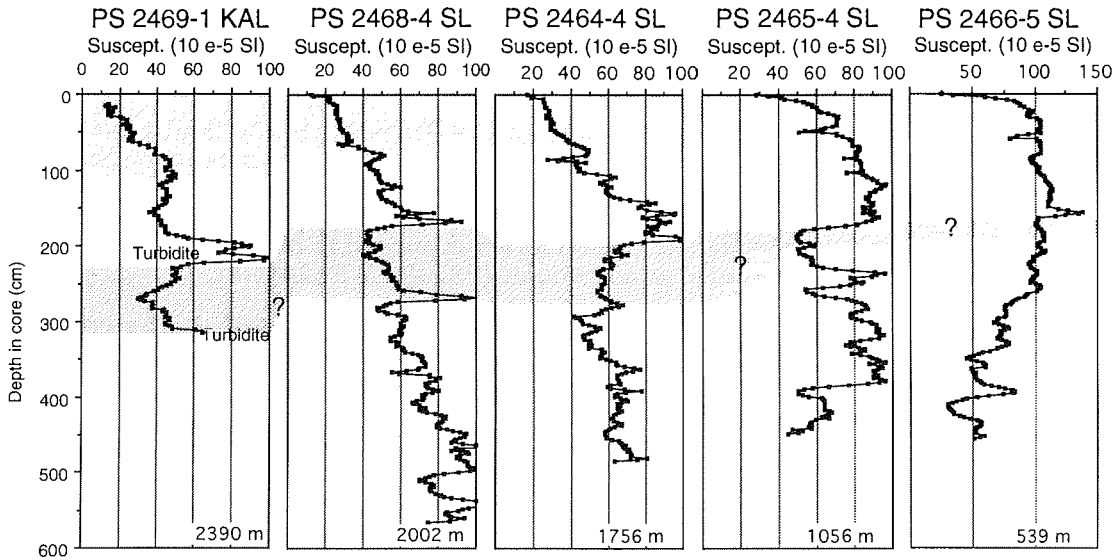
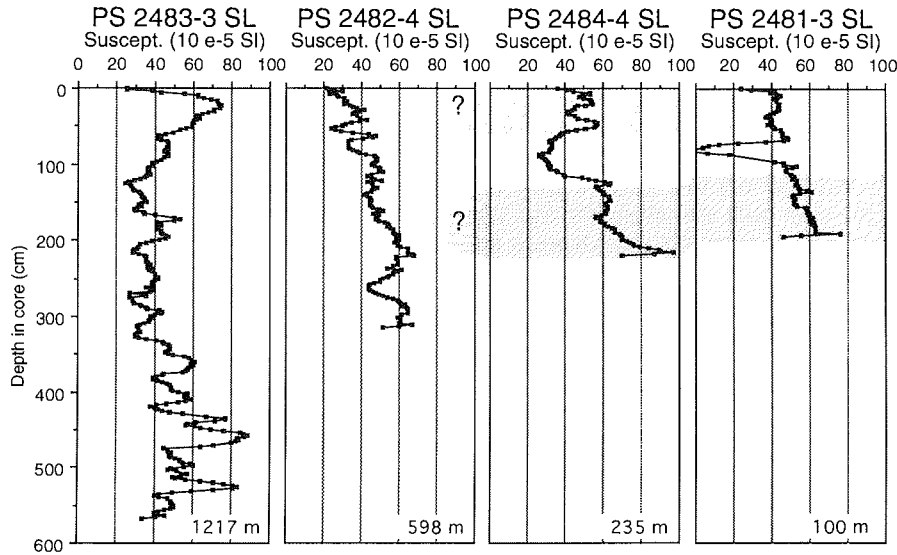


Fig. 8.4.2-7: Magnetic susceptibility logs of cores located across the Laptev Sea continental slope (Transect F).



**Fig. 8.4.2-8:** Magnetic susceptibility logs of cores located across the Laptev Sea continental slope (Transect G).



**Fig. 8.4.2-9:** Magnetic susceptibility logs of cores located across the Laptev Sea continental slope (Transect E).

between 3-4 m depth in Cores PS2471-4 and PS2483-3. Moreover, the lithologies of both cores resemble each other. In contrast, the remaining shallower sites across Transect E have rather different lithology and susceptibility records (PS2482-4, PS2484-4, PS2481-3). Exclusively, the uppermost sediment cores from a water

depth of 235 m (PS2484-4) and 100 m (PS2481-3), respectively, show similar magnetic susceptibility records (Fig. 8.4.2-9).

Magnetic susceptibility logs from the easternmost Transects H and G (Fig. 8.4.2-6 and Fig. 8.4.2-8) have also been successfully applied for core correlation. Lithologically, there is no apparent change with core depth. Within Core PS2469-1 of Transect G, numerous high amplitude and high frequency variations in magnetic susceptibility could be attributed to sand layers supposed to be of turbiditic origin, which could also be detected in adjacent cores (PS2468-4, PS2464-4).

The interpretation of magnetic susceptibility logs from Transect H remains highly tentative. Though correlation of the upper 1-1.5 m of the sediment sequence seems to be possible, the correlation of the lower sequence is rather doubtful, indicated by question marks in Fig. 8.4.2-6.

**Physical properties:** Along the sampling transects on the Laptev Sea continental slope, physical properties were measured on box cores (GKG) and long undisturbed gravity cores (KAL). The cores from each transect can in general be correlated (Fig. 8.4.2-10). However, important differences in properties have been found between sediments retrieved from the eastern and western part of the Laptev Sea slope.

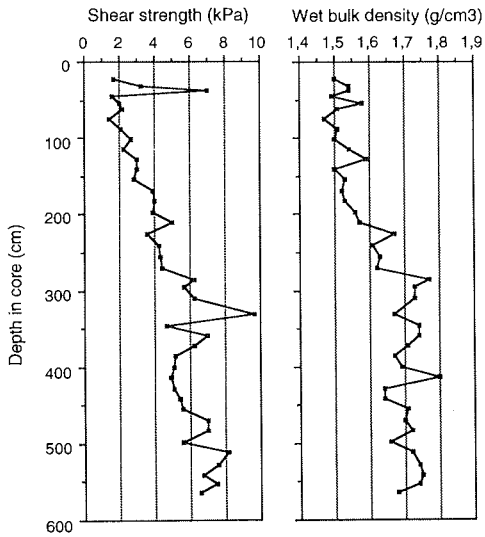
In KAL-cores PS2456-3 and PS2469-1, collected on the lower slope of the eastern Transects H and G, shear strength and bulk density generally increases with depth in the upper 2-3 m of the sediment sequence. Below, a stratified sequence of sandy turbidites shows more constant physical properties with no clear trend, suggesting more rapid sedimentation rates. The lithologically very homogeneous Core PS2458-4 (KAL), located on the middle part of the slope, shows linearly increasing shear strength and bulk densities in the upper 5 m of sediments. Below, more or less constant shear strength values were measured.

On the western Laptev Sea slope (Transect F) another trend in physical properties can be observed. KAL-cores PS2473-4 and PS2474-3 show generally increasing shear strength and bulk density in the upper 2-3 m of sediment. Below, a 2-4 m thick sequence with linearly decreasing bulk densities and a shear strength curve with no obvious trend can be seen. The reason for the observed decrease in bulk density over several metres is speculative until further physical property and mineralogical-geochemical data will be available. However, a high organic carbon content in combination with large porosity and a fast deposition rate could have influenced the observed trend. In the lowermost part of the two KAL-cores an abrupt increase in bulk density reflects the transition to turbidite dominated sediments.

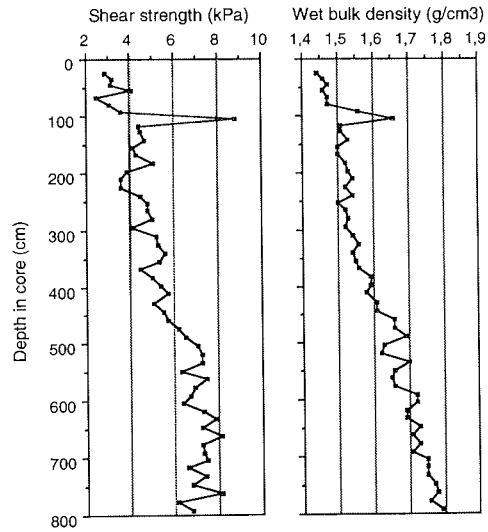
**Depositional environment:** The sediment composition indicates a strong supply of terrigenous material across the Laptev Sea shelf to the continental margin. Additional evidence for this source comes from the relatively high content of plant fragments and from findings of freshwater and shallow marine bivalves in cores from the middle and lower slope. Most of the fine-grained material may be transported in suspension by currents across the shelf. However, significant amounts of sediment may also be rafted by sea ice, as indicated by findings of sediments in

Transect H

**PS 2456-3 KAL**

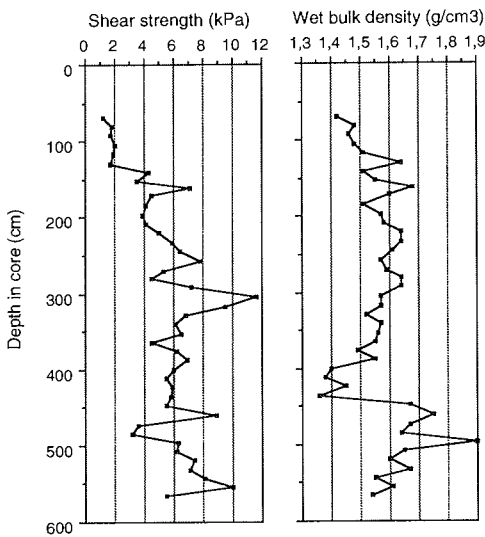


**PS 2458-4 KAL**



Transect F

**PS 2473-4 KAL**



**PS 2474-3 KAL**

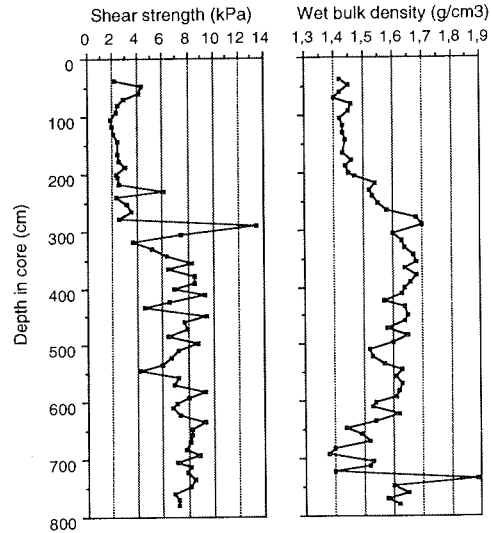


**Fig. 8.4.2-10:** Physical properties (shear strength and wet bulk density) of KAL-cores located across the Laptev Sea continental slope, Transect H and Transect F.

sea ice (see Chapter 6). Except for the shelf samples (partly reworked?) and the westernmost Transect E, the core tops and sediment cores contain only minor portions of coarse-grained sand and gravel. This suggests that sediment-raffing by glacier ice seems to be unlikely in the modern Laptev Sea and never was the dominant sedimentary process during the time interval covered by the sediment cores. Mixing of sediment by bioturbation is extremely strong on the shelf and upper slope. Vertical chitinous worm tubes with a length up to 30 cm indicate a very thick upper mixed sediment layer. Although the degree of benthic coverage is decreasing downslope, bioturbation is still an important environmental process, which prevents any stratification.

The high amount of Fe-sulphides and Mn-precipitations in many sediment cores must be attributed to the decay of marine organic matter by the activity of sulphate-reducing bacteria. This process is active only under reducing conditions, i.e. with no contact to sea water and without the presence of free oxygen in the pore water. Since bottom waters on the Laptev Sea continental margin have a "normal" oxygen content, if compared to the rest of the Arctic Ocean (see Chapter 5), the strong bacterial activity (see Chapter 7) indicates a rapid burial of high amounts of marine organic matter by high sedimentation rates before a sufficient oxidation from sea water could take place. This process apparently is less important for the lower slope of the western Laptev Sea, where brownish and olive greenish colours indicate a "normal" deep-sea oxidation and/or a lower supply of marine organic matter to this area. Here, the sediment colour is probably determined by clay minerals, iron oxides etc. Investigations of chlorophyll in the surface waters (see Chapter 7) support the view of higher biological productivity in the eastern Laptev Sea.

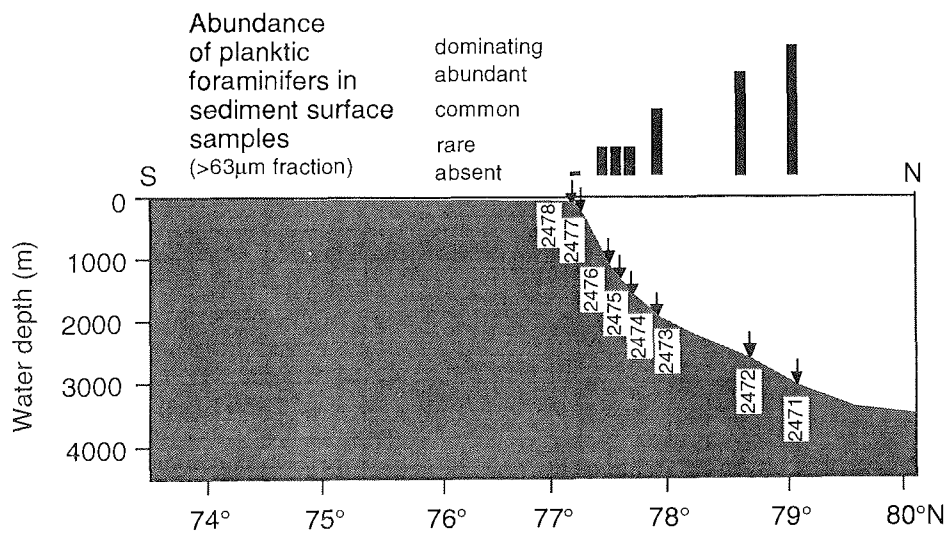


**Fig. 8.4.2-11:** Abundance of planktic foraminifers in sediment surface samples from the western Laptev Sea, Transect F.

The correlation of the magnetic susceptibility records of the sediment cores indicates a strong downslope decrease of sedimentation rates. Apparently, sedimentation rates on the uppermost slope (100-500 m water depth) are approximately ten times

higher than on the lower slope. The strongly decreasing supply of terrigenous material to greater water depths is also apparent from the increasing amount of planktic foraminifers in the coarse fraction of the surface sediments (Fig. 8.4.2-11). Although conditions for planktic life become unfavorable to the North (perennial ice, colder waters), the downslope decreasing dilution by terrigenous material make planktic foraminifers become the dominant coarse fraction component in surface sediments from the lower slope, whereas they are rare on the upper slope.

The obviously high sedimentation rates on the upper slope of the Laptev Sea continental margin and the homogeneity of the sediment cores down to approximately 9 m core depth suggest that environmental conditions did not change significantly during the time interval covered by these cores. It can be speculated that these sediments consist entirely of Holocene deposits. During the last glaciation, the sea level dropped by approximately 120 m and the coastline of the Laptev Sea must have been located near the present shelf break. Considering the probably strongly different sediment transport mechanisms to the shelf break during the late Pleistocene (river transport?) and the Holocene (currents, suspension, sea ice rafting), one should expect lithologic differences between the slope sediments from both time intervals.

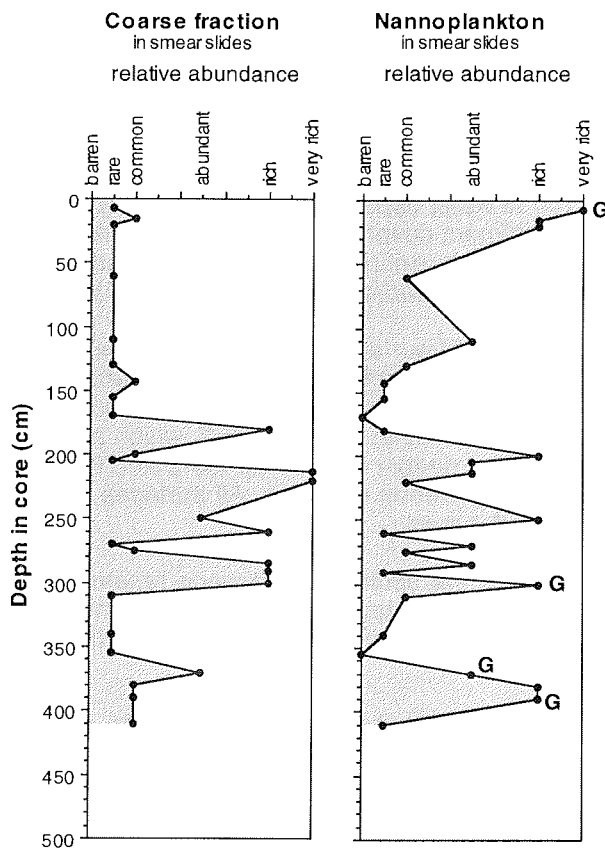


Fig. 8.4.2-12: Comparison of abundances of planktic foraminifers and nannoplankton in Core PS2471-4 from the western Laptev Sea continental slope, Transect F.

However, no lithologic variability can be observed in the cores from the upper slope. The cores from the lower slope, which contain sandy layers, may span over a longer time interval, possibly several glacial-interglacial cycles. This is supported by findings of coccoliths of *Gephyrocapsa* sp., which has proven to be a useful indicator for Arctic interglacial sediments (GARD 1988). The occurrence of this species at 300-400 cm in lower slope Core PS2471-4 (Fig. 8.4.2.-12) may indicate the presence of sediments from the last interglacial (Oxygen Isotope Stage 5). By applying radiometric and isotopic measurements, it will be possible to decipher the history of sedimentary environments of the Laptev Sea continental margin.

To summarize the observations, the sedimentary environment of the Laptev Sea continental margin is characterized by comparatively high sedimentation rates of terrigenous material and strong bioturbation. The deposition of relatively high amounts of terrigenous and marine organic matter and, in many areas, bacterial activity and insufficient oxidation lead to the generation of Fe-sulphides and Mn-precipitations, which determine the dark gray colour of the sediments.

#### 8.4.3 *Sediments from the Vilkitski Strait*

**Lithological description:** Five short (approximately 40 cm, GKG) and four long sediment cores (up to 9 m, SL) were obtained in Vilkitski Strait from 130-230 m water depth. Three cores west of Cape Chelyuskin are located in the northern part (PS2450-3), in the middle (PS2452-3) and in the southern part (PS2451-3) of Vilkitski Strait (see Fig. 8.2-2). Core PS2485-2 was recovered east of Cape Chelyuskin. A further attempt to obtain a core at location PS2486 from the top of a hummock located at 100 m water depth in the center of the Vilkitski Strait failed. Only a few centimeter-thick sediment cover was recovered, resting on stones, gravel and coarse sand. The gravel was entirely of the same kind of metamorphic rock suggesting that it is derived from bedrock exposed at that location.

Box cores show even sediment surfaces covered by a diverse benthic community. The benthos comprises ophiuredeans, crinoids, ascideans, small bivalves, polychaets, hydrozoans and many chitinous worm tubes. Few but large stones (up to 10 cm) could be found on stations PS2451 and PS2452, which are characterized by silty sandy sediment surfaces. The deeper Cores PS2450-2 and PS2485-1 are more fine-grained, consisting of homogeneous silty clay. All surfaces, however, are coloured dark yellowish brown to dark brown.

The uppermost 10-15 cm of the sediment sequence resembles the corresponding surfaces in colour and lithology. At approximately 10 cm core depth, the sediment is diagenetically altered, which results in dark brown, partly rusty colours and a markedly increased stiffness.

Underlying sediments are generally characterized by gray to dark gray, sandy, clayey silts or sandy, silty clays. Black streaks, layers and spots of iron-sulphides and manganese precipitations, typical for these sediments, are responsible for the dark sediment color. The iron-sulphides and manganese precipitations presumably generated during the decay of enrichments of organic matter by sulphate reduction. Thin sand layers, supposed to be turbidites, mainly occur in the lower part of the

sediment column, whereas dropstones and fragments of bivalves can be observed over the entire sediment sequence.

**Magnetic susceptibility:** Four up to nine metre long sediment cores were recovered in Vilkitzki Strait from 130-230 m water depth. Corresponding magnetic susceptibility logs vary in the range of 50-100  $\cdot 10^{-5}$  SI (Fig. 8.4.3-1). Because of large differences in this narrow depositional environment, it is not yet possible to achieve a correlation based on the magnetic susceptibility.

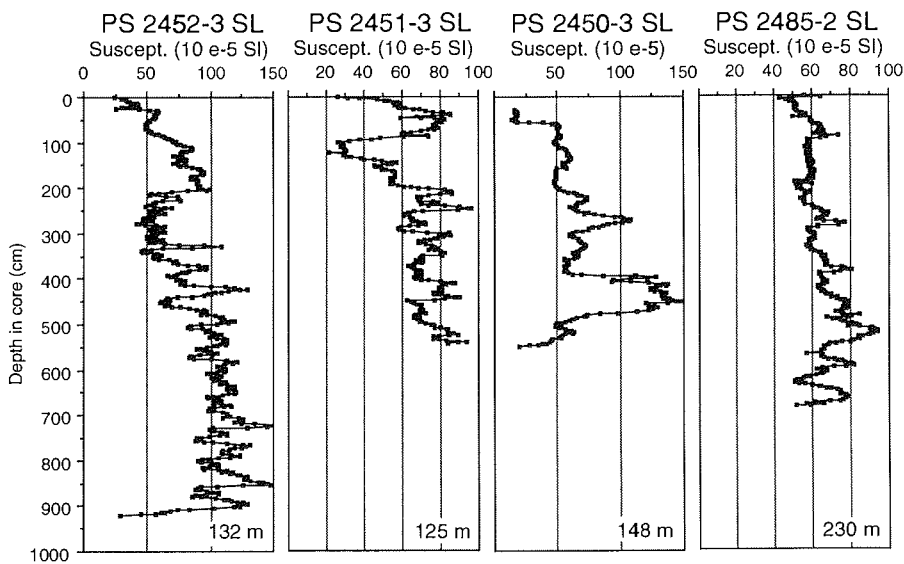


**Fig. 8.4.3-1:** Magnetic susceptibility logs of sediments cores from Vilkitzki Strait.

**Physical properties:** Measurement of shear strength and bulk density was limited to box cores and a few gravity cores. Gravity Core PS2450-3 displays a trend of normal consolidated behaviour with shear strength increasing with depth at a rate of about 1 kPa/m (Fig. 8.4.3-2). More stiff, olive-coloured intervals (3-4 m subbottom depth) deviate from this trend. In gravity Core PS2451-3, zones of high increase in shear strength are found between units with more or less constant properties. This pattern may be related to major changes in depositional conditions (changes in sediment source, current velocity or sea level). However, the physical properties do not support an ice-loading of at least the upper 5 m sediment sequence in the Vilkitzki Strait.

**Depositional environment:** From the lithological core descriptions, it becomes evident that the depositional environment must rapidly have changed in time and space. Correlation of cores recovered from the regionally restricted area of Vilkitzki Strait is not possible. However, the PARASOUND sub-bottom profiling interpretations allow to reconstruct a rather detailed picture of the glacially influenced depositional environment (see Chapter 8.1).

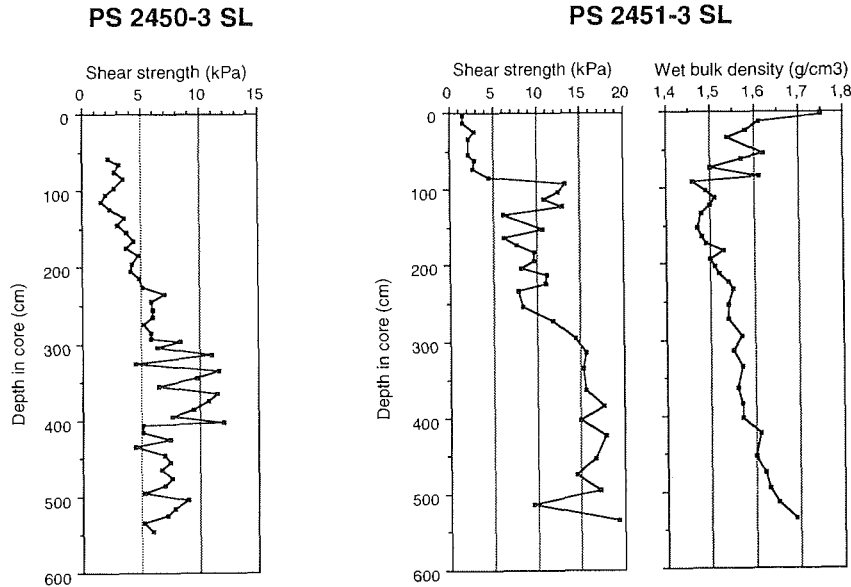


Fig. 8.4.3-2: Selected physical property logs of sediment cores from Vilkitski Strait

## 8.5 Geochemical Changes in the Sediments

### 8.5.1 Pore Water Geochemistry

The sea water is in continuous interaction with the sediments at the seafloor. Its composition is a result of these reactions. Shelf areas are in a transition position between the river estuaries and the deep sea where drastic changes of the environment take place. The extensive shelves surrounding the Arctic Ocean play an important role for material fluxes and contribute to the general oceanic element transport and budget. A knowledge of what enters and what leaves the sediments is necessary for the understanding of the geochemical cycles and processes in this region. Reactions related to changes in the environment preferably occur in the pore water. Reactions in the solid phase of the sediment are of minor importance. In the line of this study, selected parameters of surface sediment environment and components of primary diagenetic dissolution and precipitation were measured.

**Sampling and measurements:** Sediments for pore water sampling were collected with a standard 12 tube Multicorer (MUC), tube diameter of 6 cm. This way of sampling gives the best probability to retain an undisturbed sediment-bottom water interface, which is necessary for oxygen measurement and pore water sampling of the uppermost sediments. Immediately after the return of the MUC on deck, three sub-cores were brought to the laboratory and kept at 4° C. The storage time of the sediment cores until the end of measurement and pore water sampling was not more than 24-36 h. In Table 8.5.1-1, all stations are listed where pore water sampling and/or oxygen measurements were carried out.

Station	Core-#	Latitude	Longitude	Water depth (m)	Porewater sampling	Oxygen measurements
6	2440-3	81°12,87'N	30°36,51'E	186	x	
7	2441-2	81°28,08'N	30°53,54'E	412	x	
14	2442-2	81°41,79'N	30°19,85'E	2848	x	
19	2445-2	82°45,01'N	40°12,06'E	2994	x	x
20	2446-2	82°23,92'N	40°53,60'E	2026	x	x
24	2447-3	82°09,91'N	42°02,30'E	1024	x	x
25	2448-2	82°07,37'N	42°32,79'E	520	x	x
28	2450-1	78°01,99'N	102°18,52'E	152	x	x
29	2451-1	77°42,48'N	102°10,12'E	144	x	x
30	2452-1	77°53,25'N	101°37,43'E	134	x	x
31	2453-1	76°30,23'N	133°21,21'E	37	x	x
32	2454-1	78°42,64'N	132°17,45'E	2976	x	x
33	2455-2	79°38,92'N	130°34,78E	3425	x	x
34	2456-1	78°29,11'N	132°54,86'E	2534	x	x
38	2458-2	78°08,14'N	133°19,14'E	769	x	x
39	2459-1	78°06,03'N	133°30,78E	532	x	x
41	2461-1	77°54,65'N	133°33,77'E	73	x	x
43	2462-2	77°24,30'N	133°33,19'E	54	x	x
46	2464-1	77°28,60'N	125°53,68'E	1750	x	x
47	2465-2	77°11,20'N	126°08,13'E	1020	x	
49	2467-2	77°05,38'N	126°15,47'E	332	x	x
50	2468-2	77°41,41'N	125°52,01'E	1990	x	x
52	2469-2	78°04,14'N	125°01,17'E	2343	x	x
53	2470-2	79°13,65'N	122°52,09'E	3236	x	x
54	2471-2	79°09,45'N	119°45,03'E	3051	x	x
56	2472-2	78°40,00'N	118°44,48'E	2621	x	x
58	2473-2	77°59,16'N	118°34,82'E	1930	x	x
59	2474-1	77°40,82'N	118°34,59'E	1517		x
60	2475-2	77°31,94'N	118°27,28'E	1104	x	x
62	2476-2	77°23,68'N	118°11,61'E	531	x	x
64	2477-2	77°15,02'N	118°33,22'E	225	x	x
65	2478-2	77°10,49'N	118°43,67'E	108	x	x
66	2479-1	77°31,34'N	114°27,35'E	65	x	x
68	2481-1	78°28,38'N	110°47,33'E	101	x	x
69	2482-2	78°41,96'N	112°30,93'E	537	x	x
70	2483-1	78°45,71'N	112°42,58'E	1217	x	x

**Table 8.5.1-1:** List of stations of pore water sampling and oxygen measurements.

Shipboard laboratory analyses were done in the following sequence:

- Three samples of bottom water directly overlying the sediment were drawn for calibration of oxygen measurements by Winkler titration.
- One sample of bottom water was taken for salinity determination.
- Measurement of pH in bottom water and at the bottom water / sediment interface.
- In case of a stable pH-value, oxygen measurements were carried out, beginning in the bottom water some millimetres above the sediment surface. The oxygen electrode was then directly introduced into the sediment by a micromanipulator.
- Sediment cores were split into slices of 1 cm in thickness, beginning at the bottom-water/sediment interface. pH values in each slice was measured downcore.

- The sediment slices were cooled to 4° C and subsequently centrifuged. The pore water was collected and filtered (Satorius filters 0.45 µm pore diameter).
- The pore water samples from equivalent levels of the three cores were combined and stored at 4° C.
- The associated solid phase samples were stored under the same conditions.

The oxygen measurements were carried out by using a commercial electrode (type 737 Clark style Micro oxygen electrode, Diamont General, Ann Arbor, USA). The electrode was calibrated with nitrogen gas for the zero point and with air for the saturation point. The calibration procedure was checked by Winkler titration, carried out by G. Ilyin. The salinity of the bottom water was measured by B. Rudels on a Guideline Autosal 8000. The pH measurements were carried out with a PHM 93 Reference pH Meter (Radiometer Copenhagen) and electrodes. During a two point calibration, the zero pH and the sensitivity of the electrodes were determined on each station using an Ingold buffer solution (pH 7 and pH 9). The sensitivity of the electrodes were in the range of 95.6-100.3 %.

The vessels for pore water (Nalgene type), the Falcon centrifuge tubes and all equipment, which came into contact with the pore water samples, were thoroughly rinsed with hydrochloric acid and Milli-Q-water. The sampling of suboxic and anoxic cores was performed in a nitrogen gas-filled glove bag.

**Preliminary results:** Stations at different water depths show strong differences in the depth of oxygen penetration (Fig. 8.5.1-1). The shelf sediments have an oxygen penetration of 1-2 cm only. The oxidation front is moving downward with increasing water depth. The end point of penetration at the deepest part of the slope (> 2000 m) was not reached until 8 cm. This is caused by the lower rate of degradation of organic matter in deeper regions. This result corresponds to the decreasing of microbiological activity with increasing water depth (see Chapter 7).

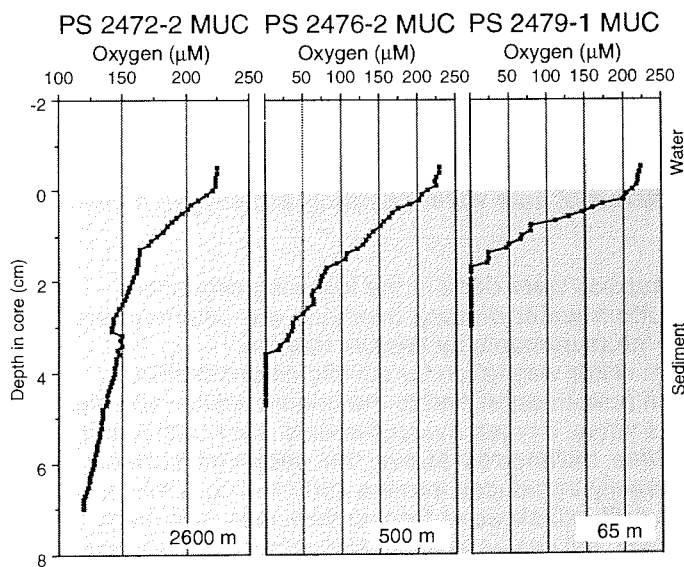


Fig. 8.5.1-1: Selected oxygen profiles in Laptev Sea sediments.

The different oxygen penetration in shelf and slope sediments has consequences for diagenetical zones and processes in the sediments. A comparison with pH-profiles (Fig. 8.5.1-2, Tab. 8.5.1-1) gives an indication that further diagenetical reactions in sediments are related to the penetration of oxygen. Consequently, the decrease of pH value is very slow in the deep water profile.

The change of the chemical environment, which follows these reactions, influences the balance of diffusive fluxes of chemical elements in the pore water. Especially the sediment depth, where the transition from oxygen and/or nitrate reduction to manganese oxide reduction takes place, is important for the capacity of element fluxes from the sediment to the bottom water.

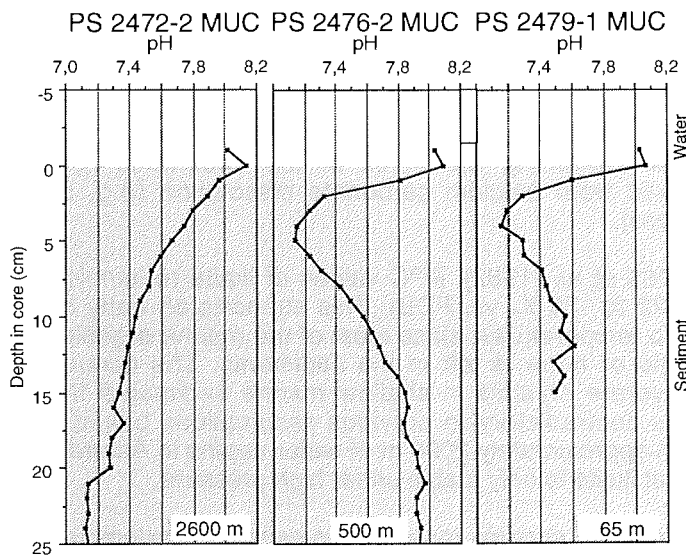


Fig. 8.5.1-2: Selected pH-profiles in sediments from the Laptev Sea.

### 8.5.2 Calcium Carbonate Hexahydrate Precipitations

Early diagenetic precipitations of calcium carbonate hexahydrate (ikaite) have been found in one sedimentary horizon of Core PS2460-3. The core site, which is from approximately 200 m water depth, is situated on the easternmost profile of the Laptev Sea continental slope (Transect H). The entire core is characterized by very dark olive gray homogeneous silty clays, presumably rich in organic matter. Downcore increasing amounts of iron-sulphides and manganese precipitations result in a nearly black colored sedimentary sequence. X-ray photographs indicate strong bioturbation. Large shallow marine bivalve fragments at ca. 100 cm and 467 cm core depth (e.g. *Yoldia amygdalea*, living recently not deeper than 70 m in the Laptev Sea) give evidence for steady downslope transport of sedimentary material. PARASOUND echosoundings (see Chapter 8.1) support excess sedimentation at that location, where sediment layers are thick and successively thinning out downslope.

In 232-238 cm core depth, a cluster of several large (up to 3 cm) crystals of calcium carbonate hexahydrate (ikaite) occur within the fine-grained sediment, occupying approximately an area of 8 cm in diameter. Nevertheless, the magnetic susceptibility log does not show any significant change. X-ray images do not indicate any subsequent change of sedimentary structures due to crystal growth (e.g. bending of sediment layers). The crystals obviously grew radially from a centerpoint. The crystals are not stable at temperatures  $>0^{\circ}$  C, but release their crystal water and deteriorate within a few hours.

The interstitial precipitation of calcium carbonate hexahydrates is obviously driven by microbial decomposition, which generates distinctive dissolved nutrient and biogenic gas patterns in pore waters and also affects major cations (FÜTTERER 1984). Thereby, high sedimentation rates as seen in Core PS2460-3 favour the burial and preservation of organic matter. The carbon of the calcium carbonate hexahydrates may result from the decomposition of organic matter under anoxic conditions. This process, which is probably initiated by sulphate-reducing bacteria, generates hydrogensulphide explaining the smell of the sediments. Calcium ions are presumably derived from calcium carbonate dissolution (e.g. shells of marine, calcareous organisms).

According to SUESS et al. (1982),  $\delta^{13}\text{C}$  values of ikaite resemble those of marine organic matter (-22 to -25 ‰ vs. PDB). This supports an early diagenetic crystal growth at sub-zero temperatures, since most of the marine organic matter was later degraded and little or none is left in the sediments. The occurrence of calcium carbonate hexahydrate crystals in shallow marine sediments from the Eurasian Shelf, however, is contradictory to previous assumptions based on findings from Bransfield Strait in approximately 2000 m of water depths in Antarctica (FÜTTERER et al. 1984, 1986) that ikaite is only stable under high pressure.

The radially grown ikaite crystals resemble so-called "Glendonites", pseudomorphs of calcite after ikaite, which have been described from various locations, e.g. the Tertiary clay and siltstone formations of Spitsbergen (THIEDE et al. 1988, NÜRNBERG 1985), and which have been used as paleoclimate indicators.

9 REFERENCES

- Barnes, P.W., Hunter, R.E., Lee, A., Reimnitz, E. & Weber, W.S.* (1985): Sediment transport by ice gouging: application of model experiments to the arctic continental shelf.- In: S.F. Ackley & W.F. Weeks (eds), *Sea Ice Properties and Processes*, CRREL Monograph, Cold Regions Research and Engineering Laboratory, Hanover, New Hampshire, pp 109-111.
- Barnett, D.* (1991): Sea ice distribution in the Soviet Arctic.- In: L. W. Brigham (ed.), *The Soviet Maritime Arctic*, Belhaven Press, London, 47-62.
- Catalano G.* (1987): An improved method for the determination of ammonia in seawater.- *Mar. Chem.* 20: 289-295.
- Chang, S.-B.R. & Kirschvink, J.L.* (1989): Magnetofossils, the magnetization of sediments and the evolution of magnetite biomineralisation.- *Ann. Rev. Earth Planet. Sci.* 17: 169-195.
- Childress, J.J. & Mickel, T.J.* (1980): A motion compensated shipboard precision balance system.- *Deep Sea Res.* 27: 965-970.
- Damuth, J.E.* (1980) Use of high-frequency (3.5-12 kHz) echograms in the study of near-bottom sedimentation processes in the deep sea: A review.- *Marine Geology* 38: 51-75.
- Fütterer, D.K. (Hrsg.)* (1984): Die Expedition Antarktis-II mit FS "Polarstern" 1983/85. Fahrtabschnitt Punta Arenas - Punta Arenas (ANT II-3).- *Berichte Polarforsch.* 18: 39-92.
- Fütterer, D.K. (Hrsg.)* (1986): Die Expedition Antarktis-IV mit FS "Polarstern" 1985/86. Fahrtabschnitt Rio de Janeiro - Punta Arenas (ANT-IV/2).- *Berichte Polarforsch.* 32: 82-114.
- Fütterer, D.K. (ed.)* (1992): ARCTIC'91: The expedition ARK-VIII/3 of RV "Polarstern" in 1991.- *Berichte Polarforsch.* 107, 267 pp.
- Gard, G.* (1988b). Late Quaternary calcareous nannofossil biochronology and paleo-oceanography of Arctic and Subarctic seas.- *Medd. Stockholms Univ. Geol. Inst.* 275: 8-45.
- Grosswald, M.G.* (1990): Late Pleistocene ice sheet in the Soviet Arctic.- In: V.M. Kotlyakov & V.E. Sokolov (eds.), *Arctic Research - Advances and prospects (Vol.2)*, Proceedings of the conference of Arctic and Nordic Countries on coordination of research in the Arctic, Academy of Sciences of the USSR, Leningrad, December 1988: 18-23.
- Hansen, L. & Grasshoff, K.* (1983): Automated Chemical Analysis. In: K. Grasshoff, M. Erhardt & K. Kremling (eds.), *Methods of Seawater Analysis*, Verlag Chemie, Weinheim, pp. 419.

*Kovacs, A. & Morey, R.M.* (1991): Sounding sea ice thickness using a portable electromagnetic induction instrument.- *Geophysics* 56: 1992-1998.

*Nowaczyk, N.* (1991): Hochauflösende Magnetostratigraphie spätquartärer Sedimente arktischer Meeresgebiete (High-resolution magnetostratigraphy of Late-Quaternary Arctic marine sediments).- *Berichte Polarforsch.* 78: 1-187.

*Nürnberg, D.* (1985): Kartierung der tertiären Schichtenfolge im südwestlichen Nathorstland, Spitzbergen.- Unveröffentl. Diplomarbeit, Univ. Kiel.

*Ramseier, R.O., Asmus, K.W., Collin, M. & Garrity, C.* (1991): Microwave properties of ice, snow, ocean and atmosphere.- In: G. Krause, J. Meincke & H.J. Schwarz (eds.), *Scientific Cruise Reports of Arctic Expeditions ARK-VI/1-4 of RV "Polarstern" in 1989.*- *Berichte Polarforsch.* 87: 66-68.

*Thiede, J., Spielhagen, R.F. & Weinelt, M.H.* (1988): Cenozoic northern hemisphere paleoclimate: an enigma of correlation of oceanic and continental stratigraphic sequences.- *Meyniana* 40: 47-53.

*Thompson, R. & Oldfield, F.* (1986): *Environmental magnetism.* Allen and Unwin, London.

10 ANNEX

10.1 Station list ARK-IX/4

Station	AWI-No.	Date	Time	Latitude	Longitude	Depth (m)	Ice cover	Activity
Bear Island Trough								
27/001	PS2439-1 PS2439-2	09.08.1993	08:06	73°38,7'N	22°55,3'E	458	0	MN
			08:53	73°38,8'N	22°55,4'E	459		MUC (20)
			09:32	73°38,8'N	22°55,3'E	459		GKG (31)
			09:58	73°38,8'N	22°55,2'E	449		MG
27/002	AWI 416	10.08.1993	06:08	76°00,0'N	14°59,0'E	339		CTD
			06:47	76°00,2'N	14°58,9'E	337		1. Mooring AWI 416
			-8:43	76°00,7'N	15°00,5'E	349		
27/003	AWI 415	10.08.1993	10:52	76°20,2'N	14°59,6'E	300		CTD
			11:10	76°20,3'N	14°59,5'E	301		SD
			11:47	76°19,4'N	14°59,7'E	315		2. Mooring AWI 415
			-13:44	76°20,1'N	14°59,3'E	317		
27/004	AWI 417		19:21	76°35,7'N	19°08,9'E	170		CTD
			19:46	76°35,7'N	19°08,8'E	174		3. Mooring AWI 417
			-21:42	76°36,4'N	19°09,4'E	183		
27/005	AWI 418	11.08.1993	22:38	76°35,1'N	19°40,5'E	205		CTD
			22:55	76°35,1'N	19°40,4'E	215		4. Mooring AWI 418
			00:18	76°35,7'N	19°39,6'E	210		
Barents Sea, Profile A								
27/006	PS2440-1 PS2440-2 PS2440-3 PS2440-4 PS2440-5	12.08.1993	10:00	81°12,2'N	30°34,9'E	185	9	CTD
			10:00 - 16:13	"	"	"		Ice station
			10:41	81°12,2'N	30°34,9'E	185		HN
			10:07	81°12,2'N	30°34,9'E	185		SD
			10:46	81°12,3'N	30°35,5'E	187		BO
			11:07	81°12,4'N	30°35,7'E	188		MN
			11:30	81°12,5'N	30°35,9'E	187		BO
			11:56	81°12,6'N	30°36,2'E	187		MUC (BIO)
			12:25	81°12,6'N	30°36,3'E	198		MG
			12:48	81°12,8'N	30°36,5'E	187		MUC (10)
			13:08	81°12,9'N	30°36,6'E	186		MUC
			13:20	81°12,9'N	30°36,6'E	188		MN
			13:44	81°13,0'N	30°36,7'E	196		GKG (32)
			14:19	81°13,2'N	30°36,9'E	199		SL (empty)
17:00	81°13,7'N	30°36,7'E	170	begin AGT				
17:15	81°13,8'N	30°37,2'E	200	end AGT				
27/007	PS2441-1 PS2441-2 PS2441-3	13.08.1993	21:38	81°26,3'N	30°54,7'E	412	9-10	Hydrophone
			23:35	81°27,1'N	30°51,9'E	501		CTD
			23:49	81°27,1'N	30°52,1'E	503		SD
			00:24	81°27,4'N	30°52,4'E	517		BO
			00:40	81°27,5'N	30°52,9'E	525		MN
			01:28	81°27,7'N	30°53,3'E	543		BO
			01:51	81°27,9'N	30°53,5'E	560		MUC
			02:27	81°28,1'N	30°53,5'E	574		MUC
			03:09	81°28,3'N	30°53,9'E	589		GKG (31.5)
			03:58	81°28,5'N	30°54,1'E	603		MG
27/008			04:44	81°28,8'N	30°53,9'E	609		CTD

Station	AWI-No.	Date	Time	Latitude	Longitude	Depth (m)	Ice cover	Activity		
27/009			08:27	81°32,0'N	30°31,1'E	920		CTD		
			09:26	81°32,2'N	30°31,3'E	967		SD		
27/010			10:59	81°33,3'N	30°16,5'E	1305		CTD		
27/011			13:07	81°34,1'N	30°14,9'E	1564		CTD		
			13:23	81°34,1'N	30°15,0'E	1570		SD		
27/012			15:48	81°36,6'N	30°15,4'E	2196		CTD		
27/013			19:19	81°39,2'N	30°14,9'E	2616		Hydrophone		
27/014		14.08.1993	20:15 - 7:00	81°39,5'N	30°15,2'E	2657	9-10	Ice station		
			20:57	81°39,7'N	30°15,3'E	2597		CTD		
			21:40	81°39,8'N	30°15,7'E	2695		BO		
			21:58	81°39,9'N	30°15,9'E	2701		MN		
			23:59	81°40,4'N	30°17,8'E	2756		BO		
			00:16	81°40,5'N	30°18,0'E	2765		CTD		
			00:21	81°40,5'N	30°18,0'E	2766		SD		
			00:55	81°40,6'N	30°18,5'E	2770		HN		
	PS2442-1		03:07	81°41,1'N	30°20,0'E	2806		MUC (BIO)		
			04:25	81°41,4'N	30°20,0'E	2828		MG		
	PS2442-2		05:48	81°41,8'N	30°19,9'E	2848		MUC (31)		
	PS2442-3		07:15	81°42,3'N	30°19,8'E	2876		GKG (empty)		
	PS2442-4	09:03	81°43,0'N	30°20,9'E	2915	GKG (40)				
	PS2442-5	10:38	81°43,3'N	30°21,3'E	2944	SL (200/180)				
27/015			11:29	81°43,5'N	30°22,0'E	2960		CTD		
Barents Sea, transit between Profile A and C										
27/016		15.08.1993	09:42	82°11,6'N	34°29,9'E	2456	10	MN		
			9:45 - 14:45	82°11,6'N	34°29,9'E	2456		Ice station		
	PS2443-1		12:45	82°12,1'N	34°35,1'E	2463		GKG (empty)		
	PS2443-2		13:52	82°12,2'N	34°36,8'E	2464		GKG (55)		
	PS2443-3		14:58	82°12,2'N	34°37,9'E	2462		SL (600/400)		
27/017		16.08.1993	9:20 - 13:57	82°29,0'N	37°42,9'E	2562	9-10	Ice station		
			10:07	82°29,1'N	37°42,9'E	2565		GKG (empty)		
	PS2444-1		11:30	82°29,2'N	37°44,4'E	2566		GKG (43)		
	PS2444-2		12:48	82°29,2'N	37°45,5'E	2564		SL (600/466)		
27/018		17.08.1993	07:07	82°33,5'N	39°19,2'E	2598		CTD		
			09:45	82°33,7'N	39°18,8'E	2610		CTD		
			10:00 - 14:38	82°33,7'N	39°18,9'E	2612		Ice station		
			12:12	82°33,9'N	39°20,1'E	2617		CTD		
			12:25	82°33,9'N	39°20,2'E	2616		SD		
			13:03	82°33,9'N	39°20,8'E	2615		CTD		
Barents Sea, Profile C										
27/019		18.08.1993	06:14	82°45,1'N	40°12,6'E	2971	9-10	CTD		
			06:39	82°45,2'N	40°12,5'E	2972		BO		
			06:59	82°45,2'N	40°12,6'E	2973		BO		
			07:17	82°45,2'N	40°12,6'E	2973		CTD		
			9:00 - 0:13	82°45,4'N	40°12,2'E	2988			Ice station	
			09:13	82°45,5'N	40°12,3'E	2988			MN	
			09:29	82°45,4'N	40°12,2'E	2989			SD	
			11:00	82°45,6'N	40°12,5'E	2994			CTD	
			12:38	82°45,8'N	40°13,5'E	2996			HN	
			14:22	82°45,9'N	40°14,8'E	2996			MUC (BIO)	
	PS2445-1									

Station	AWI-No.	Date	Time	Latitude	Longitude	Depth (m)	Ice cover	Activity
	PS2445-2		15:44	82°45,8'N	40°15,4'E	2994		MUC (32)
			17:08	82°45,8'N	40°15,3'E	2993		MG
	PS2445-3		18:50	82°45,8'N	40°14,6'E	2995		GKG (38)
	PS2445-4		20:20	82°46,0'N	40°13,6'E	2999		KAL (750/725)
			21:44	82°46,0'N	40°13,0'E	3004		MG (empty)
			23:48	82°46,3'N	40°12,8'E	3012		MG (empty)
27/020		19.08.1993	18:00	82°23,2'N	40°54,9'E	1987	9-10	CTD
			18:00 - 03:42	"	"	"		Ice station
			18:30	82°23,2'N	40°54,8'E	1980		BO
			18:50	82°23,3'N	40°54,6'E	1980		BO
			19:11	82°23,3'N	40°54,4'E	1982		CTD
			19:51	82°23,3'N	40°54,0'E	1988		MN
			21:28	82°23,4'N	40°52,9'E	2002		CTD
			21:30	82°23,4'N	40°52,9'E	2002		SD
	PS2446-1	20.08.1993	23:32	82°23,7'N	40°52,5'E	2019		MUC (BIO)
			00:25	82°23,8'N	40°52,7'E	2023		MG (empty)
			01:28	82°23,9'N	40°53,2'E	2027		MG
	PS2446-2		02:32	82°23,9'N	40°53,6'E	2026		MUC (29)
	PS2446-3		03:28	82°24,0'N	40°53,6'E	2025		GKG (37)
	PS2446-4		04:40	82°23,8'N	40°54,5'E	2022		KAL (750/645)
			05:39	82°23,8'N	40°54,5'E	2019		MG (empty)
			06:32	82°23,8'N	40°54,4'E	2018		MG
27/021			09:00	82°19,4'N	41°26,0'E	1795		CTD
27/022			13:00	82°16,0'N	41°36,3'E	1507		CTD
			13:18	82°16,0'N	41°36,4'E	1509		SD
			14:00	82°16,1'N	41°36,8'E	1512		CTD
27/023			16:56	82°12,0'N	41°52,4'E	1195		CTD
27/024			19:15 - 0:39	82°09,7'N	42°02,7'E	1195	9-10	Ice station
			19:42	82°09,7'N	42°02,6'E	997		BO
			19:58	82°09,7'N	42°02,6'E	996		BO
			20:17	82°09,6'N	42°02,3'E	1003		CTD
			21:03	82°09,6'N	42°02,2'E	1005		SD
			21:17	82°09,6'N	42°02,2'E	1006		MN
	PS2447-1	21.08.1993	22:42	82°09,8'N	42°02,1'E	1013		MUC (BIO)
	PS2447-2		23:24	82°09,8'N	42°02,2'E	1017		MUC (BIO)
			00:00	82°09,8'N	42°02,7'E	1021		MG
	PS2447-3		00:33	82°09,9'N	42°02,3'E	1024		MUC (30)
	PS2447-4		01:21	82°09,6'N	42°02,7'E	1024		GKG (43)
	PS2447-5		02:09	82°10,0'N	42°03,1'E	1025		SL (600/417)
			02:44	82°10,0'N	42°03,3'E	1025		MG
27/025			04:44	82°07,4'N	42°29,8'E	508	9-10	CTD
			05:38	82°07,4'N	42°34,0'E	504		BO
			05:51	82°07,4'N	42°34,0'E	502		BO
			06:08	82°07,4'N	42°34,2'E	504		MN
	PS2448-1		07:05	82°07,4'N	42°33,4'E	511		MUC (BIO)
			07:48	82°07,4'N	42°33,1'E	516		MG
	PS2448-2		08:13	82°07,4'N	42°32,8'E	520		MUC (30)
	PS2448-3		08:47	82°07,4'N	42°32,3'E	534		GKG (60)
	PS2448-4		09:28	82°07,5'N	42°31,8'E	553		SL (600/388)

Station	AWI-No.	Date	Time	Latitude	Longitude	Depth (m)	Ice cover	Activity
27/026			10:38	82°05,6'N	42°43,5'E	386		CTD
27/027			14:00 - 20:00	82°01,3'N	43°33,1'E	289	9-10	Ice station
			14:09	82°01,3'N	43°33,1'E	289		CTD
			14:55	82°01,4'N	43°33,7'E	289		BO
			15:11	82°01,4'N	43°33,8'E	285		BO
			15:25	82°08,4'N	43°33,9'E	285		MN
	PS2449-1		15:58	82°01,4'N	43°34,2'E	287		MUC (BIO)
			16:32	82°01,4'N	43°34,3'E	286		MG
	PS2449-2		16:47	82°01,4'N	43°34,5'E	287		MUC (5)
	PS2449-3		17:19	82°01,4'N	43°34,6'E	286		GKG (10)
		21.08.1993	21:01	82°01,7'N	43°33,2'E	284		begin AGT
			21:24	82°01,4'N	43°34,0'E	292		end AGT
Vilkitsky Strait								
27/028		26.08.1993	09:07	78°02,2'N	102°20,2'E	158	3-4	BO
			09:26	78°02,2'N	102°19,6'E	157		CTD
			09:57	78°02,0'N	102°19,0'E	154		SD
			09:59	78°02,0'N	102°19,0'E	154		MN
	PS2450-1		10:24	78°02,0'N	102°18,5'E	152		MUC (BIO/GEO)
			10:46	78°02,0'N	102°17,9'E	151		MG
	PS2450-2		11:14	78°01,8'N	102°18,3'E	148		GKG (41)
			11:39	78°01,9'N	102°17,5'E	149		GKG (BIO)
Heli	R9423801		12:00	78°10,0'N	103°05,0'E			Sea-ice sampling
	PS2450-3		12:08	78°01,9'N	102°17,0'E	148		SL (600/551)
			12:52	78°02,0'N	102°20,0'E	153		begin AGT
			13:06	78°02,1'N	102°20,9'E	158		end AGT
27/029		27.08.1993	03:21	77°42,2'N	102°22,5'E	140		BO
			03:39	77°42,4'N	102°21,2'E	142		MN
	PS2451-1		04:11	77°42,5'N	102°19,1'E	144		MUC (BIO/GEO)
			04:36	77°42,5'N	102°17,8'E	144		MG
	PS2451-2		04:59	77°42,4'N	102°17,3'E	143		GKG (40)
			05:27	77°42,0'N	102°14,3'E	135		GKG (BIO)
			05:55	77°41,6'N	102°10,3'E	128		CTD
	PS2451-3		07:01	77°41,3'N	102°11,1'E	125		SL (700/544)
Heli	R9423901	27.08.1993	07:00	78°08,0'N	102°48,0'E			Sea-ice sampling
			07:30	77°40,5'N	102°07,3'E	120		begin AGT
			07:45	77°40,5'N	102°05,1'E	120		end AGT
27/030			09:58	77°52,9'N	101°46,2'E	140		CTD
			10:36	77°53,0'N	101°42,3'E	138		BO
			10:52	77°53,1'N	101°41,1'E	138		BO
			11:10	77°53,2'N	101°39,3'E	135		MN
	PS2452-1		11:32	77°53,3'N	101°37,4'E	134		MUC (BIO/GEO)
			12:04	77°53,4'N	101°36,7'E	133		MG
	PS2452-2		12:23	77°53,5'N	101°35,5'E	132		GKG (41)
			12:51	77°53,7'N	101°34,2'E	132		GKG (BIO)
	PS2452-3		13:26	77°53,8'N	101°32,8'E	132		SL (1005/921)
			14:00	77°53,8'N	101°28,4'E	130		begin EBS
			14:10	77°53,7'N	101°27,1'E	130		end EBS
Heli	R9424001	28.08.1993	10:00	77°40,0'N	100°31,9'E			Sea-ice sampling
Heli	R9424301	31.08.1993	10:00	75°46,0'N	121°54,0'E			Sea-ice sampling

Station	AWI-No.	Date	Time	Latitude	Longitude	Depth	Ice	Activity
						(m)	cover	
Laptev Sea, Profile H								
27/031	PS2453-1 PS2453-2 PS2453-3	01.09.1993	06:40 06:55 07:26 07:35 07:50 08:12 08:33 09:06 09:36 09:46 10:07 10:14 16:02	76°29,8'N 76°29,5'N 76°30,0'N 76°30,1'N 76°30,2'N 76°30,5'N 76°30,9'N 76°31,4'N 76°32,2'N 76°32,1'N 76°31,8'N 76°31,8'N 76°31,7'N	133°10,3'E 133°11,3'E 133°20,4'E 133°20,7'E 133°21,2'E 133°21,3'E 133°21,0'E 133°20,8'E 133°19,8'E 133°20,5'E 133°19,0'E 133°19,3'E 133°19,1'E	39 39 38 38 37 38 38 38 37 38 37 38 38	0	begin AGT end AGT BO MN MUC (21) GKG (41) GKG (BIO) SL (/158) begin EBS end EBS CTD CTD SD
27/032	PS2454-1	02.09.1993	04:05 06:08 07:57 08:36 08:56 09:13 10:00 11:22 13:00 15:20 15:45	78°43,1'N 78°42,9'N 78°42,6'N 78°42,4'N 78°42,2'N 78°42,4'N 78°42,4'N 78°42,4'N 78°42,6'N 78°42,7'N 78°42,7'N	132°22,0'E 132°21,3'E 132°20,8'E 132°22,0'E 132°22,1'E 132°22,2'E 132°21,2'E 132°19,9'E 132°17,5'E 132°33,8'E 132°39,4'E	2987 2987 2963 2965 2961 2961 2960 2962 2976 3012 3028	0	CTD MN CTD BO BO CTD HN MG MUC (BIO/GEO) begin AGT end AGT
27/033	PS2455-1 PS2455-2 PS2455-3 PS2455-4	03.09.1993	02:58 3:04 - 14:04 05:53 06:56 06:56 09:54 11:36 12:29 12:39 12:50 15:29	79°38,7'N 79°38,7'N 79°39,0'N 79°39,0'N 79°39,0'N 79°38,9'N 79°39,1'N 79°39,4'N 79°39,4'N 79°39,5'N 79°40,5'N	130°33,0'E 130°33,0'E 130°35,8'E 130°36,1'E 130°36,1'E 130°34,8'E 130°32,1'E 130°30,8'E 130°30,6'E 130°30,4'E 130°29,5'E	3420 3420 3427 3420 3420 3425 3429 3428 3423 3430 3438	8	CTD ice station MUC (BIO) CTD SD MUC (33) GKG (44) CTD CTD HN SL (150/100)
27/034	PS2456-1 PS2456-2 PS2456-3	04.09.1993	23:44 00:56 01:32 04:26 06:31	78°28,5'N 78°29,1'N 78°29,3'N 78°29,0'N 78°28,9'N	132°53,8'E 132°54,9'E 132°56,1'E 133°00,1'E 133°01,9'E	2526 2534 2536 2520 2507		CTD MUC (32) CTD GKG (44) KAL (600/574)
27/035			08:04 09:44 11:34 12:08 12:22 12:41 12:46 14:02	78°22,8'N 78°23,0'N 78°23,3'N 78°23,5'N 78°23,6'N 78°23,6'N 78°23,6'N 78°23,5'N	133°03,5'E 133°04,2'E 133°05,5'E 133°06,1'E 133°06,4'E 133°06,8'E 133°07,0'E 133°09,5'E	2037 2062 2088 2160 2176 2158 2155 2151	0	CTD MN CTD BO BO CTD HN MG

Station	AWI-No.	Date	Time	Latitude	Longitude	Depth (m)	Ice cover	Activity
	PS2457-1		15:02	78°23,2'N	133°11,4'E	2019		MUC (17, BIO/GEO)
	PS2457-2		16:06	78°22,6'N	133°12,9'E	1948		MG (empty)
			17:41	78°22,4'N	133°12,4'E	1934		MG
27/036			18:53	78°18,4'N	133°16,1'E	1506		CTD
27/037			21:26	78°14,4'N	133°19,8'E	1256		CTD
			22:30	78°14,4'N	133°20,0'E	1247		CTD
27/038		05.09.1993	00:29	78°09,9'N	133°23,3'E	982	0-1	MN
			01:34	78°09,8'N	133°22,6'E	965		CTD
			01:45	78°09,7'N	133°22,7'E	952		HN
			02:01	78°09,5'N	133°23,0'E	935		BO
			02:19	78°09,2'N	133°22,9'E	914		BO
			02:37	78°09,0'N	133°23,3'E	893		CTD
			03:59	78°08,4'N	133°20,7'E	828		MG
	PS2458-1		04:31	78°08,2'N	133°20,0'E	796		MUC (BIO)
	PS2458-2		05:10	78°08,1'N	133°19,1'E	769		MUC (31)
			06:17	78°09,7'N	133°22,4'E	950		GKG (BIO)
			07:00	78°09,8'N	133°23,8'E	960		GKG (BIO)
	PS2458-3		07:45	78°10,0'N	133°23,7'E	981		GKG (46)
	PS2458-4		08:35	78°10,0'N	133°23,9'E	983		KAL (800/800)
			09:43	78°10,6'N	133°25,3'E	1033		begin AGT
			09:58	78°10,7'N	133°26,1'E	1039		end AGT
27/039			11:52	78°06,0'N	133°31,1'E	533	0	CTD
			12:09	78°06,0'N	133°31,4'E	528		HN
			12:41	78°06,0'N	133°32,4'E	514		MN
			13:27	78°05,8'N	133°34,3'E	446		BO
			13:42	78°05,7'N	133°34,8'E	432		BO
			14:41	78°06,3'N	133°36,4'E	493		begin EBS
			14:51	78°06,2'N	133°35,8'E	498		end EBS
	PS2459-1		16:05	78°06,0'N	133°31,5'E	532		MUC (31)
			16:34	78°05,9'N	133°30,8'E	511		MG
			17:12	78°05,9'N	133°31,1'E	520		GKG (BIO)
	PS2459-2		17:54	78°05,9'N	133°30,8'E	517		GKG (41)
			18:28	78°06,0'N	133°30,3'E	525		GKG (BIO)
	PS2459-3		19:08	78°06,0'N	133°30,3'E	523		SL (1000/689)
			19:53	78°06,0'N	133°32,3'E	525		begin AGT
			20:08	78°06,0'N	133°32,9'E	514		end AGT
27/040			21:06	78°04,4'N	133°33,4'E	215	0	CTD
			21:20	78°04,4'N	133°33,0'E	222		HN
			21:49	78°04,5'N	133°32,4'E	243		MN
			22:07	78°04,6'N	133°32,3'E	254		BO
			22:24	78°04,7'N	133°32,6'E	257		BO
	PS2460-1		22:52	78°04,4'N	133°34,1'E	213		MUC (BIO)
			23:20	78°04,4'N	133°34,2'E	217		MG (empty)
			23:30	78°04,4'N	133°34,5'E	217		MG
	PS2460-2		23:52	78°04,4'N	133°34,9'E	215		MUC (19)
		06.09.1993	00:32	78°04,5'N	133°36,3'E	216		GKG (BIO)
	PS2460-3		01:02	78°04,3'N	133°36,5'E	191		GKG (32)
			01:32	78°04,5'N	133°36,5'E	203		GKG (BIO)
	PS2460-4		02:19	78°04,5'N	133°35,9'E	204		SL (1100/913)

Station	AWI-No.	Date	Time	Latitude	Longitude	Depth (m)	Ice cover	Activity
			02:48	78°04,6'N	133°34,9'E	231		begin AGT
			03:03	78°04,5'N	133°33,8'E	233		end AGT
27/041			04:59	77°54,4'N	133°33,9'E	72	0-1	CTD
			05:00	77°54,4'N	133°33,9'E	72		HN
			05:13	77°54,2'N	133°33,6'E	72		CTD
			05:40	77°54,0'N	133°33,1'E	71		SD
			05:54	77°54,3'N	133°33,4'E	72		MN
Heli	R9424901		06:00	77°56,6'N	131°28,6'E			Sea-ice sampling
			06:08	77°54,4'N	133°33,5'E	72		CTD
			06:28	77°54,4'N	133°33,4'E	72		BO
			06:38	77°54,4'N	133°33,2'E	73		BO
			06:57	77°54,5'N	133°33,3'E	73		begin EBS
			07:07	77°54,6'N	133°33,7'E	73		end EBS
	PS2461-1		07:11	77°54,7'N	133°33,8'E	73		MUC (25)
	PS2461-2		08:17	77°54,5'N	133°33,4'E	73		GKG (BIO)
	PS2461-3		08:16	77°54,6'N	133°33,3'E	73		GKG (31)
			08:41	77°54,7'N	133°33,2'E	73		GKG (BIO)
			09:08	77°55,0'N	133°33,4'E	73		SL (400/250)
			09:32	77°54,8'N	133°34,4'E	72		begin AGT
			09:47	77°54,7'N	133°35,4'E	71		end AGT
27/042			12:46	77°39,7'N	133°34,5'E	61		CTD
27/043			15:46	77°24,3'N	133°34,2'E	53	3-5	CTD
			15:55	77°24,1'N	133°34,7'E	53		HN
			16:11	77°23,9'N	133°35,7'E	53		MN
			16:43	77°24,1'N	133°33,5'E	54		BO
			16:54	77°24,1'N	133°33,1'E	54		BO
			17:10	77°24,1'N	133°33,1'E	54		begin EBS
			17:20	77°24,2'N	133°33,2'E	54		end EBS
	PS2462-1		17:35	77°24,4'N	133°33,1'E	54		MUC (BIO)
	PS2462-2		17:56	77°24,3'N	133°33,2'E	54		MUC (15)
	PS2462-3		18:20	77°24,3'N	133°33,3'E	55		GKG (BIO)
			18:39	77°24,3'N	133°33,4'E	54		GKG (33)
			19:00	77°24,3'N	133°33,3'E	54		GKG (BIO)
	PS2462-4		19:29	77°24,5'N	133°32,7'E	55		SL (400/272)
			19:51	77°24,5'N	133°33,0'E	54		begin AGT
			20:02	77°24,3'N	133°33,7'E	54		end AGT
Laptev Sea, Profile G								
27/044		07.09.1993	04:52	77°02,0'N	126°23,2'E	94	6	CTD
			05:15	77°02,0'N	126°24,3'E	93		HN
			05:20	77°01,9'N	126°24,5'E	93		MN
			05:35	77°01,8'N	126°24,9'E	92		BO
			05:44	77°01,8'N	126°25,0'E	92		BO
Heli	R9425001		06:00	77°00,3'N	125°49,2'E			Sea-ice sampling
			06:08	77°01,9'N	126°25,4'E	93		begin EBS
			06:18	77°02,1'N	126°25,6'E	94		end EBS
	PS2463-1		06:44	77°02,8'N	126°25,6'E	93		MUC (BIO)
	PS2463-2		07:17	77°02,1'N	126°26,3'E	93		MUC (GEO)
			07:44	77°01,8'N	126°24,9'E	92		GKG (BIO)
	PS2463-3		08:15	77°01,8'N	126°24,8'E	92		GKG (31)

Station	AWI-No.	Date	Time	Latitude	Longitude	Depth (m)	Ice cover	Activity
	PS2463-4		08:37	77°01,8'N	126°25,0'E	92		GKG (BIO)
			09:04	77°01,8'N	126°25,4'E	92		SL (empty)
			09:32	77°02,3'N	126°25,3'E	96		begin AGT
			09:47	77°02,6'N	126°25,0'E	96		end AGT
27/045		08.09.1993	16:10 - 4:00	77°28,4'N	125°54,1'E	1750	10	Ice station
27/046			04:37	77°28,2'N	126°05,1'E	1754		CTD
	PS2464-1		05:30	77°28,1'N	126°05,9'E	1748		SD
			07:18	77°28,6'N	125°53,7'E	1753		MUC (30)
			07:46	77°28,5'N	125°53,7'E	1752		CTD
	PS2464-2		09:07	77°28,6'N	125°53,8'E	1754		GKG (BIO)
Heli	R9425111		10:09	77°28,8'N	125°54,2'E	1760		GKG (36)
	PS2464-3		10:00	77°24,3'N	126°12,8'E			Sea-ice sampling
	PS2464-4		11:12	77°29,1'N	125°54,8'E	1756		SL (empty)
			12:40	77°29,1'N	125°54,8'E	1756		SL (500/485)
27/047			15:54	77°10,9'N	126°14,4'E	995	9	CTD
			16:33	77°10,8'N	126°16,1'E	995		MN
			17:35	77°10,7'N	126°18,4'E	973		CTD
			18:37	77°10,5'N	126°20,8'E	922		BO
			18:51	77°10,4'N	126°20,7'E	918		BO
			19:23	77°10,3'N	126°21,4'E	896		MG
	PS2465-1		20:35	77°10,7'N	126°12,3'E	1009		MUC (BIO)
	PS2465-2		21:22	77°11,2'N	126°08,1'E	1025		MUC (31)
			22:08	77°10,9'N	126°13,4'E	1009		GKG (BIO)
	PS2465-3		22:50	77°11,0'N	126°13,4'E	1026		GKG (30)
			23:36	77°11,3'N	126°13,8'E	1015		GKG (BIO)
	PS2465-4	09.09.1993	00:24	77°11,5'N	126°14,7'E	1056		SL (600/448)
			01:28	77°11,7'N	126°19,2'E	1006		begin AGT
			01:43	77°11,7'N	126°20,4'E	1016		end AGT
27/048			04:37	77°07,7'N	126°21,3'E	512	7-8	CTD
			05:05	77°07,8'N	126°22,1'E	520		HN
			05:27	77°07,6'N	126°22,9'E	533		MN
			05:28	77°07,6'N	126°23,0'E	537		HN
			06:09	77°07,7'N	126°24,4'E	560		BO
			06:23	77°07,7'N	126°24,7'E	541		BO
			07:07	77°07,6'N	126°23,4'E	500		begin EBS
			07:17	77°07,7'N	126°22,4'E	526		end EBS
			08:02	77°07,7'N	126°21,4'E	522		MG
			08:42	77°07,8'N	126°21,5'E	513		MUC (empty)
	PS2466-1		09:10	77°07,9'N	126°22,4'E	561		MUC (BIO)
	PS2466-2		09:58	77°07,5'N	126°19,2'E	538		MUC (30)
Heli	R9425201		10:00	77°09,1'N	125°51,0'E			Sea-ice sampling
			10:36	77°07,8'N	126°20,1'E	546		GKG (BIO)
	PS2466-3		11:05	77°08,1'N	126°21,2'E	552		GKG (28)
			11:44	77°08,2'N	126°22,9'E	610		GKG (BIO)
	PS2466-4		12:36	77°08,1'N	126°21,6'E	542		SL ( /200)
	PS2466-5		13:31	77°07,8'N	126°22,7'E	539		SL (460/455)
			14:13	77°07,8'N	126°25,0'E	556		begin AGT
			14:28	77°07,6'N	126°24,3'E	530		end AGT
27/049			16:12	77°05,9'N	126°18,8'E	218	9	CTD

Station	AWI-No.	Date	Time	Latitude	Longitude	Depth (m)	Ice cover	Activity
	PS2467-1 PS2467-2  PS2467-3		16:18 17:14 17:32 17:56 18:39 18:55 19:28 19:58 20:32 20:47 21:06 21:21	77°05,8'N 77°06,2'N 77°06,0'N 77°06,1'N 77°06,2'N 77°05,8'N 77°05,4'N 77°05,0'N 77°05,0'N 77°04,7'N 77°04,7'N 77°04,7'N	126°19,4'E 126°20,9'E 126°21,5'E 126°20,1'E 126°17,6'E 126°17,0'E 126°15,5'E 126°14,8'E 126°13,4'E 126°12,3'E 126°10,7'E 126°08,8'E	200 260 166 287 292 240 332 195 284 180 180 360		HN MN BO BO MG MUC (BIO) MUC (25) GKG (BIO) GKG (19) GKG (BIO) begin AGT end AGT
27/050	PS2468-1 PS2468-2 PS2468-3 PS2468-4	10.09.1993	04:31 04:40 4:40 - 14:15 05:08 06:59 08:34 08:48 09:34 10:35 11:38 12:43 13:53 15:36 15:51 19:50	77°43,7'N 77°43,7'N " 77°43,5'N 77°42,5'N 77°41,8'N 77°41,7'N 77°41,4'N 77°41,4'N 77°41,4'N 77°41,6'N 77°41,7'N 77°41,4'N 77°41,1'N	125°45,3'E 125°45,8'E " 125°47,0'E 125°50,6'E 125°51,4'E 125°51,4'E 125°51,3'E 125°51,4'E 125°52,1'E 125°53,6'E 125°56,1'E 125°55,1'E 125°54,2'E	1990 1990 " 2025 1919 1981 1983 1981 1985 1900 1991 2002 1992 1993	9	CTD HN Ice station MN CTD BO BO MG MUC (BIO) MUC (36) GKG (46) SL (700/565) begin AGT end AGT CTD
27/051				77°52,1'N	125°34,1'E	2297		CTD
27/052	PS2469-1  3311  PS2469-2 PS2469-3	11.09.1993	3:20 - 10:00 03:25 04:44 05:32 07:20  07:51 09:07	78°07,2'N 78°07,2'N 78°06,2'N 78°05,5'N 78°04,4'N  78°04,1'N 78°03,6'N	125°02,6'E 125,02,6'E 125°03,2'E 125°03,2'E 125°01,8'E  125°01,2'E 125°00,0'E	2410 2410 2390 2392 2351  2343 2332	9-10	Ice station CTD KAL (350/346) CTD Deployment of a meterological buoy on ice MUC (empty) GKG (47)
27/053	PS2470-1 PS2470-2 PS2470-3 PS2470-4	12.09.1993	02:19 02:57 3:00 - 13:50 04:58 05:00 07:07 07:20 07:31  08:18 09:43 11:24 12:58 14:33	79°15,6'N 79°15,4'N 79°15,3'N 79°14,6'N 79°14,6'N 79°13,9'N 79°13,8'N 79°53,32'N  79°13,7'N 79°13,6'N 79°13,7'N 79°13,4'N 79°13,0'N	122°53,1'E 122°53,3'E 122°53,4'E 122°53,8'E 122°53,3'E 122°52,3'E 122°52,2'E 125°54,0'E  122°51,7'E 122°51,3'E 122°52,1'E 122°53,1'E 122°54,4'E	3244 3244 3244 3239 3239 3238 3237  3236 3237 3236 3234 3233	9-10	CTD MN Ice station CTD HN BO BO Deployment of a meterological buoy on ice MG MUC (BIO) MUC (28) GKG (41) GKG (41)

Station	AWI-No.	Date	Time	Latitude	Longitude	Depth (m)	Ice cover	Activity
Laptev Sea, Profile F								
27/054		13.09.1993	05:35	79°11,3'N	119°56,4'E	3039	7-8	begin AGT
			05:55	79°11,8'N	119°56,2'E	3042		end AGT
			8:30 - 20:55	79°11,3'N	119°54,3'E	3073		Ice station
			08:34	79°11,3'N	119°54,3'E	3073		CTD
			09:32	79°11,1'N	119°54,3'E	3071		HN
			10:45	79°10,8'N	119°53,8'E	3067		MN
			12:37	79°10,4'N	119°51,9'E	3060		CTD
			13:20	79°10,2'N	119°51,0'E	3057		BO
			13:34	79°10,2'N	119°50,6'E	3057		BO
			14:29	79°10,0'N	119°49,2'E	3054		MG
	PS2471-1		15:53	79°09,7'N	119°47,2'E	3051		MUC (BIO)
	PS2471-2		17:48	79°09,5'N	119°45,8'E	3051		MUC (35)
	PS2471-3		19:25	79°09,3'N	119°46,9'E	3048		GKG (40)
	PS2471-4		20:49	79°09,1'N	119°47,6'E	3047		SL (600/416)
27/055		14.09.1993	01:28	79°02,3'N	118°14,7'E	2874		CTD
27/056			13:57	78°40,2'N	118°42,7'E	2615	9-10	CTD
			14:30	78°40,1'N	118°42,7'E	2615		HN
			15:51	78°40,2'N	118°42,7'E	2615		MN
			17:34	78°40,1'N	118°43,3'E	2616		CTD
			18:06	78°40,1'N	118°43,5'E	2617		BO
			18:17 - 1:43	78°40,1'N	118°43,5'E	2617		Ice station
			18:20	78°40,1'N	118°43,6'E	2617		BO
			19:17	78°40,1'N	118°44,2'E	2619		MG
	PS2472-1		20:41	78°40,0'N	118°44,5'E	2620		MUC (BIO)
	PS2472-2		21:58	78°40,0'N	118°44,5'E	2621		MUC (30)
	PS2472-3		23:23	78°40,0'N	118°44,3'E	2620		GKG (35)
	PS2472-4	15.09.1993	00:46	78°40,1'N	118°44,5'E	2620		SL (600/390)
			01:48	78°40,0'N	118°44,7'E	2620		MG
Heli	R9425801		08:00	78°21,2'N	117°54,0'E			Sea-ice sampling
27/057			08:26	78°20,3'N	118°23,7'E	2218		CTD
Heli	R9425811		09:00	78°21,3'N	117°12,7'E			Sea-ice sampling
27/058			17:36	78°00,2'N	118°33,2'E	1929	8-9	CTD
			18:08	78°00,2'N	118°33,4'E	1930		MN
			18:35 - 2:56	78°00,2'N	118°33,5'E	1930		Ice station
			20:28	78°00,2'N	118°34,2'E	1933		CTD
			20:37	78°00,2'N	118°34,2'E	1933		HN
			22:08	78°00,0'N	118°34,9'E	1938		BO
			22:25	77°59,9'N	118°35,0'E	1937		BO
			23:11	77°59,7'N	118°35,1'E	1937		MG (empty)
	PS2473-1	16.09.1993	00:13	77°59,5'N	118°35,1'E	1935		MUC (BIO)
	PS2473-2		01:34	77°59,2'N	118°34,8'E	1930		MUC (31)
	PS2473-3		02:44	77°58,9'N	118°34,3'E	1927		GKG (38)
	PS2473-4		03:40	77°58,7'N	118°33,7'E	1923		MG (empty)
			04:43	77°58,6'N	118°34,5'E	1919		KAL (800/562)
27/059			12:52	77°41,3'N	118°34,3'E	1528		CTD
	PS2474-1		14:09	77°40,8'N	118°34,6'E	1517		MUC (BIO)
			14:32	77°40,7'N	118°34,6'E	1513		CTD
			16:16	77°40,4'N	118°34,5'E	1502		MG

Station	AWI-No.	Date	Time	Latitude	Longitude	Depth (m)	Ice cover	Activity
	PS2474-2		17:13	77°40,2'N	118°34,5'E	1497		GKG (36)
	PS2474-3		18:23	77°40,2'N	118°34,5'E	1494		KAL (900/784)
27/060		17.09.1993	23:05	77°33,6'N	118°25,5'E	1183	9	CTD
			23:26 - 7:05	77°33,5'N	118°25,8'E	1181		Ice station
			23:30	77°33,5'N	118°25,8'E	1181		HN
			23:59	77°33,4'N	118°26,2'E	1178		MN
			01:27	77°33,0'N	118°27,1'E	1160		CTD
			02:35	77°32,6'N	118°27,5'E	1143		MN
			03:00	77°32,5'N	118°27,5'E	1137		BO
			03:13	77°32,5'N	118°27,6'E	1134		BO
			03:47	77°32,3'N	118°27,6'E	1126		MG
	PS2475-1		04:34	77°32,1'N	118°27,5'E	1100		GKG (BIO)
	PS2475-2		05:22	77°32,0'N	118°27,5'E	1108		GKG (35)
			06:07	77°31,9'N	118°27,3'E	1104		MUC (24)
			07:01	77°31,9'N	118°27,5'E	1101		MG
	PS2475-3		07:41	77°31,8'N	118°27,8'E	1097		SL (1000/800)
27/061			10:43	77°26,9'N	118°18,7'E	765		CTD
27/062			13:02	77°24,7'N	118°10,5'E	571	8-9	CTD
			13:21	77°24,5'N	118°10,9'E	556		HN
			13:54	77°24,3'N	118°11,2'E	556		MN
			14:40	77°24,1'N	118°11,4'E	545		BO
			14:57	77°24,0'N	118°11,5'E	542		BO
			15:27	77°23,9'N	118°11,5'E	538		MG
	PS2476-1		15:55	77°23,8'N	118°11,6'E	534		MUC (BIO)
	PS2476-2		16:28	77°23,7'N	118°11,6'E	531		MUC (33)
			17:04	77°23,6'N	118°11,5'E	525		GKG (BIO)
	PS2476-3		17:34	77°23,5'N	118°11,5'E	524		GKG (36)
			18:04	77°23,4'N	118°11,5'E	520		GKG (BIO)
	PS2476-4		18:34	77°23,4'N	118°11,6'E	521		SL (1000/634)
27/063			23:10	77°18,1'N	118°25,1'E	365		CTD
27/064		18.09.1993	01:32	77°15,9'N	118°31,8'E	242	8	CTD
			1:32 - 8:15	"	"	"		Ice station
			01:44	77°15,8'N	118°32,0'E	238		HN
			02:07	77°15,7'N	118°32,4'E	231		MN
			02:30	77°15,5'N	118°32,7'E	225		BO
			02:45	77°15,4'N	118°32,8'E	221		BO
			03:10	77°15,3'N	118°33,0'E	221		MG
	PS2477-1		03:34	77°15,2'N	118°33,2'E	230		MUC (BIO)
	PS2477-2		03:59	77°15,0'N	118°33,2'E	225		MUC (34)
			04:28	77°14,9'N	118°33,2'E	196		GKG (BIO)
	PS2477-3		04:53	77°14,8'N	118°33,2'E	193		GKG (32)
			05:15	77°14,7'N	118°33,1'E	190		GKG (BIO)
	PS2477-4		05:47	77°14,6'N	118°32,9'E	187		SL (600/589)
			06:29	77°14,7'N	118°30,9'E	191		begin AGT
			06:44	77°14,5'N	118°32,2'E	181		end AGT
			07:20	77°14,6'N	118°31,8'E	188		begin EBS
			07:30	77°14,7'N	118°31,1'E	195		end EBS
27/065			14:38	77°11,1'N	118°44,2'E	107	8-9	CTD
			14:47	77°11,0'N	118°44,2'E	106		HN

Station	AWI-No.	Date	Time	Latitude	Longitude	Depth	Ice	Activity
						(m)	cover	
			15:09	77°10,9'N	118°44,2'E	104		MN
			15:21	77°10,8'N	118°44,2'E	103		BO
			15:34	77°10,7'N	118°44,2'E	101		BO
	PS2478-1		15:52	77°10,6'N	118°44,1'E	107		MUC (BIO)
	PS2478-2		16:15	77°10,5'N	118°43,7'E	108		MUC (18)
			16:43	77°10,3'N	118°43,1'E	95		GKG (BIO)
	PS2478-3		17:01	77°10,3'N	118°42,6'E	101		GKG (20)
			17:24	77°10,2'N	118°41,8'E	96		GKG (BIO)
			17:43	77°10,2'N	118°41,3'E	97		MG
Laptev Sea, transit between Profile F and E								
27/066	PS2479-1	19.09.1993	11:59	77°31,3'N	114°27,4'E	65		MUC (BIO/GEO)
Laptev Sea, Profile E, NE of Maly Taymyr Island								
27/067		20.09.1993	02:04	78°16,1'N	109°14,0'E	50	7	CTD
			02:16	78°16,1'N	109°14,0'E	50		HN
			02:33	78°15,9'N	109°14,8'E	51		MN
			02:43	78°15,8'N	109°14,9'E	51		BO
			02:51	78°15,8'N	109°14,8'E	51		BO
			02:59	78°15,8'N	109°14,9'E	51		MUC (empty)
	PS2480-1		03:22	78°15,8'N	109°14,7'E	51		MUC (10)
			03:43	78°15,7'N	109°14,9'E	51		GKG (BIO)
	PS2480-2		04:03	78°15,7'N	109°14,7'E	51		GKG (15)
Heli	R9426301		04:00	78°19,2'N	106°47,6'E			Sea-ice sampling
			04:22	78°15,5'N	109°14,5'E	51		GKG (BIO)
	PS2480-3		04:48	78°15,5'N	109°14,5'E	51		SL (empty)
			05:25	78°15,3'N	109°14,7'E	51		begin EBS
			05:35	78°15,1'N	109°14,4'E	51		end EBS
			05:53	78°15,3'N	109°14,6'E	51		begin AGT
			06:09	78°15,6'N	109°15,5'E	51		end AGT
			6:34 - 7:09	78°15,8'N	109°13,7'E	50		Ice measurements
27/068			13:02	78°28,1'N	110°49,4'E	101	9-10	CTD
			13:04	78°28,2'N	110°48,5'E	101		HN
			13:32	78°28,2'N	110°47,8'E	102		MN
			13:46	78°28,3'N	110°47,8'E	100		BO
			13:59	78°28,3'N	110°47,7'E	102		BO
			14:22	78°28,3'N	110°47,6'E	101		MG
	PS2481-1		14:41	78°28,3'N	110°47,5'E	100		MUC (BIO)
	PS2481-2		15:11	78°28,4'N	110°47,3'E	101		GKG (42)
			15:33	78°28,4'N	110°47,4'E	100		GKG (BIO)
	PS2481-3		16:00	78°28,4'N	110°47,3'E	100		SL (200/195)
			16:38	78°28,6'N	110°47,3'E	100		begin EBS
			16:48	78°28,5'N	110°47,2'E	101		end EBS
			17:06	78°28,4'N	110°46,9'E	101		begin AGT
			17:21	78°28,1'N	110°46,0'E	101		end AGT
27/069		21.09.1993	3:45 - 8:30	78°41,5'N	112°31,8'E	517	10	Ice station
			03:57	78°41,5'N	112°31,8'E	518		CTD
			03:59	78°41,5'N	112°31,8'E	518		HN
			04:43	78°41,6'N	112°31,5'E	535		MN
			05:23	78°41,7'N	112°31,4'E	546		BO
			05:38	78°41,7'N	112°31,3'E	549		BO

Station	AWI-No.	Date	Time	Latitude	Longitude	Depth (m)	Ice cover	Activity
			06:15	78°41,8'N	112°31,2'E	554		MG
	PS2482-1		06:51	78°41,9'N	112°31,1'E	557		MUC (BIO)
	PS2482-2		07:22	78°42,0'N	112°30,9'E	557		MUC (30)
			07:57	78°42,1'N	112°30,8'E	565		GKG (BIO)
	PS2482-3		08:27	78°42,1'N	112°30,7'E	577		GKG (20)
			09:01	78°42,2'N	112°30,7'E	574		GKG (BIO)
	PS2482-4		09:37	78°42,2'N	112°30,3'E	598		SL (500/315)
			10:07	78°42,3'N	112°30,1'E	608		MG
27/070			12:15	78°45,0'N	112°42,0'E	1140	10	CTD
			12:44	78°45,1'N	112°41,6'E	1140		MN
			14:23	78°45,3'N	112°41,7'E	1155		CTD
			14:28	78°45,3'N	112°41,6'E	1157		HN
			15:33	78°45,4'N	112°41,7'E	1173		BO
			15:48	78°45,5'N	112°41,6'E	1177		BO
			16:20	78°45,5'N	112°41,8'E	1189		MG
			16:40	78°45,5'N	112°41,9'E	1192		MUC (empty)
	PS2483-1		17:45	78°45,6'N	112°42,0'E	1205		MUC (30)
			18:33	78°45,7'N	112°42,2'E	1210		GKG (BIO)
	PS2483-2		19:17	78°45,7'N	112°42,2'E	1216		GKG (44)
	PS2483-3		20:24	78°45,7'N	112°42,6'E	1217		SL (700/568)
			21:05	78°45,7'N	112°42,4'E	1219		MG
27/071		22.09.1993	03:55	78°34,8'N	111°22,2'E	240	10	CTD
			04:08	78°34,8'N	111°22,2'E	240		HN
			04:28	78°34,8'N	111°22,2'E	240		MN
			04:54	78°34,9'N	111°22,4'E	240		BO
			05:08	78°34,9'N	111°22,5'E	240		BO
			05:32	78°34,9'N	111°22,6'E	239		MG
			06:06	78°34,9'N	111°22,6'E	240		MUC (empty)
	PS2484-1		06:27	78°34,9'N	111°22,9'E	235		MUC (31)
			06:58	78°34,9'N	111°23,0'E	240		GKG (BIO)
	PS2484-2		07:46	78°34,9'N	111°23,2'E	235		GKG (37)
			08:07	78°34,9'N	111°23,1'E	235		GKG (BIO)
			08:27	78°34,9'N	111°23,0'E	242		MG
	PS2484-3		08:51	78°34,9'N	111°22,9'E	235		SL (400/221)
<b>Vilkitsky Strait</b>								
27/072		23.09.1993	18:16	77°53,9'N	105°06,8'E	228		CTD
	PS2485-1		18:51	77°54,0'N	105°05,0'E	229		GKG (ca. 45)
	PS2485-2		19:20	77°54,0'N	105°03,2'E	230		SL (/900/689)
			19:57	77°54,5'N	105°04,0'E	229		begin AGT
			20:13	77°54,6'N	105°02,7'E	229		end AGT
27/073			21:46	77°59,5'N	104°37,5'E	132		CTD
	PS2486-1		22:21	77°59,5'N	104°35,6'E	118		SL (empty)
	PS2486-2		22:41	77°59,4'N	104°34,6'E	122		GKG (empty)
27/074		24.09.1993	02:50	78°17,5'N	105°30,7'E	194		CTD

List of used abbreviations in the station list ARK IX/4

MN	Multi net
MUC	Multi corer
GKG	Großkastengreifer
MG	Multi grab
CTD	Conductivity, temperature, depth probe
SD	Secchi disk
HN	Hand net
BO	Bongo net
SL	Gravity corer
AGT	Aggassiz trawl
KAL	Kastenlot
EBS	Epibenthos sledge
Heli	Helicopter flight

The data in the station list represent:

for:

ice stations:                      begin and end of work on ice

geological stations:

(MUC, GKG, SL, KAL)      bottom contact

biological stations:

(GKG, MUC, MG)              bottom contact

(AGT + EBS)                  begin and end of bottom contact

oceanographic stations:

(CTD)                              begin of first water contact

(Bongo, SD, HN)                begin of first water contact

10.2 Benthos sampling list

Date	Station#	Geo-#	Gear	Depth (m)	Position N	Position E	Position N*	Position E*
<b>Bear Island Trough</b>								
09.08.93	27/001	2439	MG	449	73°38,8'	22°55,2'		
<b>Northern Barents Sea Slope</b>								
12.08.93	27/006	2440-1	MUC-BIO	197	81°12,61'	30°36,20'		
12.08.93	27/006	2440-2	MUC-GEO	187	81°12,80'	30°36,44'		
12.08.93	27/006	2440-3	MUC-BIO	186	81°12,87'	30°36,51'		
12.08.93	27/006	2440	MG	198	81°12,6'	30°36,3'		
12.08.93	27/006	2440-4	GKG-GEO	196	81°13,02'	30°36,72'		
12.08.93	27/006	2440	AGT	170-200	81°13,7'	30°36,7'	81°13,8'	30°37,2'
12.08.93	27/007	2441-1	MUC-BIO	560	81°27,88'	30°53,47'		
12.08.93	27/007	2441-2	MUC-GEO	574	81°28,08'	30°53,54'		
12.08.93	27/007	2441-3	GKG-GEO	589	81°28,30'	30°53,85'		
13.08.93	27/007	2441	MG	603	81°28,5'	30°54,1'		
13.08.93	27/014	2442-1	MUC-BIO	2806	81°41,10'	30°19,95'		
13.08.93	27/014	2442-2	MUC-GEO	2848	81°41,79'	30°19,85'		
13.08.93	27/014	2442-4	GKG-GEO	2915	81°43,0'	30°20,9'		
15.08.93	27/014	2442	MG	2828	81°41,40'	30°20,03'		
16.08.93	27/016	2443-2	GKG-GEO	2464	82°12,15'	34°36,75'		
18.08.93	27/017	2444-1	GKG-GEO	2566	82°29,20'	37°44,40'		
18.08.93	27/019	2445-1	MUC-BIO	2996	82°45,84'	40°14,75'		
18.08.93	27/019	2445-2	MUC-GEO	2994	82°45,81'	40°15,36'		
18.08.93	27/019	2445	MG	2993	82°45,8'	40°15,3'		
19.08.93	27/019	2445-3	GKG-GEO	2995	82°45,83'	40°14,54'		
19.08.93	27/020	2446-1	MUC-BIO	2019	82°23,72'	40°52,54'		
20.08.93	27/020	2446-2	MUC-GEO	2026	82°23,92'	40°53,60'		
20.08.93	27/020	2446-3	GKG-GEO	2025	82°23,94'	40°53,63'		
20.08.93	27/020	2446	MG	2027	82°23,90'	40°53,16'		
20.08.93	27/020	2446	MG	2018	82°23,75'	40°54,41'		
20.08.93	27/024	2447-1	MUC-BIO	1013	82°09,78'	42°02,16'		
20.08.93	27/024	2447-2	MUC-BIO	1017	82°09,82'	42°02,15'		
20.08.93	27/024	2447-3	MUC-GEO	1024	82°09,91'	42°02,30'		
21.08.93	27/024	2447-4	GKG-GEO	1024	82°09,59'	42°02,74'		
21.08.93	27/024	2447	MG	1021	82°09,88'	42°02,7'		
21.08.93	27/024	2447	MG	1025	82°10'	42°03,3'		
21.08.93	27/025	2448-1	MUC-BIO	511	82°07,42'	42°33,43'		
21.08.93	27/025	2448-2	MUC-GEO	520	82°07,37'	42°32,79'		
21.08.93	27/025	2448-3	GKG-GEO	534	82°07,42'	42°32,25'		
21.08.93	27/025	2448	MG	516	82°07,43'	42°33,10'		
21.08.93	27/027	2449-1	MUC-BIO	287	82°01,38'	43°34,16'		
21.08.93	27/027	2449-2	MUC-GEO	287	82°01,36'	43°34,48'		
21.08.93	27/027	2449-3	GKG-GEO	286	82°01,35'	43°34,63'		
21.08.93	27/027	2449	MG	286	81°01,37'	43°34,31'		
21.08.93	27/027	2449	AGT	284-292	82°01,7'	43°33,18'	82°01,39'	43°34'
<b>Vilkitsky Strait</b>								
26.08.93	27/028	2450-1	MUC-BIO	152	78°01,99'	102°01,99'		
26.08.93	27/028	2450-2	GKG-GEO	148	78°01,83'	102°18,24'		
26.08.93	27/028	2450-B	GKG-BIO	149	78°01,9'	102°17,5'		
26.08.93	27/028	2450	MG	151	78°02,0'	102°17,9'		
26.08.93	27/028	2450	AGT	153-157,5	78°19,5'	102°19,99'	78°02,11'	102°20,9'
27.08.93	27/029	2451-1	MUC-BIO	144	77°42,48'	102°17,27'		
27.08.93	27/029	2451	MG	144	77°42,5'	102°17,8'		
27.08.93	27/029	2451-2	GKG-GEO	143	77°42,43'	102°17,27'		
27.08.93	27/029	2451-B	GKG-BIO	135	77°42,0'	102°14,3'		
27.08.93	27/029	2451	AGT	120	77°40,53'	102°07,3'	77°40,53'	102°05,13'

27.08.93	27/030	2452-1	MUC-BIO	134	77°53,25'	101°37,43'		
27.08.93	27/030	2452-2	GKG-GEO	132	77°53,52'	101°35,54'		
27.08.93	27/030	2452-B	GKG-BIO	132	77°53,7'	101°34,2'		
27.08.93	27/030	2452	MG	133	77°53,42'	101°36,71'		
27.08.93	27/030	2452	EBS	130	77°53,75'	101°28,41'	77°53,70'	101°27,05'

**Laptev Sea**

01.09.93	27/031	2453	AGT	39	76°29,83'	133°10,29'	76°29,48'	133°11,31'
01.09.93	27/031	2453-1	MUC-GEO	37	76°30,23'	133°21,21'		
01.09.93	27/031	2453-2	GKG-GEO	38	76°30,53'	133°21,32'		
01.09.93	27/031	2453-B	GKG-BIO	38	76°30,9'	133°21,0'		
01.09.93	27/031	2453	EBS	37-38	76°32,15'	133°19,82'	76°32,12'	133°20,46'
02.09.93	27/032	2454	MG	2962	78°42,4'	132°19,9'		
02.09.93	27/032	2454-1	MUC-BIO	2976	78°42,64'	132°17,45'		
02.09.93	27/032	2454	AGT	3012-3028	78°42,68'	132°33,8'	78°42,70'	132°39,41'
03.09.93	27/033	2455-1	MUC-BIO	3427	79°39,01'	130°35,75'		
03.09.93	27/033	2455-2	MUC-GEO	3425	79°38,82'	130°34,78'		
03.09.93	27/033	2455-3	GKG-GEO	3429	79°39,012'	130°32,13'		
03.09.93	27/034	2456-1	MUC-GEO	2534	78°29,11'	132°54,86'		
03.09.93	27/034	2456-2	GKG-GEO	2520	78°29,04'	133°00,10'		
04.09.93	27/035	2457-1	MUC-BIO	2019	78°23,19'	133°11,43'		
05.09.93	27/035	2457(-2)	MUC-GEO (MG)	2130	78°23,50'	133°09,57'		
05.09.93	27/035	2457	MG	2151	78°23,5'	133°09,57'		
05.09.93	27/035	2457	MG	1934	78°22,4'	133°12,4'		
05.09.93	27/038	2458	MG	828	78°08,4'	133°20,7'		
05.09.93	27/038	2458-1	MUC-BIO	796	78°08,19'	133°19,94'		
05.09.93	27/038	2458-2	MUC-GEO	769	78°08,14'	133°19,14'		
05.09.93	27/038	2458-B1	GKG-BIO	950	78°09,7'	133°22,4'		
05.09.93	27/038	2458-3	GKG-GEO	981	78°09,95'	133°23,86'		
05.09.93	27/038	2458-B2	GKG-BIO	982	78°09,9'	133°23,8'		
05.09.93	27/038	2458	AGT	1033-1039	78°10,58'	133°25,26'	78°10,70'	133°26,06'
05.09.93	27/039	2459	EBS	493-498	78°06,27'	133°36,38'	78°06,19'	133°35,79'
05.09.93	27/039	2459-1	MUC-GEO	532	78°06,03'	133°31,46'		
05.09.93	27/039	2459	MG	511	78°05,92'	133°30,8'		
05.09.93	27/039	2459-B1	GKG-BIO	520	78°05,9'	133°31,1'		
05.09.93	27/039	2459-2	GKG-GEO	517	78°05,95'	133°30,31'		
05.09.93	27/039	2459-B2	GKG-BIO	525	78°06,0'	133°30,3'		
05.09.93	27/039	2459	AGT	525-514	78°6,02'	133°32,27'	78°6,03'	133°32,93'
05.09.93	27/040	2460-1	MUC-BIO	213	78°04,38'	133°34,06'		
05.09.93	27/040	2460	MG	217	78°04,4'	133°34,2'		
05.09.93	27/040	2460-2	MUC-GEO	215	78°04,43'	133°34,87'		
06.09.93	27/040	2460-B1	GKG-BIO	216	78°04,5'	133°36,3'		
06.09.93	27/040	2460-3	GKG-GEO	191	78°04,33'	133°36,47'		
06.09.93	27/040	2460-B2	GKG-BIO	203	77°04,5'	133°36,45'		
06.09.93	27/040	2460	AGT	231-233	78°04,56'	133°34,9'	78°04,52'	133°33,77'
06.09.93	27/041	2461	EBS	73	77°54,48'	133°33,29'	77°54,62'	133°33,65'
06.09.93	27/041	2461-1	MUC-GEO	73	77°54,65'	133°33,77'		
06.09.93	27/041	2461-B1	GKG-BIO	73	77°54,5'	133°33,4'		
06.09.93	27/041	2461-2	GKG-GEO	73	77°54,62'	133°33,25'		
06.09.93	27/041	2461-B2	GKG-BIO	73	77°54,7'	133°33,2'		
06.09.93	27/041	2461	AGT	72-71	77°54,83'	133°34,37'	77°54,66'	133°35,39'
06.09.93	27/043	2462	EBS	54	77°24,1'	133°33,09'	77°24,24'	133°33,20'
06.09.93	27/043	2462-1	MUC-BIO	54	77°24,35'	133°33,11'		
06.09.93	27/043	2462-2	MUC-GEO	54	77°24,30'	133°33,19'		
06.09.93	27/043	2462-B1	GKG-BIO	55	77°24,3'	133°33,3'		
06.09.93	27/043	2462-3	GKG-GEO	54	77°24,28'	133°33,35'		
06.09.93	27/043	2462-B1	GKG-BIO	54	77°24,3'	133°33,3'		
06.09.93	27/043	2462	AGT	54	77°24,46'	133°32,96'	77°24,32'	133°33,68'

07.09.93	27/044	2463	EBS	93-94	77°01,9'	126°25,4'	77°02,1'	126°25,6'
07.09.93	27/044	2463-1	MUC-BIO	93	77°02,83'	126°25,55'		
07.09.93	27/044	2463-2	MUC-GEO	93	77°02,08'	126°26,31'		
07.09.93	27/044	2463-B1	GKG-BIO	92	77°01,8'	126°24,9'		
07.09.93	27/044	2463-3	GKG-GEO	92	77°01,76'	126°26,31'		
07.09.93	27/044	2463-B2	GKG-BIO	92	77°01,8'	126°25,0'		
07.09.93	27/044	2463	AGT	96	77°02,32'	126°25,30'	77°02,63'	126°25,01'
08.09.93	27/046	2464-1	MUC-GEO	1753	77°28,60'	125°53,68'		
08.09.93	27/046	2464-B	GKG-BIO	1754	77°28,6'	125°53,8'		
08.09.93	27/046	2464-2	GKG-GEO	1760	77°28,79'	125°54,17'		
08.09.93	27/047	2465	MG	896	77°10,3'	126°21,4'		
08.09.93	27/047	2465-1	MUC-BIO	1009	77°10,74'	126°12,29'		
08.09.93	27/047	2465-2	MUC-GEO	1025	77°11,20'	126°08,13'		
08.09.93	27/047	2465-B1	GKG-BIO	1009	77°10,85'	126°13,4'		
08.09.93	27/047	2465-3	GKG-GEO	1026	77°11,01'	126°11,48'		
08.09.93	27/047	2465-B2	GKG-BIO	1015	77°11,25'	126°13,8'		
09.09.93	27/047	2465	AGT	1006-1016	77°11,67'	126°19,17'	77°11,65'	126°20,41'
09.09.93	27/048	2466	EBS	500-526	77°07,64'	126°23,35'	77°07,67'	126°22,38'
09.09.93	27/048	2466	MG	522	77°07,72'	126°21,4'		
09.09.93	27/048	2466-1	MUC-BIO	561	77°07,94'	126°22,38'		
09.09.93	27/048	2466-2	MUC-GEO	538	77°07,52'	126°19,24'		
09.09.93	27/048	2466-B1	GKG-BIO	546	77°07,75'	126°20,1'		
09.09.93	27/048	2466-3	GKG-GEO	552	77°08,05'	126°21,24'		
09.09.93	27/048	2466-B2	GKG-BIO	610	77°08,2'	126°22,9'		
09.09.93	27/048	2466	AGT	556-530	77°07,83'	126°25,04'	77°07,6'	126°24,33'
09.09.93	27/049	2467	MG	292	77°06,17'	126°17,59'		
09.09.93	27/049	2467-1	MUC-BIO	240	77°05,82'	126°17,04'		
09.09.93	27/049	2467-2	MUC-GEO	332	77°05,38'	126°15,47'		
09.09.93	27/049	2467-B1	GKG-BIO	195	77°05,0'	126°14,8'		
09.09.93	27/049	2467-3	GKG-GEO	284	77°04,99'	126°13,36'		
09.09.93	27/049	2467-B2	GKG-BIO	180	77°04,7'	126°12,3'		
09.09.93	27/049	2467	AGT	180-360	77°04,7'	126°10,7'	77°04,7'	126°08,8'
10.09.93	27/050	2468	MG	1981	77°41,44'	125°51,3'		
10.09.93	27/050	2468-1	MUC-BIO	1985	77°41,36'	125°51,40'		
10.09.93	27/050	2468-2	MUC-GEO	1990	77°41,41'	125°52,07'		
10.09.93	27/050	2468-3	GKG-GEO	1991	77°41,58'	125°53,55'		
10.09.93	27/050	2468	AGT	1992-1993	77°41,43'	125°55,09'	77°41,10'	125°54,16'
11.09.93	27/052	2469-1	MUC-GEO	2443	78°04,14'	125°01,17'		
11.09.93	27/052	2469-2	GKG-GEO	2332	77°03,58'	125°00,01'		
12.09.93	27/053	2470	MG	3236	79°13,7'	122°51,7'		
12.09.93	27/053	2470-1	MUC-BIO	3237	79°13,64'	122°51,29'		
12.09.93	27/053	2470-2	MUC-GEO	3236	79°13,65'	122°52,09'		
12.09.93	27/053	2470-3	GKG-GEO	3233	79°12,96'	122°54,37'		
12.09.93	27/053	2470	MG	3229	79°11,6'	122°55,2'		
13.09.93	27/054	2471	AGT	3039-3042	79°11,33'	119°56,37'	79°11,81'	119°56,22'
13.09.93	27/054	2471	MG	3054	79°09,95'	119°49,23'		
13.09.93	27/054	2471-1	MUC-BIO	3051	79°09,71'	119°47,19'		
13.09.93	27/054	2471-2	MUC-GEO	3051	79°09,45'	119°45,83'		
13.09.93	27/054	2471-3	GKG-GEO	3048	79°09,29'	119°46,89'		
14.09.93	27/056	2472	MG	2619	78°40,1'	118°44,2'		
14.09.93	27/056	2472-1	MUC-BIO	2620	78°40,02'	118°44,50'		
14.09.93	27/056	2472-2	MUC-GEO	2621	78°40,00'	118°44,48'		
14.09.93	27/056	2472-3	GKG-GEO	2620	78°40,04'	118°44,29'		
14.09.93	27/056	2472	MG	2620	78°39,98'	118°44,74'		
15.09.93	27/058	2473-1	MUC-BIO	1935	77°59,51'	118°35,14'		
15.09.93	27/058	2473-2	MUC-GEO	1930	77°59,16'	118°34,82'		
15.09.93	27/058	2473-3	GKG-GEO	1927	77°58,88'	118°34,25'		
15.09.93	27/059	2474-1	MUC-BIO	1517	77°40,82'	118°34,59'		
15.09.93	27/059	2474	MG	1502	77°40,36'	118°34,5'		
16.09.93	27/059	2474-2	GKG-GEO	1497	77°40,24'	118°34,52'		

16.09.93	27/060	2475	MG	1126	77°32,28'	118°27,56'		
16.09.93	27/060	2475-B	GKG-BIO	1100	77°32,05'	118°27,5'		
17.09.93	27/060	2475-1	GKG-GEO	1108	77°31,98'	118°27,45'		
17.09.93	27/060	2475-2	MUC-GEO	1104	77°31,94'	118°27,28'		
17.09.93	27/060	2475	MG	1101	77°31,88'	118°27,47'		
17.09.93	27/062	2476	MG	538	77°23,93'	118°11,5'		
17.09.93	27/062	2476-1	MUC-BIO	534	77°23,80'	118°11,60'		
17.09.93	27/062	2476-2	MUC-GEO	531	77°23,68'	118°11,61'		
17.09.93	27/062	2476-B1	GKG-BIO	525	77°23,55'	118°11,45'		
17.09.93	27/062	2476-3	GKG-GEO	524	77°23,51'	118°11,45'		
17.09.93	27/062	2476-B2	GKG-BIO	520	77°23,4'	118°11,45'		
17.09.93	27/064	2477	MG	221	77°15,27'	118°33,04'		
17.09.93	27/064	2477-1	MUC-BIO	230	77°15,15'	118°33,17'		
18.09.93	27/064	2477-2	MUC-GEO	225	77°15,02'	118°33,17'		
18.09.93	27/064	2477-B1	GKG-BIO	196	77°14,85'	118°33,2'		
18.09.93	27/064	2477-3	GKG-GEO	193	77°14,77'	118°33,17'		
18.09.93	27/064	2477-B2	GKG-BIO	190	77°14,65'	118°33,05'		
18.09.93	27/064	2477	AGT	191-181	77°14,72'	118°30,92'	77°14,49'	118°32,21'
18.09.93	27/064	2477	EBS	188-195	77°14,63'	118°31,8'	77°14,72'	118°31,14'
18.09.93	27/065	2478-1	MUC-BIO	107	77°10,63'	118°44,05'		
18.09.93	27/065	2478-2	MUC-GEO	108	77°10,49'	118°43,67'		
18.09.93	27/065	2478-B1	GKG-BIO	95	77°10,3'	118°43,1'		
18.09.93	27/065	2478-3	GKG-GEO	101	77°10,28'	118°42,58'		
18.09.93	27/065	2478-B2	GKG-BIO	96	77°10,2'	118°41,75'		
18.09.93	27/065	2478	MG	97	77°10,24'	118°41,336'		
18.09.93	27/066	2479-1	MUC-BIO/GEO	65	77°31,34'	114°27,35'		
20.09.93	27/067	2480-1	MUC-GEO	51	78°15,75'	109°14,73'		
20.09.93	27/067	2480-B1	GKG-BIO	51	78°15,7'	109°14,9'		
20.09.93	27/067	2480-2	GKG-GEO	51	78°15,69'	109°14,74'		
20.09.93	27/067	2480-B2	GKG-BIO	51	78°15,5'	109°14,5'		
20.09.93	27/067	2480	EBS	51	78°15,25'	109°14,65'	78°15,07'	109°14,37'
20.09.93	27/067	2480	AGT	51	78°15,32'	109°14,58'	78°15,56'	109°15,53'
20.09.93	27/068	2481	MG	101	78°28,29'	110°47,56'		
20.09.93	27/068	2481-1	MUC-GEO	100	78°28,31'	110°47,47'		
20.09.93	27/068	2481-2	GKG-GEO	101	78°28,38'	110°47,33'		
20.09.93	27/068	2481-B	GKG-BIO	100	78°28,4'	110°47,4'		
20.09.93	27/068	2481	EBS	100-101	78°28,62'	110°47,28'	78°28,47'	110°47,16'
20.09.93	27/068	2481	AGT	101	78°28,37'	110°46,92'	78°28,05'	110°46,00'
20.09.93	27/069	2482	MG	554	78°41,84'	112°31,24'		
20.09.93	27/069	2482-1	MUC-BIO	557	78°41,90'	112°31,05'		
21.09.93	27/069	2482-2	MUC-GEO	557	78°41,96'	112°30,93'		
21.09.93	27/069	2482-B1	GKG-BIO	565	78°42,05'	112°30,8'		
21.09.93	27/069	2482-3	GKG-GEO	577	78°42,09'	112°30,65'		
21.09.93	27/069	2482-B2	GKG-BIO	574	78°42,15'	112°30,65'		
21.09.93	27/069	2482	MG	608	78°42,27'	112°30,08'		
21.09.93	27/070	2483	MG	1189	78°45,5'	112°41,8'		
21.09.93	27/070	2483-1	MUC-GEO	1205	78°45,64'	112°42,01'		
21.09.93	27/070	2483-B	GKG-BIO	1210	78°45,65'	112°42,15'		
21.09.93	27/070	2483-2	GKG-GEO	1216	78°45,74'	112°42,23'		
21.09.93	27/070	2483	MG	1219	78°45,7'	112°42,5'		
21.09.93	27/071	2484	MG	239	78°34,9'	111°22,6'		
21.09.93	27/071	2484-1	MUC-GEO	240	78°34,94'	111°23,15'		
21.09.93	27/071	2484-B1	GKG-BIO	240	78°34,9'	111°23,0'		
22.09.93	27/071	2484-2	GKG-GEO	235	78°34,91	111°22,93'		
22.09.93	27/071	2484-B2	GKG-BIO	235	78°34,9'	111°23,1'		
22.09.93	27/071	2484	MG	242	78°34,9'	111°22,99'		
<b>Vilkitsky Strait</b>								
22.09.93	27/072	2485-1	GKG-GEO	229	77°54,01'	105°04,98'		
22.09.93	27/072	2485	AGT	229	77°54,54'	105°04,00'	77°54,65'	105°02,69'
23.09.93	27/073	2486-2	GKG-GEO	122	77°59,44'	104°35,61'		

Device Sample-#	GKG PS2440-4	GKG PS2442-4	GKG PS2443-2	GKG PS2444-1	GKG PS2445-3	GKG PS2446-3	GKG PS2448-1	GKG PS2452-2	GKG PS2453-2	GKG PS2462-3	GKG PS2465-3	GKG PS2467-3
Depth in core	(cm)											
	0	0	5	0	0	0	0	0	0	0	0	0
		5	20	31	30	25	31	9	16	18	15	10
		31	40	42			50	25	41	33	30	
		42	50									
Device Sample-#	SL PS2443-3	SL PS2444-2	KAL PS2445-4	KAL PS2446-4	SL PS2447-5	SL PS2448-4	SL PS2450-3	SL PS2451-3	SL PS2453-3	KAL PS2456-3	KAL PS2458-4	SL PS2460-4
Depth in core	(cm)											
	0	0	20	20	20	12	25	0	5	30	20	1
	100	10	70	50	26	30	100	15	50	38	30	10
	200	32	75	60	32	41	150	40	70	43	50	20
	300	45	77	80	80	51	200	60	125	50	100	60
	400	52	80	100	95	78	247	85	135	57	200	120
		60	90	120	116	100	251	97	158	70	300	160
		66	105	150	130	150	258	99		90	400	210
		76	116	200	190	180	293	140		170	500	230
		82	120	250	210	240	296	160		205	600	270
		95	125	300	215		305	200		213	700	310
		125	140	320	340		350	240		220	800	330
		130	158	350	400		380	300		240		370
		155	203	370			398	340		270		410
		166	225	390			402	370		290		430
		200	253	400			411	420		299		470
		250	300	420			450	450		350		510
		320	400	450			455	500		400		530
		266		480			470	540		470		570
		366		500			490			500		610
		466		520			508			540		630
		CC		550			525			560		670
				580			550			573		710
				600								730
				620								770
												810
												830
												870
												908

10.3 List of smear slides prepared and examined during the cruise

Device Sample-#	GKG PS2468-3	GKG PS2470-4	GKG PS2472-3	GKG PS2473-3	GKG PS2474-2	GKG PS2476-3	GKG PS2477-3	GKG PS2478-3	GKG PS2483-2
Depth in core	(cm)								
	0	0	0	10	0	0	0	0	0
	20	20	20	13	10	13	5	15	10
	40	35	35	20	20	20	30		20
				30	30	35			40
Device Sample-#	SL PS2465-4	KAL PS2469-1	SL PS2471-4	KAL PS2473-4	KAL PS2474-3	SL PS2476-4	SL PS2483-3		
Depth in core	(cm)								
	1	13	7	50	30	0	0		
	7	63	16	100	50	12	10		
	10	113	20	120	90	26	40		
	40	264	60	150	130	40	65		
	70	310	110	200	150	80	80		
	100	315	130	250	200	130	100		
	140		143	268	220	140	110		
	170		148	300	250	190	135		
	200		155	328	300	230	150		
	240		170	350	350	240	165		
	270		180	400	400	280	170		
	300		185	440	450	330	177		
	340		190	450	500	350	195		
	370		195	500	520	390	220		
	400		200	560	550	430	240		
	440		205		580	450	260		
			213		598	490	265		
			220		630	530	272		
			250		650	550	278		
			260		662	580	280		
			270		700	590	290		
			275		740	633	295		
			285		747		298		
			290		749		310		
			300		760		330		
			310		768		340		
			320		780		350		
			340				360		
							568		

## 10.4 Graphical Core Descriptions

### Legend:

#### Lithology

	sand		foraminiferal ooze
	sandy silt		nannofossil ooze
	sandy clay		diatomaceous ooze
	sandy silty clay		radiolarian ooze
	silt		volcanic ash
	silty clay		chert / porcellanite
	clay		pebbles, dropstones
	diamicton		sediment clasts mudclasts

• smear slides

/// // changes in core scale

#### Structure

	bioturbation
	stratification
	lamination
	coarsening upward sequence
	fining upwards sequence
	sharp boundary
	gradational boundary
	transition zone

**PS2439-2 (GKG)**

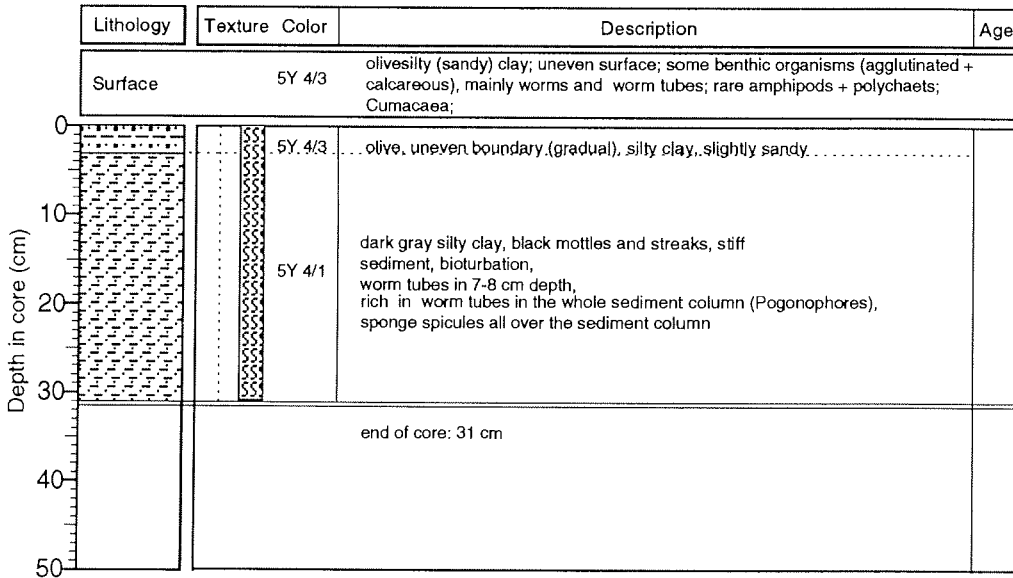
Barents Sea, Bear Island Trough

**ARK IX/4 (ARCTIC 93)**

Recovery: 0.31 m

73°38,8'N 22°55,3'E

Water depth: 459 m



**PS2440-4 (GKG)**

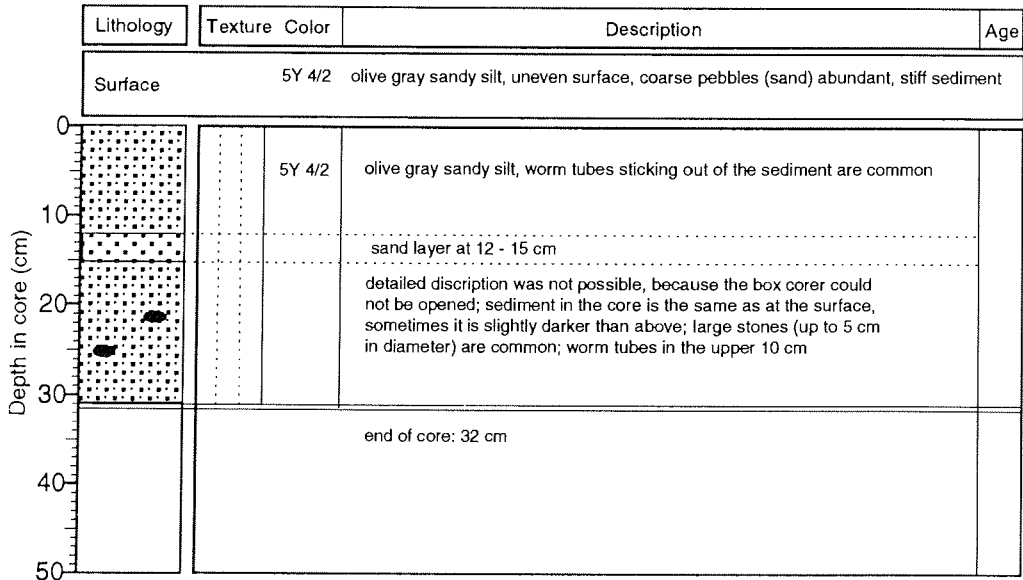
Barents Sea, Profile A, north of Quitoya

**ARK IX/4 (ARCTIC 93)**

Recovery: 0.32 m

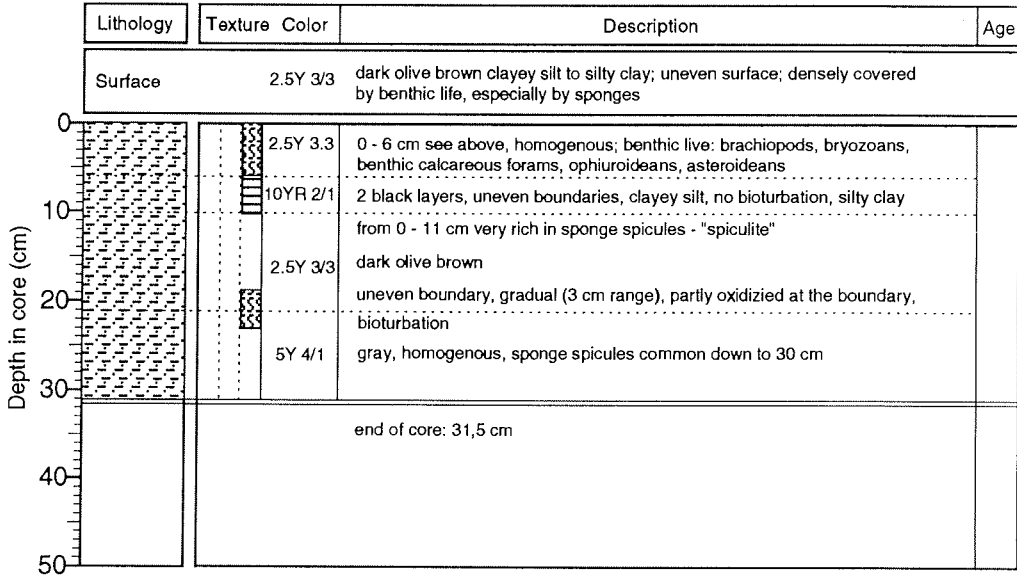
81°13,02'N 30°36,72'E

Water depth: 196 m



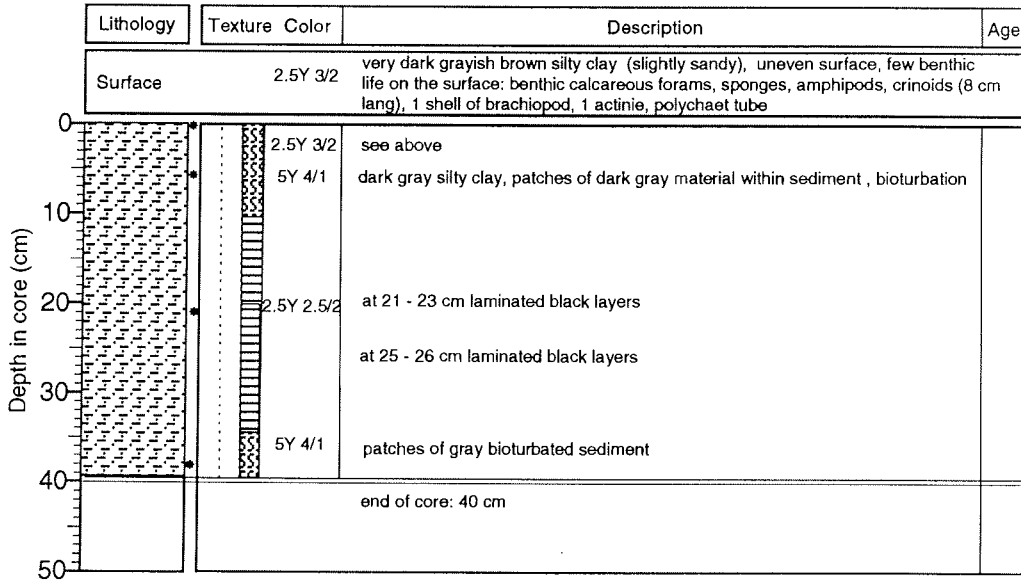
**PS2441-3 (GKG) Barents Sea, Profile A, north of Quitoya ARK IX/4 (ARCTIC 93)**

Recovery: 0.31 m      81°28,30'N 30°53,85'E      Water depth: 589 m



**PS2442-4 (GKG) Barents Sea, Profile A, north of Quitoya ARK IX/4 (ARCTIC 93)**

Recovery: 0.40 m      81°43,0'N 30°20,9'E      Water depth: 2915 m



**PS2443-2 (GKG)**

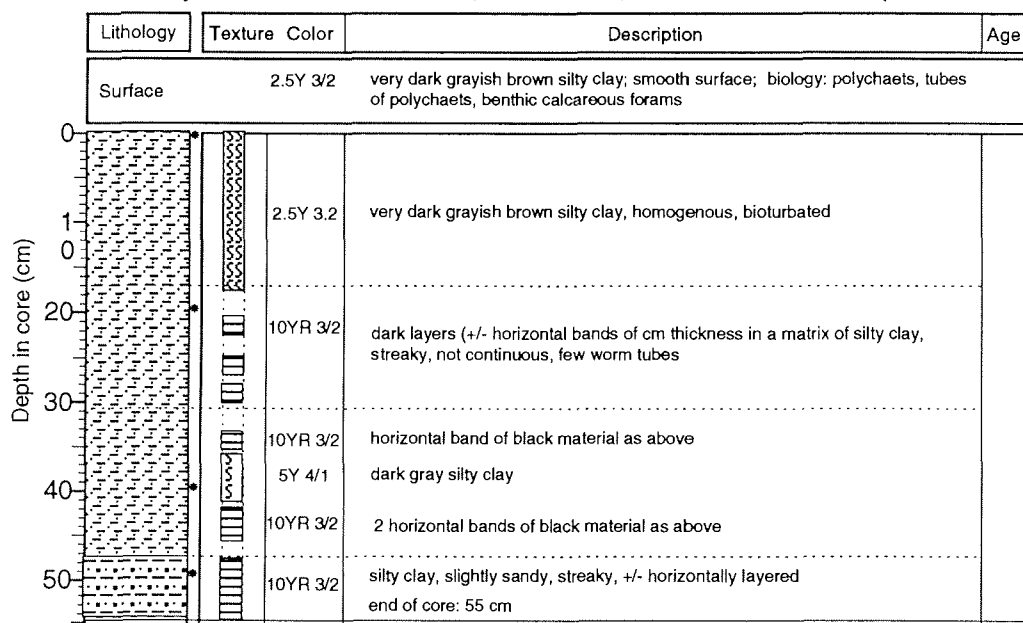
Barents Sea, transit to Profile C

**ARK IX/4 (ARCTIC 93)**

Recovery: 0.55 m

82°12,15'N 34°36,75'E

Water depth: 2464 m



**PS2444-1 (GKG)**

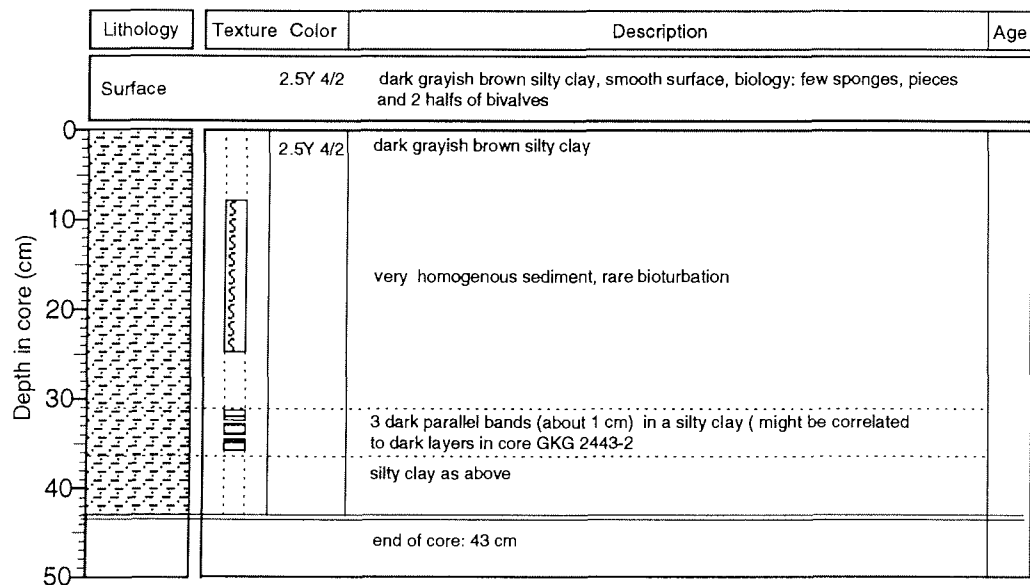
Barents Sea, transit to Profile C

**ARK IX/4 (ARCTIC 93)**

Recovery: 0.43 m

82°29,20'N 37°44,40'E

Water depth: 2566 m



PS2444-2 SL

Recovery: 4.66 m

Barents Sea,  
transit from Profile A to C  
82°29,17'N , 37°45,54 E

ARK IX/4 (ARCTIC 93)

Water depth: 2564 m

Lithology	Texture Color	Description	Age
	10YR 3/3	dark brown silty clay, homogenous	
		4 layers of dark (black) organic rich clayey silt, intercalated by sediment as above	
	10YR 3/3	dark brown silty clay, homogenous	
	10YR 3/4	dark yellowish brown silty clay, slightly lighter than above	
	7.5 Y 3/2	layers of dark (black) organic rich clayey silt, burrows, boundaries not sharp but gradual into dark yellowish brown silty clay	
	5Y 3/1	reddish oxidized layer of silty clay	
	5Y 3/1	very dark olive gray silty clay, bioturbated, dark streaks	
	5Y 3/2	dark olive silty clay	
	5Y 4/1	dark gray clayey silt, slightly sandy, dark streaks	
		at 110 cm black particles (3 mm)	
	10YR 3/2	4 layers of reddish (pinkish) clay	
	5Y 4/4	olive sandy silt, dropstone (3 cm) at 131 cm, oxidized worm burrows at 127 cm, very stiff sediment	
	5Y 4/1	dark gray sandy silty clay (diamicton), soft, dropstones	
		silicified carbonate dropstone (4 cm) at base,	
		at 202 cm one large dropstone (2 cm)	
		at 235 cm coal particles abundant (stage 6??)	
		dropstones all over the core	
		at 287 and 294 cm 1 large dropstone (2 cm)	
		end of core: 4.66 m	

PS2445-3 (GKG)

Barents Sea, Profile C

ARK IX/4 (ARCTIC 93)

Recovery: 0.38 m

82°45,83'N 40°14,54'E

Water depth: 2995 m

Lithology	Texture	Color	Description	Age
Surface	10YR 3/2		very dark grayish brown silty clay , even surface, benthic calcareous foraminifers ( <i>Pyrgo sp.</i> ) and bivalve shells common	
	10YR 3/2		homogenous silty clay 0-20 cm <i>Pyrgo sp.</i> common	
			end of core 38 cm	

PS2445-4 KAL

Barents Sea slope, Profile C

ARK IX/4 (ARCTIC 93)

Recovery: 7.25 m

82°45,97'N 40°13,6'E

Water depth: 2999 m

Lithology	Texture Color	Description	Age
	10YR3/2	very dark grayish brown silty clay, homogenous, abundant <i>Pyrgo sp.</i> down to 20 cm grayish patches between 40 and 50 cm	
layered; boundary gradual			
	5Y 4/1	76 - 80 cm: 5Y 2.5/2; 10YR 3/2; 5Y 3/2, silty clay stiff layers, laminated, some are yellowish,	
	5Y 4/1	dark gray, silty clay with dark streaks in lower part	
	5Y 4/1	silty clay, slightly reddish, gray streaks	
	2.5Y 4/2	silty clay, slightly reddish at the top, grayish streaks + laminae at 115-123 cm	
	5Y 3/1	mud clasts and rare dropstones	
	5Y 3/1	very dark olive gray layer of fine sand (turbidite?)	
	5Y 3/1	very dark olive gray sandy clayey silt	
	5Y 4/2	dark olive silty clay, reddish-brownish colored, 2 dark-olive layers	
		some black patches	
		brownish reddish colors black layer	
	5Y 4/1	gradual boundary, black layer, grayish streaky sediment, mud clasts	
	5Y 3/1	very dark olive gray sandy clayey silt (diamictic), homogenous, some cm-sized dropstones in the whole sequence down to the base of the core	
// // //			
		end of core: 7.25 m	

PS2446-3 (GKG)

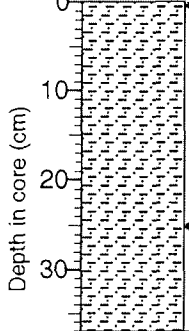
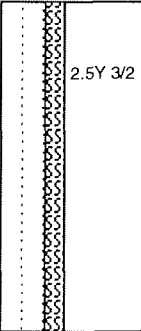
Barents Sea, Profile C

ARK IX/4 (ARCTIC 93)

Recovery: 0.37 m

82°23,94'N 40°53, 63'E

Water depth: 2025 m

Lithology	Texture Color	Description	Age
Surface	2.5Y 3/2	very dark grayish brown silty clay, even, slightly disturbed (crack in the middle of core reaching down to core bottom) surface, benthic calcareous forams abundant, worm burrows	
 <p>Depth in core (cm)</p>	 <p>2.5Y 3/2</p>	<p>very dark grayish brown silty clay, homogenous, strongly bioturbated, sometimes streaky</p>	
		<p>end of core 37 cm</p>	



PS2446-4 KAL

Barents Sea slope  
N Franz-Josef Land, Profile C  
82°23.82' N 40°54.46' E

ARK IX/4 (ARCTIC 93)

Recovery: 6.50 m

Water depth: 2022 m

Lithology	Texture	Color	Description	Age
		5Y 3/1	very dark olive gray sandy clayey silt, at the boundary sandy silt	
		5Y 4/2	olive gray sandy silty clay	
		5Y 3/2	layer of dark olive gray sandy silty clay	
		5Y 4/2		
		5Y 3/2	very dark olive gray with some olive-yellowish streaks, sandy silty clay	
		5Y 3/1		very dark gray, 3 cm thick layer of sandy gravel and rounded stones
		5Y 3/1	very dark gray sandy silty clay, with abundant dropstones of different sizes at 615 cm one large dropstone of 7 cm	
	end of core 6.50 m			
7				
8				
9				
10				

PS2447-4 (GKG)

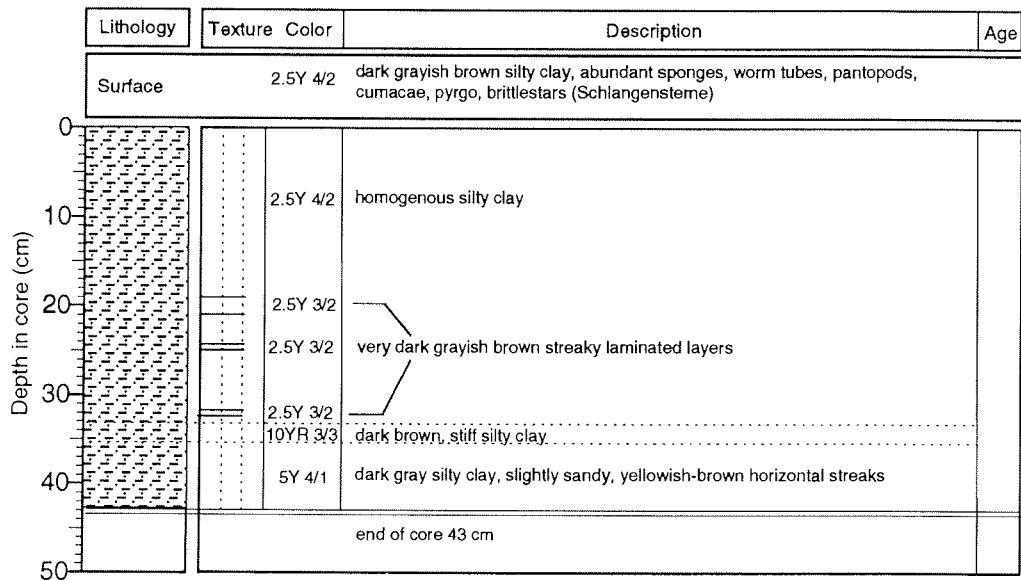
Barents Sea, Profile C

ARK IX/4 (ARCTIC 93)

Recovery: 0.43 m

82°09,91'N 42°02,74'E

Water depth: 1024 m



PS2447-5 SL

Barents Sea slope  
N Franz-Josef-Land, Profile C  
82° 09,7'N 42° 02,7'E

ARK IX/4 (ARCTIC 93)

Recovery: 4.17 m

Water depth: 1025 m

Lithology	Texture	Color	Description	Age
		10YR3/2	very dark grayish brown silty clay, homogenous	
		10YR2/2	very dark brown layer of sandy silt, rich in organic material, gradual boundaries	
		5YR3/2	very dark brown layer of silty clay, rich in organic material	
		5Y4/3	dark brown sandy silt	
		5Y3/2	dark olive gray sandy silty clay, becoming increasingly olive at upper 7 cm of unit, here also rusty layers due to diagenesis	
		5Y2.5/1	black layer of silty sand	
		5Y 3/2	dark olive gray sandy silty clay, small mud clasts abundant, sometimes laminated	
			135-156 cm: enriched in coal fragments	
			some cm-sized dropstones	
		5Y 3/2	dark olive gray sandy clayey silt (diamicton), small mud clasts abundant	
	5Y 3/1	very dark olive gray sandy clayey silt, rich in gravel, no coal fragments dropstones (-5 cm) at 210 cm, 237 cm, 265 cm, 293 cm, 333 cm, 364 cm, 377 cm, 406 cm		
	5Y 3/1			
end of core 4.17 m				

PS2448-3 (GKG)

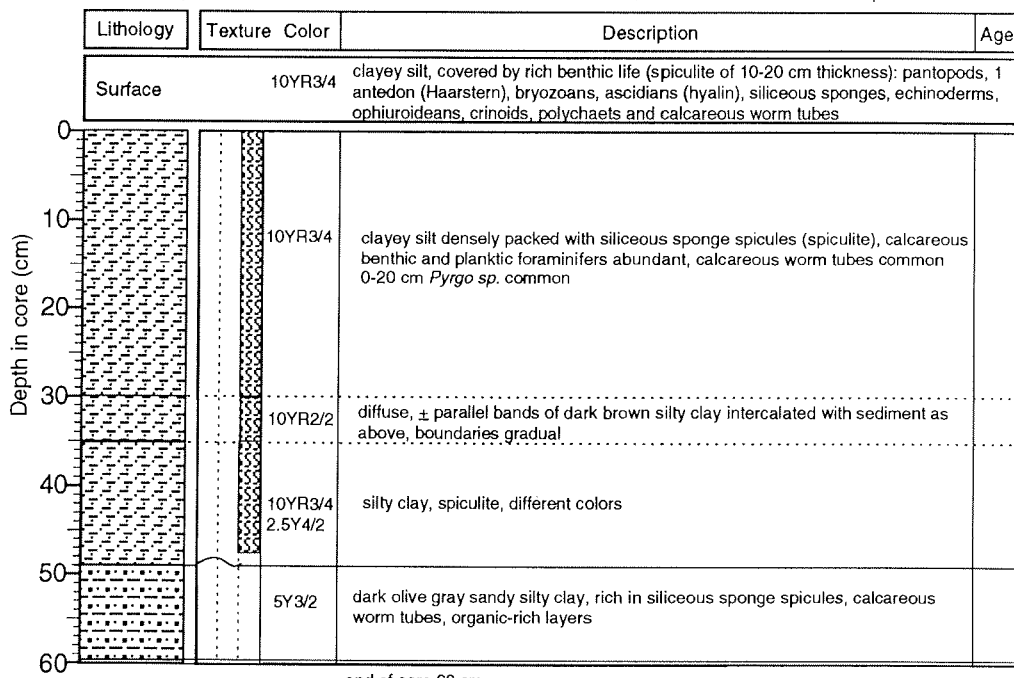
Barents Sea, Profile C

ARK IX/4 (ARCTIC 93)

Recovery: 0.60 m

82°07,42'N 42°32,24'E

Water depth: 534 m



end of core 60 cm

PS2448-4 SL

Barents Sea slope  
N° Franz-Josef-Land, Profile C  
82° 07,4' N - 42° 29,8' E

ARK IX/4 (ARCTIC 93)

Recovery: 3.52 m

Water depth: 553 m

Lithology	Texture Color	Description	Age
	10YR3/4	dark yellowish brown silty clay, rich in siliceous sponge spicules generating spiculite; sponge spicules mostly enriched in layers or patches; calcareous worm tubes abundant; at base gradual change in color, strongly bioturbated	
	2.5Y4/4	olive brown silty clay	
	10YR3/3	dark brown sandy clayey silt, more greenish than above, calcareous worm tubes abundant	
	10YR3/2	layer of very dark grayish brown silty clay, enriched in sponge spicules	
	10YR3/3	dark brown silty clay	
	2.5Y4/4	sandy clayey silt, different colors due to intensive bioturbation, thick layers and patches of sponge spicules, at base silty clayey sand fining upwards; dropstones (-4 cm) at base	
	5Y 3/1	very dark olive gray sandy clayey silt (diamicton) coal fragments and dropstones abundant sandy layer with gravel (-0.5 cm), slightly more olive	
	5Y 3/1	very dark olive gray sandy clayey silt = diamicton; rich in coal fragments and dropstones comparable to lithology in cores KAL 2445, 2446, and 2447 large dropstones (-3 cm) at 153 cm, 194 cm, 206 cm,	
		1 cm thick layered silty clay	
		at 297-298 cm thin sandy layer with uneven upper and lower boundaries at 298-315 cm: sandy clayey silt with abundant dropstones, but more olive	
		very dark olive gray sandy clayey silt = diamicton; rich in coal fragments and dropstones silty sand, fining upwards	
		end of core 3.52 m	

**PS2449-3 (GKG)**

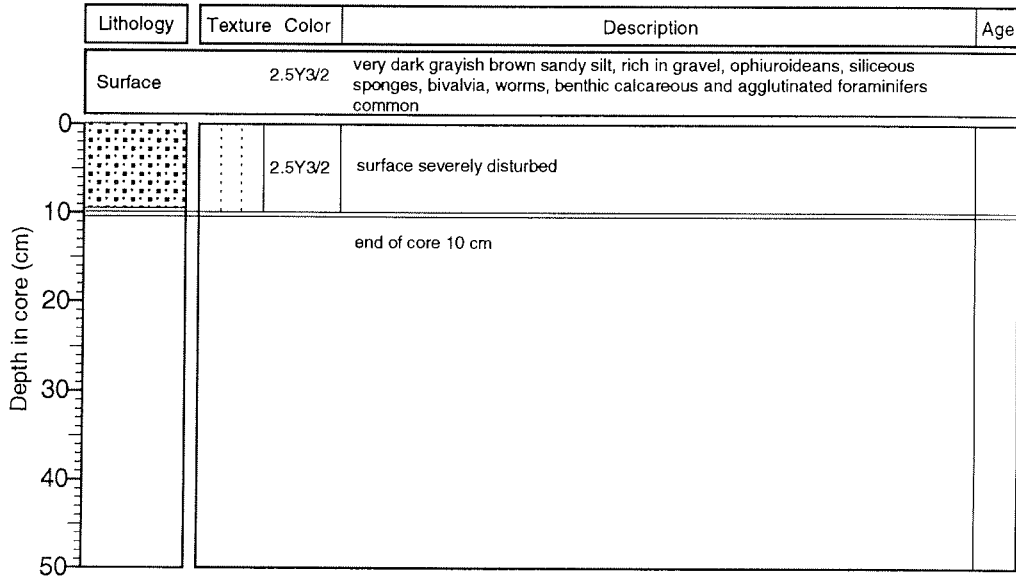
Barents Sea, Profile C

**ARK IX/4 (ARCTIC 93)**

Recovery: 0.10 m

82°01,35'N 43°34,63'E

Water depth: 286 m



**PS2450-2 (GKG)**

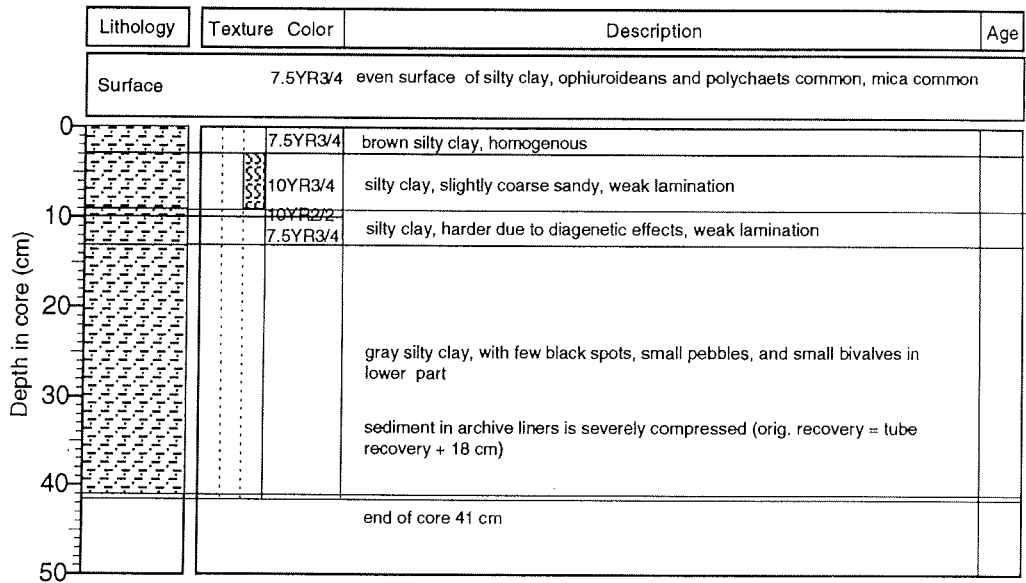
Northern Vilkitsky Strait

**ARK IX/4 (ARCTIC 93)**

Recovery: 0.41 m

78°01,99'N 102°18,52'E

Water depth: 152 m



PS2450-3 (SL)

N`Vilkitsky Strait

ARK IX/4 (ARCTIC 93)

Recovery: 5.51 m

78°01,88`N 102°16,96`E

Water depth: 148 m

Lithology	Texture	Color	Description	Age
0				
core liner is not opened, because of high water content and disturbance (s. 2450-2 GKG)				
1				
<p>5Y 3/2 dark olive gray very fine silty clay, homogenous, rich in Fe/Mn precipitates (- 0.5 cm) through the entire section</p> <p>5Y 3/2 fine silty clay, homogenous, rich in Fe/Mn</p> <p>from 238 cm downcore: silty clay, strongly enriched in Fe/Mn precipitates, often Fe/Mn rich layers (at: 239 cm, 241 cm, 242 cm, 247 cm)</p>				
2				
<p>5Y 2.5/1 layer of Fe/Mn enrichment (black), gradual boundary</p> <p>5Y 3/2 dark olive gray silty clayey sand; black laminae at 260 cm, and 174 - 278 cm; dropstones at 264 cm and 270 cm</p>				
3				
<p>dark olive gray sand layer with abundant dropstones (- 1cm)</p> <p>black layer (5Y 2.5/1) of silty sand, rich in Fe/Mn</p>				
<p>5Y 4/4 olive silty clay, changing to olive gray colors, with some greenish to brownish colors intercalated by</p> <p>5Y 4/2 silty clay, very stiff, no dropstones</p>				
4				
<p>between 397 and 405 cm: 3 dark brown sand layers (10YR 3/3), oxidized colors, grading into very dark grayish brown clays (2.5Y 3/2) upwards (turbidite sequence); one dropstone (2 cm) at 401 cm</p> <p>5Y 3/1 very dark gray sandy silt, black streaks and laminae, high sand content in the upper 30 cm of the unit, decreasing sand content downcore</p>				
5.51				
<p>from 450 to 551 cm: very dark gray clayey silt to silty clay, intercalated by black layers (5Y 2.5/2) at 464 cm, 477 cm, 504 cm, 508 cm, 518 cm, 532 cm</p>				

end of core: 5.51 m

PS2450-3 (SL)

N`Vilkitsky Strait

ARK IX/4 (ARCTIC 93)

Recovery: 5.51 m

78°01,88`N 102°16,96`E

Water depth: 148 m

Lithology	Texture	Color	Description	Age
			core liner is not opened, because of high water content and disturbance (s. 2450-2 GKG)	
		5Y 3/2	dark olive gray very fine silty clay, homogenous, rich in Fe/Mn precipitates (- 0.5 cm) through the entire section	
		5Y 3/2	fine silty clay, homogenous, rich in Fe/Mn	
			from 238 cm downcore: silty clay, strongly enriched in Fe/Mn precipitates, often Fe/Mn rich layers (at: 239 cm, 241 cm, 242 cm, 247 cm)	
		5Y 2.5/1	layer of Fe/Mn enrichment (black), gradual boundary	
		5Y 3/2	dark olive gray silty clayey sand; black laminae at 260 cm, and 174 - 278 cm; dropstones at 264 cm and 270 cm	
			dark olive gray sand layer with abundant dropstones (- 1cm)	
			black layer (5Y 2.5/1) of silty sand, rich in Fe/Mn	
		5Y 4/4	olive silty clay, changing to olive dark grayish colors, with some greenish to brownish colors	
		5Y 4/2	intercalated by silty clay, very stiff, no dropstones	
			between 397 and 405 cm: 3 dark brown sand layers (10YR 3/3), oxidized colors, grading into very dark grayish brown clays (2.5Y 3/2) upwards (turbidite sequence); one dropstone (2 cm) at 401 cm	
		5Y 3/1	very dark gray sandy silt, black streaks and laminae, high sand content in the upper 30 cm of the unit, decreasing sand content downcore	
			from 450 to 551 cm: very dark gray clayey silt to silty clay, intercalated by black layers (5Y 2.5/2) at 464 cm, 477 cm, 504 cm, 508 cm, 518 cm, 532 cm	

end of core: 5.51 m

PS2450-3 (SL)

N`Vilkitsky Strait

ARK IX/4 (ARCTIC 93)

Recovery: 5.51 m

78°01,88`N 102°16,96`E

Water depth: 148 m

Depth in core (m)	Lithology	Texture	Color	Description	Age
0				core liner is not opened, because of high water content and disturbance (s. 2450-2 GKG)	
1			5Y 3/2	dark olive gray very fine silty clay, homogenous, rich in Fe/Mn precipitates (- 0.5 cm) through the entire section	
2			5Y 3/2	fine silty clay, homogenous, rich in Fe/Mn	
				from 238 cm downcore: silty clay, strongly enriched in Fe/Mn precipitates, often Fe/Mn rich layers (at: 239 cm, 241 cm, 242 cm, 247 cm)	
			5Y 2.5/1	layer of Fe/Mn enrichment (black), gradual boundary	
			5Y 3/2	dark olive gray silty clayey sand; black laminae at 260 cm, and 174 - 278 cm; dropstones at 264 cm and 270 cm	
3				dark olive gray sand layer with abundant dropstones (- 1cm)	
				black layer (5Y 2.5/1) of silty sand, rich in Fe/Mn	
			5Y 4/4	olive silty clay, changing to olive gray colors, with some greenish to brownish colors intercalated by	
			5Y 4/2	silty clay, very stiff, no dropstones	
4				between 397 and 405 cm: 3 dark brown sand layers (10YR 3/3), oxidized colors, grading into very dark grayish brown clays (2.5Y 3/2) upwards (turbidite sequence); one dropstone (2 cm) at 401 cm	
			5Y 3/1	very dark gray sandy silt, black streaks and laminae, high sand content in the upper 30 cm of the unit, decreasing sand content downcore	
5.51				from 450 to 551 cm: very dark gray clayey silt to silty clay, intercalated by black layers (5Y 2.5/2) at 464 cm, 477 cm, 504 cm, 508 cm, 518 cm, 532 cm	

end of core: 5.51 m

PS2451-2 (GKG)

Vilkitsky Strait

ARK IX/4 (ARCTIC 93)

Recovery: 0.40 m

77°42,43'N 102°17,27'E

Water depth: 143 m

Lithology	Texture Color	Description	Age
Surface	10YR3/4	even surface of silty sand, few ophiuroideans, crinoids, ascidians, small bivalves, polychaets and worm tubes, few dropstones (-5 cm), mica common	
	10YR3/4	dark yellowish brown silty sand as above	
		gradual color change from yellowish brown to dark gray	
	5Y 3/1	very dark gray sandy clayey silt (gray diamicton), dropstones (- 5cm) and coal fragments abundant, black streaks and lamination in parts	
		sediment in archive liners is severely compressed (orig. recovery = tube recovery + 20 cm)	
		end of core 40 cm	

PS2451-3 (SL)

S`Vilkitsky Strait

ARK IX/4 (ARCTIC 93)

Recovery: 5.44 m

77°42,2' N 102°22,5' E

Water depth: 140 m

Lithology	Texture	Color	Description	Age
0		10YR 3/4	dark yellowish brown very sandy silt	
		10YR 3/6	very dark yellowish brown silty sand, diagenetically altered horizon, mud clasts to the diagenesis-horizon	
		5Y 3/1	very dark grayish brown sandy silt, with oxidized streaks + patches belonging to the diagenesis-horizon	
		5Y 4/1	very dark gray sand, homogenous, with few dark spots (Fe/Mn precipitates)	
		5Y 4/1	dark gray silty clay, black patches + mottles (not as much as in 2450-3 SL), sandy layers are intercalated	
			between 60 and 70 cm enrichment of Fe/Mn mottles	
		5Y 4/2	olive gray sandy clayey silt, intercalated by one black layer (5Y 2.5/1) of organic rich sandy silt	
1		10YR 3/4	layered section: rusty layers of dark yellowish brown (10YR 3/4) sandy silt, diagenetically altered, sharp contacts;	
		5Y 4/2	intercalated with olive gray (5Y 4/2) silty clay, 1 dropstone (-5 mm) at 117 cm	
		5Y 4/1	dark gray silty clay, homogenous, one black layer of organic rich silty clay (0.5 cm thickness) in 131 cm depth, sharp boundaries	
		5Y 4/1	dark gray silty clay, homogenous, black mottles (Fe/Mn precipitates) common all over the core	
2			at 233 and 250 cm some bigger dropstone (- 3 cm)	
		5Y 4/1	dark gray silty clay, homogenous, becoming gradually darker to very dark gray silty clay, few dropstones, black mottles (Fe/Mn precipitates)	
3		5Y 3/1	very dark gray silty clay	
			at 393 cm one bigger dropstone (-1 cm)	
		5Y 3/1	very dark gray silty clay, homogenous, few dropstones, black mottles (Fe/Mn precipitates) over the entire section, in the lower part black layers at 428-430 cm, 439-440 cm, 442-443 cm, 459 cm, 476 cm, no sharp boundaries	
5			one bigger (-1 cm) dropstone at 522 cm	
			end of core: 5.44 m	
6				

PS2452-2 (GKG)

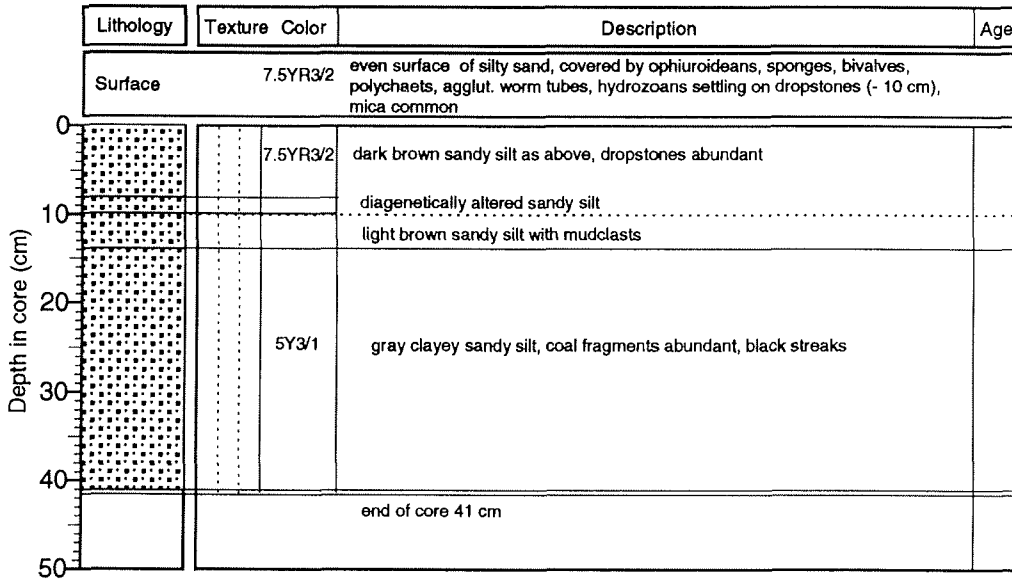
Southern Vilkitsky Strait

ARK IX/4 (ARCTIC 93)

Recovery: 0.41 m

77°53,52'N 101°35,45'E

Water depth: 132 m



PS2453-2 (GKG)

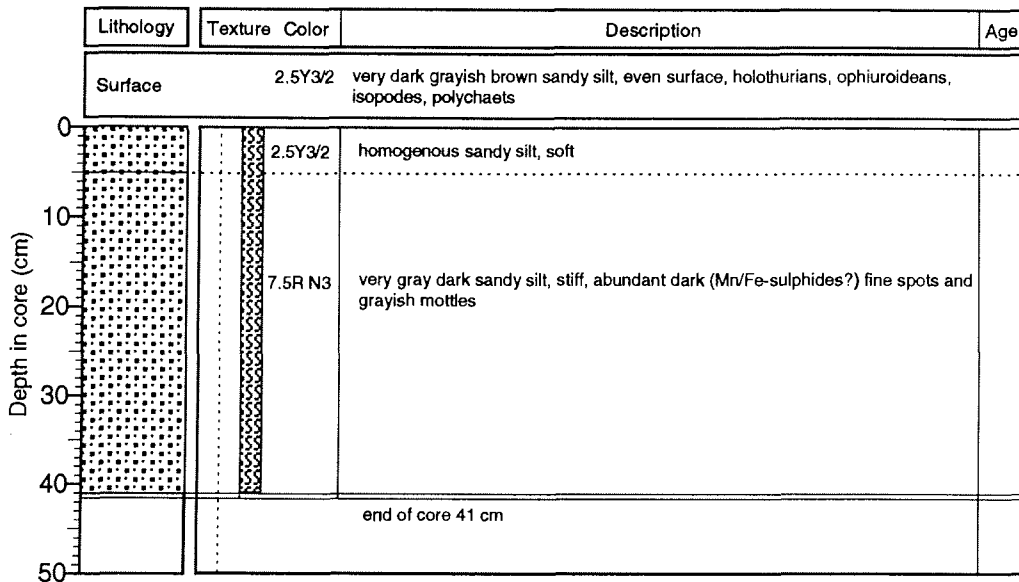
Eastern Laptev Sea shelf

ARK IX/4 (ARCTIC 93)

Recovery: 0.41 m

76°30,53'N 133°21,32'E

Water depth: 38 m



PS2453-3 SL

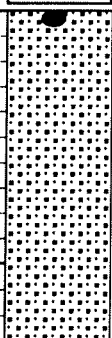
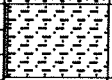
Eastern Laptev Sea shelf

ARK IX/4 (ARCTIC 93)

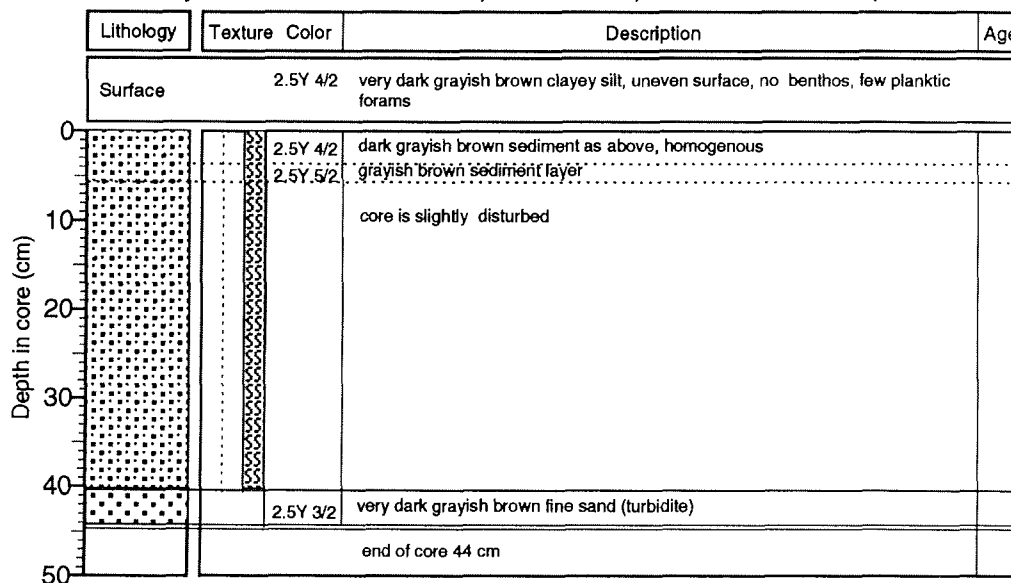
Recovery: 1.58 m

76°31,04'N 133°20,8'E

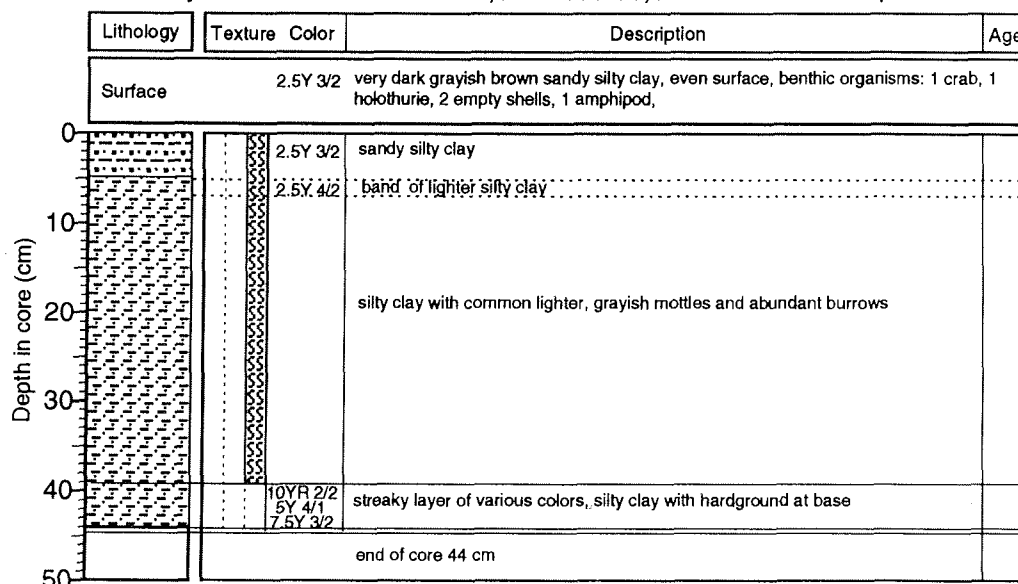
Water depth: 38 m

Depth in core (m)	Lithology	Texture	Color	Description	Age
	0				1 cm-sized dropstone at 3 cm depth
			7.5YR N3	very gray dark sandy silt, stiff, abundant (Mn, Fe-precipitates), fine spots and grayish mottles	
1			7.5YR N3	see above	
			5Y 3/1	very dark gray silty clay, stiffer than above (higher values for susceptibility !), homogenous, less fine spots and grayish black mottles (Fe, Mn-precipitates)	
	end of core 1.58 m				
2					
3					
4					
5					

**PS2455-3 (GKG)** Eastern Laptev Sea, Profile H **ARK IX/4 (ARCTIC 93)**  
 Recovery: 0.44 m 79°39,12'N 130°32,13'E Water depth: 3429 m



**PS2456-2 (GKG)** Eastern Laptev Sea, Profile H **ARK IX/4 (ARCTIC 93)**  
 Recovery: 0.44 m 78°29,04'N 133°00,10'E Water depth: 2520 m



PS2456-3 (KAL)

Laptev Sea, Profile H

ARK IX/4 (ARCTIC 93)

Recovery: 5.74 m

78°28,86`N 133°01,90`E

Water depth: 2507 m

Depth in core (m)	Lithology	Texture Color	Description	Age
0		10YR 3/4	dark yellowish brown silty clay, homogenous	
		10YR 2/2	very dark brown clayey silt, convex boundary	
		5Y 3/1	silty clay, layer of different brownish colors	
		10YR 3/2	hardground, diagenetically altered clayey silt, reddish-brownish, rusty	
		5Y 3/1	very dark gray silty clay, homogenous	
		5Y 3/1	very dark grayish brown, clayey sandy silt, diagenetically altered, rusty colors	
		5Y 3/1	very dark gray silty clay, homogenous, bioturbated	
			sandy layer	
1		2.5Y 3/2	very dark grayish brown, every 2-3 cm black layers of Fe/Mn-precipitates, comparable to shelf cores, but layers instead of spots	
		2.5Y 3/2	sediment see above	
2		2.5Y 3/2	no more Fe/Mn rich layers and spots	
		5Y 3/1	very dark gray layer of clayey silt, more olive, sharp boundaries	
		2.5Y 3/2	no more Fe/Mn layers	
		2.5Y 3/2	sediment see above, Fe/Mn rich layers, layers partly with sharp boundaries	
3		5Y 3/1	very dark gray silty clay, no Fe/Mn - sulfides	
		5Y 3/1	very dark gray, sand layer, fining upwards, turbidite, slightly darker than above	
		5Y 3/1	very dark gray silty clay, with few spots of Fe/Mn precipitates (no layers)	
			olive colored streaks (1-3 cm) of the same material at 308, 332, 356, 380, 470 cm	
			sandy turbidites fining upwards are common at 366, 392, 426, 450, 462, 492, 499 cm	
4				
5				

**PS2456-3 (KAL)**

Laptev Sea, Profile H

**ARK IX/4 (ARCTIC 93)**

Recovery: 5.74 m

78°28,86`N 133°01,90`E

Water depth: 2507 m

Lithology	Texture	Color	Description	Age
		5Y 3/1	very dark gray silty clay  sandy turbidites at 525, 532, 538 cm	
		2.5Y N2	black layers of silty clay at 488 cm, 497 cm, 537 cm, 548 cm, 554 cm, 562 cm, 568 cm,	
	end of core 5.74 m			

**PS2458-3 (GKG)**

Eastern Laptev Sea, Profile H

**ARK IX/4 (ARCTIC 93)**

Recovery: 0.46 m

78°09,95`N 133°23,71`E

Water depth: 981 m

Lithology	Texture	Color	Description	Age
Surface		10YR 3/3	dark brown silty clay, even surface, very high biological activity: abundant polychaets (Maldanidae?), 3 pantopods, 2 amphipods, few benthic forams, abundant fecal pellets, pogonophores	
		10YR 3/3	dark brown silty clay	
		10YR 2/2	very dark brown layer of silty clay	
		10YR 3/3 with 5Y 3/1	dark brown silty clay with patches of very dark olive gray silty clay very high bioturbation	
		10YR 2/2	very dark brown irregular layers of silty clay between 16 and 20 cm, very irregular boundary	
		5Y 3/1	very dark olive gray silty clay, high bioturbation, brownish patches from above	
	end of core 46 cm			

PS2458-4 KAL

Eastern Laptev Sea, Profile H

ARK IX/4 (ARCTIC 93)

Recovery: 8.00 m

78°09,95`N 133°23,86`E

Water depth: 983 m

Lithology	Texture	Color	Description	Age
0		10 YR 3/3	dark brown silty clay, disturbed by coring	
		10 YR 2/2	very dark brown/dark brown layers of silty clay, irregular boundary (see GKG)	
1		5Y 3/1	very dark olive gray silty clay, brownish patches from above	
			from 70 cm downcore: increasing number of Fe/Mn-precipitates	
			at ca. 100 cm typical number of Fe/Mn precipitates reached	
			• smear slides at 200 + 300 cm	
4			at ca. 400 cm: bivalve shells (0,5 cm)	
			at 453 cm: calcareous shell fragments	
5			slightly lighter color, at 508 - 530 cm dark layers of Fe/Mn enrichment (see 2456-3 KAL)	
			at 656 cm: calcareous shell fragments	
			• smear slides at 600 cm	
7				
8			from 773 cm to core base no more Fe/Mn spots, just silty clay of same color, homogenous	
end of core: 8.00 m				

**PS2459-2 (GKG)**

Eastern Laptev Sea, Profile H

**ARK IX/4 (ARCTIC 93)**

Recovery: 0.41 m

78°05,92`N 133°30,78`E

Water depth: 517 m

Lithology	Texture	Color	Description	Age
Surface				
		2.5Y 3/2	very dark grayish brown silty clay, even surface, worm tubes common, sticking out of the sediment or lying on the surface,	
		2.5Y 3/3	grayish brown silty clay becoming very dark brown at the base	
		10YR 2/2	very dark brown layer of clayey silt	
		5Y 3/2	dark olive gray silty clay, intercalated by brownish streaks, layers and patches from above	
		10YR 2/2	very dark brown layer of clayey silt	
		10YR 3/3	diagenetically altered horizon of dark brown clayey silt	
		5Y 3/2	dark olive gray silty clay as at 10 cm, less brown patches	
		10YR 3/3	diagenetically altered horizon as at 14 cm	
		2.5Y N4	dark gray silty clay, homogenous	
	2.5Y N3	very dark gray silty clay, homogenous		
end of core 41 cm				

**PS2460-3 (GKG)**

Eastern Laptev Sea, Profile H

**ARK IX/4 (ARCTIC 93)**

Recovery: 0.32 m

78°04,33`N 133°36,47`E

Water depth: 191 m

Lithology	Texture	Color	Description	Age
Surface				
		7.5YR 3/2	dark brown sandy silt, even surface, with brittle stars	
		7.5YR 3/2	brown sandy silt, homogenous	
			gray sandy clay, homogenous	
		2.5Y 4/0		
end of core 32 cm				

PS2460-4 SL

Eastern Laptev Sea, Profile H

ARK IX/4 (ARCTIC 93)

Recovery: 9.08 m

78°04,49'N 133°35,86'E

Water depth: 204 m

Lithology	Texture Color	Description	Age
0	10YR 3/2	very dark grayish brown silty clay,	
		mixing zone of both sediment types, brownish patches and streaks in grayish matrix	
	5Y 3/1	very dark olive gray silty clay, stiff, homogenous	
		at 43-48, 56-60, 73-81 cm stripes of slightly darker sediment	
		darker than above, silty clay, area of increased number of Fe/Mn precipitates and patches	
		silty clay, homogenous, no Fe/Mn-precipitates	
	5Y 3/1	very dark olive gray silty clay, rich in Fe/Mn-precipitates	
		at ca. 100 cm: bivalve fragments	
		at 232-238 cm: IKAITE - crystal (3 cm),	
		from 284 cm downcore increasingly black, H <sub>2</sub> S smell !!!	
	5Y 3/1	very dark olive gray silty clay, rich in Fe/Mn spots	
		465 - 468 cm: large bivalve fragments (3 cm), <i>Yoldia amygdalea</i> (shallow marine form, living recently between 10 to 70 m)	
		the sediment color is changing from gray to black downcore	

PS2460-4 SL

Laptev Sea, Profile H

ARK IX/4 (ARCTIC 93)

Recovery: 9.08 m

78°04,49'N 133°35,86'E

Water depth: 204 m

Lithology	Texture Color	Description	Age
5	5Y 3/1	nearly black sediment as above	
	5Y 2.5/1	black sediment	
6	5Y 2.5/1	nearly black sediment as above	
7	5Y 3/1	very dark olive silty clay, sharp boundaries	
		between 723 - 742 cm slightly more olive	
	5Y2.5/1	black silty clay	
8	5Y 3/1	very dark olive silty clay, sharp boundaries	
		between 806 - 810 cm slightly more olive	
	5Y2.5/1	black silty clay	
		at 868 - 870 cm bivalve fragment	
9		end of core 9.08 m	
10			

PS2461-2 (GKG)

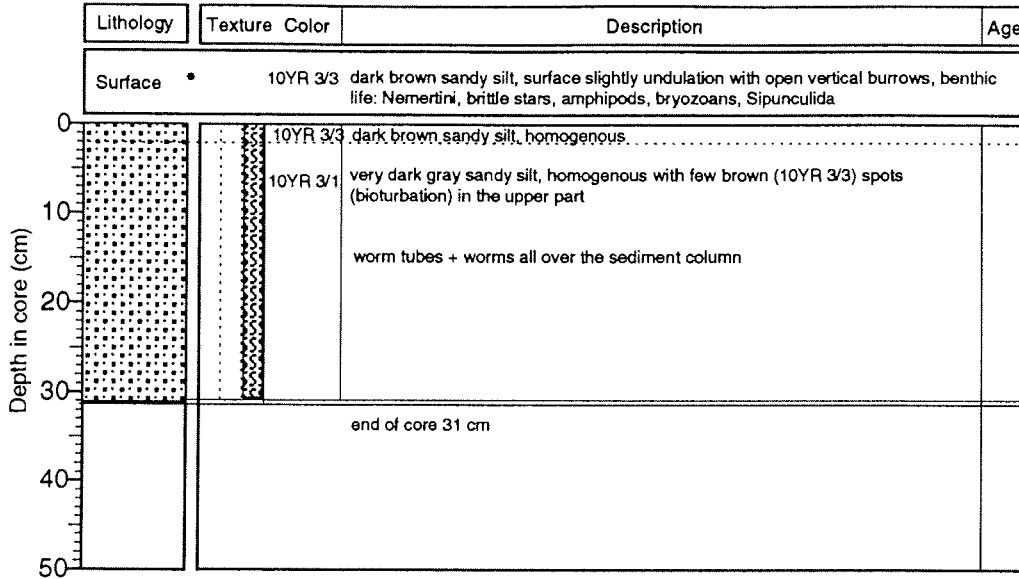
Laptev Sea, Profile H

ARK IX/4 (ARCTIC 93)

Recovery: 0.31 m

77°54,62' N 133°33,25' E

Water depth: 73 m



PS2462-3 (GKG)

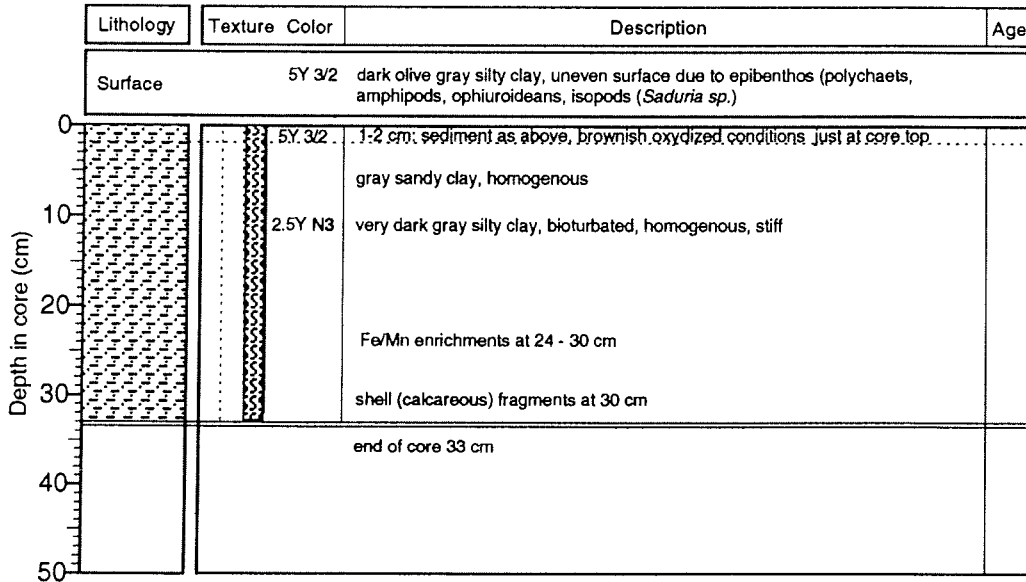
Eastern Laptev Sea, Profile H

ARK IX/4 (ARCTIC 93)

Recovery: 0.33 m

77°24,28' N 133°33,35' E

Water depth: 54 m



**PS2463-3 (GKG)**

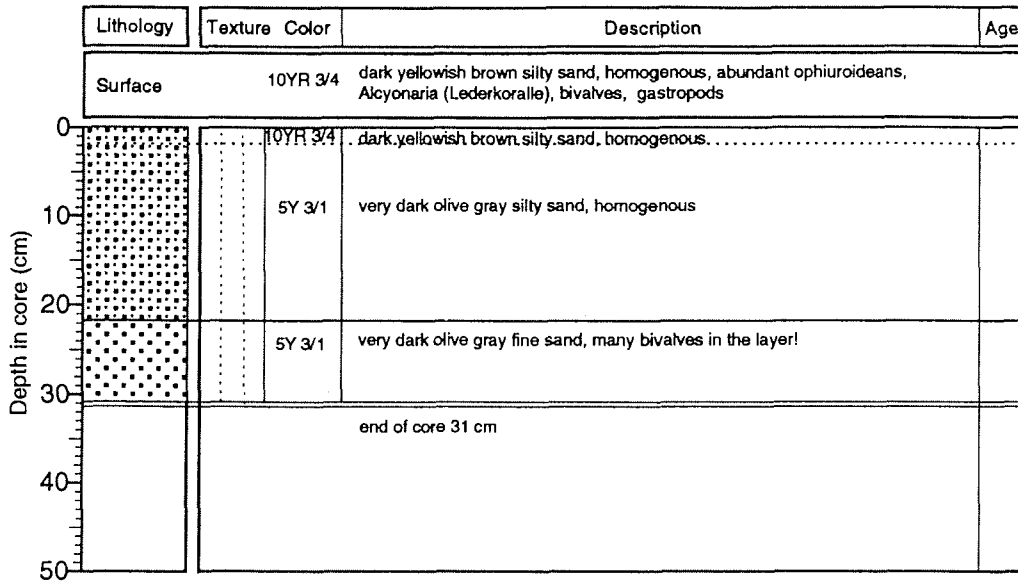
Laptev Sea, Profile G

**ARK IX/4 (ARCTIC 93)**

Recovery: 0.31 m

77°01,76'N 126°24,77'E

Water depth: 92 m



**PS2464-2 (GKG)**

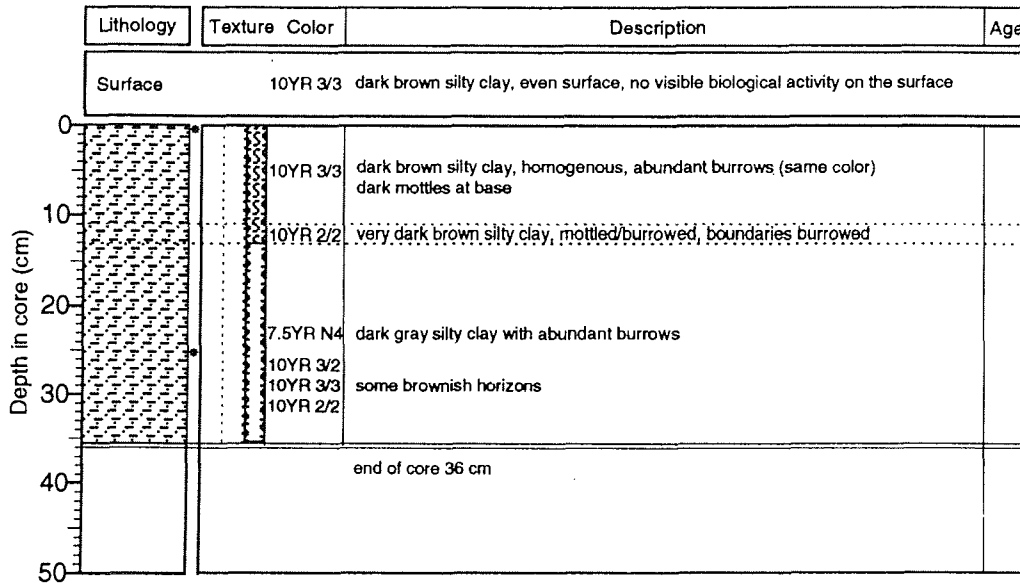
Laptev Sea, Profile G

**ARK IX/4 (ARCTIC 93)**

Recovery: 0.36 m

77°28,79'N 125°54,17'E

Water depth: 2025 m



PS2465-3 (GKG)

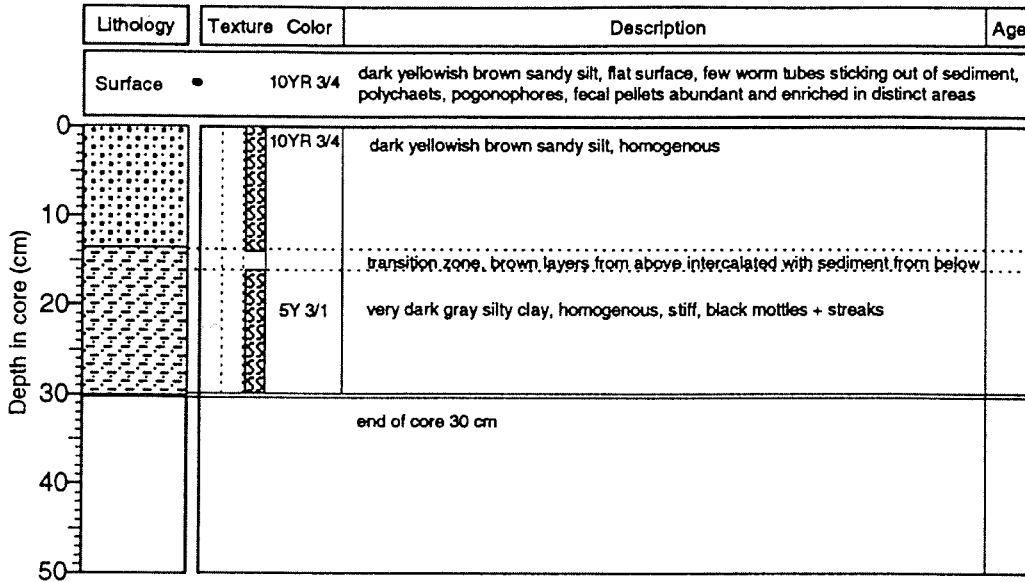
Laptev Sea, Profile G

ARK IX/4 (ARCTIC 93)

Recovery: 0.30 m

77°11,01'N 126°13,35'E

Water depth: 1026 m



PS2465-4 (SL)

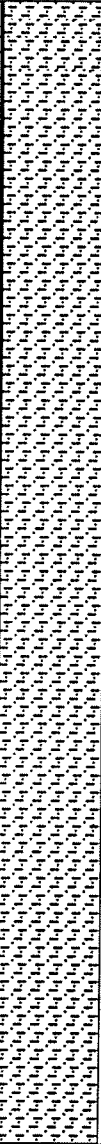
Laptev Sea, Profile G

ARK IX/4 (ARCTIC 93)

Recovery: 4.48 m

77°11,48'N 126°14,70'E

Water depth: 1056 m

Lithology	Texture Color	Description	Age
	10YR 3/4	dark yellowish brown silty clay	
		mixing zone of sediment from above and below, slightly diagenetically altered	
	5Y 4/1	dark gray homogenous silty clay	
		from 27 cm downcore: increasing amount of Fe/Mn precipitates, some material slightly darker due to Fe/Mn enrichment	
	5Y 3/1	dark gray silty clay as above, rich in spots of Fe/Mn precipitates	

end of core: 4.48 m

PS2466-3 (GKG)

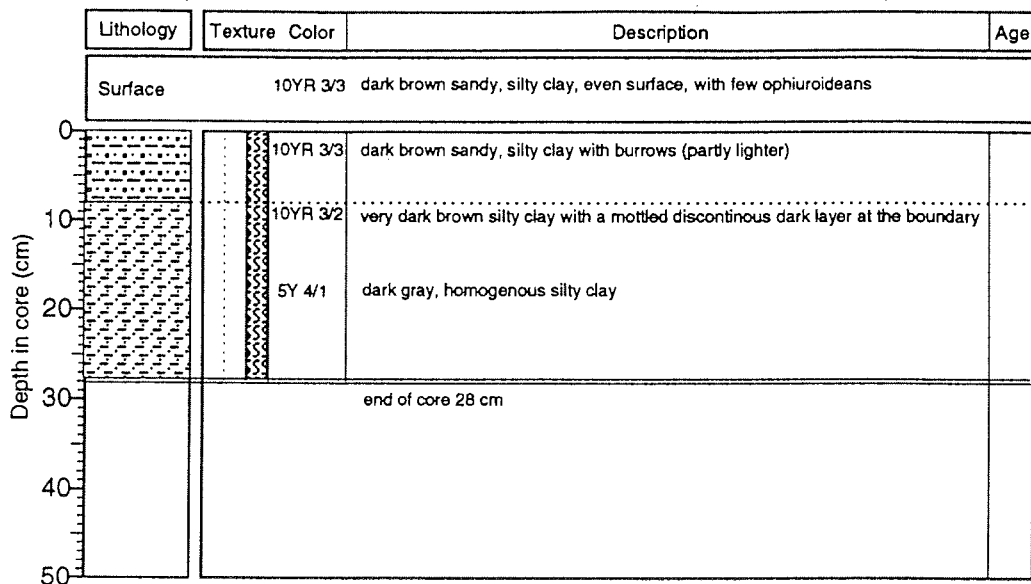
Laptev Sea, Profile G

ARK IX/4 (ARCTIC 93)

Recovery: 0.28 m

77°08,05`N 126°21,24`E

Water depth: 552 m



PS2467-3 (GKG)

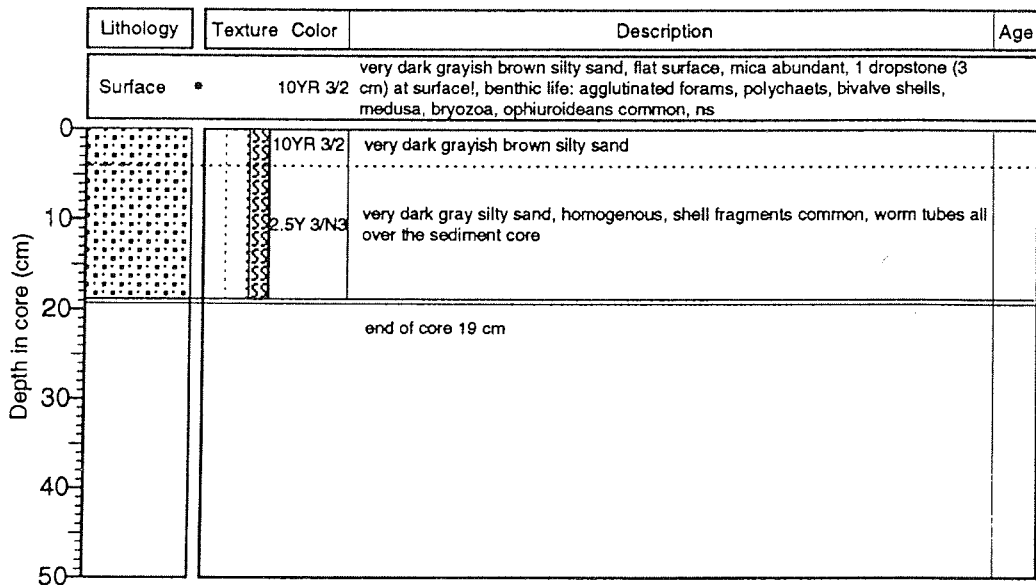
Laptev Sea, Profile G

ARK IX/4 (ARCTIC 93)

Recovery: 0.19 m

77°04,99`N 126°13,36`E

Water depth: 284 m



PS2468-3 (GKG)

Laptev Sea, Profile G

ARK IX/4 (ARCTIC 93)

Recovery: 0.46 m

77°41,58'N 125°53,55'E

Water depth: 1991 m

Lithology	Texture Color	Description	Age
Surface	10YR 3/2	very dark grayish brown silty clay, even surface, rare benthic life on the surface	
<p>Depth in core (cm)</p>	10YR 3/3	dark brown silty clay, homogenous, rare lighter, grayish burrows	
	10YR 2/2	sequence of brownish, streaky laminated layers of silty clay, irregular mottling, one large burrow (gray) at 26-29 cm	
	10YR 3/3		
	10YR 2/2		
	10YR 3/3	dark gray silty clay, homogenous, some irregular/streaky laminated layers (10YR 3/3), number of laminated layers increasing to the top of the section	
10YR 2/2			
	end of core 46 cm		

PS2469-1 (KAL)

Laptev Sea, Profile G

ARK IX/4 (ARCTIC 93)

Recovery: 5.51 m

78°06,17'N 125°03,21'E

Water depth: 2390 m

Lithology	Texture	Color	Description	Age
		10YR 3/4	dark yellowish brown silty clay, homogenous	
		10YR 3/1	in the upper part homogenous silty clay as above, intercalated by dark streaks and layers (very dark gray) and patches in the lower part grading into olive gray silty clay, homogenous, dark streaks and patches as above	
		5Y 4/2		
		5Y 4/1	dark gray homogenous silty clay	
			olive streaks/layers (5Y 4/3) with sharp contacts at 95-96 cm, 112-113 cm, 137-139 cm, 158-159 cm	
		5Y 4/2	olive gray silty clay	
		5Y 3/1	olive gray silty clay, intercalated by turbidity layers, mottled;	
		5Y 4/2	sandy dark gray turbidite layers at: 187-188 cm, 191-193 cm, 196-198 cm, 211-213 cm, 216-217 cm; at 200 cm one olive streak	
		5Y 4/2	olive gray silty clay	
		5Y 4/2	olive streaks (5Y 4/3) at 233-234 cm, 251-252 cm, 266-267 cm, 279-280 cm, 306-308 cm	
		5Y 4/2		
		5Y 4/2		
		5Y 4/2		
	5Y 3/1	dark gray sandy layer		
			end of core: 3.15 m (+ core catcher: 3.46 m)	

PS2469-3 (GKG)

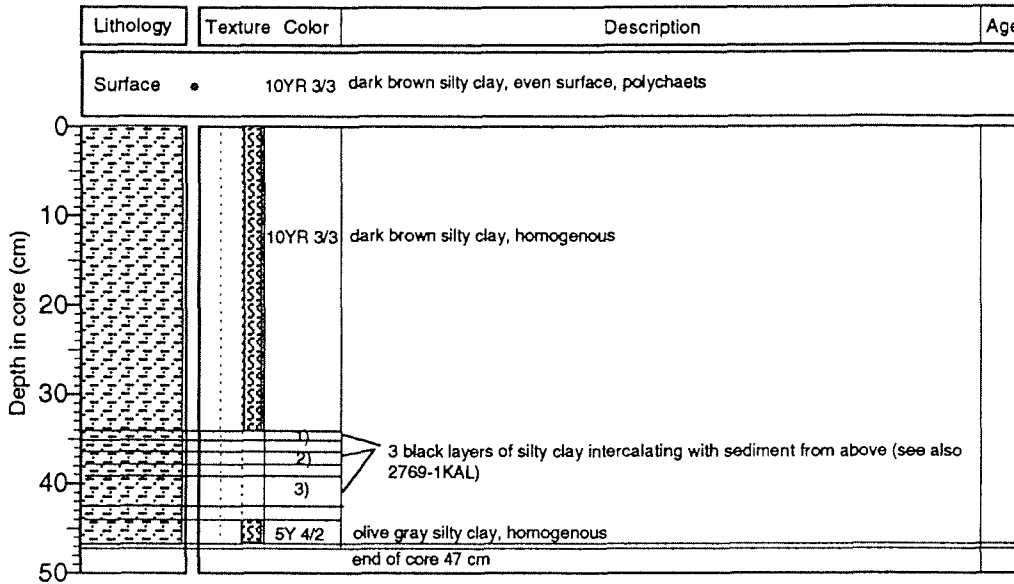
Laptev Sea, Profile G

ARK IX/4 (ARCTIC 93)

Recovery: 0.47 m

77°03,58'N 125°00,01'E

Water depth: 2332 m



PS2470-4 (GKG)

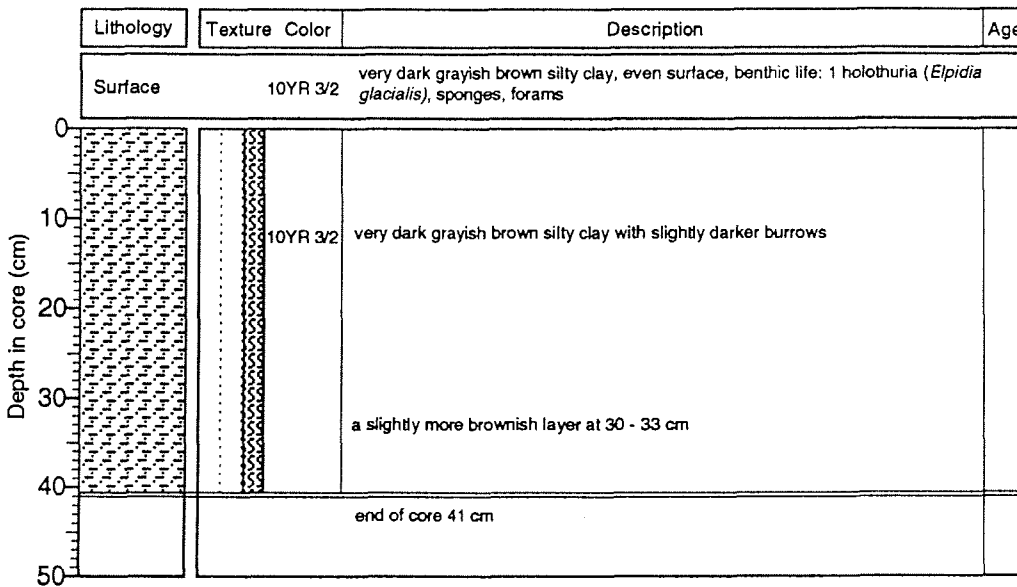
Laptev Sea, Profile G

ARK IX/4 (ARCTIC 93)

Recovery: 0.41 m

79°12,96'N 122°54,37'E

Water depth: 3233 m



PS2471-3 (GKG)

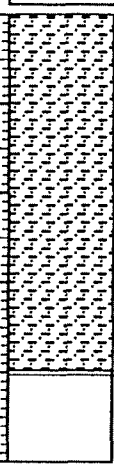
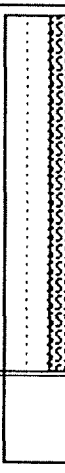
Laptev Sea, Profile F

ARK IX/4 (ARCTIC 93)

Recovery: 0.40 m

79°09,29'N 119°46,89'E

Water depth: 3048 m

Lithology	Texture	Color	Description	Age
Surface		10YR 3/2	dark brown silty clay	
			10YR 3/2 dark brown silty clay, homogenous with faint grayish mottles and rare light grayish burrows (Ø 1 cm)	
			slightly more brownish at 37 - 40 cm	
			end of core 40 cm	

PS2471-4 (SL)

Laptev Sea, Profile F

ARK IX/4 (ARCTIC 93)

Recovery: 4.16 m

79°09,07'N 119°47,55'E

Water depth: 3047 m

	Lithology	Texture Color	Description	Age
0			lost of 1 - 7 cm	
		10YR 3/4	dark yellowish brown silty clay, soft, homogenous	
			between 40 - 47 cm: colors becoming gradually more grayish brown	
		10YR 4/2	dark grayish brown silty clay	
		10YR 2/1	black layer of silty clay, mottled with patches and streaks	
1		10YR 4/2	dark grayish brown silty clay, homogenous	
		2.5Y 5/4	light olive brown silty clay	
		10YR 4/2	dark grayish brown silty clay	
		2.5Y 5/4	light olive brown silty clay	
			color becoming slightly darker downcore	
		5Y 4/4	3 layers of dark yellowish brown silty clay, diagenetically altered, stiff, rusty colors within an olive silty clay, black mottles are common	
		10YR 4/4		
		2.5Y 3/2	very dark grayish brown silty clay, clayey in the lower and silty in the upper part	
		5Y 4/1		
2		5Y 4/2	olive gray soft clay	
		5Y 4/2	stiff layers of dark gray sand, turbidites, olive gray silty clay, soft, intercalated in between the turbidites	
		2.5Y 4/4	olive brown silty clay	
		5Y 4/1	dark gray sandy silt layer	
			silty clay of olive brownish colors, intercalated by several thin turbidites (sand, 10YR 4/3, brown), thin black layers and diagenetically altered stiff layers of clayey silt	
3		2.5Y N3	very dark gray clay, homogenous, soft	
		2.5Y 4/2	dark grayish brown sand layer, stiff	
		5Y 4/2	olive gray silty clay, homogenous, bioturbated	
		5Y 4/3	olive sand layers with dropstones (-2 cm)	
		5Y 3/2	dark olive gray sequence of turbidites: sandy layers grading into clay sequences	
4		5Y 4/2	thin sand layer at 391 cm	
		5Y 4/2	olive gray silty clay, slightly diagenetically altered, stiff	
5				

PS2472-3 (GKG)

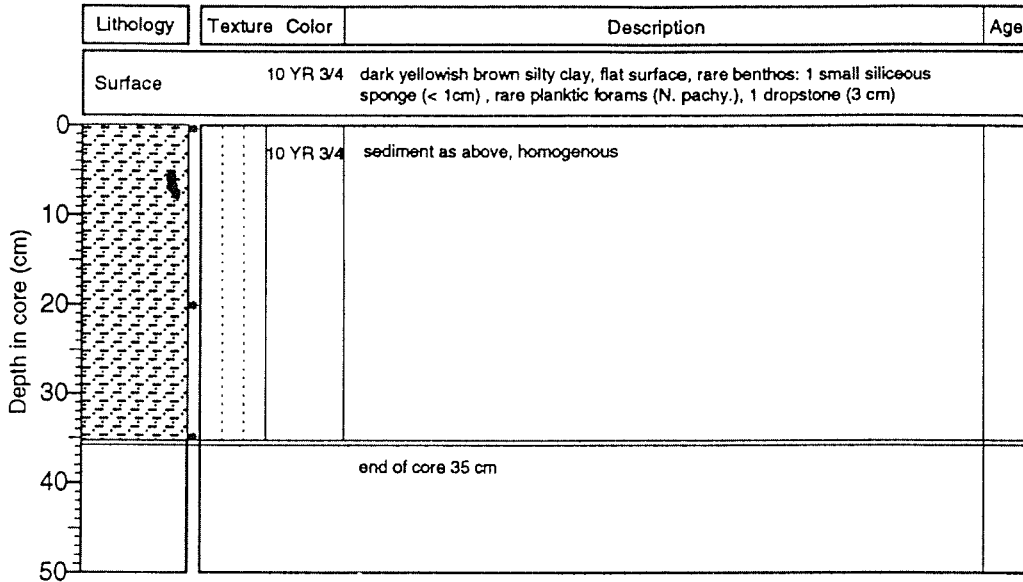
Laptev Sea, Profile F

ARK IX/4 (ARCTIC 93)

Recovery: 0.35 m

78°40,04'N 118°44,29'E

Water depth: 2620 m



PS2473-3 (GKG)

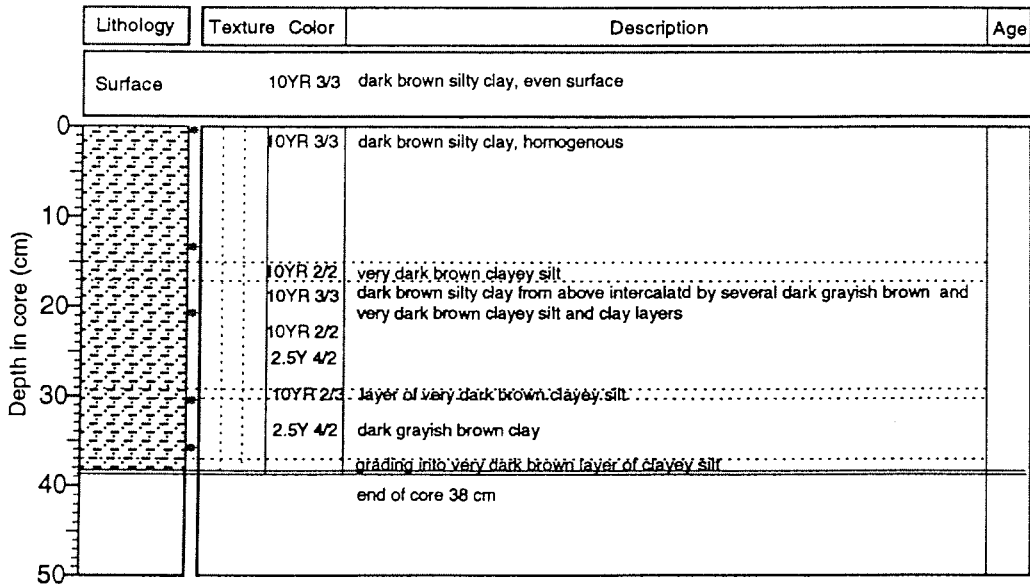
Laptev Sea, Profile F

ARK IX/4 (ARCTIC 93)

Recovery: 0.38 m

77°58,88'N 118°34,25'E

Water depth: 1927 m



PS2473-4 (KAL)

Laptev Sea, Profile F

ARK IX/4 (ARCTIC 93)

Recovery: 6.15 m

77°58,57'N 118°34,50'E

Water depth: 1919 m

Lithology	Texture Color	Description	Age
0		no exact depth of core due to superpenetration	
		intensively disturbed interval	
	5Y 3/2	dark olive gray silty clay	
	5Y 3/2/ 5Y 2.5/1	dark olive gray silty clay with some black patches at 53 cm	
1		between 95 and 100 cm, increasing number of black patches	
	5Y 3/2	dark olive gray silty clay	
	5Y 4/2	olive gray silty clay, only very few black patches below this boundary, more olive colored	
	5Y 4/2	olive gray silty clay, becoming more and more olive, homogenous	
2		olive silty clay, some brownish streaks between 330 - 333 cm	
	5Y 4/3	some dark olive/brownish irregular patches in silty clay	
	5Y 4/3	patchy structure dark olive and olive silty clay	
	5Y 4/3	olive silty clay, homogenous	
		2 very dark grayish brown (2.5Y 3/2) layers of silty clay at 268-270 and 275 - 277 cm, in between olive silty clay	
3		one olive-brown layer of silty clay	
	5Y 3/2	dark olive gray silty clay, homogenous	
	5Y 3/2/ 2.5Y 4/4	intensive olive brown irregular layer, more olive brown than olive gray	
	5Y 4/1	338-379 cm dark gray homogenous silty clay with very few black patches	
	5Y 4/1	some olive brown (2.5Y 4/4) layers in dark gray silty clay	
4		dark gray homogenous silty clay	
		some more black patches to the boundary	
	5Y 3/2	dark olive gray sandy silt (turbidite?)	
	5Y 4/2	olive gray silty clay, more olive to the lower boundary	
	5Y 4/1	sequence of sandy silt turbidites of different thickness in silty clay at 459, 460, 463, 465, 467, 468, 470, 473, 476, 478, 486, 489, 492, 494 cm	
5			

PS2473-4 (KAL)

Laptev Sea, Profile F

ARK IX/4 (ARCTIC 93)

Recovery: 6.15 m

77°58,57'N 118°34,50'E

Water depth: 1919 m

Depth in core (m)	Lithology	Texture Color	Description	Age
	5	[Hatched pattern]	5Y 4/2	495 - 512 cm olive gray fine silty clay
	2.5Y 4/4		olive- brown silty clay, homogenous	
6			end of core: 6.15 m	
7				

PS2474-2 (GKG)

Laptev Sea, Profile F

ARK IX/4 (ARCTIC 93)

Recovery: 0.36 m

77°40,24'N 118°34,52'E

Water depth: 1497 m

Depth in core (cm)	Lithology	Texture Color	Description	Age
	Surface		10YR 3/3	dark brown silty clay, uneven surface, no benthos visible, but large holes (bioturbation?, destruction?)
0	[Hatched pattern]	10YR 3/3	dark brown silty clay, homogenous	
10		10YR 3/3 10YR 3/1	mottled layer of dark brown and very dark gray silty clay	
		10YR 3/3	mottled layer of dark brown and dark gray silty clay	
20		5Y 4/1	mottled layer of dark brown and dark gray silty clay	
		10YR 3/3 10YR 3/1 5Y 4/1	mottled layer of dark brown, very dark olive gray, and dark gray silty clay	
30		10YR 3/3 5Y 4/1	mottled layer of dark brown and dark gray silty clay	
40			end of core 36 cm	
50				

PS2474-3 (KAL)  
Recovery: 7.84 m

Laptev Sea, Profile F  
77°40,15'N 118°34,5'E

ARK IX/4 (ARCTIC 93)  
Water depth: 1494 m

Depth in core (m)	Lithology	Texture Color	Description	Age
0		10YR 3/3	destroyed core top, dark brown silty clay, homogenous; (see 2475-1 GKG)	
		10YR 3/3 5Y 4/1 10YR 3/1	silty clay, mottled: two to three colors: dark brown, to dark gray to very dark gray	
1		5Y 4/1	dark gray homogenous silty clay  a few olive bands at : 66-68, 77-78, 82-83, 94-95, 120-122 cm	
2		5Y 4/1	dark gray silty clay, Fe/Mn precipitates in spots and bands are abundant	
			from here to the base of the core decreasing amount of spots and layers of Fe/Mn precipitates	
		5Y 4/2	olive-gray band of silty clay	
		5Y 4/1	dark gray homogenous silty clay, with very few black Fe/Mn rich spots	
4			olive gray bioturbated silty clay, homogenous, appears significantly more olive than upper gray part due to many olive colored bands; one dropstone (1cm) at 393 cm	
5		5Y 4/1	dark gray, homogenous silty clay, with few black spots	
		2.5Y 3/2	2 layers of very dark grayish brown silty clay, sharp boundaries	
		5Y 4/1	dark gray homogenous silty clay, rich in Fe/Mn, appears slightly darker than above due to black spots	
6		5Y 4/1	between 578 and 610 cm: sequence of dark gray homogenous clay, intercalated by olive layers, regions of abundant Fe/Mn precipitates in spots and layers	
		5Y 3/1		

PS2474-3 (KAL)

Laptev Sea, Profile F

ARK IX/4 (ARCTIC 93)

Recovery: 7.84 m

77°40,15'N 118°34,50'E

Water depth: 1494 m

	Lithology	Texture Color	Description	Age
6		5Y 4/1		
		5Y 4/1	area of abundant black Fe/Mn spots and stripes	
			black stripes of silty clay, Fe/Mn-rich; intercalating homogenous dark gray clay, relatively sharp contacts	
			at 673 cm one dropstone (0,5 cm)	
			black stripes of silty clay, no sharp boundaries	
7		5Y 4/1	dark gray clay, abundant Fe/Mn spots and stripes	
		5Y 4/1/5Y 2.5/1	dark gray and black silty clay, mottled	
		5Y 5/1 4Y 4/1 5Y 2.5/1	sequence of several turbidites, thin sand layers (0.5 cm) grading upwards into silty clay, different colors: gray, dark gray, black	
8			end of core 7.84 m	

PS2475-1 (GKG)

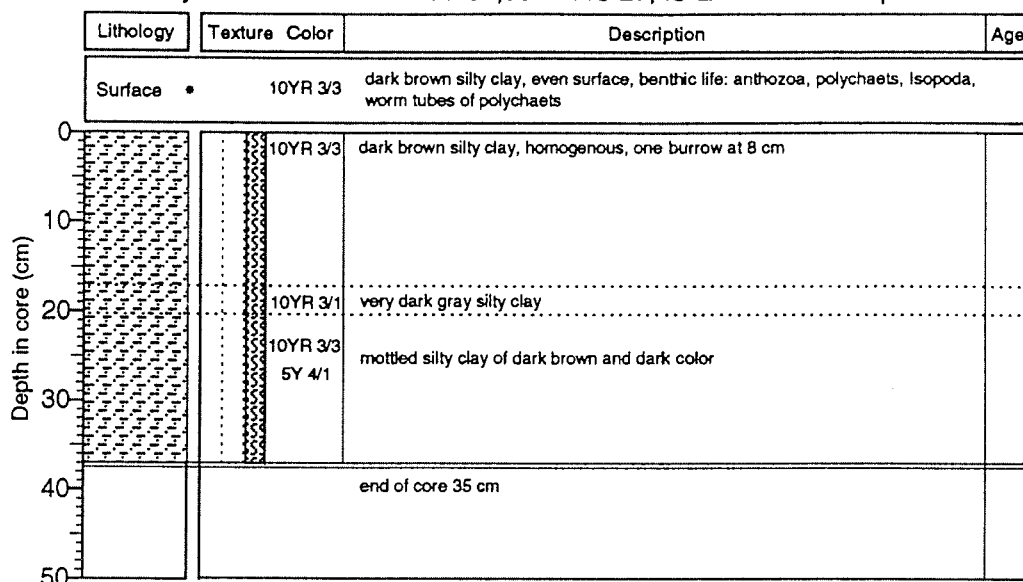
Laptev Sea, Profile F

ARK IX/4 (ARCTIC 93)

Recovery: 0.35 m

77°31,98'N 118°27,45'E

Water depth: 1108 m



PS2476-3 (GKG)

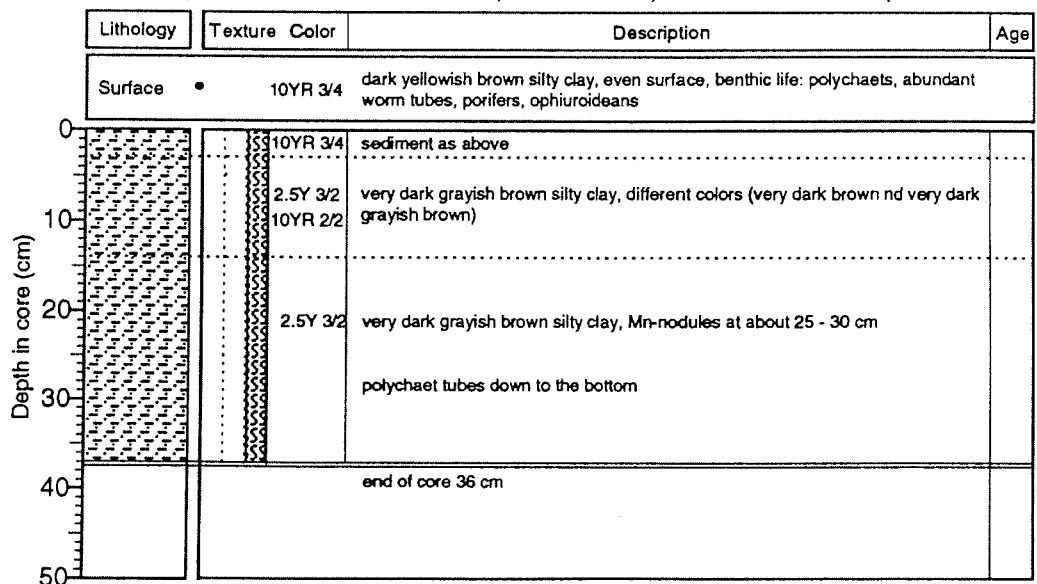
Laptev Sea, Profile F

ARK IX/4 (ARCTIC 93)

Recovery: 0.36 m

77°23,51'N 118°11,45'E

Water depth: 524 m



PS2477-3 (GKG)

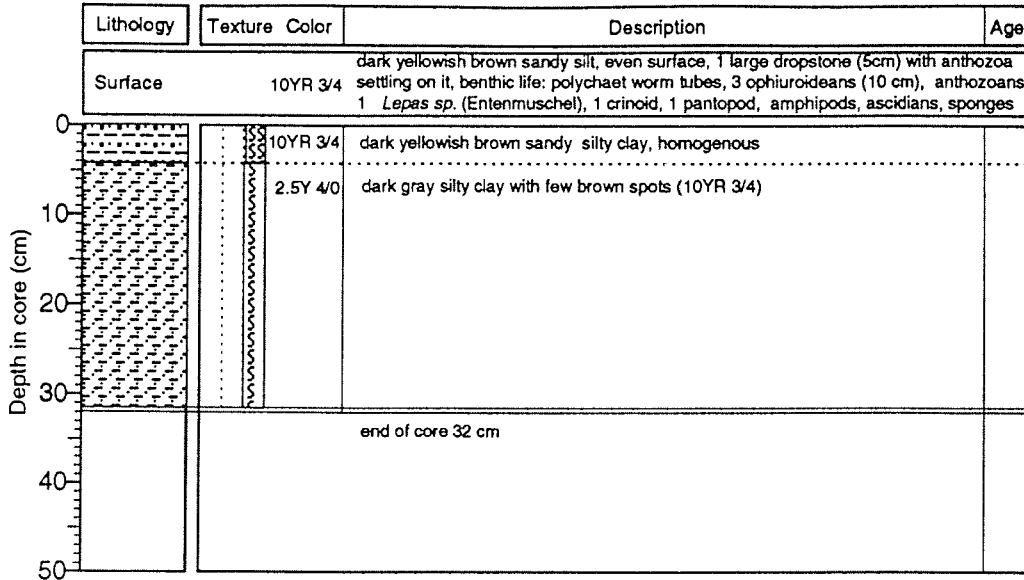
Laptev Sea, Profile F

ARK IX/4 (ARCTIC 93)

Recovery: 0.32 m

77°14,77'N 118°33,22'E

Water depth: 193 m



PS2478-3 (GKG)

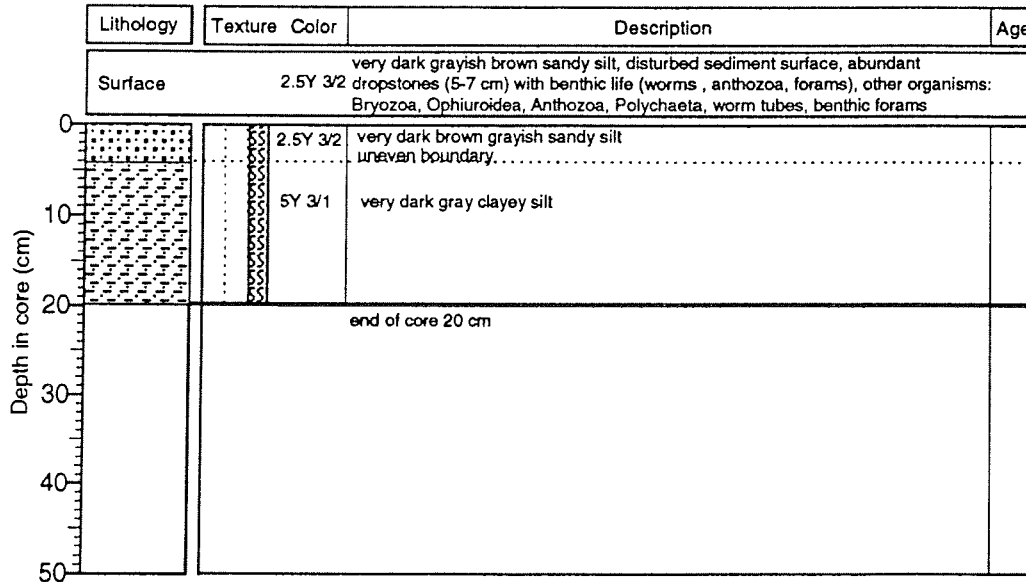
Laptev Sea, Profile F

ARK IX/4 (ARCTIC 93)

Recovery: 0.20 m

77°10,28'N 118°42,58'E

Water depth: 101 m



PS2480-2 (GKG)

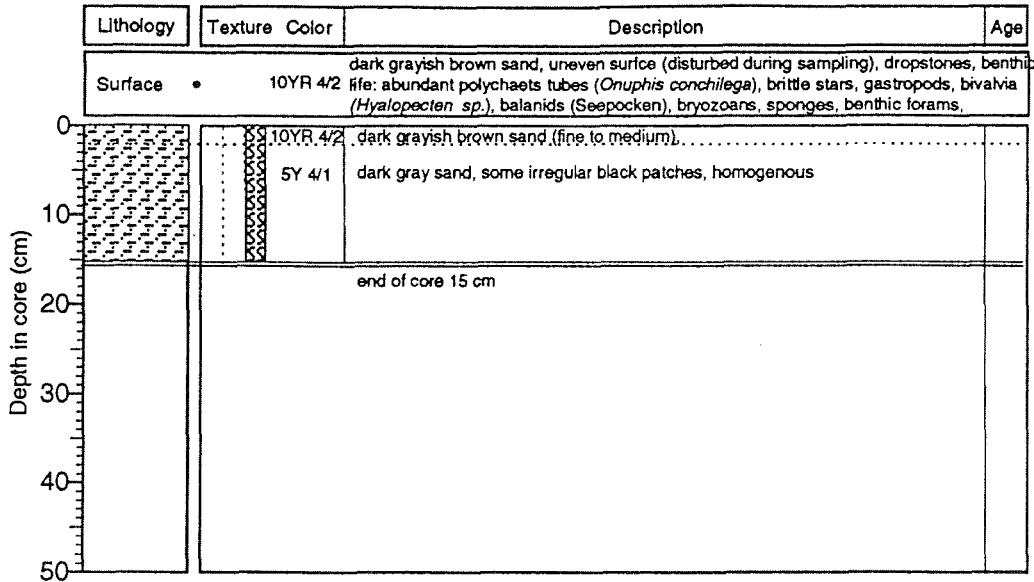
Laptev Sea, Profile E

ARK IX/4 (ARCTIC 93)

Recovery: 0.15 m

78°15,69'N 109°14,74'E

Water depth: 51 m



PS2481-2 (GKG)

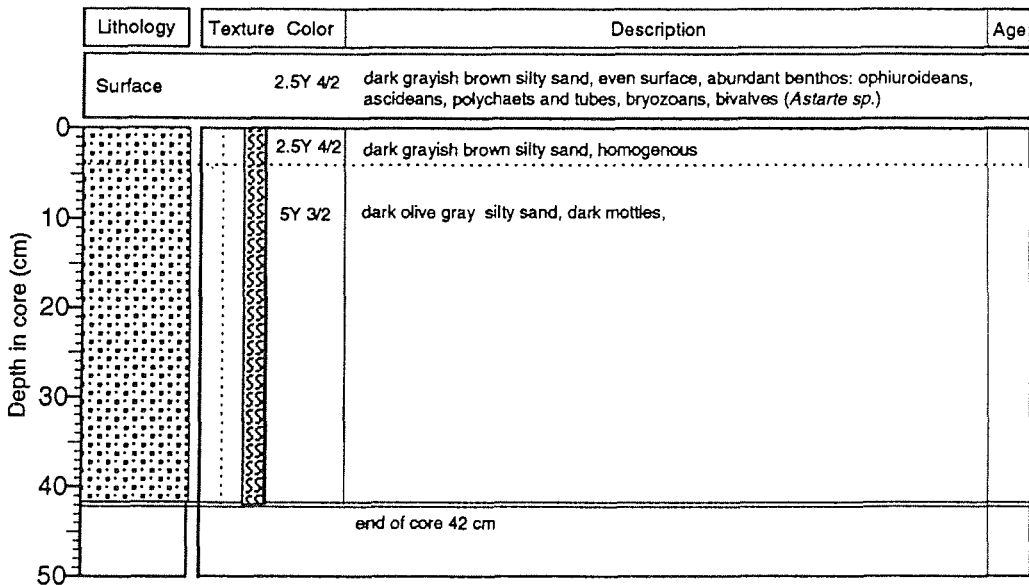
Laptev Sea, Profile E

ARK IX/4 (ARCTIC 93)

Recovery: 0.42 m

78°28,38'N 110°47,33'E

Water depth: 101 m



PS2482-2 (GKG)

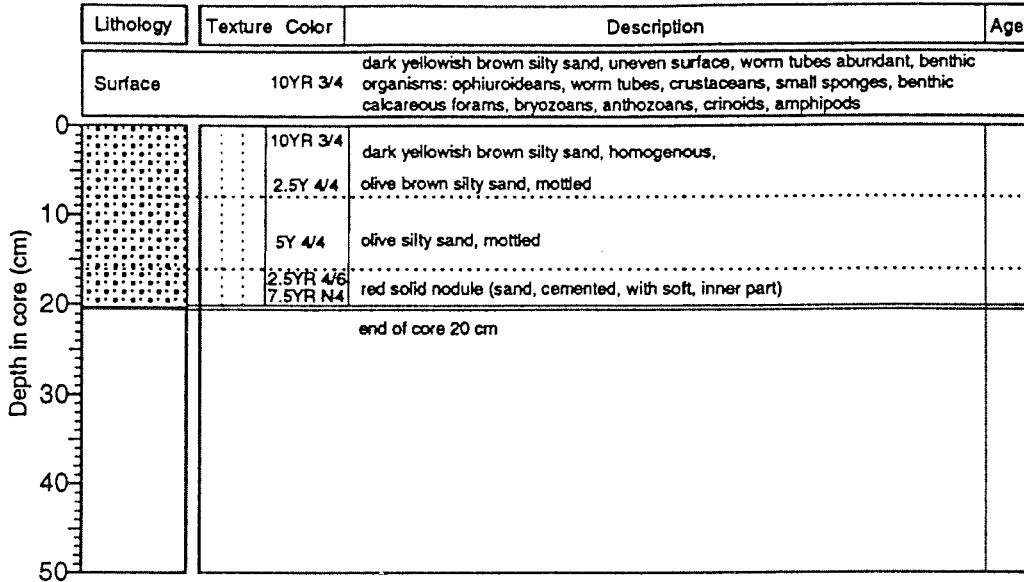
Laptev Sea, Profile E

ARK IX/4 (ARCTIC 93)

Recovery: 0.20 m

78°41,96'N 112°30,65'E

Water depth: 577 m



PS2483-2 (GKG)

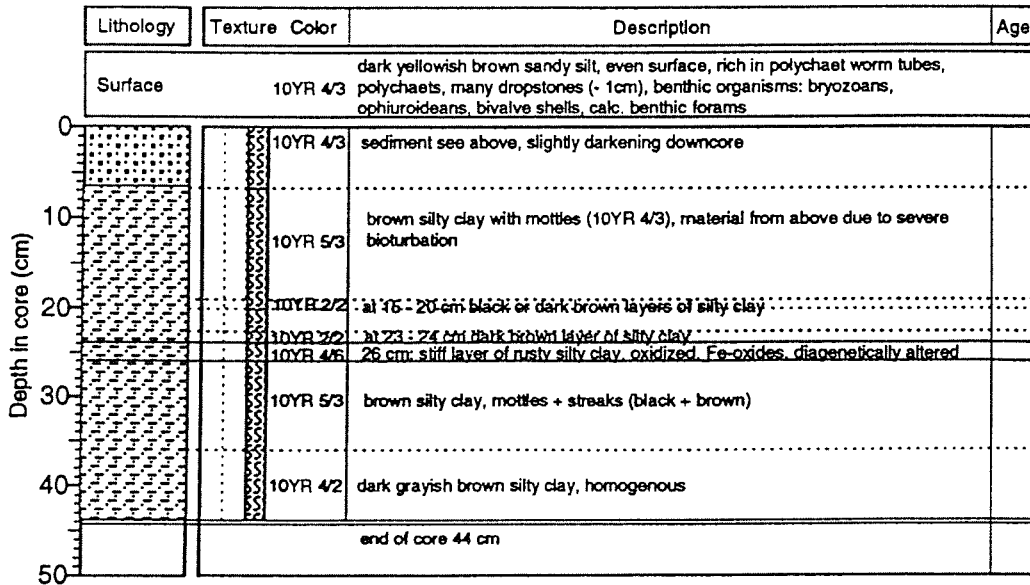
Laptev Sea, Profile E

ARK IX/4 (ARCTIC 93)

Recovery: 0.44 m

78°45,74'N 112°42,23'E

Water depth: 1216 m



PS2483-3 (SL)

Laptev Sea, Profile E

ARK IX/4 (ARCTIC 93)

Recovery: 5.68 m

78°45,71'N 112°42,58'E

Water depth: 1217 m

Depth in core (m)	Lithology	Texture Color	Description	Age
0		10YR 3/4	dark yellowish brown clayey silt, homogenous	
		2.5Y 4/4	olive brown silty clay, uneven gradual boundary, bioturbated few black streaks and mottles olive brown silty clay, homogenous, bioturbated, color grading downcore from 2.5Y 4/4 to 2.5Y 5/4	
1		2.5Y 5/4	light olive brown silty clay, homogenous	
		2.5Y 3/2	2 black to dark brown layers of clay intercalated in very dark grayish brown clay clay with various colors: rusty reddish and black mottles + streaks at 126-130 cm, 141 cm	
		2.5Y 4/2	dark grayish brown clay, transition zone with gradual color change	
		2.5Y N4	dark gray clay, homogenous	
			sand layer, turbidite, grading upwards	
2		5Y 4/2	at 205 cm: very thin sand layer	
		5Y 4/2	gradual transition of colors	
		10YR 4/3	brown/dark brown clay, oxidized colors	
		2.5Y 4/4	olive brown silty sand	
		2.5Y 4/4	olive brown clayey silt, homogenous	
		2.5Y 4/4	2 dark yellowish brown (10YR 3/4), (rusty) sand layers in sandy silt	
		2.5Y 4/4	olive brown sandy silt	
		5Y 3/1	sequence of very dark gray sandy silt intercalated by some thick + thin turbidites coarse sand with dropstones (1-1cm) + mud clasts (2-2cm)	
3		5Y 3/1	pink layer of silty clay very dark sandy silt coarse sand layer	
		5Y 3/1	several thin sand layers -0.3 cm	
		5Y 3/2	dark olive gray homogenous clay	
		5Y 4/2	dark gray (5Y 4/1) sand layers in olive gray sandy clayey silt, grading upwards	
		5Y 4/4	olive sandy clayey silt, homogenous	
		5Y 4/4	rusty layer of silty clay olive sandy silty clay, homogenous sand lense (2 cm) at 386-388 cm	
4			at 414 cm: 1 dropstone (2 cm) at the boundary to lower unit: oxidizing colors (rusty) sand layer, grading upwards into olive clayey silt	
		2.5Y N3	sequence of turbidites, very dark gray sandy silt intercalated by many thin sand layers Fe-oxide rich sand layer	
		2.5Y N3	sequence of sandy turbidites intercalated in sandy silt	
		5Y 4/2	uneven boundary olive gray clayey silt, homogenous, at 494 cm 1 dropstone (2 cm)	
5				

PS2483-3 (SL)

Laptev Sea, Profile E

ARK IX/4 (ARCTIC 93)

Recovery: 5.68 m

78°45,71'N 112°42,58'E

Water depth: 1217 m

Lithology	Texture Color	Description	Age
	5Y 4/2	olive gray silty clay 2 sand layers at 503 - 506 cm and 511 - 515 cm in silty clay	
	5Y 4/2	olive gray silty clay, homogenous, bioturbated	
		sand layer, grading upwards	
	5Y 4/2 5Y 4/3	olive gray to olive clay	
		end of core: 5.68 m	

PS2484-2 (GKG)

Laptev Sea, Profile E

ARK IX/4 (ARCTIC 93)

Recovery: 0.37 m

78°34,91'N 111°23,15'E

Water depth: 235 m

Lithology	Texture Color	Description	Age
Surface	10YR 4/2	dark grayish brown sandy clay, even surface, fecal pellets, benthic organisms: crinoideans, polychaets, porifers, anthozoans, sponges	
	10YR 4/2	dark grayish brown sandy silty clay	
	2.5Y 5/4 2.5Y 4/2	light olive brown silty clay, mottled with dark grayish brown patches	
	10YR 3/2	very dark grayish brown Fe-band	
		end of core 37cm	

## 10.5 General guidelines for data and sample distribution

By mutual understanding participating scientists in *Polarstern* cruise ARK-IX/4 agreed on general guidelines for the exchange of material and data obtained during the expedition. Because specific needs vary strongly between disciplines each participating disciplinary group set up its own specific guideline to best meet the specific demands.

To optimize information for those not participating in the cruise or associated by shorebased studies a list of potential working titles has been attached. Names of major contributors are given in italics.

### 10.5.1 Physical and chemical oceanography

#### 10.5.1.1 Statement for the distribution of oceanographic and hydrochemical data

The oceanographical and hydrochemical data obtained during ARK IX/4 will be hold by the principal investigators responsible for the respective measurements. These are for

##### *CTD data*

- Bert Rudels, Institut für Meereskunde, Troplowitzstr.7, 2000 Hamburg 54, Germany, Phone: 49-40-41235756, Fax: 49-40-5605926
- Leonid Timokhov, Arctic and Antarctic Research Institute, Bering Str. 38, 199397 St. Petersburg, Russia, Phone: (812) 3523971 Fax: (812) 3522688, Telex: 121423 NILAS SU, e-mail: aaricoop@sovam\_com
- Robin Muench, Science Applications International Corporation, 13400B Northup Way 36, Bellevue, WA 98005, USA, Fax: (206) 7479211
- Ursula Schauer, Alfred-Wegener-Institute für Polar- und Meeresforschung, Am Handelshafen, 27515 Bremerhaven, Germany, Fax: 49-471-4831425

##### *ADCP data*

- Robin Muench, Science Applications International Corporation, 13400B Northup Way 36, Bellevue, WA 98005, USA, Fax: (206) 7479211
- Ursula Schauer, Alfred-Wegener-Institute für Polar- und Meeresforschung, Am Handelshafen, 27515 Bremerhaven, Germany, Fax: 49-471-4831425
- Leonid Timokhov, Arctic and Antarctic Research Institute, Bering Str. 38, 199397 St. Petersburg, Russia, Phone: (812) 3523971 Fax: (812) 3522688, Telex: 121423 NILAS SU, e-mail: aaricoop@sovam\_com

##### *nutrients and ammonia*

- Anna Luchetta, Istituto Talassographico di Trieste, Viale R. Gessi 2, 34123 Trieste, Italia, Fax: 0039-40-308941, Phone: 0039-40-305506

##### *oxygen*

- Anna Luchetta, Istituto Talassographico di Trieste, Viale R. Gessi 2, 34123 Trieste, Italia, Fax: 0039-40-308941, Phone: 0039-40-305506
- Genadiy Iljin, Marine Biological Institute, Vladimirskaja st. 17, 183023 Murmansk Russia

*total carbonate*

- Kristina Olsson & Leif Anderson, Institutionen för Analytisk och Marin Kemi, GU/CTH, Kemigården 3, S-41296 Göteborg, Phone: 46-31-7722777, Fax: 46-31-7722785, e-mail: kristina@amc.chalmers.se

*freon and krypton*

- William Smethie & Guy Mathieu, Lamont-Doherty Earth Observatory, Palisades, NY 10964 USA, Phone: 914-3592900, e-mail: bsmeth@lamont.ldeo.columbia.edu

*helium, tritium, <sup>14</sup>C and <sup>18</sup>O*

- Reinhold Bayer & Markus Frank, Institut für Umweltphysik, Im Neuenheimer Feld 366, D-69120 Heidelberg, Germany, Phone: 49-6221-563335, Fax: 49-6221-563405, e-mail: br@uphys1.uphysn.uni-heidelberg.de, fm@uphys1.uphysn.uni-heidelberg.de

*barium*

- Kelly Falkner, Oregon State University-Oceanography, 560SW 15th Street, Corvallis OR 97331-2201, USA, Fax: (503) 737 2064

*trace Metals*

- Chris Measures, University of Hawaii, Dept of Oceanography, Honolulu HI 96822, USA,

*radio isotopes*

- Lee Cooper, Oak Ridge National Laboratory, Environmental Sciences Division, PO Box 2008, MS 6038, Bldg. 1505, USA, Fax: (615) 576-8646

*methane*

- Keith Kvenvolden, US Geological Survey, 345 Middlefield Road, MS-999, Menlo Park CA 94025 3591, USA, Fax: (415) 3543191

A copy of all data will be provided to Russian authorities according to the regulations of working in the economical zone of foreign countries. Copies should be sent to the Arctic and Antarctic Research Institute as soon as the various analyses are finished and data are available. Data of the CTD- and ADCP-measurements will be provided by the end of the cruise.

During two years after the analysis, the responsibility for the distribution of the data rests with the respective shipboard participants and principal investigators.

10.5.1.2 List of working titles for oceanographic and hydrochemical themes

- Distribution of water masses along the Eurasian basins continental slope (from CTD and tracer data).- *U. Schauer, AWI, R. Muench, SAIC, L. Anderson & K. Olsson, AMK, U. Bayer & M. Frank, IUH, A. Luchetta & P. Ponitz, ITT, G. Ilyin, MMBI, W. Smethie & G. Mathieu, L-DEO, B. Rudels, ZMK, L. Timokhov, AARI*
- Tracking the fate of Arctic river waters by geochemical means (from rosette samples).- *K.K. Falkner, Oregon State University OSU*

- The circulation in the upper layers at the Eurasian basins continental slope (from ADCP-, CTD-, and tracer-data).- *U. Schauer, AWI, R. Muench, SAIC, L. Anderson & K. Olsson, AMK, U. Bayer & M. Frank, IUH, A. Luchetta & P. Ponitz, ITT, G. Ilyin, MMBI, W. Smethie & G. Mathieu, L-DEO, B. Rudels, ZMK, L. Timokhov, AARI*
- The outflow of shelf brine water from the northwestern Barents Sea (from mooring data).- *U. Schauer, AWI, R. Muench, SAIC*
- Analyses of the ADCP data for internal wave phenomena (from ADCP and CTD data).- *R. Muench, SAIC, U. Schauer, AWI, Pinkel, SIO, D'Asaro & Padman, University of Wahington UW*
- Hydrography of surface melt puddles on Arctic sea ice (from nutrients, total carbonate, oxygen and salinity data).- *A. Luchetta & P. Ponitz, ITT, G. Ilyin, MMBI, L. Anderson & K. Olsson, AMK, L. Timokhov, AARI*
- Double diffusive convection and intrusive mixing in Arctic ocean intermediate waters (from CTD data).- *B. Rudels, ZMK*
- Large scale thermohaline circulation in the Arctic ocean: comparison between model and measurement (from CTD data).- *G. Lohmann & U. Schauer, AWI, B. Rudels, ZMK*
- <sup>228</sup>Radium as a tracer of shelf waters in the surface Arctic Ocean.- *M. Rutgers v.d. Loeff, AWI et al.*

## 10.5.2 Remote sensing

### 10.5.2.1 Guidelines for the exchange of remote sensing data

The recommendation for the exchange of remote sensing data is designed to provide guidelines for the data exchange practice for data collected during ARK-IX/4 to optimize the information base between the different working groups. All collected data are properties of the investigating institution.

- The Alfred Wegener Institute (AWI) shall archive all AVHRR raw data in a binary format and produce rectified data sets for the areas of main interest.
- The line-scan measurements in the visible and infrared spectral range and the airborne radar measurements received from the INTAARI radar flights are archived in the AWI.
- The Arctic and Antarctic Research Institute (AARI) carries out the long wave and the short wave energy surface flux and estimates the microwave emissivities of several arctical surface types during the ice stations.
- The INTAARI investigates ice thickness measurements with an geographic radar system based on the different backscattering properties of ice and water.

Every participating organisation should prepare their own data sets and the main processed data products in a clearly arranged manner. Any investigator wishing to request above mentioned data from the expedition ARK-IX/4 shall submit a request to the responsible institution. Therefore every investigator should be prepared to provide any other participant with a small amount of data after short time and free of costs.

The data distribution in a larger amount to other participants of ARK-IX/4 experiment should be possible in a cooperative way. The obtained data should be employed only for own studies. The transmission to non participant groups of ARK-IX/4 requires the agreement of the proprietor.

#### 10.5.2.2 Tentative scientific working titles on remote sensing themes

- Improvement of sea ice concentration algorithms.- *V. Alexandrov, AARI, Th. Martin, AWI*
- Sea ice classification from remote sensing.- *V. Alexandrov, AARI, H. Eicken & Th. Martin, AWI*
- Detecting new ice in the Laptev Sea polynia.- *Th. Martin, AWI*
- Sea ice drift in the Laptev Sea derived from satellite data and drifting buoy trajectories.- *H. Eicken & Th. Martin, AWI*
- Backscattering characteristics of summer melting sea ice.- *Th. Martin, AWI*
- Microwave signatures of sea ice.- *A. Darovskikh, AARI*
- Determination of ice thickness by remote sensing technique.- *H. Eicken, AWI, S. Syrtsov, INTAARI*
- Drift pattern of icebergs and their importance in the Laptev Sea.- *V. Alexandrov, AARI, H. Eicken & Th. Martin, AWI*
- Fast ice distribution and sediment transport in the Laptev Sea.- *H. Eicken & Th. Martin, AWI, E. Reimnitz, USGS*

#### 10.5.3 Physical sea-ice studies

##### 10.5.3.1 Data exchange and joint data evaluation for ARK-IX/4 sea-ice studies

Data collected by the sea-ice research groups will be exchanged between groups and made available to others upon request. Apart from data exchange for information and interpretation, the right to publish data or work resulting out of data analysis lies with the group that has collected a particular data set. Hence, any study drawing on data from another group should result in a joint project as those outlined below.

- Ship-board observations of sea-ice conditions met along the cruise track.- *H. Eicken & T. Martin, AWI, E. Reimnitz, USGS and observers group*  
A report tabulating all observations, summarizing important features will be prepared along with photographs of ice conditions and selected AVHRR satellite maps by the end of 1993 and handed to all members of the observation teams and others interested.
- Albedo data and data on energy exchange over sea ice.- *B. Ivanov & A. Alexandrov, AARI*  
A compilation of albedo data collected over different ice surfaces has been made available to H. Eicken, AWI and E. Reimnitz, USGS.-
- Spectral albedos.- *E. Reimnitz, USGS, H. Eicken, AWI*  
Spectral albedo data collected by H. Eicken and computed total albedos have been made available to B. Ivanov, AARI and E. Reimnitz, USGS; E. Reimnitz' data will be made available after processing.
- Thickness, structure and properties of sea ice.- *H. Eicken & J. Weissenberger, AWI, R. Gradinger, IPÖ*  
Ice thickness profiles, ice station data, ice-core stratigraphies, temperature profiles and salinity profiles have been compiled by H. Eicken & R. Pac, AWI and made available to all sea-ice researchers and others interested.
- Sea-ice sediments.- *E. Reimnitz, USGS*  
Sediment concentrations and related data obtained at ice stations will be made available to B. Ivanov, AARI, H. Eicken, AWI for sites of spectral/total albedo measurements, other data are available on request.
- Melt-puddle data.- *H. Eicken, AWI, R. Gradinger, IPÖ, G. Ilyin,MMBI, B. Ivanov, AARI, A. Luchetta, ITT, K. Olsson, AMK*  
Data have been exchanged or will be exchanged in the near future and are available to others on request.
- Ice biology.-  
Data available upon request (see also report prepared by ice-biology group).
- Video-Flight data.- *H. Eicken, AWI*  
Results obtained from image analysis of helicopter video flights will be made available to B. Ivanov & V. Alexandrov, AARI and others interested after processing by the end of 1993.
- Microwave emissivities and thermal radiation of different ice surfaces.-*A. Darovskich, AARI*  
Data available after processing upon request.
- Distribution and sizes of icebergs.- *H. Eicken, AWI*  
Shipboard and helicopter observations of icebergs along with evaluation of the INTAARI radar flights have been made available to V. Alexandrov, AARI. Publications and data on the glaciology of Severnaya Zemlya Islands pertaining to iceberg production will be made available through V. Alexandrov, AARI.

Joint data evaluation is planned on:

- Distribution, structure and hydrography of meltpuddles on Arctic sea ice.- *H. Eicken, T. Martin, J. Weissenberger & R. Pac, AWI, A. Alexandrov & B. Ivanov, AARI, R. Gradinger, IPÖ, G. Ilyin, MMBI, A.Luchetta & P. Ponitz, ITT, K. Olsson, AMK*
- Icebergs from the Severnaya Zemlya Islands.- *H. Eicken, T. Martin & N.N., AWI, V. Alexandrov, AARI*
- Field measurements of total and spectral albedos of sediment-laden Arctic sea ice.- *E. Reimnitz, USGSm B. Ivanov, AARI, H. Eicken, AWI*
- Regional energy exchange over summer Arctic sea ice.- *B. Ivanov & V. Alexandrov, AARI, H. Eicken & T. Martin, AWI*

#### 10.5.4 Sea-ice biology

##### 10.5.4.1 Distribution procedure for ice biological samples and data

All samples and data collected during the RV *Polarstern* cruise ARK-IX/4 are to be identified by the AWI ice core labelling code, including the ship cruise number, the Julian day of sampling and the ice core number.

Distribution of material and data is as follows:

- Samples for enumeration of abundance of ice organisms (algae, protozoa, metazoa) will be kept by Institute for Polar Ecology (IPÖ).
- Samples for determination of nutrients and algal pigments (chlorophyll a) will be distributed to Institute for Polar Ecology (IPÖ) Kiel and Alfred Wegener Institute (AWI) Bremerhaven.
- Samples of under-ice fauna:
  - amphipods collected with traps will be processed at AWI Bremerhaven;
  - mesozooplankton collected with pumps will be processed in IPÖ Kiel;
  - video recordings will be processed at AWI Bremerhaven.
- Cultures of ice metazoans for experimental purposes will be processed by IPÖ Kiel and AWI Bremerhaven.

Recognizing the tremendous investments in time, and energy expended by the members of the expedition's scientific party, preference shall be given to sample requests from shipboard participants and their laboratories. For 18 months after the expedition, the collected material/data shall be limited to shipboard participants, and their shorebased collaborators agreed upon by the participating institutes. Costs associated with transfer of samples shall be accounted for by the requesting party.

Russian scientific requests, as for taxonomic and other treatments will be given a high priority. Data of the different groups collaborating on board will be available for all on request. In case of use for publication, the partner collecting/providing the data has to be informed in advance in any case.

As responsible scientists for communication who should be contacted for detailed informations and requests will serve R. Gradinger, Institute for Polar Ecology (IPÖ) Kiel and M. Poltermann and J. Weissenberger, Alfred Wegener Institute (AWI) Bremerhaven.

#### 10.5.4.2 Tentative scientific working titles and collaborations for sea-ice biological studies

- Arctic sea ice brine communities: Growth and grazing activity of bacteria and auto- and heterotrophic protists.- *R. Gradinger, IPÖ*
- On the role of mesozooplankton organisms for coupling processes between sea ice and pelagial.- *R. Gradinger, H. Hanssen & K. Knickmeier, IPÖ*
- First observations on under-ice phytoplankton blooms in Arctic seas.- *R. Gradinger, IPÖ, A. Luchetta, ITT, M. Poltermann, AWI*
- Abundance of autotrophic and heterotrophic pico- and nanoflagellates and metazoans in sea ice of the Barents and Laptev Sea.- *C. Friedrich & R. Gradinger, IPÖ*
- Relation of physical, chemical and biological properties in Arctic sea ice.- *H. Eicken & J. Weissenberger, AWI, R. Gradinger, IPÖ*
- Taxonomy of Arctic sea ice nematodes.- *A.V. Tschesnov, Moscow State University, C. Friedrich & R. Gradinger, IPÖ, F. Riemann, AWI*
- Taxonomy of Arctic sea ice ciliates.- *N. Wilbert, University of Bonn, C. Friedrich & R. Gradinger, IPÖ*
- Taxonomy of sea ice diatoms from the Barents Sea and Laptev Sea.- *Okolodkov, ZISP, R. Gradinger, IPÖ*
- Ecophysiological investigations on Arctic sea ice protozoa and metazoa.- *C. Friedrich & R. Gradinger, IPÖ*
- Use of endoscope technique for investigation of sea ice organisms distribution and behaviour.- *J. Weissenberger, AWI*
- Distribution and behaviour of under-ice amphipods in the Barents and Laptev Seas.- *M. Poltermann, AWI*
- Migration of sea ice metazoans under natural conditions.- *J. Weissenberger, AWI*
- Resistance of Arctic sea ice communities against pollution.- *J. Weissenberger, AWI*
- Calculation of brine flow in ice floes using stain dilution experiments.- *J. Weissenberger, AWI*

#### 10.5.5 Marine biological investigations

##### 10.5.5.1 Sample and data distribution procedures for benthic and planktic biological material

All biological material and data sampled during the ARK-IX/4 of RV *Polarstern* are to be labelled with the ship's station numbers, indicating the gear used.

Distribution of material has been agreed upon as follows:

- Phytoplankton material and suspended matter and microbiological samples will be kept by Alfred Wegener Institute (AWI-Bio-II).
- Zooplankton material is distributed between the Institute of Oceanology Moscow (IORAS; multinet material, bongo net 0.5 mm), the Murmansk Marine Biological Institute (MMBI; bongo net 0.2 mm), the Institute for Polar Ecology Kiel (IPÖ; other bongo and part of multi nets), and the Alfred Wegener Institute Bremerhaven; (AWI-Bio-II; parts of multi and bongo nets).
- Macro-zoobenthos samples will be stored and processed at Alfred Wegener Institute (AWI-Bio-I; mainly quantitative infauna material), the Zoological Institute St. Petersburg (ZISP; mainly trawled material for taxonomic treatment) and at the Institute for Polar Ecology Kiel (IPÖ; epifauna, including trawled material).
- Meiofauna samples are treated and kept by the University of Oldenburg (UOI; in collaboration with AWI).
- Selected material from trawls will be processed by Alfred Wegener Institute (AWI) for analyses of trace organic contaminants.

The Alfred Wegener Institute (AWI) is to be informed about any other distribution of samples and material, also if material is given to taxonomists outside the above mentioned institutions for proper identification or more detailed studies.

For 18 months following the expedition, samples and data shall be limited to shipboard participants and their shorebased collaborators agreed upon by the participating institutes. For taxonomical identifications, material may be distributed earlier.

Recognizing the tremendous investments in time and energy expended by the members of the expedition's scientific party and the Alfred Wegener Institute, in general, preference shall be given to sample requests from shipboard participants and their laboratories. Russian scientific requests, such as for taxonomic and other treatments will be given a high priority.

Data of the different groups collaborating on board will be available for all. In case of use for publication, the partner collecting/providing the data is to be informed in advance to any use. Costs associated with transfer of samples shall be accounted for by the requesting party.

Dr. Eike Rachor, AWI, is prepared to serve as a communication address in all mentioned above matters.

#### 10.5.5.2 List of the intended scientific work on biological material and data

- 1) Phytoplankton and particulate matter in the water column (samples taken from rosette water bottles):
  - Comparative studies of the phytoplankton and particle flux regimes of the northern Barents and Laptev Seas. - (Distribution of chlorophyll-a and phaeopigments, analyses of phytoplankton species, of particulate carbon, nitrogen and silicate, total particulate matter) *E.-M. Nöthig & K. Springer, AWI*  
Cooperation: P. Wassmann, Univ. Tromsø (Particle flux in the northern Barents Sea)
- 2) Organic matter input into sediments and benthic microbial activities, (samples taken from multiple corers):
  - Input of organic material into the sediments of Barents and Laptev Seas.- *A. Boetius, E.-M. Nöthig & K. Lochte, AWI*
  - Microbial biomass distribution and microbial activities in the degradation of organic material along the Arctic continental slopes.- *A. Boetius, & K. Lochte, AWI*
  - Regulation of hydrolytic enzymes of marine bacteria.- *A. Boetius, AWI*
- 3) Zooplankton samples taken by multi-, bongo- and hand nets, including under-ice samples
  - Species and biomass distribution and community analyses of zooplankton in the northern Barents and Laptev Seas, including zoogeographical aspects.-
    - Deep water station samples *K. Kosobokova, IORAS; & H.-J. Hirche, AWI.*
    - Shallow water stations including southern Laptev Sea: *H. Hanssen & K. Knickmeyer, IPÖ.*
    - Epipelagic bongo-net samples (200 mm): *S. Timofeev, MMBI.*
  - Size distribution of epipelagic crustacean zooplankton.- *S. Timofeev, MMBI*
  - Populations structures of euphausiaceans and chaetognaths; larval plankton.- *S. Timofeev, MMBI*
  - Egg production and determination of the reproductive status of dominant copepod species.- *K. Kosobokova, IORAS, H.-J. Hirche, AWI & H. Hanssen, IPÖ*
  - Grazing rates of copepods, estimated by gut fluorescence measurements.- *H. Hanssen & K. Knickmeyer, IPÖ*
  - Hydromedusae in the waters along the Eurasian slopes.- *K. Kosobokova, IORAS*
  - Species composition of under-ice fauna and comparison with the pelagic fauna.- *H. Hanssen, K. Knickmeyer & R. Gradinger, IPÖ* (s. M. Poltermann, AWI for comparison with zoobenthos)

#### Cooperation:

- E. Markhaseva, ZISP*, for near-bottom zooplankton with special regard of the copepod family of Aetideidae;  
*V. Petryashov, ZISP* for Zooplankton in the shallow Laptev Sea;

- 4) Zoobenthos and fishes (samples taken by multi-corer, multi-grab, large box grab, epibenthos sledge and Agassiz trawl)
- Zoogeography of the benthic fauna in the northern Barents and Laptev Seas, including Vilkitsky Strait and the adjacent deep basins.- *B. Sirenko, ZISP, E. Rachor, AWI, K. Hinz, IPÖ, P. Martinez, UOI, et al.*
  - Taxonomy and biogeography of benthic macro-invertebrates along the continental slope of Barents and Laptev Seas.- *B. Sirenko & collaborators, ZISP*
  - Abundance, biomass and diversity of the meiofauna along transects in the Barents and Laptev Seas and their correlation with biotic and abiotic environmental factors.- *P. Martinez, UO*
  - Taxonomy and zoogeography of harpacticoid copepods in the northern Barents and Laptev Seas.- *P. Martinez, UO*
  - Temporary meiofauna / young macrozoobenthos as indicators of reproductive and recruitment processes in the benthos of the northern Barents and Laptev Seas.- *C.- P. Günther, AWI, & P. Martinez, UO*
  - Epifauna community analyses of the shelf and continental slope areas in the northern Barents and the Laptev Seas.- *K. Hinz, IPÖ, M. Schmid, IPÖ, D. Piepenburg, IPÖ, B. Sirenko, ZISP, E. Rachor, AWI, & J. Gutt, AWI*
  - Comparative ecophysiological studies of macrobenthic and planktonic invertebrates from the Barents and Laptev Seas.- *M. Schmid, K. Hinz, K. Knickmeyer, H. Hanssen & M. Spindler, IPÖ*
  - Changes in the endofauna distribution and structure along the continental slopes of Barents and Laptev Seas and the significance of organic matter transport from the shelves to the Arctic deep basins.- *E. Rachor, AWI*
  - Pelago-benthic coupling in the Barents and Laptev Seas - a first comparison.- *E. Nöthig, AWI, K. Springer, AWI, A. Boetius, AWI, U. Bathmann, AWI, H.-J. Hirche, AWI, H. Gonzalez, AWI, H.Hanssen, IPÖ & E. Rachor, AWI*
  - Taxonomy and zoogeography of the fish fauna along the slopes of the northern Barents and Laptev Seas.- *N. Chernova & A. Neyelov, ZISP*
  - Under-ice macrofauna and its relation to the benthos in the Arctic Ocean.- *M. Poltermann, AWI*
  - Halogenated organic compounds in benthic animals from Laptev and northern Barents Seas.- *K. Weber & H. Goerke, AWI*
  - Benthic communities in relation to bottom topography, sediment properties and depositional processes in the Laptev and Barents Seas.- *E. Damm, AWI-P; F. Niessen, AWI; N. Nørgaard, GEOMAR; D. Nürnberg, C. Schubert, R. Stein, M. Wahsner & A. Boetius, AWI; K. Hinz, IPÖ; P. Martinez, UO; E. Rachor, AWI & B. Sirenko, ZISP,*

*Cooperation:*

Zoological Institute St. Petersburg, Moscow State University, Zoological Museum Moscow for taxonomy of benthic invertebrates;  
Murmansk Marine Biological Institute for Barents Sea benthic communities and their variability;  
V. Petryashov, Zoological Institute St. Petersburg for Zoobenthos in the shallow Laptev Sea;  
M. Vincx, University of Gent for meiofauna of the Arctic deep basins;  
I. Kröncke, Senckenberg Research Institute Wilhelmshaven for Macrofauna of the Arctic deep basins.

10.5.6 Marine geology

10.5.6.1 Sediment sample distribution guidelines for ARK-IX/4 material

The sample distribution guidelines for ARK-IX/4 are designed to guarantee a fair distribution of material, to minimize the duplication of scientific effort and maximize the scientific return from these valuable samples.

The Alfred Wegener Institute (AWI) shall serve as the core repository for all ARK-IX/4 sediment samples. AWI will be responsible for the distribution of samples to shipboard and shorebased investigators. AWI will maintain a record of all samples that have been distributed and the nature of the investigations being undertaken. This information will be available to investigators on request.

All cores collected on the expedition will be labelled and recorded according to the AWI and *Polarstern* standard scheme. Samples distributed from these cores will be labelled with a standard identifier which will include a core identifier and the interval from which the sample was removed. This standard identifier should be associated with all data reported; residues of samples should remain labelled so that they can be related to earlier data.

Any investigator wishing to request samples from the expedition shall submit, in writing, a sample request to AWI. The request should contain a statement of the nature of the proposed research, the size and approximate number of samples required to complete the study. Costs associated with the taking and/or receiving samples from the AWI repository shall be accounted for by the requesting party.

For twelve months following the expedition, sampling shall be limited to shipboard participants and shorebased investigators agreed upon by the geoscience participants during the expedition. Recognizing the tremendous investment of time and energy expended by members of the expeditions's scientific party, in general preference shall be given to sample requests from shipboard participants.

For further information, please, contact the curator of the AWI Sediment Core & Data Repository: Dr. Hannes Grobe,

Alfred Wegener Institute for Polar and Marine Research  
D-27569 Bremerhaven, Germany  
Tel.: +49-471-4831-220  
Fax: +49-471-4831-149 / e-mail [grobe@vax.awi-bremerhaven.dbp.de](mailto:grobe@vax.awi-bremerhaven.dbp.de)

#### 10.5.6.2 Tentative scientific working titles on sampled geological material and data

- The Eurasian Arctic Shelf during the last Glaciation: Ice Cap versus Local Glaciers. Indication from high resolution seismic cross sections: Barents Sea to Laptev Sea.- *F. Niessen, AWI*
- Sub-marine ice gouges in the Laptev and Kara Seas as seen on high resolution seismic tracks. Evidence for ice grounding and sediment reworking on the Siberian Shelf.- *F. Niessen & H. Eicken, AWI E. Reimnitz, USGS* in cooperation with H. Kassens, GEOMAR
- High resolution seismic stratigraphy of an Arctic continental margin (Laptev Sea): Implications for late Quaternary sea level changes.- *F. Niessen, AWI*
- Stable oxygen and carbon isotopes in planktic foraminifers from Arctic ocean surface sediments: Reflection of the low salinity surface water layer.- *R. F. Spielhagen, GEOMAR et al.*
- Variability of Late Quaternary paleoenvironment and Siberian river runoff into the Arctic ocean: Evidence from foraminiferal isotope data. ( $\delta^{18}\text{O}$ ,  $\delta^{13}\text{C}$  of planktic and benthic foraminifers from selected long and short cores, AMS- $^{14}\text{C}$ -dating).- *R. F. Spielhagen, GEOMAR, R. Stein, AWI*
- Environmental changes in the Late Quaternary Eurasian Arctic: Evidence from distribution and composition of the coarse fraction in ARK-IX/4 sediment cores. (Analysis of the  $>63\ \mu\text{m}$  fraction: biogenic versus terrigenous components, composition of terrigenous fraction).- *N. Nörsgaard-Pedersen & R. Spielhagen, GEOMAR*
- $^{230}\text{Th}$  and  $^{10}\text{Be}$  in ARK-IX/4 sediment cores: Dating and reconstruction of Late Quaternary environmental changes.- *A. Eisenhauer & A. Mangini, IUH, R. Spielhagen, GEOMAR*
- Planktic foraminifers in ARK-IX/4 sediment cores: Evidence for Late Quaternary environmental changes from micropaleontological analysis. (Abundance and micropaleontology of planktic foraminifers).- *H. Bauch, GEOMAR*
- Palynology of ARK-IX/4 sediment cores: Evidence for changes of vegetation and river runoff in Late Quaternary northern Eurasia. (Pollen, spores and dinocysts in sediment cores).- *J. Matthießen, GEOMAR*
- Physical properties of ARK-IX/4 sediment cores: Changes of sedimentation and accumulation rates in the Late Quaternary. (Results of dry and wet bulk density, shear strength, and magnetic susceptibility measurements).- *N. Nörsgaard-Pedersen & H. Kassens, GEOMAR, F. Niessen, AWI*
- Barium in Arctic shelf, slope and deep-sea sediments.- *D. Nürnberg, AWI*
- Eurasian continental margin depositional environments: a comparison between Barents Sea and Laptev Sea during glacial/interglacial times. (Parasound, lithology, susceptibility, phys. prop., radiographs, smear slides).- *D. Nürnberg, AWI and shipboard scientific party*

- Calcium substitution by magnesium in Arctic planktic foraminifers.- *D. Nürnberg, AWI*
- Clay minerals in sea-ice from the central Arctic Ocean: evidence for Laptev Sea as a source area. (sea ice and sediment surface clay mineral data from ARCTIC'91, ARK-IX/4).- *D. Nürnberg & M. Wahsner, AWI, E. Reimnitz, USGS, T. Letzig, H. Kassens & I. Wollenburg, GEOMAR*
- Ikaite occurrence in Eurasian continental margin sediments.- *C. Schubert, D. Nürnberg & D.K. Fütterer, AWI*
- Terrigenous sediment transport along the Barents Sea continental margin into central parts of the Arctic ocean: evidence from clay mineralogy. (clay mineral data from ARCTIC'91, Franz-Joseph Land and ARK-IX-4).- *M. Wahsner, D. Nürnberg & F. Niessen, AWI*
- Clay minerals in Arctic Ocean surface and subsurface sediments: indikator for source areas of the terrigenous material and for transportation mechanisms between shelf and deep-sea areas.- *M. Wahsner, C. Vogt, D. Nürnberg & R. Stein, AWI*
- Relationship of grain-size distribution, structure and physical properties in sediments from the Eurasian shelf and the central Arctic ocean.- *M. Wahsner, AWI, N. Nørgaard-Pedersen, GEOMAR*
- Long-term geochemical and mineralogical changes in deep-sea cores of the Arctic ocean: indications of climatic changes in the Quaternary.- *M. Wahsner, AWI*
- Investigation of the anorganic element budget in sediment cores from the Eurasian shelf areas with special reference to manganese and iron precipitates.- *M. Wahsner, AWI, E. Damm, AWI-P*
- Changes in amount and composition of total organic carbon in central Arctic ocean and shelf region sediments during the late Quaternary.- *C. Schubert & R. Stein, AWI*
- Coals in central Arctic Ocean sediments as a tracer for source regions.- *C. Schubert & R. Stein, AWI*
- Heavy mineral distribution in central Arctic ocean and shelf region sediments: evidence for different source areas?- *R. Stein, AWI et al.*
- Organic carbon cycle: Input of terrigenous organic carbon from the Lena river and marine organic carbon productivity on the shelf region of the Laptev Sea.- *C. Schubert & R. Stein, AWI*
- Long-chain alkenones in surface water and sediments from the Laptev Sea shelf region and central Arctic Ocean as a tool for paleotemperature and paleoenvironment reconstructions.- *C. Schubert, AWI*
- Radionuclide contamination in the Arctic Basin ecosystem (from GKG samples).- *L.W. Cooper, ORNL*

- Analysis of radionuclides in sediment samples from the Laptev Sea (from GKG subcores PS2450 through PS2484).- *L. Timokhov, AARI, et al.*
- Anthropogenic pollution of the Arctic Seas (radionuclides, PCB, heavy metals, hydrocarbons in sediments of the northern Barents and Laptev Seas).- *G. Ilyin, MMBI*
- Oxygen in pore water in shelf and slope sediments of the Laptev Sea.-*E. Damm, AWI-P*
- Gradients of nutrients in pore water of the Laptev Sea.- *E. Damm, AWI-P, A. Luchetta & P. Ponitz, ITT*
- Degradation of organic matter and nutrients flux through the sediment/bottom water interface in shelf sediments of the Laptev Sea.- *E. Damm, AWI-P*
- Early diagenetic zones in Laptev Sea and their dependence on different environments of sedimentation.- *E.Damm, AWI-P, F.Niessen, AWI et al.*
- The geochemistry composition in relation to early diagenetic processes in shelf and slope sediments of the Laptev Sea.- *E. Damm, AWI-P*
- Benthic communities in relation to bottom topography, sediment properties, and depositional processes in the Laptev and Barents Seas.- *E. Damm, AWI-P, F. Niessen, D. Nürnberg, C. Schubert, R. Stein, M. Wahsner, A. Boetius & E. Rachor, AWI, K. Hinz, IPÖ, P. Martinez, BIO, B. Sirenko, ZISP, N. Nørgaard-Pedersen, GEOMAR*

10.6 Participating Institutions

Country and Institution Participants / Teilnehmerzahl

Federal Republic of Germany

AWI	Alfred Wegener Institute for Polar and Marine Research Columbusstraße D-27568 Bremerhaven	17
AWI-P	Alfred Wegener Institute for Polar and Marine Research Research Center Potsdam Postfach 60 01 49 D-14401 Potsdam	1
BIO	Department of Biology University of Oldenburg Ammerländer Heerstraße 114-118 D-26129 Oldenburg	1
GEOMAR	GEOMAR-Research Center Wischhofstraße 1-3 D-24148 Kiel	2
IPO	Institute for Polar Ecology Wischhofstraße 1-3 D-24148 Kiel	4
HSW	Helikopter Service Wasserthal GmbH Kätnerweg 43 D-22393 Hamburg	4
IUH	Institute for Environmental Physics University of Heidelberg Im Neuenheimer Feld 366 D-69120 Heidelberg	1
SWA	Seewetteramt Hamburg Deutscher Wetterdienst Bernhard-Nocht-Straße 76 D-20359 Hamburg	2

Italy / Italien

ITT	Istituto Talassografico di Trieste Viale Romolo Gessi, 2 I-34123 Trieste	2
-----	--	---

Russia / Russland

AARI	The Arctic and Antarctic Research Institute Uliza Beringa 38 St. Petersburg 199226	4
MMBI	Murmansk Marine Biological Institute Russian Academy of Sciences Murmansk 183 203	2
RGM	ROSKOMGIDROMET Per. Pavlika Morozova 12 Moscow, 123376	1
IORAS	P.P. Shirshov Institute of Oceanology Russian Academy of Sciences 23 Krasikova Moscow, 117218	1
ZISP	Zoological Institute Russian Academy of Sciences Universitetskaya nab. 1 St. Petersburg 199034	1

Ukrania / Ukraine

INTAARI	INTAARI Joint Enterprise c/o Kharkov Institute of Radioelectronics Lenin A. 14 Kharkov, 310057	1
---------	---	---

Sweden / Schweden

AMK	Department of Analytical and Marine Chemistry Chalmers University of Technology and University of Göteborg S-41296 Göteborg	1
-----	--	---

U.S.A.

L-DEO	Lamont-Doherty Earth Observatory Columbia University Palisades, N.Y. 10964	1
USGS	United States Geological Survey 345 Middlefield Road Menlo Park, CA 94025	1
SAIC	Science Applications International Corp. 13400B Northup Way, Suite 36 Seattle, WA 98005-2025	1

10.7 Participants and ship's crew

<u>name / Name</u>		<u>Institution / Insitut</u>
Alexandrov	Vitali	AARI
Boetius	Antje	AWI
Bogdanov	Vladimir	AARI
Böhm	Joachim	HSW
Brinkmann	Dirk	HSW
Büchner	Jürgen	HSW
Damm	Ellen	AWI-P
Darovskikh	Andrei	AARI
Eicken	Hajo	AWI
Frank	Markus	IUH
Friedrich	Christine	IPÖ
Fütterer	Dieter Karl (Chief Scientist)	AWI
Gradinger	Rolf	IPÖ
Hanssen	Heinrich	IPÖ
Hillebrandt	Marc-Oliver	HSW
Hinz	Katja	IPÖ
Ilyin	Gennady	MMBI
Ivanov	Boris	AARI
Kosobokova	Kseniya	IORAS
Krylov	Nicolay (Ice Pilot)	MSC
Lambert	Hans-Peter	SWA
Lensch	Norbert	AWI
Lohmann	Gerrit	AWI
Luchetta	Anna	ITT
Martin	Thomas	AWI
Martinez Arbizu	Pedro	BIO
Mathieu	Guy Georges	D-DEO
Muench	Robin	SAIC
Niessen	Frank	AWI
Nörgaard-Pedersen	Niels	GEOMAR
Nürnberg	Dirk	AWI
Olsson	Kristina	AMK
Pác	Regina	AWI
Poltermann	Michael	AWI
Poniz	Paula	ITT
Rachor	Eike	AWI
Reimnitz	Erk	USGS
Röd	Erhard	SWA
Rudels	Bert	ZMK
Schauer	Ursula	AWI
Schubert	Carsten	AWI
Sirenko	Boris	ZISP
Spielhagen	Robert	GEOMAR
Springer	Karin	AWI
Syrtssov	Sergey	INTAARI
Timofeev	Sergey	MMBI
Timokhov	Leonid	AARI
Wahsner	Monika	AWI

Weissenberger  
Witte

Jürgen  
Hannelore

AWI  
AWI

Ships Crew / Schiffspersonal ARK-IX/4

Master	Jonas	Heinz G.W.
Chief Mate	Müller	Manfred E.
1st Officer	Rodewald	Martin
2nd Officer	Grundmann	Uwe
2nd Officer	Wege	Dieter
Doctor	Blass	Carl-Christian
Radio Officer	Wanger	Karl-Heinz
Radio Officer	Geiger	Horst
Chief Engineer	Schulz	Volker
1st Engineer	Erreth	Monostory Gy
2nd Engineer	Ziemann	Olaf
3rd Engineer	Fengler	Rolf Rüdiger
Electronician	Lembke	Udo
Electronician	Muhle	Helmut
Electronician	Greitemann-Hackl	Andreas
Electronician	Roschinsky	Jörg
Electrician	Schuster	Georg
SBM	Zulauf	Reinhard
Carpenter	Marowsky	Klaus
A.B.	Bindernagel	Knuth
A.B.	Winkler	Michael
A.B.	Schmidt	Michael
A.B.	Reitz	Marcel
A.B.	Soage Curra	Jose
A.B.	Iglesias Bermudez	Bal
A.B.	Pousada Martines	Sat
A.B.	Ponte Dourado	Raul
Motorman	Müller	Klaus
Motorman	Carstens	Erwin
Motorman	Husung	Udo
Motorman	Dufner	Gustav
Motorman	Arias Iglesias	Enrique
Motorman	Heurich	Erwin
Cook	Kubicka	Egon
Cook Mate	Heuneke	Heino
Cook Mate	Wübber	Heinz
1st Steward	Scheel	Gerhard
Stewardess/Nurse	Hoffmann	Susanne
Stewardess	Hildebrandt	Bärbel
Stewardess	Hoppe	Martha
2nd Steward	Yang	Chien-Chang
2nd Steward	Yu	Kwok-Yuen
2nd Steward	Amran	Busro
Laundryman	Chang	Chin Chun